Origin of Overpressure and Pore Pressure Prediction in Carbonate Reservoirs of the Abadan Plain Basin

Vahid Atashbari

Australian School of Petroleum

The University of Adelaide

This thesis is submitted in fulfilment of the requirements for the degree of Doctor of Philosophy in the Australian School of Petroleum, Faculty of Engineering, Computer & Mathematical Sciences, The University of Adelaide

November 2016

THE UNIVERSITY of ADELAIDE

Table of Contents

Abstract

This thesis analyses overpressure throughout the Abadan Plain Basin and evaluates pore pressure in this basin using conventional petroleum industry methods, as well as two new proposed pore pressure prediction methods. Overpressures in the Abadan Plain Basin are primarily exist within carbonates, whereas most previously published overpressure analysis has been undertaken in shale-dominated clastic rocks. Overpressure in this basin is encountered in two main zones, primarily the Gachsaran and Gadvan/Fahliyan formations. South-west to north-east oriented thickening and shortening, as result of Arabia-Eurasia collision, has affected the pressure regime within the Gachsaran Formation, but seemed ineffectual to the Gadvan and Fahliyan overpressures.

In order to analyse overpressure origins and test conventional pore pressure prediction methods, a discrimination scheme was applied to remove the impact of lithology on the log recordings, resulting in isolating the minor shale interbeds within, and as a representative of, the carbonate sequences. Disequilibrium compaction was identified as the primary origin of overpressure in the Abadan Plain Basin. Eaton's (1972) pore pressure prediction method was applied on the filtered shale data with an exponent of 1.0 for sonic velocity, 0.1 for resistivity, and 5 for density data. Bowers' (1995) method was also tested and, while it accurately predicted pore pressure in the Gadvan and Fahliyan formations, it underestimates pore pressure in shallower formations.

This thesis also introduces a new 'compressibility method' for pore pressure prediction, developed by the author, that uses porosity-compressibility correlations. This new 'compressibility method' provided reliable pore pressure prediction results in the studied wells. Alternatively, overpressure as a result of sediment compaction is also estimated using Biot's (1941) general theory of three-dimensional consolidation. A generalised compaction model was constructed, and the resulting modelled pore pressure provides a reasonable estimate of observed pore pressure.

Statement

This work contains no material which has been accepted for the award of any other degree or diploma in any university or other tertiary institution and, to the best of my knowledge and belief, contains no material previously published or written by another person, except where due reference has been made in the text. The thesis was professionally reviewed and edited for textual errors by an approved proof reader.

I give consent to this copy of my thesis, when deposited in the University Library, being available for loan and photocopying.

28/11/2016

Vahid Atashbari Date

For a thesis that does not contain work already in the public domain

I certify that this work contains no material which has been accepted for the award of any other degree or diploma in my name, in any university or other tertiary institution and, to the best of my knowledge and belief, contains no material previously published or written by another person, except where due reference has been made in the text. In addition, I certify that no part of this work will, in the future, be used in a submission in my name, for any other degree or diploma in any university or other tertiary institution without the prior approval of the University of Adelaide and where applicable, any partner institution responsible for the joint-award of this degree.

I give consent to this copy of my thesis, when deposited in the University Library, being made available for loan and photocopying, subject to the provisions of the Copyright Act 1968.

I also give permission for the digital version of my thesis to be made available on the web, via the University's digital research repository, the Library Search and also through web search engines, unless permission has been granted by the University to restrict access for a period of time.

VAHID ATASHBARI

28/11/2016

Acknowledgments

I'd like to express my great thanks to my principal supervisor, Dr. Mark Tingay, for his support and genuine advices on the concepts and techniques for identifying overpressure origin and employing pore pressure prediction methods. I also thank my co-supervisor, Dr. Khalid Amrouch, and my former co-supervisor, Dr. Rosalind King, for their consultation and collaborations on the geological principles.

I also express great thanks to Dr. Saeid Jamshidi for his help in advancing my skills in MatLab software and Mr. Hossein Khoshdel for his generous assistance in helping me to work with Petrel modelling package.

Finally, my sincere thanks to my wife, mum, dad and two brothers for their continuous support and kind understanding all throughout my degree. I wouldn't have succeeded without their support and encouragement.

List of Symbols

P_h: hydrostatic pressure

σ: stress

σ': effective stress

σ_v: lithostatic pressure

σ_{max}: effective stress at the onset of unloading

ρ: density

ρ_b: bulk density

ρ_f: fluid density

ρ_{ma}: matrix density

ρ_{shale}: shale density

ρ_{normal}: density of normally compacted shale

g: gravitational acceleration

z: depth

ϕ: porosity

P: pressure

GR: Gamma ray

Δt: measured interval transit time

Δt_{ma}: matrix interval transit time

Δt_f: pore fluid interval transit time

Δt_{normal}: interval transit time of normally compacted shale

R_{shale}: shale resistivity

R_{normal}: resistivity of normally compacted shale

V: sonic velocity

V_{normal}: sonic velocity of normally compacted shale

V_0: sonic velocity at the surface

V_{max}: sonic velocity at the onset of unloading

V_b: bulk volume

V_p: pore volume

P_p: pore pressure

A: Bowers' regional parameters

B: Bowers' regional parameters

cs: an empirical regional correction factor for unconsolidated sediments

P_h: hydrostatic pressure

σ_v: lithostatic pressure

σ_{max}: effective stress at the onset of unloading

γ: exponent

η: empirically derived constant in Gardner's equation

B: empirically derived constant in Gardner's equation

α': a coefficient that measures the ratio of the liquid volume squeezed out to the volume change of the soil in an unconfined loading

α: Biot's poroelastic parameter

ν: Poisson's ratio

G: shear modulus

C: compressibility

C_b: bulk compressibility

C_r: rock compressibility

C_{bc}: bulk compressibility versus confining pressure

C_{bp}: bulk compressibility versus pore pressure

C_{pc}: pore compressibility versus confining pressure

C_{pp}: pore compressibility versus pore pressure

Cr: matrix compressibility

Q: a coefficient that measures the amount of liquid that can be forced into the sample under pressure while the volume of the sample is kept constant

1/H: a measure of the sample compressibility for a change in fluid pressure

1/R: measures the change in liquid phase content for a given change in fluid pressure

θ: the increment of liquid phase volume per unit volume of soil

q: flow rate

A: area

k: permeability

h: thickness

μ: viscosity

U: unloading parameter

x: Eaton exponent

CHAPTER 1- Introduction

1.1. Project Background

This project investigates the distribution and origin of overpressure in the Abadan Plain Basin, with a focus on understanding overpressures in carbonate formations and to develop reliable pore pressure prediction methods. Accurate estimation of pore pressure is essential in almost all aspects of the oil and gas field exploration and development (Bhagwan et al., 1998; Fertl and Chilingarian, 1977; Henning et al., 2002; Holbrook et al., 1995; O'Connor et al., 2011; Tang et al., 2011; Tingay et al., 2009). Differences in pore pressure estimation could lead to drastic changes in reserve evaluation, and particularly in under-saturated oil reservoirs with solution gas, where gas bubbles can emerge below a certain pressure (Baltensperger et al., 2012). Accurate pore pressure knowledge is particularly critical in drilling and completion, both for drilling safety (avoidance of blowouts and well control lost-time incidents) and in order to select appropriate strength casing activities (Ahmed et al., 2011; Anderson et al., 1973; Badri et al., 2001; Fertl and Chilingarian, 1977; Holbrook et al., 1995; Hooyman et al., 2003; Huffman et al., 2011; Rocha et al.). For example, the 'window' of safe drilling mud weight in overpressured formations is narrower than in normally pressured sediments (Daniel, 2001). Knowledge of overpressures is also used to evaluate the maximum buoyancy pressure that a top seal can support, which indicates the maximum height of hydrocarbon column (Caillet, 1993; Gaarenstroom et al., 1993; Yassir and Addis, 2002).

Overpressure is primarily generated due to an imbalance between overburden loading and the ability for fluid to be expelled from pore spaces (Green and Wang, 1986; Waples and Couples, 1998a). In the case of an undrained compaction, a rock attempts to lose porosity at a rate faster than pore fluid can be expelled through surrounding impermeable or low permeability seal (Green and Wang, 1986; Magara, 1975; Smith, 1971). The resultant overpressure inhibits further compaction, which creates the commonly observed 'undercompaction' signature on porosity-vertical stress trends (Bowers, 1995). It is this abnormally high porosity associated with overpressure (and the direct link between porosity and vertical effective stress) that forms the basis of all commonly used petroleum industry pore pressure prediction methods (Bowers, 1995;

Eaton, 1972; Lindberg et al., 1980). The conventional pore pressure prediction methods are applied in shales, and involve estimating effective stress, and then pore pressure, from the value of measured porosity (or a proxy, such as velocity of resistivity), with respect to a normal compaction trend (Bowers, 1995, 2001; Eaton, 1972; Fertl and Chilingarian, 1987; Ransom, 1986). However, recent years have witnessed growing observations of significant overpressures being observed in non-clastic rocks, such as carbonates and volcanics, even in shale-poor environments (Baltensperger et al., 2012; Conybeare and Shaw, 2000; Lun et al., 2013; O'Connor et al., 2010; O'Connor et al., 2011). The overpressures observed in non-clastic lithologies are often quite dangerous, and are especially problematic because they typically display no porosity anomaly, nor any obvious relationship between porosity and effective stress (O'Connor et al., 2010; Rudolph et al., 2015). For example, the porosity in many carbonates is often more affected by diagenetic processes, such as chemical compaction, fracturing, dolomitization and brecciation, rather than effective stress. These unusual, and hazardous, overpressures remain an enigma for pore pressure specialists, as it is uncertain how such overpressures form, and conventional pore pressure prediction methods are unreliable in carbonates.

The Abadan Plain Basin offers an excellent opportunity to study, in detail, the origin of overpressures in carbonate rocks, and to test existing and new methods for pore pressure prediction in this difficult lithology. The Abadan Plain Basin is located on the northern edge of the Arabian Plate, and immediately adjacent to the Zagros deformation front. The structures in this basin are primarily related to those commonly seen through the Arabian Plate, with north-south oriented anticlines. The basin is stratigraphically simpler than the Zagros Fold-Thrust Belt, which is extensively folded and currently tectonically active (DeMets et al., 2010; DeMets et al., 1990; Falcon, 1974; Lacombe et al., 2007; McClusky et al., 2000; McQuarrie, 2004; Mouthereau et al., 2007; Nilforoushan et al., 2003; Vernant et al., 2004). This basin is prolific, with hydrocarbon accumulations with an estimated 80 billion barrels of proven oil in place. Despite the great economic importance of this basin, several aspects of the basin's geology have not been properly studied. There are numerous excellent field-scale geological studies, but these have not been put together in a basin-wide regional study. Moreover, the Abadan Plain Basin was repeatedly studied in conjunction with the Dezful Embayment and yet there are few studies exclusively conducted on this basin. In particular, The Abadan Plain Basin hosts significant magnitude overpressures in carbonate reservoirs in the Fahylian Formation

(below ~3600m), with overpressures also being encountered in some fields in the shallower carbonate Gachsaran Formation at the northern end of the basin (Abdollahie Fard et al., 2006b; Alavi, 2007). The overpressured sequences of the Abadan Plain Basin have been frequently penetrated by exploration and production drilling, and thus there exists a good dataset to undertake the first detailed study of overpressures in this basin, and to provide new insight and methods for understanding overpressures, and improving pore pressure prediction, in carbonates.

1.2. Project Aims

The aim of this research is to investigate the occurrence of overpressures and their origins in the Abadan Plain Basin, and to use oilfield data to predict pore pressure, with a particular focus on carbonate formations. As such, this research seeks to achieve the following three primary aims.

1. Prepare a basin-wide pressure model to understand pressure distribution regime and implications for well drilling and field development in the Abadan Plain Basin.
2. Determine the characteristics and mechanisms of overpressure generation in the Abadan Plain Basin.
3. Test pore pressure prediction strategies, including proposing new methods, in carbonates.

1.3. Thesis Plan

This thesis starts with an overview of regional geology of the Abadan Plain Basin and tectonic settings of the Arabia-Eurasia plate collision. The different characteristics of the geologic structures of the Abadan Plain enable defining of the boundaries of the basin, and distinguish it from the surrounding assemblages.

The basin and field-scale distribution of overpressures throughout the Abadan Plain Basin is examined in Chapter 3, and demonstrates that overpressures occur basin-wide in the Gadvan and Fahliyan formations, and occasionally in the Gachsaran Formation in the northern end of the basin. The distribution of overpressures, when compared to the regional geology, can be used to suggest overpressure generation mechanisms, which is examined in Chapters 4 and 5.

Chapter 4 undertakes a literature review of overpressure origins, with particular emphasis on mechanisms likely to occur in carbonates, as well as identifying plausible mechanisms in the Abadan Plain Basin.Detailed petrophysical analysis of the overpressured shales in the Abadan Plain Basin, explaining how different mechanisms affect petrophysical rock properties, is then conducted in Chapter 5.Petrophysical analysis indicates that disequilibrium compaction is the dominant overpressure generation mechanism in this basin.

Chapters 6, 7, 8 and 9 are focused on pore pressure prediction in the Abadan Plain Basin. Chapter 6 describes the calculation and distribution of the vertical stress magnitude, which is a key input to pore pressure prediction methods, and was also used in the petrophysical analysis in Chapter 5.

Conventional pore pressure prediction methods can be used in deposits where there is a certain relationship between porosity and vertical stress. However, after discussing diagenesis and porosity evolution of carbonates in Chapter 7, carbonate rocks in the Abadan Plain Basin are determined to be ‘stress-insensitive’, and thus, likely unsuitable for conventional pore pressure prediction methods. Chapter 8 and 9 tests and compares the current ‘state of the art’ in pore pressure prediction in carbonates (Chapter 8) with new methods developed herein. In Chapter 8, a dataset of carefully discriminated shale interbeds are incorporated with the Eaton (1972) and Bowers (1995) methods to predict pore pressure using sonic, resistivity and density logs. Although the results are generally reliable in the logged zones, there were several issues that may suggest inaccuracy of these methods in carbonates. A set of complementary techniques, using compressibility attributes of rocks, to predict pore pressure and estimate maximum potential overpressure, specifically generated within carbonate rocks, are provided in Chapter 9. These tools combined with the shale-based pore pressure prediction method give the best possible solution to study overpressures in carbonates.

CHAPTER 2- Regional Geology of the Abadan Plain Basin

2.1. Introduction and Geographical Setting of the Abadan Plain Basin

The Abadan Plain Basin is located in the area covering the southwest of Iran and southeast of Iraq. It is a foredeep basin to the southwest of Zagros foreland (Saadatinejad and Sarkarinejad, 2011). The Abadan Plain Basin is located at the outer edge of the Zagros deformation front and adjacent to the Persian Gulf–Mesopotamian foreland basin (Figure 2-1; Alavi, 2007) . This basin is bounded along its northern and eastern margin by the Dezful Embayment (Figure 2-1). It extends into Iraq at its northern end and into the Persian Gulf to the south (Figure 2-1). Moallemi and Kermanshah (2012) have defined a wider area for the Abadan Plain Basin which covers almost all areas of Kuwait and northern Persian Gulf with an extension towards Saudi Arabia. Although there are similarities between the geological structures (such as depth to basement and trend of anticlines) in those areas, I have accepted those of published researches which have defined the Abadan Plain Basin as the area between Zagros Deformation Front and the Iran-Iraq border. Due to hydrodynamic connections between some structures on both sides of the border, my definition of the basin covers a narrow margin in the south of Iraq (Figure 2-1)

The structures in the Abadan Plain Basin haven't been studied in in the context of an independent basin, and were generally considered through studies of the Zagros Fold-Thrust Belt or in conjunction with the Dezful Embayment in particular. The geology of the Abadan Plain Basin is primarily controlled by the Zagros Orogeny, associated with the collision between the Arabian and Eurasian Plates. Therefore, geological explanation of the Abadan Plain comes from a comprehensive study of collisional-related tectonics of Zagros Orogeny and Arabian and Eurasian plates tectonics. The lack of unique investigation of the Abadan Plain Basin has become one of the drivers for this research; to study more attributes of a basin that is one of the region's most prolific hydrocarbon environments.

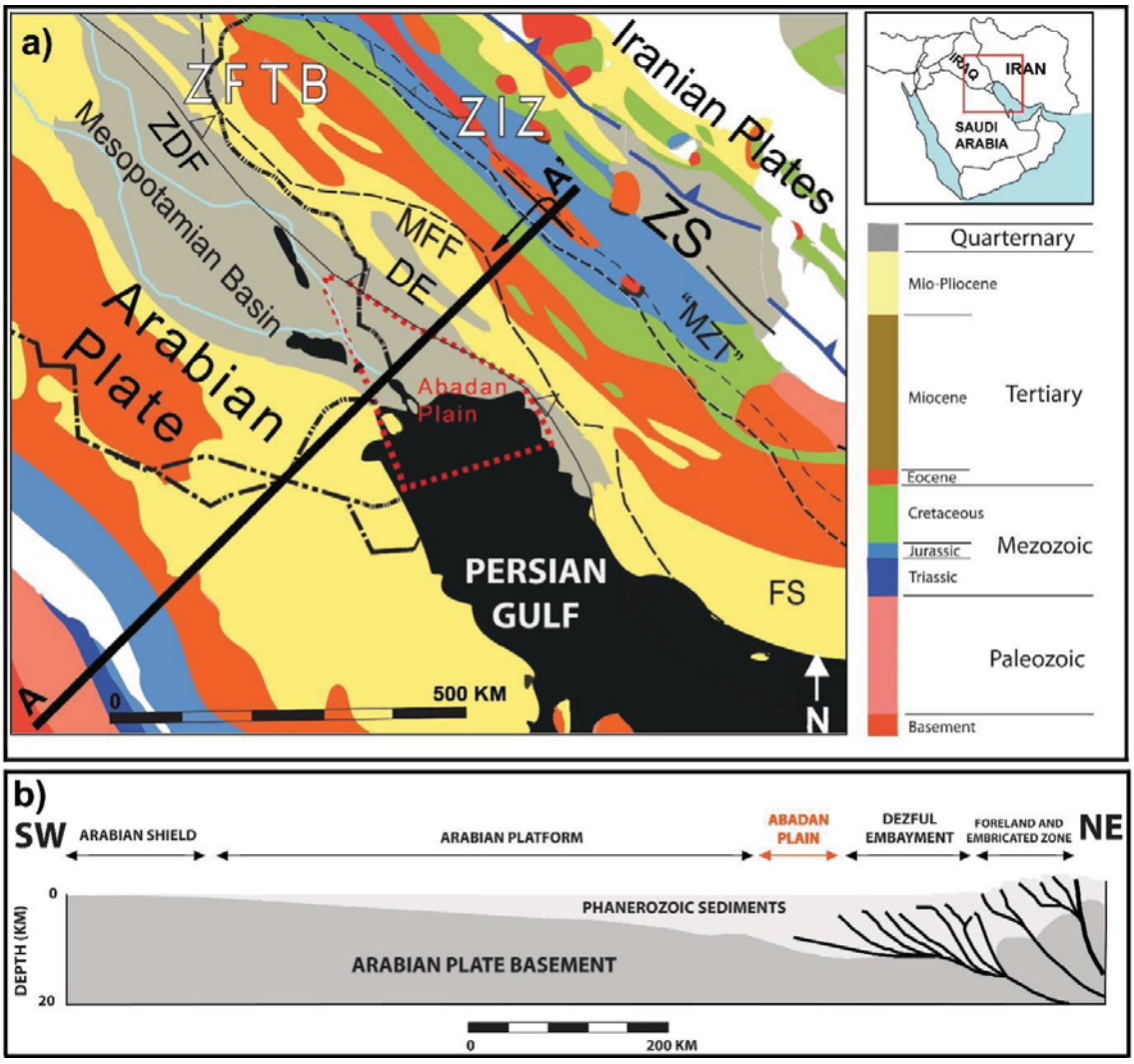

Figure 2-1 – (a) Simplified geologic map of the Arabian Plate and Zagros Fold-Thrust Belt modified from (Alavi, 2007); ARAMCO (1968). Abbreviations: DE: Dezful Embayment, FS: Fars Salient, MFF: Mountain Front Flexure, MZT: Main Zagros Thrust, ZIZ: Zagros Thrust Zone, ZDF: Zagros Deformation Front, ZIZ: Zagros Imbricate Zone, ZS: Zagros structure. Abadan Plain Basin is bounded by the Zagros front fault to the north and north-east. The location of section A-A' is also indicated. (B) Simplified cross-section across the Arabian Shield, Arabian Platform and the ZFTB along line A–A' modified from Abdollahie Fard et al. (2006b). The Arabian basement is exposed in the SW. Depth to basement is at its maximum in the Dezful Embayment while the basement gets shallower due to the tectonic thrusting towards NE.

According to British Petroleum (2014), the Middle East is the host to nearly 48% of the world's proven oil reserves and 43% of world's proven gas reserves. A vast majority of these reserves (and almost all of the giant fields) are placed on the Arabian plate or across the Zagros folded area.

Some specific conditions that gave rise to the current basin could be noted as (Ghorbani, 2002):

- almost continuous deposition of limestone, argillaceous limestone, marly limestone and evaporites from Permian up to Pliocene in a marine environment;
- existing source rock, reservoir and cap rock in adequate placement;
- lack of intense tectonic activities during the period Permian up to Pliocene (post collision tectonic settings), and;
- lack of metamorphic or magmatic activity since the Permian.

The southern part of Eurasia, that includes Iran, is often considered to have been a stable block which was affected by only gentle epeirogenic movements throughout the Palaeozoic (Falcon, 1974). As such, the Abadan Plain Basin has different attributes than the Zagros Fold-Thrust Belt, such as less seismicity and lack of anticlinal expressions at the surface. Moreover, the majority of anticlines in the Abadan Plain Basin have north-south oriented axes, while those in the Zagros are primarily oriented north-west to south-east. Structural trends in the Abadan Plain Basin are similar to the structures in Kuwait, north of Persian Gulf and northeast of Saudi Arabia (Motiei, 1995).

2.2. Abadan Plain Basin Tectonic History

The tectonic system of the Abadan Plain Basin hasn't been well studied and, despite the significant differences discussed previously, is often considered as a non-folded zone bounded by the Zagros deformation front to the north and east and thus is studied in conjunction with structures in the Zagros and the Arabian Plate. The majority of deep-seated anticlines in Cretaceous and older units in the Abadan Plain Basin and Dezful Embayment are upright and symmetrical (Abdollahie Fard et al., 2006b). In the Abadan Plain Basin, the structural trend extends to the basement which, when considering the existence of a steep fault in the core of anticlines, indicates the possible impact of basement on faulting (Abdollahie Fard et al., 2006b). The dominant trend of structural closure in this basin in the offshore oilfields is north to south oriented, which becomes north-east to south-west oriented in the offshore fields.

The movement of the Afro-Arabia plate towards the Eurasia Plate, and subsequent closure of the Tethyan Ocean (Berberian and King, 1981; Falcon, 1974; Takin, 1972), have been followed by the continent-continent collision of the Zagros Orogen. Sarkarinejad and Azizi (2008) suggest that continent-continent collision resulted in triclinic dextral transpression, although (Saadatinejad and Sarkarinejad, 2011) noted the key role of extension, expressed by normal faulting and asymmetric grabens. Contrary to this, oceanic crust is still subsiding under the Iranian plate along the Oman Subduction Zone (Abdollahie Fard et al., 2006b). Alavi (2004) classified the Neoproterozoic–Phanerozoic stratigraphy of the collision-affected region into four major zones, based on their tectonosedimentary features, which consist of megasequences, including several lithostratigraphic units, bounded by unconformities.

1- Marine and non-marine deposits of evaporites and associated volcanic and sedimentary layers overlain by siliciclastic and carbonates that have accumulated in an extensional pull-apart setting during the uppermost Neoproterozoic to possibly Devonian.
2- The former group is overlain uncomfortably by the Permian to Triassic (Sharief, 1982; Szabo and Kheradpir, 1978) platform succession that consists of basal conglomerates and sandstones related to the continental rifting (Berberian, 1995; Sepehr and Cosgrove, 2004).
3- Then, accumulations on a north to north-east oriented shallow (Neo-Tethyan) continental-shelf have deposited during the lowermost Jurassic to upper Turonian stage of the upper Cretaceous epoch (James and Wynd, 1965). This phase has been identified as a passive continental margin with sea-floor spreading to the north-east by Berberian (1995).
4- Finally, upper Cretaceous to recent marine, paralic, and continental deposits overlie the older sequences.

The Tethys ocean was closed by the time of Oligocene-Miocene epochs, and the rapid shift in sedimentation towards more detritic facies marks the passage from passive margin to foreland basin conditions (Molinaro et al., 2004). In fact, the main tectonic attribute in this region is the Arabian-Eurasian collision, and based on the time of the collision, the regional depositional history has been divided into several periods (Figure 2-2). The exact time of the Arabia-Eurasia plate collision initiation isn't clear and a wide range of times has been proposed. The most accepted timeframe for the collision is late Cretaceous, considering ophiolite obduction (Alavi,

1994; Allen et al., 2004; Berberian and King, 1981; Yilmaz, 1993) and the Zagros Orogeny that started in the Middle Maastrichtian (Alavi, 2007). However, Mouthereau et al. (2012) identified three stages of the collision: initiation, crustal thickening and uplift/deformation which took place at 35 Ma, 25 Ma and 15-12 Ma respectively.

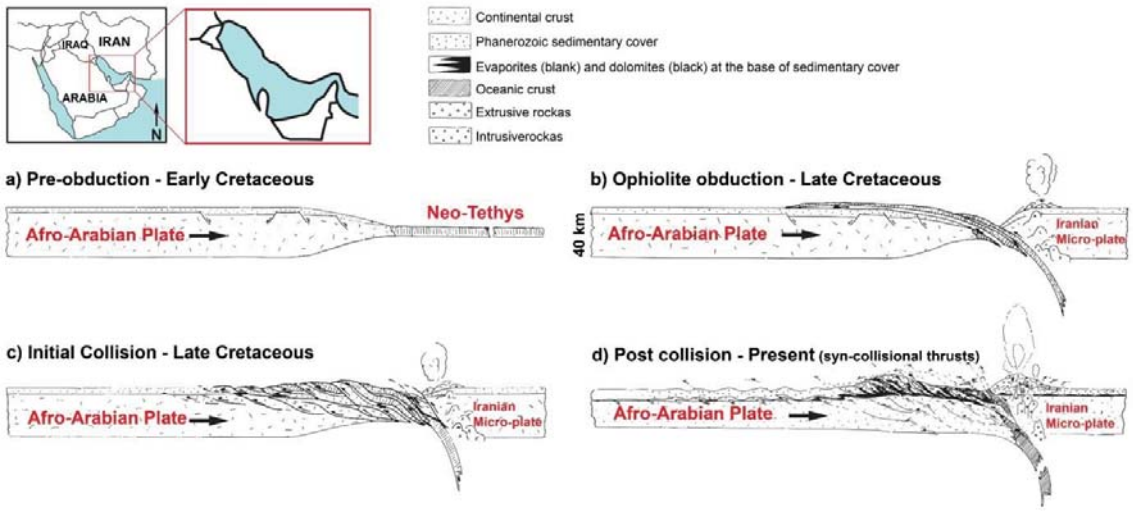

Figure 2-2 - Schematic cross sections illustrating pre-obductional and obductional-initial collisional steps in the evolution of the Zagros collision zone, modified from Alavi (1994).

Contrary to this, Philip et al. (1989) considered the separation of eastern and western Great Caucasus by a system of left-lateral strike-slip faults to be the result of the beginning of the continental collision at 5 Ma. They also noted an intensified deformation during the Middle Pliocene (3.5 Ma). However, investigations such as (Robertson, 2000) on the Neotethyan Oceanic Basin have indicated its closure was due to the diachronous collision in Eocene-Oligocene which ended in 23 Ma during the collision. It is notable that the Arabian-Eurasion plate convergence, and resulting folding, is currently active (DeMets et al., 2010; DeMets et al., 1990; Falcon, 1974; Lacombe et al., 2007; McClusky et al., 2000; McQuarrie, 2004; Mouthereau et al., 2007; Nilforoushan et al., 2003; Vernant et al., 2004). A schematic reconstruction of Africa-Arabia and Eurasia is presented in Figure 2-3 where the possible movement of the Arabian plate towards Eurasia was estimated between 300 and 500 km since initial

collision (Dewey et al., 1989). Agard et al. (2011) outlined the following period/regimes as the main attributes and geodynamics of the Zagros Orogeny:

(1) Mid to late Cretaceous time (115–85 Ma) corresponds to a distinctive period of perturbation of subduction processes and inter-plate mechanical coupling marked by blueschist exhumation and upper plate fragmentation;
(2) Paleocene–Eocene time (60–40 Ma) witnesses slab break-off, major shifts in arc magmatism and distributed extension within the upper plate;
(3) From Oligocene time onwards (30±5 Ma to present), collision develops with a progressive SW migration of deformation and topographic build-up (Sanandaj-Sirjan Zone (SSZ): 20–15 Ma, High Zagros: ~ 12–8 Ma; Simply Folded Belt (SFB): 5–0 Ma), and is accompanied by a second, late Miocene slab break-off (~ 10 Ma to present).

Figure 2-3 - Plate reconstructions for the convergence of Africa-Arabia and Eurasia modified after Allen et al. (2004) and Dewey et al. (1989). Numbers are ages in Ma. There has been roughly 300–500 km of Arabia-Eurasia convergence since the initial collision at 20– 30 Ma. This is comparable with the convergence recognized within the collision zone (Allen et al., 2004).

Falcon (1974) proposed that sediments, which deposited after the south-westerly migration of belts of synorogenic basin development in the Zagros Orogeny, came from the north-east and were from local uplifts. According to Alavi (1994), the Zagros Orogeny consists of three parallel belts:

1- Urumieh–Dokhtar magmatic assemblage to the northeast (UDMA), with its oldest rock deposited in Early Cretaceous and peak magmatic activity in the Eocene.
2- the Zagros imbricate zone (ZIZ) at the southwest of UDMA, which includes both the "Sanandaj–Sirjan zone" and the "Zagros thrust zone" of Stoecklin (1968).
3- the Zagros Fold–Thrust Belt (ZFTB) is the same as the "simple folded zone" of Falcon (1961), which extends parallel and to the southwest of the ZIZ.

None of the aforementioned zones cover Abadan Plain Basin, as they are defined, but due to the structural impact of the Zagros folding on the basement and Phanerozoic sediments of the Arabian plate, they have been considered from a geographic and tectonic point of view. The main structures in the Abadan Plain Basin are part of broader assemblages that include the Arabian Platform and Iran Micro-plate. The East Arabian Block limits the southern extension of the Abadan Plain Basin. Different trends of the structures in Arabian plate are presented in Figure 2-4 with dashed lines. The north-south trend is dominant in the centre and west of Arabia while north-east to south-west trend is prevalent in the eastern parts of the plate. Zagros structure at the north and north-east edge of the plate is expressed as several sets of thrusts and folds in a north-west to south-east orientation.

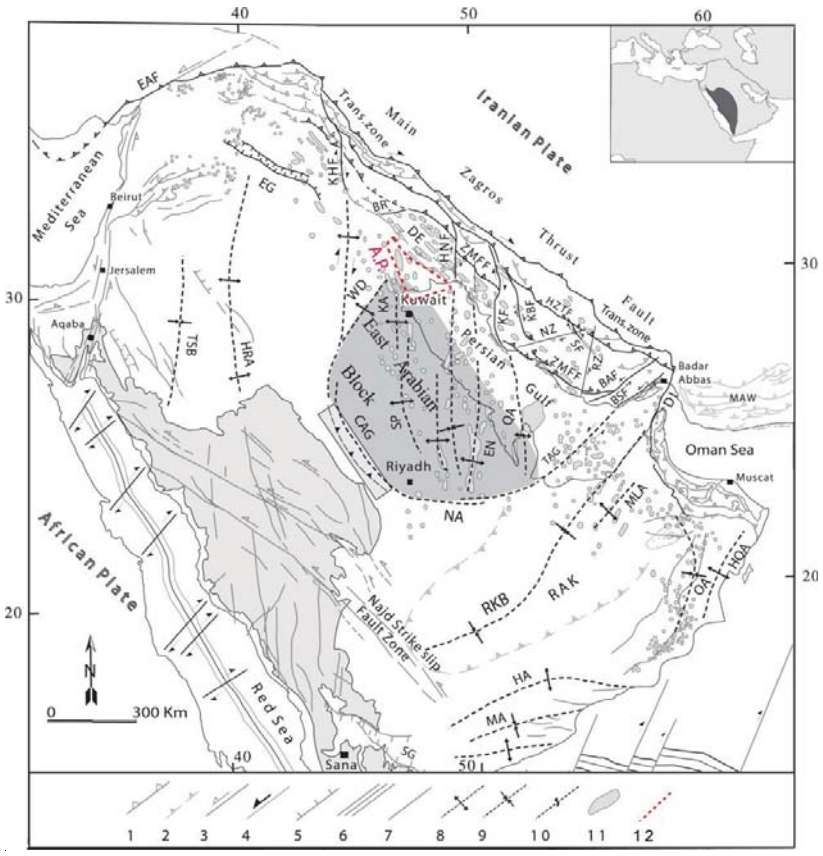

Figure 2-4 - Main structures in the Arabian plate, modified from Bahroudi (2003). (1) Contractional Fault, (2) Intercontinental basin, (3) Strike-slip faults: DI, Dibba Fault; BSF, Bostaneh Fault; BAF, Bastak Fault; RZ, Razak Fault; NZ, Nezamabad Fault; SF, Savastan Fault Zone; KBF, Kar Bas Fault Zone; KF, Kazeron Fault Zone; HNF, Hendijan Fault; BR, BalaRud Fault; and KHF, Khanqin Fault; EAF, East Anatolian Fault; (4) Transform Fault, (5) Normal Fault, (6) Spreading Axis, (7) Master Fracture, (8-10) Basement lineaments in Arabia (Anticline/Arch, Syncline/Basin, and Flexure) including TSB, Tabuk Basin; MH, Mardin High; EG, Euphrates Anah Graben; HRA, Hail Ga'ara Rutbah Arch; WSB, Widyan Basin; TAG, Trans Arabian lineament; CAG, Central Arabian Graben; KA, Kuwait Arch; SP, Summan Platform; EN, En Nala Safaniya Trend; QA, Qatar Arch; RKB, Rub Al Khali Basin; MLA, Mender Lekhwair High;OA, Oman basin lineament; HQA, Huqf Arch; WD, Wadi Al-Batin lineament; HA, Hadhramout Arch; MA, Mukalla Arch; NA, Nisah-sahba lineament; SG, Sadah Graben, (11) Oil and gas fields, (12) The Abadan Plain Basin.

The platform on which the Abadan Plain Basin is located generally has the same attributes of the Arabian platform. Abdollahie Fard et al. (2006b), based on Sattarzadeh et al. (1999), has characterised three main basement-involved deep-seated trends in Abadan Plain: NE–SW, N–S and NW–SE. Furthermore, according to a series of geological attributes, such as seismic activity, magnetic imprints, gravity anomalies, and reactivation of younger exposed structures, Alavi (2007) identified some reactivated pre-Zagros structures in the basement of the ZFTB. He classified reactivated

pre-Zagros structures into three main groups, attributed to three major geotectonic events, which have affected the Afro-Arabian Plate: N-S trend, NW-SE trend, and NE-SW trend. This is consistent with Abdollahie Fard et al.'s (2006b) classification of the basement. The basement-involved horst system of N-S structures is predominant in this region. This trend is attributed to the Pan-African orogeny, or Pan-African structural grain, which has been superimposed by the Zagros fold near the Zagros deformational front (Abdollahie Fard et al., 2006b), and seems to be following the trend of the Neoproterozoic orogenic belt with magnetic anomalies indicated by Johnson and Stewart (1995) on the Arabian Plate (Figure 2-5).

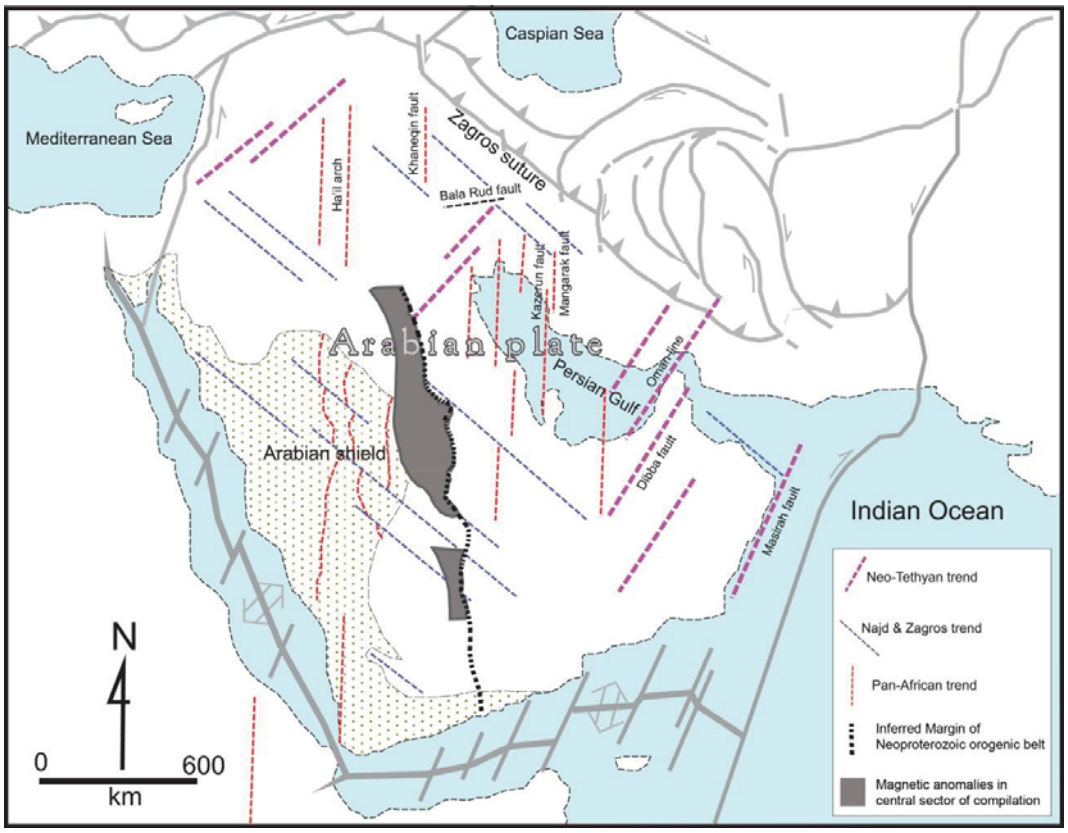

Figure 2-5 - Prominent basement-rooted lineaments in the Arabian continental crust (modified after Alavi ,2007) showing the inferred margins of Neoproterozoic crust of the type exposed on the Arabian-Nubian as defined by Johnson and Stewart (1995).

Tectonic plate movement and the resulting closure of the Neo-Tethys Ocean were the principal drivers for most strata deformations in central and southern Iran, Iraq, and the

Persian Gulf region. Major geological features (i.e. faults) are frequent in the fold area, but absent in the Abadan Plain Basin. However, the region remains under a compressional stress regime and several active faults play a significant role in surface deformations across the Zagros structure. Figure 2-6 represents the seismic event map of the ZFTB and northern Arabia. The earthquakes are notably distributed along the major fault, while the magnitude of the seismic events is significantly higher along the fault. The depth and magnitude of earthquakes decrease in a south-west direction (from ZFTB towards Arabia, including the Abadan Plain Basin). The seismic events in the Abadan Plain area are distinctively shallower in depth, and smaller in magnitude, than those of the ZFTB.

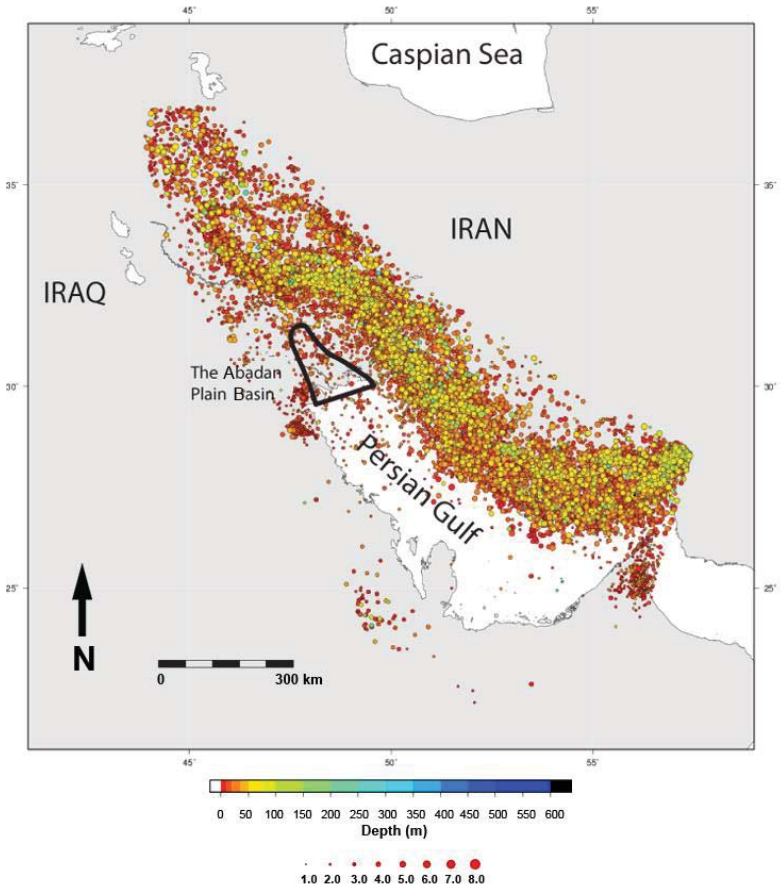

Figure 2-6 – Seismic event map of the Zagros Fold-Thrust Belt and northern Arabia from 01 January 1900 to 01 November 2014. Data are from the International Seismological Centre. A total of 15,727 events were recorded. The Abadan Plain Basin has been shown with a black polygon where the intensity of seismic events is lower than those of in Zagros area and seismic events occur in shallower depths.

The majority of the formations containing oil and gas accumulation were either deposited by the time of the Arabian-Eurasia collision, and deformed as a consequence, or deposited during the continuous collision and experienced some degree of deformation.

2.3. Abadan Plain Basin Stratigraphy

The majority of the sediments in Middle East are marine sequences deposited in the Tethys Oceanic environment. There are few outcrops of deep formations in the Abadan Plain Basin and the surface in this region consists of Quaternary deposits (Haghi Pour and Aghanabati, 1988). Shallow deposits (present to Oligocene) mainly consist of sandstone, conglomerates and evaporites. From Eocene to Cretaceous, deposits are several combinations of carbonate and clay/shales with minor sandstone interlayers. Jurassic to Permian deposits consist of three types of evaporites, carbonates and shales, while sandstone and conglomerates are present in the older horizons. The Hormuz salt formation lies immediately above the Pan-African basement and is extensive over the entire region. Murris (1980) summarised the sedimentation processes of the Middle East including the Abadan Plain Basin as follows.

1. From the late Carboniferous to the Early Jurassic, the region has been covered by a very shallow carbonate platform with evaporitic central depressions and clastic incursions from the west.
2. From the Middle Jurassic to the Turonian, intershelf basins have been breaking up the shallow carbonate platform, which differentiated the platform further. Clastic deposits reached their maximum development while coming from the west during early to middle Albian.
3. The late Turonian to early Senonion Alpine orogeny affected the Tethyan region, causing a major change in the depositional system.
4. Flysch-type sediments, coming from the rising orogene in the east, formed a shale-filled open-marine foredeep.
5. Large-scale overthrusting and ophiolite were emplaced due to the late Campanian to early Maestrichtian paroxysm, after which, stable conditions

returned and a stable carbonate platform was left in the west as well as a shaly successor basin in the east. This has been followed by a clastic material supply on the eastern flank of the basin due to an isostatically rising orogenic belt.

6. During early to middle Oligocene, the depositional basin narrowed considerably, which could be a result of a pronounced drop in worldwide sea level (Vasil and Mitcham Jr., 1979).
7. The basin was covered by carbonate rocks and evaporites during the late Oligocene to middle Miocene.
8. Finally, clastic rocks were deposited on the carbonates and evaporites during Miocene and the Pliocene.

Several clay type formations, as well as evaporites, provide a sealing for some underlying reservoirs that host significant hydrocarbon accumulations. Furthermore, despite the tectonic activity of the Zagros Orogeny, the Abadan Plain Basin has experienced less topographical deformation, and more erosion, than the main Zagros Orogenic Belt (Abdollahie Fard et al., 2006b; Alavi, 2007). According to the concept of lithospheric flexure (the crustal thickening as a result of mountain belt evolution), the trend of depth to basement steadily decreases from north-east to south-west over the Iranian microplate (Figure 2-7).

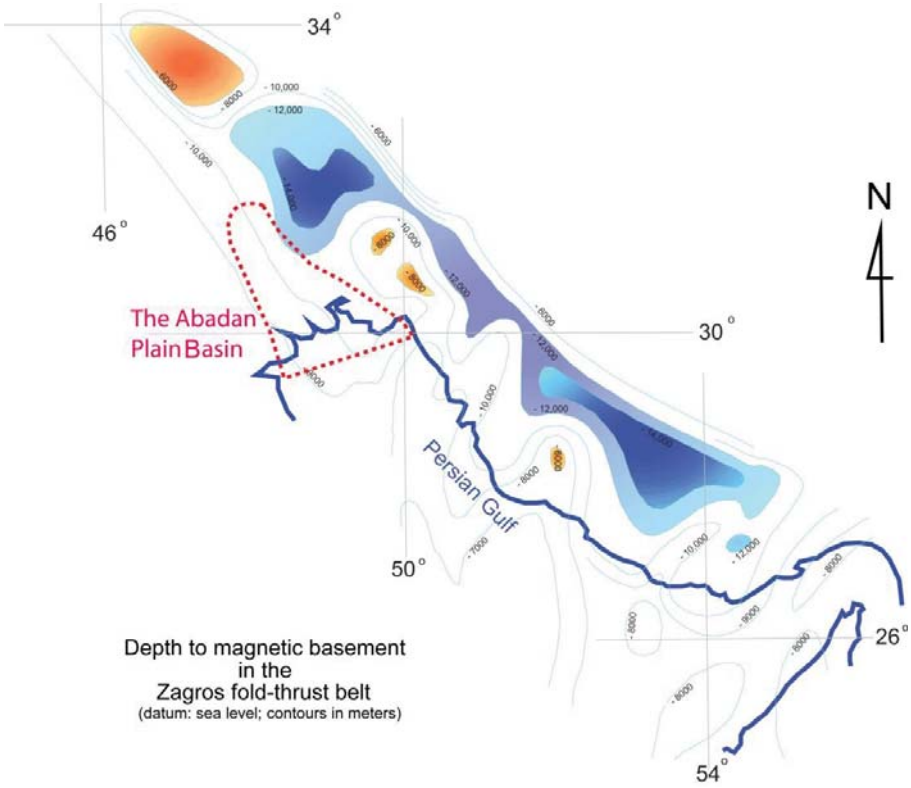

Figure 2-7 - Top-magnetic basement map of the Zagros Fold-Thrust Belt (modified after Alavi, 2007 and Morris, 1977) Blue and orange shades indicate basement 'lows' and 'highs', respectively.

Abdollahie Fard et al. (2006b) and Alavi (2007) have classified the depositional environment of the Dezful Embayment and Abadan Plain Basin into four distinct areas.

1. Marine and continental foreland (includes deposits from late Cretaceous to present).
2. Passive continental margin (Jurassic to late Cretaceous).
3. Continental rifting (Permian to Triassic).
4. Epicontinental platform (Cambrian to Permian).

According to this classification, all sediments later than the Ilam formation are in the marine and continental foreland group, while the underlying formations investigated in this research are considered part of the passive continental margin group. Formations beyond the Fahliyan haven't been examined herein. A schematic diagram of this

classification is shown in Figure 2-8. Based on Alavi's (2007) classification, the entire range of formations investigated in this research are within the Zagros Orogeny timeframe and have been deposited during the Cretaceous to Pliocene.

Motiei (1993) classified the hydrocarbon bearing formations of the south-west of Iran into nine periods with respect to the depositional environment, and with an emphasis on oil and gas reservoirs. The area of his classification includes the Fars and Zagros Structure in south and south-west of Iran. A part of this classification for the Abadan Plain Basin and the Dezful Embayment is noted below.

1- Permian: A sea-level rise that caused the deposition of the Faraghan sandstone formation in Lower Permian, and then sequences of reef carbonates in the Middle and Upper Permian in a supertidal environment.
2- Triassic: A shallow marine and high-energy environment that formed the Khaneh Kat dolomitic formation. This formation is mainly cap rock with occasional gas shows in the porous members.
3- Lower and Middle Jurassic: A closed sea environment covering the north of the Dezful Embayment and central Iraq, in which a series of evaporites, argillaceous limestone and a few shales were deposited.
4- Upper Jurassic: A closed sea environment with evaporitic deposits, such as the Gotnia formation.
5- Lower Cretaceous: Following the sea level rise in late Jurassic, a trough existed in the Lower Cretaceous in which the Garu shale has been deposited in Northern parts of the Dezful Embayment. Concurrently, Fahliyan and Darian formations were deposited in a shallow marine environment. Ghorbani (2002) believes that the Fahliyan, Gadvan and Dariyan formations were all deposited in the trough conditions. According to Motiei (1993), the origin of sediments of the Gadvan formation were from erosion of the Arabian Shield outcrops in the Arabian Peninsula and Fars region (southern Iran).
6- Middle Cretaceous: During the Albian-Cenomanian, the Fars platform was uplifted, but with concurrent sea level rise in adjacent areas. Erosional features

are frequent prior to, and during, the Turonian. The Sarvak formation was deposited before the erosion in the Cenomanian.

7- Upper Cretaceous: Following the Turonian erosion, the Laffan shale (and concurrent Surgah shale) was deposited during the sea level rise. The Ilam neritic carbonate then overlies the Laffan shale. Gurpi accumulations dominate the entire basin from the middle Santonian.

8- Paleocene-Eocene: Cretaceous sea level rise made the depositional environment monotonic, while the Gurpi and Pabdeh formations, comprised of shale and carbonates, were deposited in a shallow marine to supertidal environment.

9- Oligocene-Miocene: Prior to this time, sea level started falling and the region was exposed to the erosion. There was a narrow trough in the region, in which Oligocene deposits accumulated. After a primary rise, there has been a sea level fall that continues until the present-day.

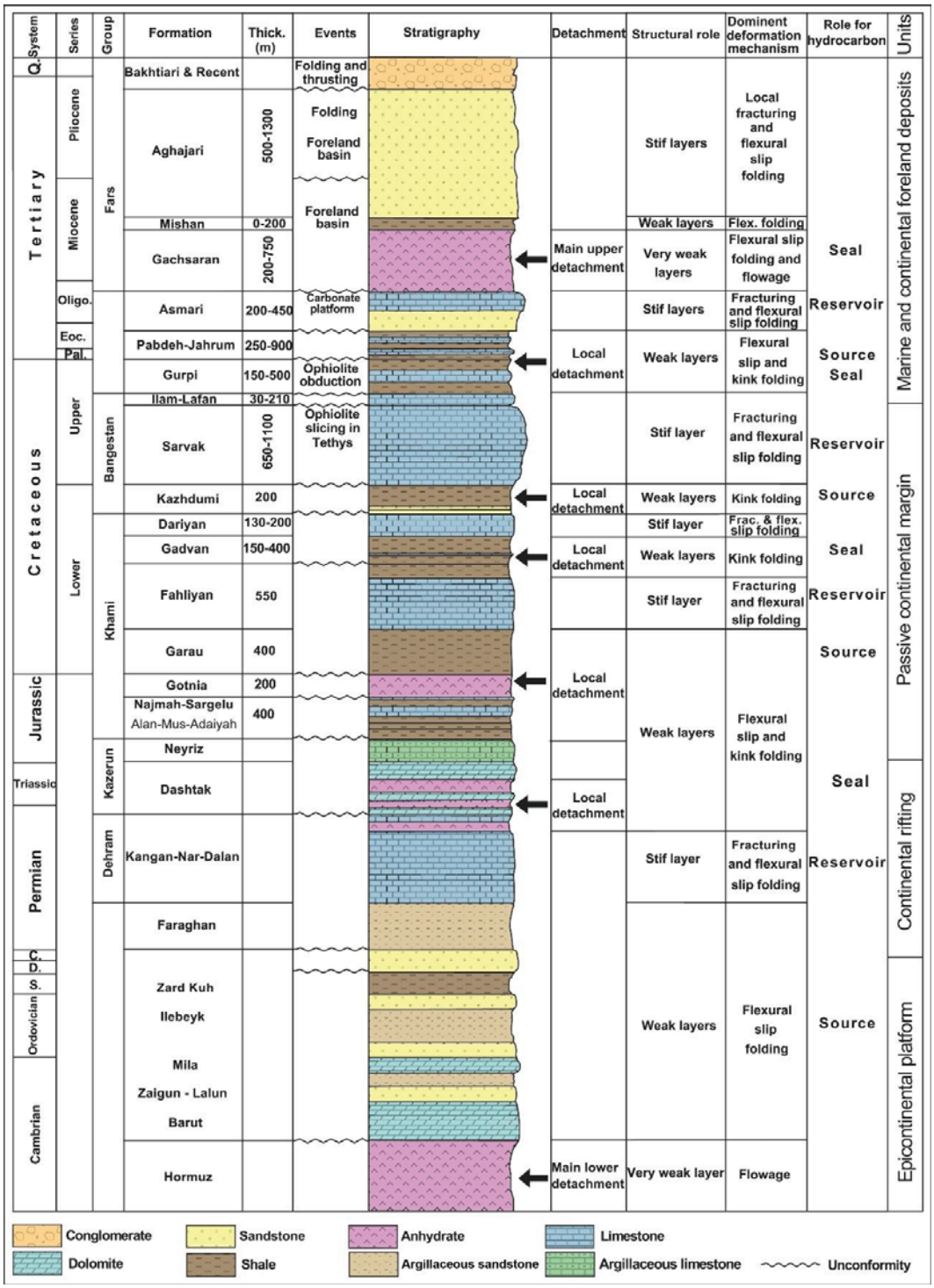

Figure 2-8 - Simplified stratigraphy of the Dezful Embayment and Abadan Plain depicting the major lithological successions and main tectonic events in the Dezful Embayment and the Abadan Plain (modified from Abdollahie Fard et al. (2006b) based on well data as well as research by Motiei (1993) and Alavi (2004)). Mechano-stratigraphy, detachments and influence on the hydrocarbon system are outlined.

In terms of structural stratigraphy of the area, several cross sections over the ZFTB have been published which vary in placement and coverage area. A few of the north-east to south-west cross sections reach to the verge of, or pass through, the Abadan Plain Basin Abdollahie Fard et al. (2006b); (Alavi, 2004, 2007; Blanc et al., 2003; Falcon, 1974; Hessami et al., 2001; McQuarrie, 2004). One of the best descriptive cross sections is provided by Abdollahie Fard et al. (2006b), which highlights thrust-related structures in the Dezful Embayment and gentle flexures of the Abadan Plain.

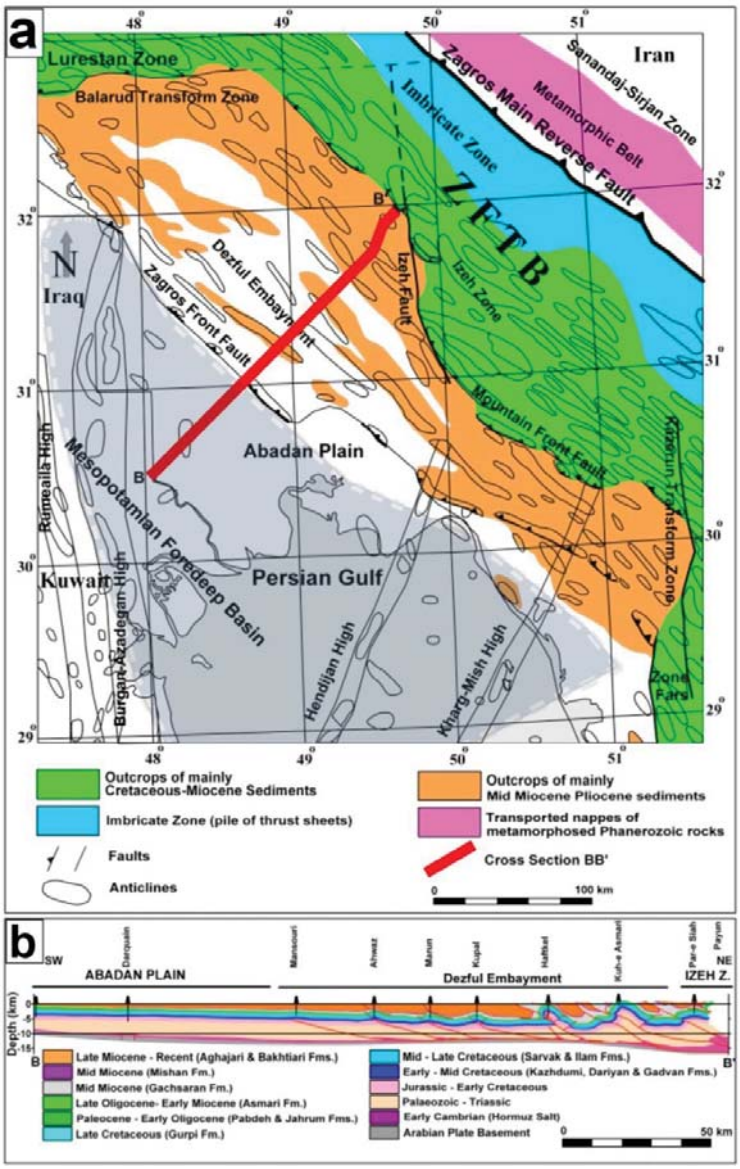

Figure 2-9 - (a) Simplified geological map of the western ZFTB modified from Abdollahie Fard et al. (2006b), using the National Iranian Oil Company (NIOC) geological map of south-west Iran at scale 1:1,000,000. The distribution of major anticlines is shown. Master thrust faults subdivide the ZFTB into different zones. Abadan Plain is highlighted and bounded by the Zagros Front Fault at the north and east, Rumeaila High at the west and Persian Gulf at the south. The north-south trending palaeohigh within the Abadan Plain Basin is orthogonal to oblique to the main north-west to south-east trend of the ZFTB. The location of section B–B_ is also shown. (b) Cross-section through the Abadan Plain and the Dezful Embayment along line B–B_, including data from recent seismic profiles and wells. Thrust related structures in the Dezful Embayment contrary to the gentle flexures in the Abadan Plain Basin are noted.

As clearly observed (Figure 2-9), there is a unique shortening trend in the thickness of formations from north-east to south-west, which reconfirms the basics of the region's present day stress regime (Rajabi et al., 2010). Major geological features (i.e. faults) are frequent in the fold area, but absent in the Abadan Plain Basin.

2.4. Exploration History in the Abadan Plain Basin

The Dezful Embayment was the first place in the Middle East where oil was explored and commercially produced in 1908. The first commercial oil field is located in Masjed Sloeyman (Owen, 2008) and it has continuously produced oil until the present-day. In the Abadan Plain Basin, hydrocarbon exploration history goes back to 1948 on the Iraqi side (Al Naqib, 1967), and to 1964 on the Iranian side (Arvandan Oil and Gas Co., 2014). The majority of the oil and gas fields in this area are onshore and located at the middle and northern part of the plain (Figure 2-10).

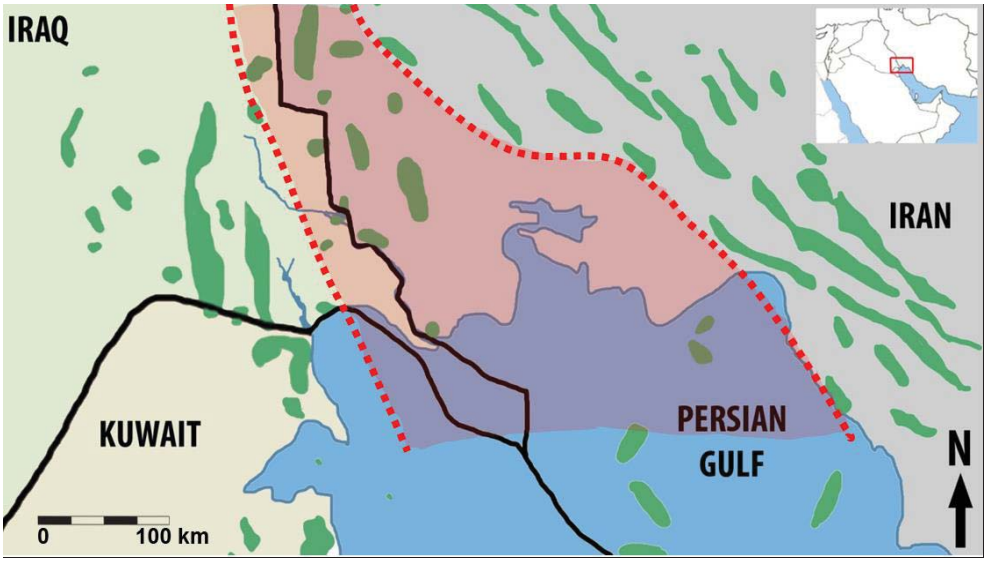

Figure 2-10 - Oil and gas fields in the Abadan Plain Basin. Abadan Plain is highlighted in red. The study area of this research consists of six fields in the north and middle of the plain, covering approximately 3500 km^2.

The late Carboniferous to Miocene sequence of the Abadan Plain Basin is similar to those in the rest of Middle East region, which are dominated by the carbonate sedimentation on a very stable, broad platform. This makes it the world's richest hydrocarbon habitat (Murris, 1980). Hydrocarbon stratigraphic traps in the shallow-marine, carbonate-dominated basin of the Abadan Plain have been formed in pre-Zagros Orogeny structures, and then been deformed and geometrically controlled by the Cretaceous tectonic setting (Abdollahie Fard et al., 2006b). Gas plays are mainly formed in some of the Permian–Triassic platform successions' mega-sequences (Alavi, 2004), while petroleum sources and reservoir rocks are formed in those of the Jurassic to recent (Ala et al., 1980; Beydoun et al., 1992; Stoneley, 1990). The reservoirs in the Abadan Plain Basin are of a stratigraphic type (Moallemi and Kermanshah, 2012), which distinguishes them from the depositional basin. There are several cases of uneconomic wells in the same reservoir as economic reserves in the Abadan Plain Basin; even wells spotted on the crest of the structure. Therefore, the uncertainties in the hydrocarbon exploration in this region increase due to the varying attributes of the deposits.

The Abadan Plain Basin is one of the richest prospects for hydrocarbon and is surrounded by several supergiant oil fields. The total proven oil in place in this basin is around 80 billion barrels and current oil production reaches 582,000 barrels per day. Planned daily oil production exceeds one million barrels, and almost all of the fields in the region are currently undergoing development phases. Reservoir formations in this basin include Asmari, Sarvak, Gadvan and Fahliyan. Structurally, the formations above the reservoir rock play the key role of sealing the porous reservoirs, while the source rocks are underneath the reservoir. The Gadvan formation is an exception, as it has both reservoir and seal attributes. The Gadvan is mainly a seal formation, but in some areas, it has a producible accumulation of hydrocarbon, which is capped by shale layers at the top of the formation. There is another prospect beyond the depth interval of this research that includes Carboniferous/Permian source rocks and accumulations in the Dehram formation (Permian geological period), and which is possibly an interesting subject for further investigations.

CHAPTER 3- Overpressures in the Abadan Plain Basin

3.1. Introduction

High pore pressures (overpressures) are a phenomenon observed in most sedimentary basins worldwide and have long been of importance for petroleum exploration and production, particularly for the safe drilling of wells (Mouchet and Mitchell, 1989). Overpressures have been frequently observed in the Abadan Plain Basin, and have resulted in several well control incidents. The aims of this chapter are to:

- Outline key terms and definitions related to pore pressure;
- discuss how pore pressure is measured in petroleum exploration;
- review previous studies of overpressure in the region, and;
- describe the distribution of overpressure in the Abadan Plain Basin.

The discussion of the evidence for and distribution of overpressure in the Abadan Plain Basin provides a prelude to the detailed analysis of the origin of overpressure (Chapter 4) and methods for pore pressure prediction (Chapters 5 and 6).

3.2. Pore pressure terminology

Pore pressure is the outwards pressure exerted by the fluids (typically water or hydrocarbons) that fill the pore spaces in rocks. However, hydrocarbons are very rare compared to the presence of water in the underground pore spaces, and thus pore pressures typically refer to water pressures. Pore pressure typically ranges between the hydrostatic pore pressure and the vertical (or overburden) stress. The hydrostatic pressure (the normal fluid pressure in the subsurface) is the pressure exerted by the weight of a static column of fluid (Mouchet and Mitchell, 1989). The

hydrostatic pressure (P_h) is a function of the height of the fluid column (z, ie. depth) and the fluid density (ρ_f), expressed as:

$$P_h = \rho_f \cdot g \cdot z \qquad \text{Equation 3-1}$$

where g is the acceleration due to gravity (approximately 9.81 $m.s^{-2}$). Fluid density in sedimentary basins typically varies between 1.00 to 1.08 $g.cm^{-3}$, depending on fluid salinity. Hence, the hydrostatic pore pressure gradient is approximately 10 MPa/km. Figure 3-1 shows the schematic trend of normal formation pressure with different fluids in the pores.

Lithostatic pressure is also known as the weight of a standard column of earth crust, normally 22.6 MPa/km (1.0 psi/ft) on average where reliable density measurement is not available (Dickinson, 1969). However, this estimate is not true in many basins and may cause erroneous further calculations (Tingay et al., 2003). Any value of pore pressure that is greater than hydrostatic pressure is known as overpressure. In a few cases, pore pressure that is close to the lithostatic pressure gradient has been observed, such as in Iceland (Zencher et al., 2006), Southern Louisiana (Jones, 1969), Brunei (Tingay et al., 2009) and the Middle East (Atashbari and Tingay, 2012b).

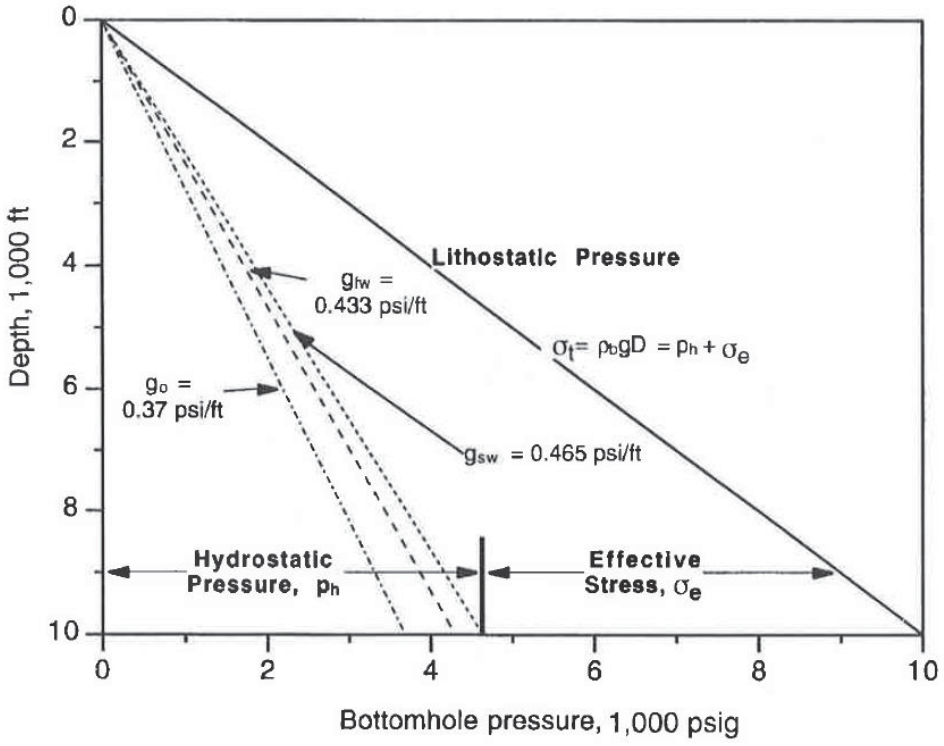

Figure 3-1 Borehole pressure gradients for different materials (Poston and Berg, 1997)

3.3. Methods for Pore Pressure Measurement

Pressure measurements are used in reservoir volumetric calculations, dynamic reservoir property determinations (such as permeability), reservoir compartmentalization analysis, reservoir fluid characterisation and well completion design (lifting systems). Pore pressure estimations are essential in the exploration of oil and gas fields, as encountering an unexpected overpressure zone poses significant risk of blow out for the drilling operation. On the other hand, the volume of the fluid in the reservoir decreases by production, causing the pore pressure to drop. Therefore, the majority of pore pressure measurements aim to evaluate the pressure regime and degree of overpressure in the pre-production conditions. However, all available field data, including production tests are considered in this research.

Formation pore fluid pressure can be measured from:

- openhole and cased hole well testing (DST);
- production or injection test;
- wireline or MWD formation interval testing tools, and;
- mud weight data.

The first two items are highly accurate production-related test methods conducted at certain depths of the reservoir (target depth). However, due to their relative scarcity (usually at most 1-3 tests in a well), the pressure recordings do not provide a depth profile. Hence, pore pressure measurement by wireline formation interval tests and mud weights are focussed on herein. Meanwhile, it is worth noting that the pressure measurement in the first three techniques could be performed using any of four types of pressure sensor (mechanical, capacitance, strain or quartz) (Schlumberger, 2006):

3.3.1. Formation Interval Testing

Wireline formation interval testers (WFIT) measure pore fluid pressures and, typically, also collect samples of formation fluids. WFIT is a generic terms referring to a number of tools such as Schlumberger's repeat formation tester (RFT) and modular dynamic tester (MDT), Baker Hughes' reservoir characterisation instrument (RCI), and Halliburton's sequential formation tester (SFT). A recent version of the MDT is shown in Figure 3-2.

Figure 3-2 Modular dynamic tester (MDT) in multi-probe mode (Ireland et al., 1992).

In general, formation interval tester tools measure the formation pressure by pulling formation fluid into the tool via a probe. The pressure inside the probe is monitored until it equilibrates with the formation pressure (pressure build-up). Then the gauge is read as pore pressure. Pressure build-up in WFIT takes a few minutes as the whole set of tool needs to move to the next test point. In the overbalanced drilling operation, drilling mud is normally kept slightly above the formation pressure. Therefore, mud materials are injected into the porous formation and can cause spuriously high pressure readings at the first few minutes of the test, when the tool samples muds from the flushed zone (Van Ruth et al., 2000). This is known as supercharging and occasionally observed in the field measurements.

Pressure transient tests vary in specifications and the volume of fluid sample to be collected in a single test run, but they are all reliable sources of pore pressure measurements in petroleum exploration. However, they have some limitations such as small number of tests taken in a well, supercharging and inability to undertake the test in low permeability formations (Van Ruth et

al., 2000). Supercharging is a disadvantage of WFITs, but can be avoided in DSTs by performing a pre-test. In a pre-test operation at any test point, the tool allows a small amount of fluid to withdraw from the formation (Smolen and Litsey, 1979). The pre-test is planned to obtain the equilibrium formation pressure by monitoring the formation adjacent to the wellbore. WFITs and DSTs are both expensive and usually run only in a few target reservoirs. Moreover, DTSs are not generally performed in highly overpressured formations (Mouchet and Mitchell, 1989). Pressure transient tests are unable to measure pore pressure in very low permeable or impermeable formations because the fluid cannot build-up in the testing chamber over a few minutes in WFITs or few hours in DTSs (Morton-Thompson and Woods, 1992). In many cases, overpressure generates and develops in fine grained, low permeability rocks (i.e. shales) and yet, pore pressure can only be measured in adjacent permeable rocks. The pressure which is measured by transient pressure tests is simply assumed to be representative of adjacent shales. However, this assumption becomes void if the permeable formation is not completely enclosed by the shale.

3.3.2. Formation Pressure Estimated from Drilling Fluid Data

During a drilling operation, the space between the annulus and drill string is filled by a fluid known as drilling fluid or drilling mud. A drilling fluid system commonly known as mud system, is the only component of the well-construction process that remains in contact with the wellbore throughout the entire drilling operation (West et al., 2006). Traditionally, muds have been classified into three categories according to the base fluid used in their preparation: air, water and oil (Caenn and Chillingar, 1996). Neff et al. (2000) classified the drilling fluids based on the nature of the base fluid, also known as the continuous phase, into two major groups: water-based fluids (WBFs) and non-aqueous based fluids (NABFs). Nowadays, the majority of drilling fluids are a complex system of water-based (WBM) or oil-based (OBM) fluids with several chemical and mineral additives (Ghazi et al., 2011). A new type of drilling fluid has emerged recently which primarily comprised of artificially formulated oil-based fluids and is called synthetic drilling fluid. Drilling fluid applications are properly explained in the drilling operation hand books, technical books, articles and operation manuals. Typical applications such as cooling and lubricating the drill bit, holding and carrying cutting out to the surface and preventing formation fluid influx into the wellbore are explained by Caenn and Chillingar

(1996), U.S. Army Corps of Engineers (2001), West et al. (2006), and Broni-Bediako and Amorin (2010).

One of the basic functions of drilling fluid is to control the pressure balance in the wellbore in order to maintain stability and prevent blowout. In conventional drilling operations, the hydrostatic pressure imposed by the drilling fluid (mud pressure) in the wellbore is usually kept above the formation pore fluid pressure and below the formation fracture pressure (termed 'overbalanced' drilling). In underbalanced drilling, which is not relevant in the wells analysed herein, mud pressure remains lower than the formation fluid pressure, allowing the formation fluid to flow into the wellbore and prevent formation damage caused by mud infiltration into the borehole wall.

Mud weight is the only data from all depths in a well and is often used as a proxy to the pore pressure and could be more reliable considering kicks, background gas, connections gas and trip gas. During an overbalance drilling, formation fluid may enter the wellbore and result a 'kick' which is controlled by increasing the mud weight to 'kill' the influx. The mud pressure required to kill a kick provides a reasonably accurate pore pressure estimate (Mouchet and Mitchell, 1989). Background gas, which is the gas entering the borehole during a drilling process, indicates that the mud in use (considering equivalent circulating density, ECD) does not overbalance the pore pressure and it is likely that pore pressure is a maximum of mud hydrostatic+ECD (Devereux, 1998). Alternatively, observing 'connection gas', which is a result of no mud circulation (zero ECD) or swabbing effect of short movement of drill string occurring during pipe connection (Schlumberger, 2015a), and detecting 'trip gas' caused by swabbing effect of pulling the drill string to surface (Schlumberger, 2015c), provides reasonable indications that the formation is just overbalanced by the mud hydrostatic (Devereux, 1998).

However, in low permeability formations such as shales where overpressures commonly develop, fluid exchange between the wellbore and formation are very few (Van Ruth et al., 2000) and mud weight may not yield an accurate estimate of pore pressure. There are several other pitfalls that limit routinely using mud weights as pore pressure estimates. For example, mud pressure may be increased above pore pressure in swelling or unconsolidated formations

to improve wellbore stability, or might be increased prior to reaching an expected depth of overpressure. The other concern regarding using mud weight as a proxy to pore pressure is that once drillers raise it for operations in a formation, they have to keep it high for the rest of the hole section, even if pore pressures return to hydrostatic deeper. This is because MW must be higher than the minimum pore pressure in the entire open hole section. It is only once that hole sections is cased off that MW can be lowered. So it is possible that any of the proposed pore pressure regressions (returns to hydrostatic or lower PP below an overpressured formation) may be deeper than they really are. The deeper sections could just be drilled with a high MW, and significant overbalance, just until the next casing point. Despite these issues, mud weight is the only available data throughout a large part of this basin and thus, was used herein with care.

Pore pressure estimation from mud weight data could be validated by direct pressure measurements such as RFT/MDT or DST. However, due to the lack of reliability of direct pressure measurements in impermeable formations (where normally no test is performed), these methods would not be as reliable over the entire wellbore. Mud weight is normally expressed as several units in the petroleum industry such as specific gravity (SG = kg/m^3 or g/cm^3) or pounds per gallon (PPG). Mud pressure is calculated from the following equation in SI units:

$$\text{EQUIVALENT CIRCULATING DENSITY } \left(\frac{kg}{m3}\right) = \frac{\text{Annular Pressure Loss (KPa)}}{\text{TVD (m)} \times 0.00981} + \text{Mud Density } \left(\frac{kg}{m3}\right) \qquad \text{Equation 3-2}$$

In conventional (overbalanced) drilling, mud pressure is typically 5-10% higher than formation pore pressure (Dickinson, 1951). In the Abadan Plain Basin, mud weight is 10% above the formation pressure in average (Figure 3-3). Mud weight approaches closer to the formation pressures in deeper sections of the wells. In this study, directly measured pore pressure greater than 11.5 MPa/km and mud weights greater than 13 MPa/km are considered as overpressure.

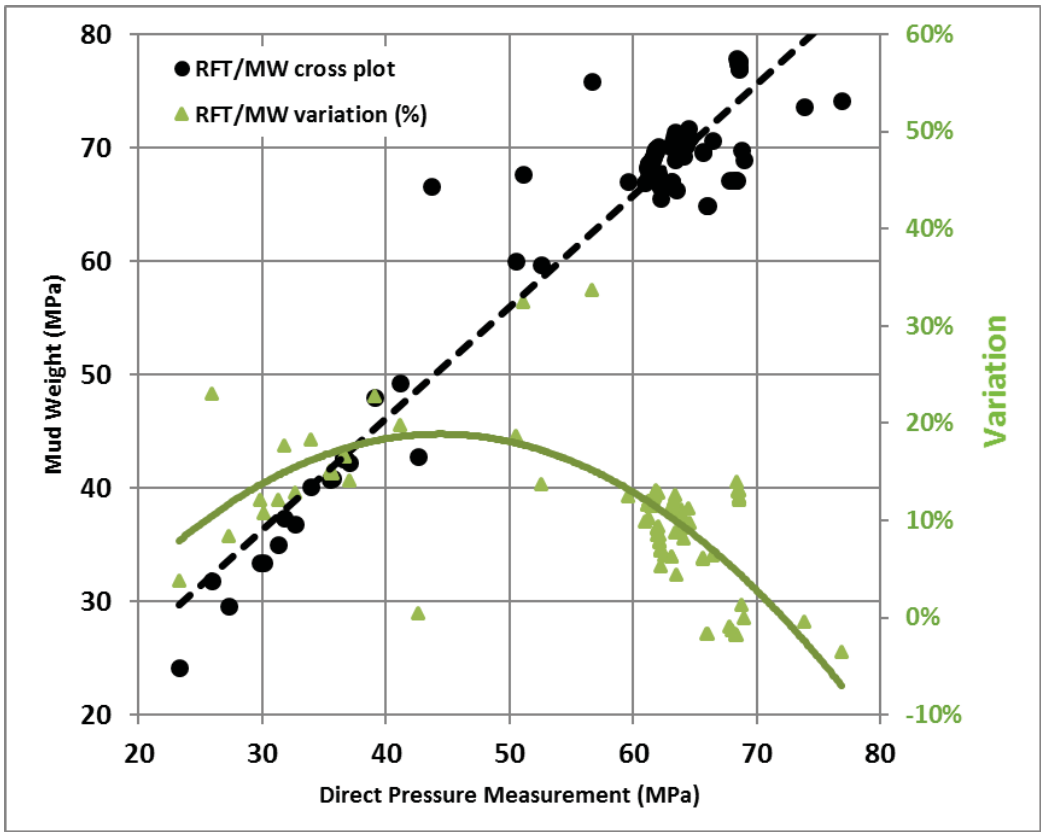

Figure 3-3 – Relationship between direct pressure measurements and mud weight in the Abadan Plain Basin. Black dots and corresponding trend line are read from left vertical axis while the variation % of mud weight with respect to direct pressure measurements is read from right vertical axis.

As an index of wellbore instability, the history of stuck tool and pipe events has been classified and presented in Figure 3-4 to obtain a better understanding of wellbore conditions. Kick and tool stuck data was missing for the wells D-14, A-6 and J-4. Stuck tool issues happen at depths as shallow as the Aghajari Formation, but most issues occur in the formations below the Sarvak Formation. Stuck tool events are categorised into being in either normally pressured or overpressured sequences (Figure 3-4a).

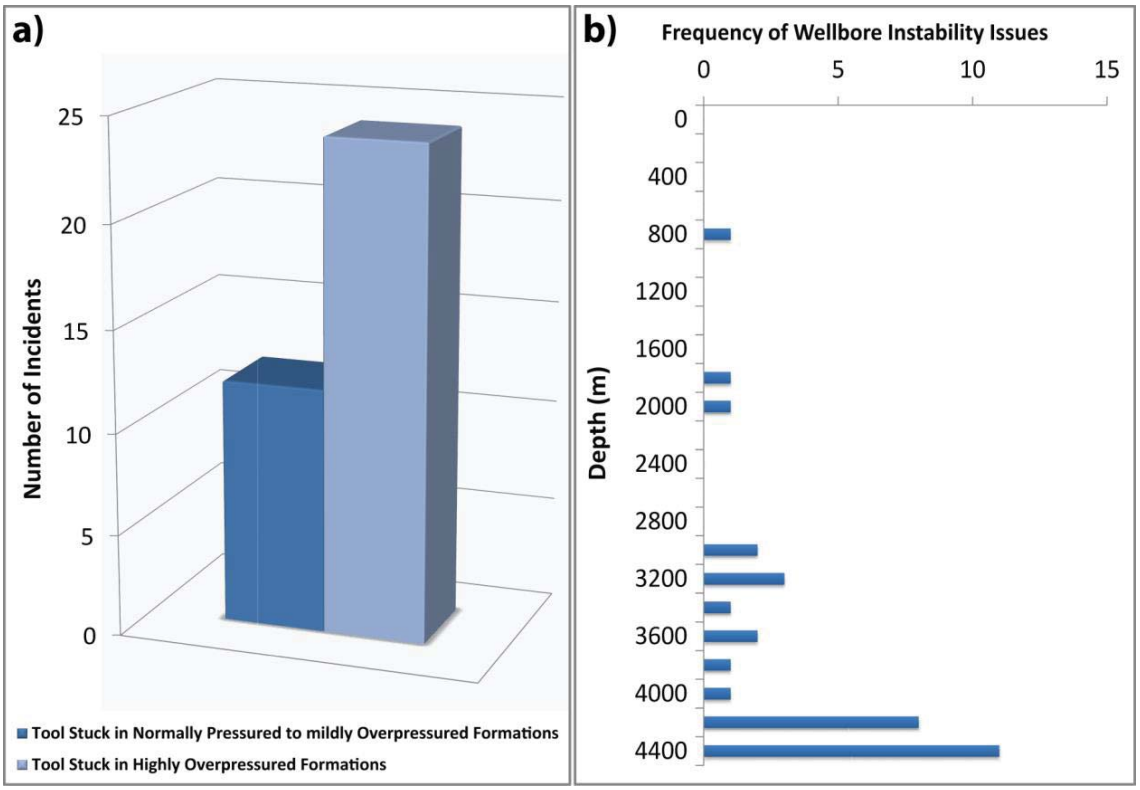

Figure 3-4 – a) Statistics of stuck tool events in the study area. A total of 36 stuck tool events (pipe, logging tools and bottom hole assemblies) have been reported. Two thirds of them were in the highly overpressured formations. b) Frequency of wellbore instability issues in the Abadan Plain Basin. The majority of incidents occurred in the overpressured formations of Gadvan and Fahliyan.

Twenty four stuck tool events out of a total of 36 (two thirds) were in the depth interval of 3900-4500m, comprising the Gadvan and Fahliyan formations. Depth interval of 3200 m to 4000 m mostly contains shale deposits and therefore, wellbore instability might have caused due to weaker mechanical strength and swelling attributes of shales. Tool stuck incidents at 4000 m depth and beyond are in the carbonate rocks and are consequences of high pore pressure which reduces the effective stress. High frequency of in these formations can be a result of overpressure or lithology (more issues in shaly formations due to shale swelling), which goes beyond the scope of this research. It is worth noting that there were no incidents reported in the Gachsaran Formation, while it was overpressured in some fields. Nevertheless, the number of wellbore instability was highest in the Gadvan and Fahliyan formations. In the light of frequency of statistical wellbore stability issues (Figure 3-4b), major concerns for the overpressured formations are also highlighted and provide a useful clue for the future wells' casing and well completion design.

3.4. Pressure data visualization

To obtain an overview of pore pressures in the area, a three-dimensional model of the mud pressure has been constructed. First, a regular grid has been created over the study region to interpolate the area between data points (Table 3-1).

Table 3-1 – Three dimensional (3D) model and gridding properties

Parameter	Value
Grid cells (nI*nJ*nGridLayers)	144*177*840
Grid nodes (nI*nJ*nGridLayers)	145*178*841
Total number of 3D grid cells	21409920
Total number of 3D grid nodes	21706210
Number of horizons	841
Number of layers	840
Total number of 2D cells	25488
Total number of 2D nodes	25810
Total number of defined 2D nodes	19818

For simplicity, layers were defined as conformably overlying each other. A Kriging regression method was used in this model. Kriging is an optimum automatic interpolation procedure (Matheron, 1973) named after the South African mining engineer D. G. Krige (Rusmussen and Williams, 2006). Overall gridded cells are shown in Figure 3-5. The dimension of the cells is 500 m by 500 m.

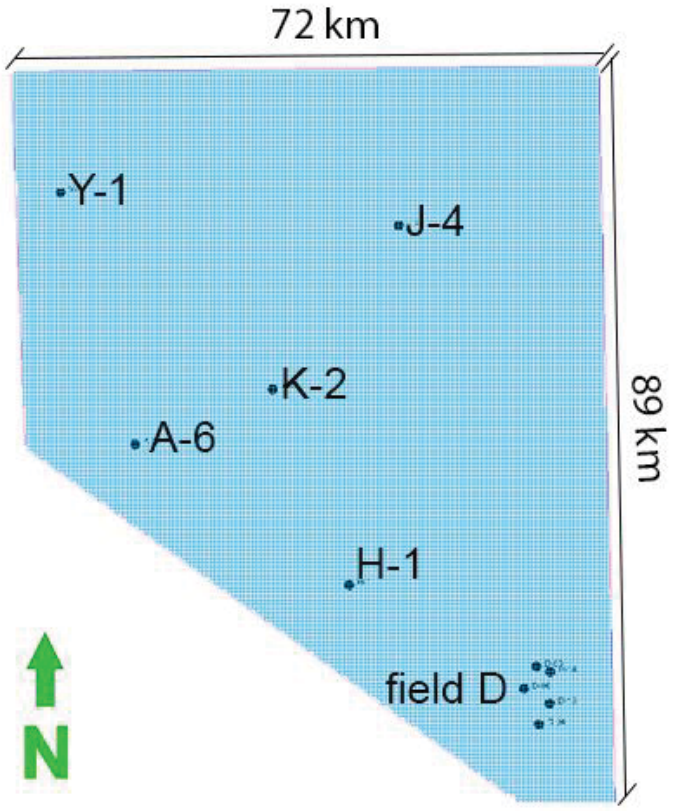

Figure 3-5 – Gridded area including all wells of this study. Each cell size is 500m by 500 m.

Then another 3D cube using Gaussian regression process was constructed. Gaussian process is based on the notion of Gaussian distribution (normal distribution) and was named after Carl Friedrich Gauss (Bishop, 2006). This cube consisted of $104 \times 104 \times 551$ grids with 10-meter depth intervals. This was limited to the area edged by the wells as shown in Figure 3-6. Due to the lateral distances between the wells, the horizontal aspects of the grids were defined 300 m. As discussed in the regional geology (Chapter 2), there is no major faulting in the region. However, this does not mean that the fields are in hydrodynamic connection, or that there are dynamic links between the structures. The visualisation is a simplified tool to demonstrate the magnitude of formation pressure and study the geographical trends of pore pressure in the region. Direct pore pressure measurements and the mud weight data are collected from the well completion, well test, geological or drilling reports (Figure 3-7 and Figure 3-8).

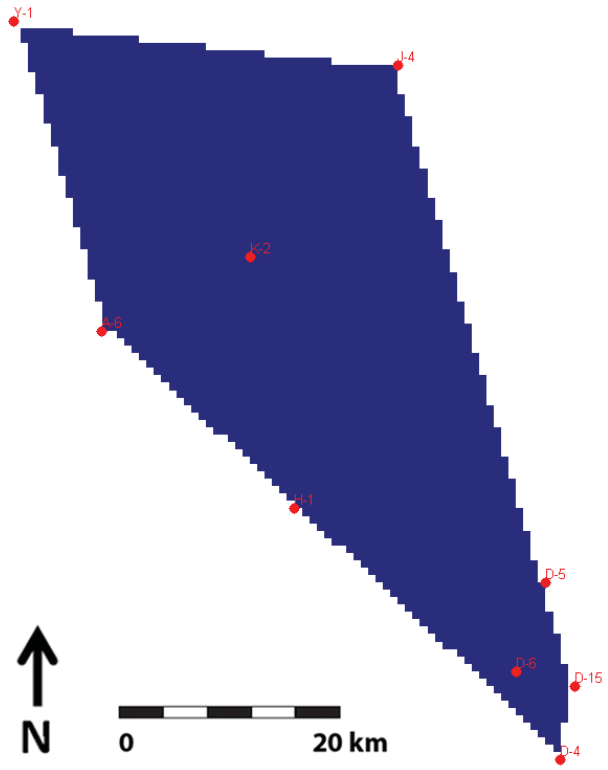

Figure 3-6 – Location of the wells on the gridded area (red circles). A grid consisting of $104 \times 104 \times 551$ grids with 10-meter depth intervals has been constructed for this region and used to interpolate pore pressure measurements between wells.

3.5. Results

There are reliable sets of mud data and RFT/MDT recordings for the wells under investigation in this study. I have classified the results to represent the pressure regime in the wells/fields.

3.5.1. Measured Pressure and Mud Data of the Wells Investigated in the Abadan Plain Basin

Direct pressure measurements are the most reliable source of information about the fluid pressure inside porous rocks. In the Abadan Plain Basin, all available data has been put together to study pressure magnitude variations and examine any regional trend in the study area. Mud

pressure exhibits some degree of overpressure gradient in the formations below 1000 m, with peak pore pressures in the Gadvan and Fahliyan formations (Figure 3-7). Direct pressure measurements confirm the existence of significant overpressure in the Gadvan/Fahliyan formations (Figure 3-8). Meanwhile, due to lack of pressure measurements over the full length of the well, mud pressure has been considered as the proxy for the formation pressure and illustrated as a 3D pressure cube (Figure 3-9) to visualise the pressure variation in the basin. Overall accordance between recorded pressure and mud pressure has been discussed earlier in this chapter.

Figure 3-7 shows the mud pressure of the wells investigated in the area of interest. There are two main abnormalities in mud weight. The shallower one is in Gachsaran formation which returns to hydrostatic pressure gradient in the underlying strata. The other substantial mud weight increase occurs in Gadvan formation and proceeds into the Fahliyan formation. In some wells, mud weight decreases within the lower section of Fahliyan formation, but remains above hydrostatic gradient. This reversal of mud weight behaviour within the Fahliyan formation is observed only in the wells of field D. Mud weight remains the same gradient or increases in the Fahliyan formation in fields A, K, H, J and Y.

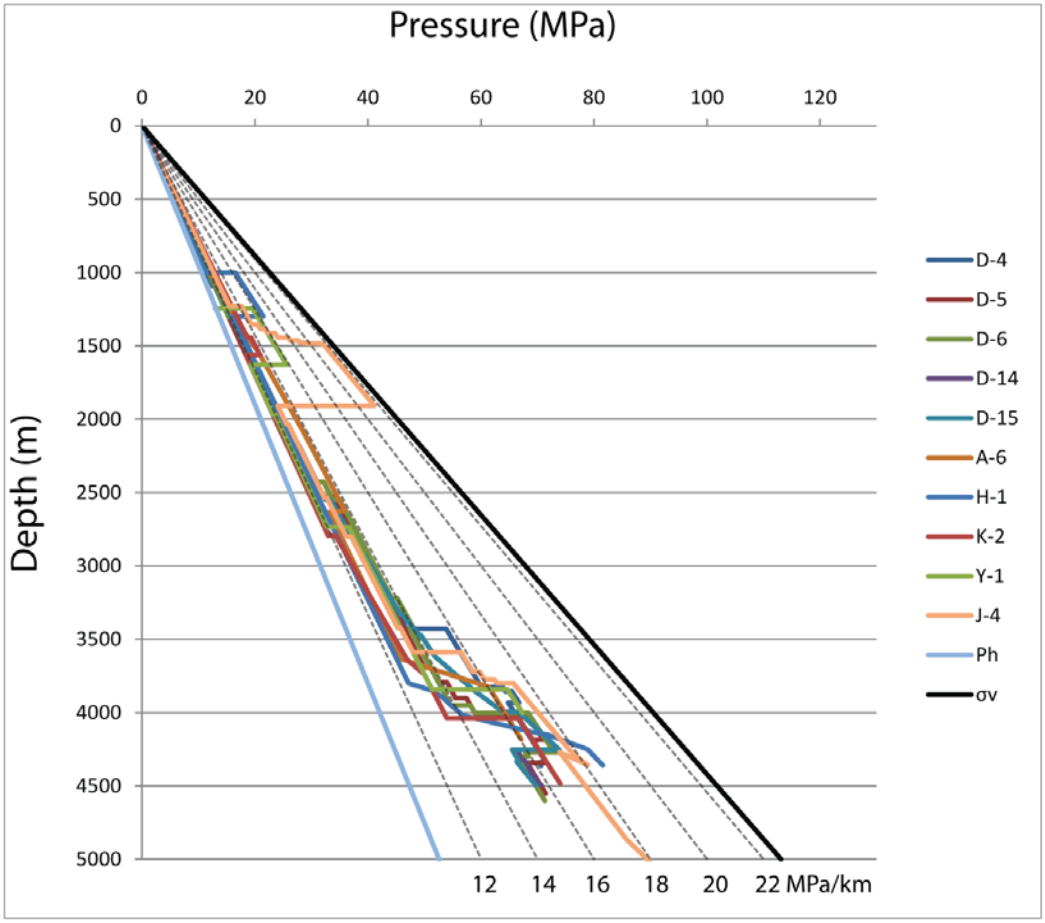

Figure 3-7 – Mud pressure of the wells studied in the Abadan Plain Basin, colour coded by wells. Hydrostatic pressure and average overburden stress are shown in light blue and black lines respectively.

RFT/MDT pressure measurements are collected from the well reports and validated with the well test results wherever possible (Figure 3-8). There are no pressure measurements in the Gachsaran Formation to validate the accuracy of pore pressure estimation from mud weight. However, the Gachsaran Formation has been frequently reported with abnormally pressures at the west and south-west of Iran (Fertl et al., 1994; Li Menggang, 2015; Zabihi Naeini and Siahkoohi, 2006) and thus, overpressures are also anticipated in the Abadan Plain. Therefore, high values of mud weight are reflecting abnormal pore pressure and were considered as a proxy for the formation pressure in this formation. The Gadvan/Fahliyan overpressure is clear at depths below 3600 m. The majority of pressure measurements lie between a 14 and 16 MPa/km gradient interval, which is generally regarded as moderate overpressure in sedimentary basins globally.

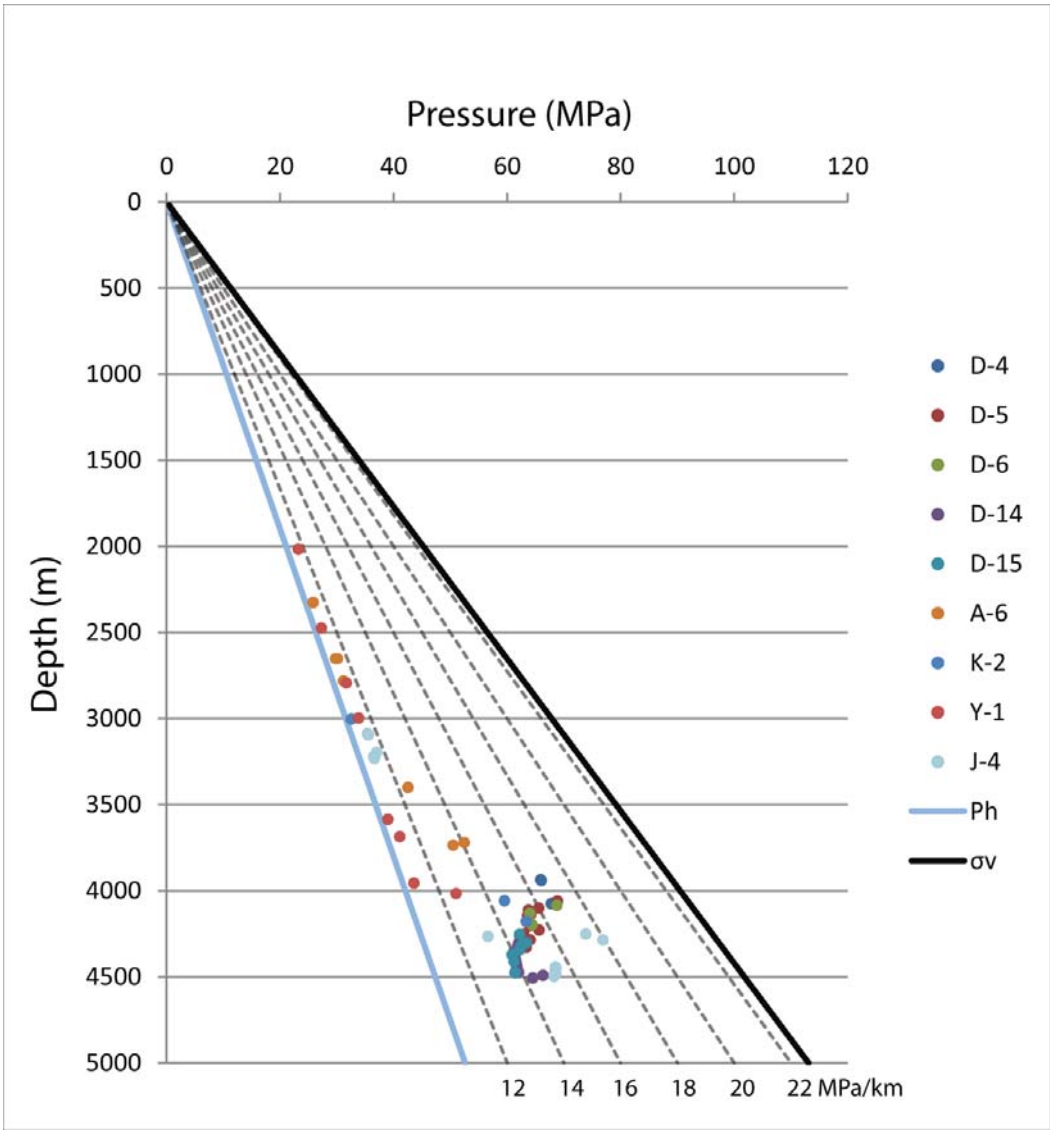

Figure 3-8 – Direct pressure measurements in the Abadan Plain Basin, colour coded by wells. Hydrostatic pressure and average overburden stress are shown in light blue and black lines respectively.

3.5.2. Pressure Cube

A three dimensional cube of the pressure data was generated to demonstrate the visualised components of formation pressure in the entire area. Well locations were noted in Figure 3-5 and Figure 3-6 and the 3D cube is presented in Figure 3-9. This cube is based on the grids described in Figure 3-5. Miocene-Oligocene deposits of the Gachsaran formation exhibits overpressure in the wells H-1, Y-1, J-4 and K-2. Mud pressure is as high as the lithostatic gradient (22 MPa/km) in the J-4 well and seems to be in a hydrostatic gradient in the wells of field D. Lower Cretaceous formations of Gadvan and Fahliyan are overpressured. The cross section of the mud pressure gradient over path through all fields and wells (Figure 3-10) shows that lateral expression of the pressure is very clear in two overpressured zones. Field D is normally pressured in the Gachsaran formation, where it is at shallower depths. This formation becomes overpressured in the northern part of the region (field Y) where it sits at a deeper elevation.

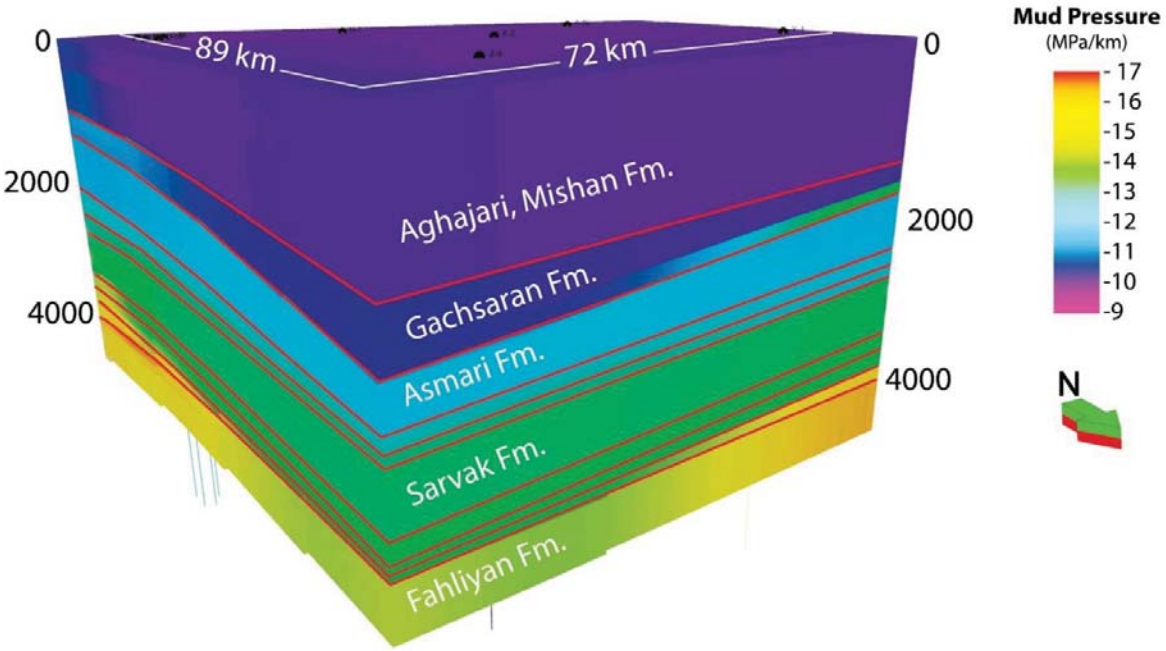

Figure 3-9 – Three dimensional (3D) model of mud pressure of the Abadan Plain Basin. Grid size is 500 m by 500 m and the total number of grids is 144*177*840. Mud pressure gradient is Color-coded as a proxy to pore pressure.

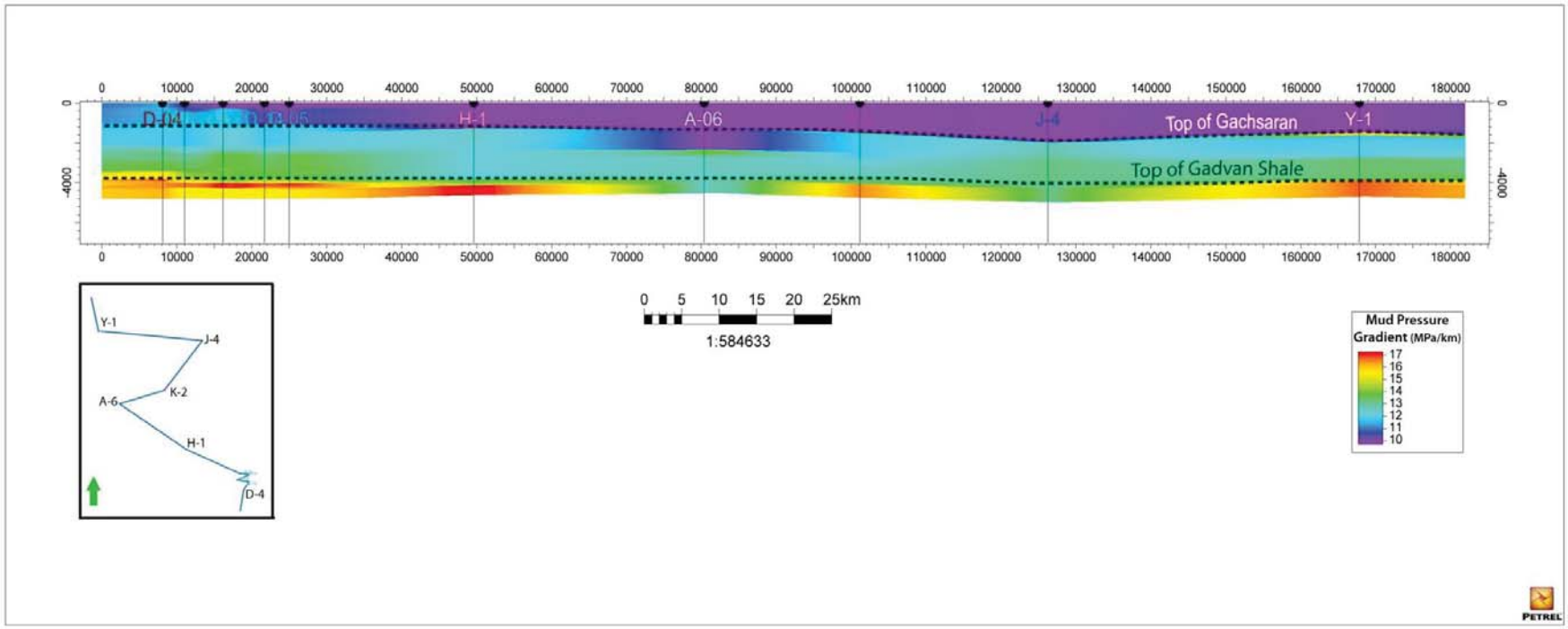

Figure 3-10 – Cross section of the wells on mud pressure. Mud pressure is colour coded in MPa/km.

The Gadvan formation is overpressured in all areas of the basin, but the variation of depth to the top of this formation differs from that of the Gachsaran formation. This will be discussed in later sections. In the following Figure 3-11, the pressure cube from different angles can be seen. The narrow overpressured horizon of the Gachsaran formation and the significant overpressured zone of the Gadvan-Fahliyan formations are clearly visible.

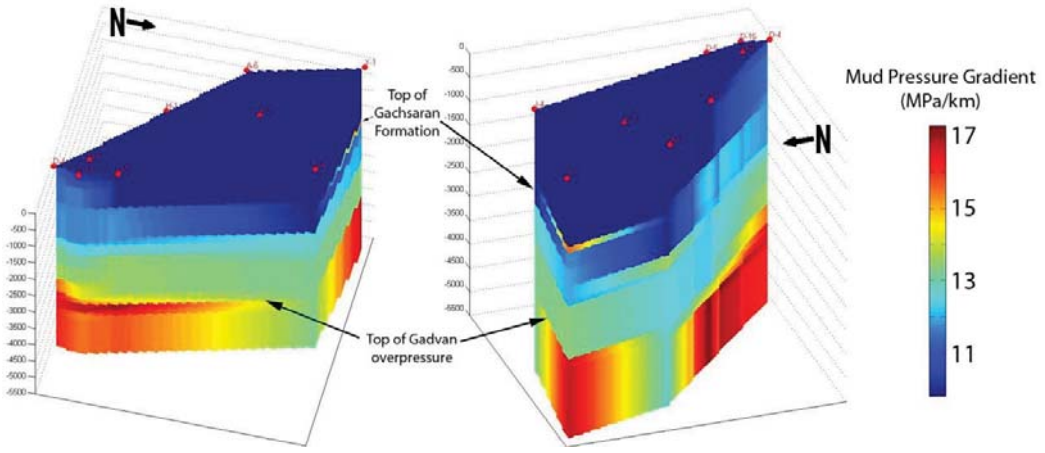

Figure 3-11 – Mud pressure from different views. Wells are shown at the surface as red points and the variation of colour indicates mud pressure in MPa/km.

The mud pressure at the top of two overpressured horizons is illustrated from different views (Figure 3-12). The Gachsaran formation is normally pressured in southern part of the region while it becomes overpressured towards north. The Gadvan and Fahliyan formations are entirely overpressured. The degree of overpressure varies from 12.7 MPa/km in field Y to 17.9 MPa/km in well J-4. The pore pressure of the Gadvan formation is overpressured in the centre of the study area and is remarkable lower than at the northern and southern edges.

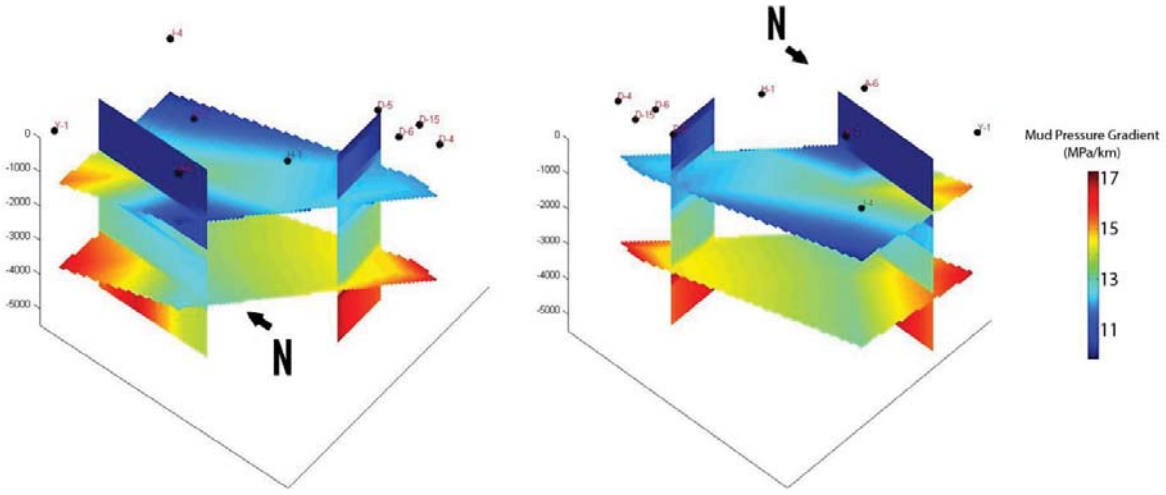

Figure 3-12 – Slices from the mud pressure cube (Figure 3-11) from different perspectives. Wells are shown at the top surface as black circles and variations in colour show mud pressure in MPa/km. The horizontal slices are at the depth of the Gachsaran and Gadvan formations.

The formations are dipping towards the north and northwest, where the basin meets the Zagros Fold-Thrust Belt. Top of formations are included to the 3-D model and regional trends are discussed in the next section.

3.5.3. Overpressured Zones

Two main zones exhibit abnormal pore pressure, and their thickness and pressure distribution are demonstrated in Figure 3-13. The first stratum is in the shallow Gachsaran Formation. Its formation top varies from 974 m deep in well H-1 to 1446 m deep in well J-4. The formation becomes deeper and thicker towards the north-east, as it approaches the Zagros fold belt (Figure 3-13). This kind of deepening and thickening towards a major fold belt is typical of foreland basin settings. Sequences in the Abadan Basin have undergone extensive foldings along the Zagros structure and become thicker as a result of planar shortening. Pore pressure in the Gachsaran formation also follows a similar trend to the depth of burial and thickness (Figure 3-14). The formation is highly ovepressured in field J where it has the closest distance to the Zagros Front Fault (or Zagros Deformation Front).

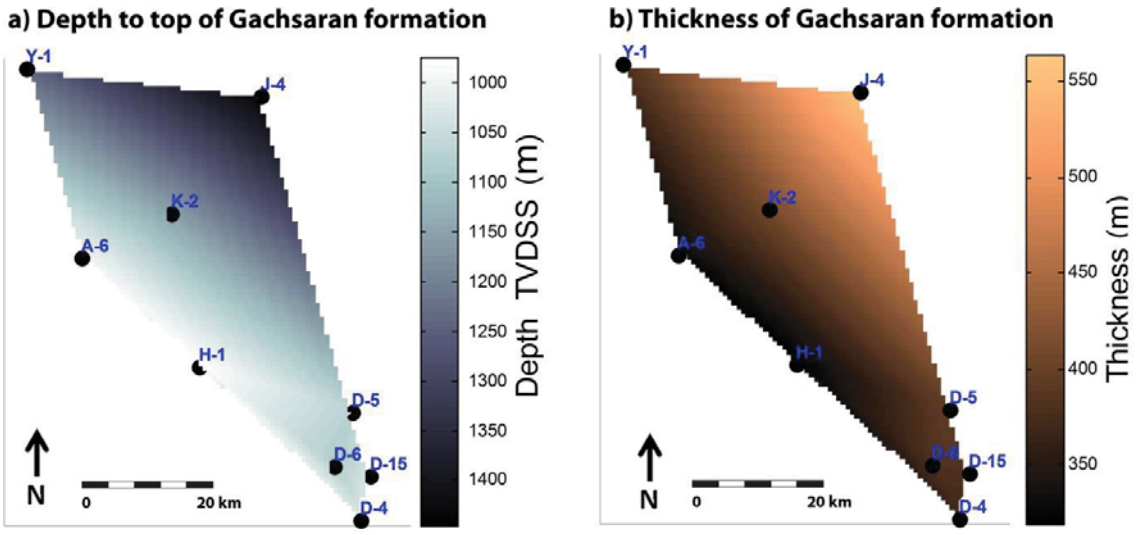

Figure 3-13 – a) Depth of the top of the Gachsaran formation. The wells' locations are indicated by black circles. b) Thickness of the Gachsaran formation in the study area.

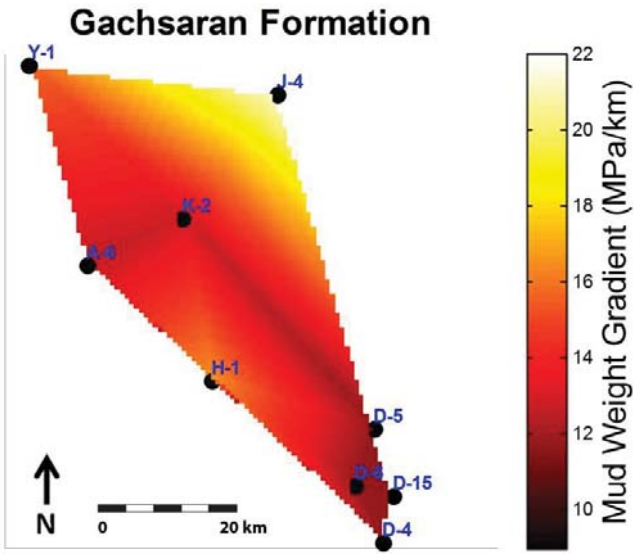

Figure 3-14 – Mud pressure gradient at the top of the Gachsaran formation. Mud pressure gradient is in MPa/km and well locations are indicated by black circles.

The second overpressured stratum is the Gadvan formation, which forms the seal or cap rock to the underlying Fahliyan formation hydrocarbon-bearing reservoirs. Both the Gadvan and Fahliyan formations are significantly overpressured and the main focus of this study. The Gadvan sealing formation gets deeper to the north-east while it becomes thicker along this orientation (Figure 3-15). The thickness varies from 21 m in Y-1 to 80 m in D-4. Similar to the Gachsaran formation, thickening behaviour of the Gadvan shale is interpreted as a result of crustal deformation at the vicinity of Zagros structure. However, pore pressure gradient does

not follow the same trend as formation depth or thickness (Figure 3-16). The formation is highly overpressured with a pressure magnitude of around 17 MPa/km in the corners of the area (fields A, J, and D) and around 13 MPa/km in the middle where fields H and K located. The maximum recorded pore pressure gradient of 17.94 MPa/km has been recorded in well J-4.

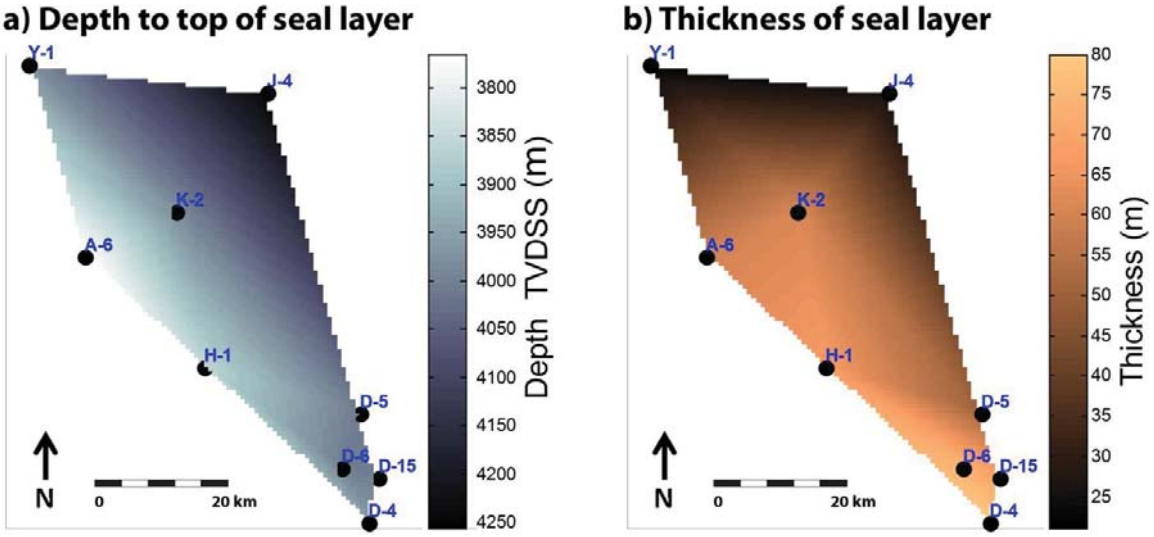

Figure 3-15 – a) Depth of seal layer in the Gadvan Formation. Well locations are indicated by black circles. b) Thickness of the seal layer in the Gadvan Formation. The seal layer consists of several sequences of shale in the lowermost section of the Gadvan Formation.

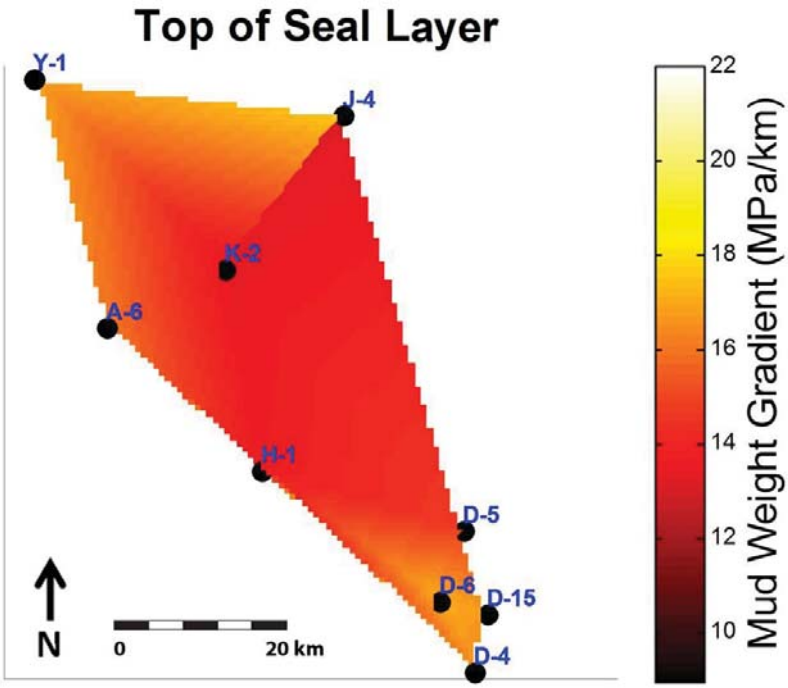

Figure 3-16 - Mud pressure gradient at the top of the shale in the Gadvan formation. Mud pressure gradient is in MPa/km. Well locations are indicated by black circles.

3.6. Discussion

Drilling mud pressure in nine wells has been used as a continuous proxy for pore pressure, with verification from direct pressure measurements, and has then been used to build a 3D pore pressure gradient volume for the Abadan Plain Basin (Figure 3-9). Pore pressure estimated from mud weight has identified two distinct overpressured horizons. A part of fields exhibited overpressure in the Gachsaran Formation while the other fields have normal pore pressure in this formation. The Gadvan and Fahliyan zone is the second overpressured sequence with various magnitudes. Detailed discussions of these findings are provided in the following sections.

3.6.1. Discussions on the Overpressures in the Gachsaran Formation

Overpressures are observed in the shallow Gachsaran formation, from 1000 m to 1500 m depth, but only in a small number of wells at the northern end of the basin. This formation is highly overpressured, with examples of pore pressures reaching sub-lithostatic magnitudes (up to 22 MPa/km), particularly in tectonically altered structures nearest to the Zagros fold-belt. Analysis of available data indicates that fields closer to the Zagros folded area exhibited a higher magnitude and wider extent of overpressure in the Gachsaran formation.

Overpressure in the Gachsaran formation is generally observed in the northern fields while it becomes normally pressured towards the south (field D). The proximity of the Zagros suggests that overpressure magnitudes may potentially have been enhanced due to tectonic activity in the Zagros area, with higher horizontal stresses enhancing typical disequilibrium compaction (Couzens-Schultz and Azbel, 2014; Yassir and Bell, 1994). However, the Gachsaran Formation also displays a thickening (from 800m near the Zagros to 370m near well D-4) and deepening towards the Zagros fold belt (Figure 3-13), as is common in sequences deposited in a foreland setting Plain (Abdollahie Fard et al., 2006b). These attributes are completely consistent with the wider scale of crustal thickness (depth to Moho) of the Abadan Plain Basin and surrounding areas (Dehghani and Makris, 1983; Mokhtari et al., 2004) where the maximum thickness is observed beneath the Zagros structure and it decreases at both sides. Hence, the increase in overpressure in the Gachsaran formation towards the Zagros fold belt may also simply be due conditions becoming increasingly more favourable for standard disequilibrium compaction overpressuring.

3.6.2. Discussions on the Overpressures in the Gadvan and Fahliyan Formations

The second overpressured sequence is the Gadvan-Fahliyan zone, which exhibits two distinct overpressure levels. Pore pressure gradients are at a maximum in the bottom of the Gadvan and the top of the Fahliyan formation. However, recorded pore pressures then typically display a 15% reduction in the pore pressure from the top to the middle of the Fahliyan formation. This can be simply due to the buoyancy interaction between the hydrocarbon and water in the

formation as the measured pore pressures deviate from hydrostatic gradient and follow a steeper trend reflecting an oil column. However, these different pressures may indicate isolated sub-layers, which, according to drilling and completion reports, is the case within the Fahliyan formation. In some wells of field D, mud weight was kept in an overestimated higher magnitude while spotting the Fahliyan Formation and it appears that as soon as the driller noticed, it has been reduced to more accurate values. It is also noted that complete mud loss has been reported in the normally pressured formations of Pabdeh and Sarvak which was due to high permeability of those formations and irrelevant to overpressure.

On geographical classification of the fields, field D differed as it sits in the middle of the plain while the rest of the fields are located in the northern area. There is no available pore pressure data in the southern part of the Abadan Plain Basin, where it enters the Persian Gulf. Overall statistics of stuck tool (pipe, logging tools and bottom hole assemblies) incidents, as an indication of unstable wellbore conditions, indicates a predominance of instability events within particular formations. Even considering that stuck tool events may be the result of drilling operational issues (rather than wellbore instability), the high frequency of the phenomena in the overpressured Gadvan and Fahliyan formations indicates that overpressure (and the consequent lower effective stress) plays a role in wellbore instability (Figure 3-4). Furthermore, it is interesting to note that the Gadvan and Fahliyan formations do not exhibit any noticeable increase in pore pressure gradient approaching the Zagros. However, the entire Gadvan/Fahliyan sequence is significantly overpressured, and the lack of significant pore pressure gradient variation makes it difficult to detect any noticeable geographical trends.

The shallower part of this overpressured zone is the Early Cretaceous Gadvan Formation. The Gadvan formation is divided into three distinct sections, with different permeabilities:

a) The moderate permeability Upper Gadvan which consists of marl, shale, silty claystone, and some interbedded argillaceous limestone.
b) The high permeability Khalij Member that varies from limestone in field Y, A and D to sandstone in field H. The Khalij Member is known as Zubeir Sand, comprised of both limestone and sandstone in field K.

c) The low permeability Lower Gadvan that is composed of several sequences of limestone and shale, interbedded with marl, and argillaceous limestone layers.

The mud weight used to drill the Gadvan Formation increases dramatically in the shaly and lower permeability sequences of the lower Gadvan formation. Gadvan shale gets thicker over the region from north to south (Figure 3-15b), whilst the highest magnitude pore pressure gradients are observed in the central and eastern parts of the study area (Figure 3-16). The burial depth of the Gadvan Formation decreases towards the south-west (Figure 3-15a). However, the mud weight as a proxy to pore pressure within the top of the Gadvan Formation spatially varies from higher magnitudes at the north and south parts of the study area to slightly lower values in the middle (fields K and H in Figure 3-16). The low permeability and shaly sequences of the Lower Gadvan are favourable for the generation of overpressures, and also provide an excellent regional seal for the underlying Fahliyan formation. The temperature gradient in the depths of the Gadvan shale supports the observation of good sealing across the lower Gadvan, and thus fluid and pressure isolation between the carbonate rich Fahliyan formation and shallower sequences (Figure 3-17).

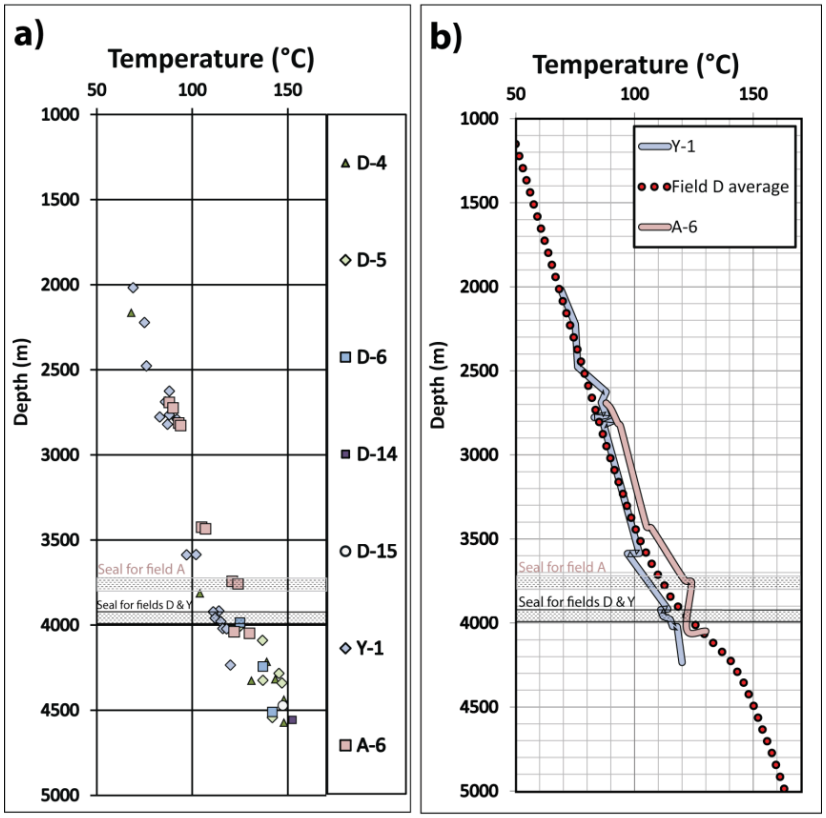

Figure 3-17 – Bottom hole temperature in the wells (left) and summarized trends (right). The average field D temperature is shown as a dashed red line compared to the trends in fields A and Y. Note that the top of the Gadvan formation in field D is at depths of around 3800 m and the top of sealing shale in the Gadvan formation is at 3900m. The top of the Gadvan formation in fields A and Y are is indicated on the graph. Temperature gradients increase at these depths and decrease in the lower parts of the Fahliyan formation which is in good agreement with the pressure measurements, where the fluid pressure tends to follow a hydrostatic gradient.

The Gadvan shale and upper section of the Fahliyan formation, that form a key pore pressure transition zone and seal, has similar properties throughout the entire region. The depth to the top of this regional seal becomes shallower from northeast to southwest (Figure 15), consistent. According to drilling mud data (Figure 3-16), pore pressure varies between 13.5 MPa/km in wells K-2 and H-1 in the middle of the region to 17.8 MPa/km in J-4 at the northeast corner of the basin. The average pore pressure is 15.7 MPa/km in this area. The high magnitude overpressure in fields Y and J could be due to the tectonic activities in the vicinity of the Zagros Fold-Thrust Belt, while the equivalent magnitude in field D, which is at the bottom-most region to the south, could be due to a greater thickness of Gadvan shale.

3.7. Conclusion

Mud weights and direct pore pressure measurements from 10 wells in 6 fields demonstrate that overpressures are observed throughout the Abadan Plan Basin. Overpressures can reach almost lithostatic magnitudes (22.0 MPa/km) and are primarily observed within two zones, the Gachsaran formation and the Gadvan/Fahliyan formations. The Gachsaran formation is overpressured in the northern part of the basin, while it exhibits normal pore pressure in the south. The Gadvan and Fahliyan formations are overpressured throughout the entire study area, and are also associated with a significant number of wellbore instability events, and are thus considered the largest drilling hazard in the basin. Low permeability shale layers in the lower Gadvan formation provide a perfect seal for the underlying Fahliyan formation. A south-west to north-east oriented increase in formation burial depth of both the Gachsaran and Gadvan formations was observed, which is due to the post-collisional crust shortening and thickening and development of formations within a foreland setting. Both the Gachsaran and Gadvan formations get deeper towards the north-east of the basin towards the Zagros fold belt. The Gachsaran Formation becomes thicker and overpressured along this direction while it is normally pressured in the fields at the bottom of the study area. However, despite having a similar burial depth trend with the Gachsaran formation, thickness of the Gadvan Shale as a sealing layer has a different trend and seems inconsecutive to the Zagros folding. Pore pressure doesn't vary significantly across the Gadvan and Fahliyan formations and both of them are entirely overpressured in this basin. Identifying overpressured intervals in the wells of the Abadan Plain Basin determines what formations need to be further investigated. In the next two chapters, possible overpressure generation mechanisms in the sedimentary basins, and more specifically within the Abadan Plain Basin, will be examined.

CHAPTER 4- Origin of Overpressure in Sedimentary Basins

4.1. Introduction

Overpressures have been identified in the Abadan Plain Basin and primarily occur in carbonate reservoirs, and also some shales. Understanding the origin of overpressure has been identified as an essential part of PP prediction (Lindberg et al., 1980; Tingay et al., 2009; van Ruth et al., 2004; Zhang, 2011). Pore pressure is required for determining the three principal effective stresses in the Earth's crust that define the in-situ state of stress (Zoback, 2007) and a significant input for accurate geomechanical models. In shales, overpressures are proposed to be primarily generated by disequilibrium compaction, but with additional possible input from kerogen-to-gas maturation and clay diagenesis (Buryakovsky et al., 2002; Lahann et al., 2001; Pinna et al., 2011; Tingay et al., 2009; Tingay et al., 2013). This has been tested in numerous regions by examining the petrophysical log response to overpressure (Bowers, 1995, 2002; Eaton, 1972; Fillippone, 1982; Lindberg et al., 1980; Ramdhan and Goulty, 2010). However, the origin of overpressure is particularly poorly understood in carbonates (Atashbari and Tingay, 2012b; O'connor et al., 2010; Weakley, 1990; Xu et al., 2007).

This chapter will undertake a literature review to examine the main overpressure generation mechanisms in sedimentary basins, before discussing the possible mechanisms of overpressure generation that are relevant to the Abadan Plain Basin. The aims of this chapter are to:

- Outline key terms and definitions related to overpressure origin;
- discuss how overpressure is generated by various mechanisms in their depositional environments;
- review previous studies of overpressure origin in depositional environments, and;
- investigate the possible origins of overpressure in the Abadan Plain Basin based on the geology of the basin.

The discussion of the potential mechanisms of overpressure in the Abadan Plain Basin provides a prelude to the petrophysical analysis of the origin of overpressure in Chapter 5.

4.2. Overpressure Generation and Development Mechanisms

Abnormal pressure can be a result of several mechanical and chemical processes that may act individually or in association with each other. The majority of overpressures are considered to be 'autochthonous' overpressure systems (Xinong et al., 2003), where there is no fluid flow into the closed system during the deposition. High-magnitude overpressures due to undercompaction and fluid expansion are of this type and occur within, or proximal to, the sediments in which they were generated (Lee and Deming, 2002; Swarbrick and Osborne, 1998; Tingay et al., 2009). In contrast, an 'allochthonous' overpressured system is where a more highly overpressured fluid flows into the system through the conduit units (lateral or vertical pressure transfer). To help identify the type and origin of overpressures in the Abadan Plain Basin, this sub-chapter will undertake a literature review of overpressure generation mechanisms and controls, with a particular focus on mechanisms that may be most applicable to the Abadan Plain Basin.

4.2.1. Disequilibrium Compaction (DC)

Clastic rocks are progressively loaded by the overburden stress as they are buried. This loading will typically cause rocks to compact and lose porosity, by either grain rearrangement (mechanical compaction) or through chemical compaction processes such as cementation (Dickinson, 1953; Hubbert and Rubey, 1961; Sclater and Christie, 1980). There is also another process that occurs over a wide geological timeframe known as secondary compression. This is defined as the time-dependant component of total settlement, which takes place after consolidation as a result of creep under constant effective stress (Patrick, 2002). Nevertheless, any form of compaction, in terms of the loss of pore volume, requires pore fluids to be expelled from the rock, and thus is a function of loading rate (e.g. burial rate or tectonic loading) and the rock's permeability (Osborne and Swarbrick, 1997b; Swarbrick and Osborne, 1996; Zhao, 2013). Overpressures can be generated when there is an imbalance between loading rate and permeability, meaning that rocks cannot expel fluids fast enough for the rock framework

(sediment grains) to support the increased load (Lee and Williams, 2000; Osborne and Swarbrick, 1997b; Zhao, 2013). Such an imbalance results in pore fluids supporting some of the increased overburden load, and becoming overpressured as a result, in a process termed disequilibrium compaction (Bruce and Bowers, 2002; Hart et al., 1995). Porous shales under the aforementioned conditions exhibit lower density than what is expected for normal compaction in that depth and are known as undercompacted (Bradley and Powley, 1994; Leftwich Jr and Engelder, 1994). This is basically because of water inclusion in the pore space whereas water has lower density than the shale grain or matrix. That anomalous characteristic of the shales is the basis of most pore pressure prediction methods, which attribute the difference between anticipated and observed petrophysical properties of shales to overpressure (i.e. Eaton, 1972; Anderson et al., 1973; Ransom, 1986; Fertl and Chilingarian, 1987; Bowers, 1995; Sayers, 2000). The pore pressure due to under-compaction increases sub-parallel to the lithostatic pressure while the fluid expansion can cause the pore pressure to rise by a rate greater than lithostatic gradient (Figure 4-1). The classic example of disequilibrium compaction overpressure occurs in the Gulf Coast of Louisiana, in which overpressure issues are commonly observed in isolated porous reservoir beds in thick shale sections, independent of depth and the geological age of the formation (Cannon and Craze, 1938; Cannon and Sullins, 1946; Dickinson, 1951; Gordon and Flemings, 1998).

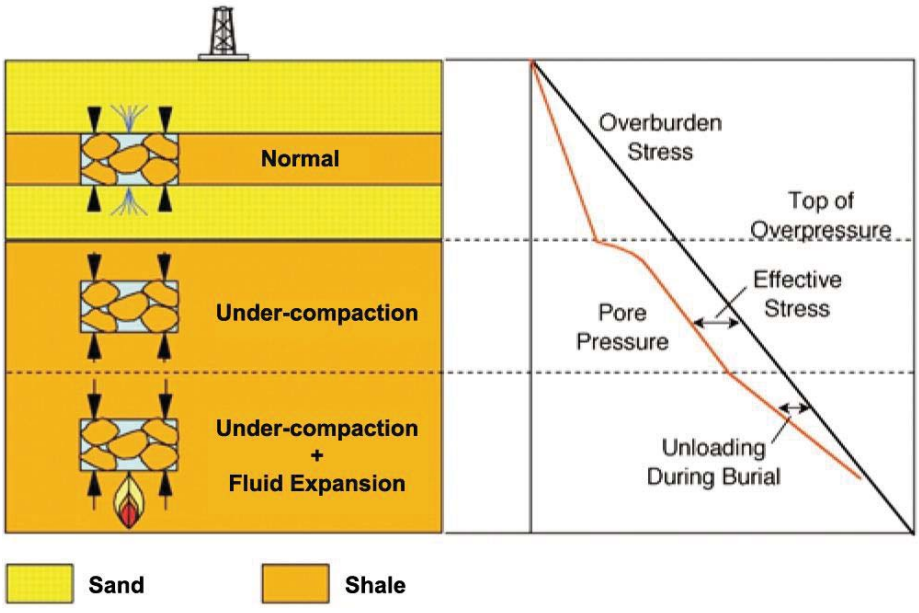

Figure 4-1 - Response of vertical effective stress to different overpressure mechanisms. Modified from Bowers (2002)

Understanding the compaction process (both mechanical and chemical) and the implications to the porosity is a key to evaluate the fluid inclusion capacity of overpressure generation (some compaction models are explained by Chilingar et al. (2002)). It must be noted that rock compaction refers to a total volume change in pore space and solid part of the rock body including matrix and grains (Newman, 1973). Pore space (porosity) compaction is larger than the rock body compaction by several orders of magnitude and, therefore, is generally considered as the index of total compaction. Porosity loss due to external loading consists of the following four sequential steps (Waples and Couples, 1998b):

(1) "A load is applied to the system of sediment+pore fluid. In many cases, this load will be the addition of new sediment at the top of the stratigraphic column.
(2) The framework of grains deforms (yields), leading to a (slight) reduction in pore volume. This step includes simple grain re-arrangement and 'true' distortional strain.
(3) The contained pore fluid(s) experience a pressure increase due to the reduction in pore space. This step results in a net transfer of some of the applied load from the framework grains to the pore fluid.
(4) The now (slightly) overpressured pore fluid flows to sites with lower potential energy (for example, the surface), if this is possible."

It must be noted that the main load in underground conditions is the overburden or vertical stress (Fatt, 1953; Hall, 1953b). For mechanical compaction, Goulty (1998) suggested a relationship between porosity and vertical stress as follows:

$$\emptyset = \emptyset_0 e^{-b\sigma_v} \qquad \text{Equation 4-1}$$

Where ϕ is porosity, ϕ_0 is the initial porosity, σ_v is the vertical stress as a function of density, and b is a constant according to King Hubbert and Rubey (1959). Waples (2001) believes that Goulty's equation (Equation 4-1) does not describe the low-rate process in which overpressure is generated. Goulty (1998) himself also stated that porosity loss should be related to the mean effective stress, instead of vertical stress. Concurrently, Harrold et al. (1999) demonstrated the significance of considering mean stress compared to vertical stress in PP predictions, particularly in deeper formations where horizontal stresses increases, and where the differences between mean stress and vertical stress expand and may result in false pore pressure predictions. However, horizontal stresses in many places are not properly evaluated

and, therefore, vertical stress or overburden is often used as the main variable (in Equation 4-1). Based on this, each rock undergoes different compaction processes depending on its physical and chemical properties. As an example, typical porosity-depth trends for shale, sandstone, chalk and shaly sandstone of the North Sea are shown in Figure 4-2 (Sclater and Christie, 1980).

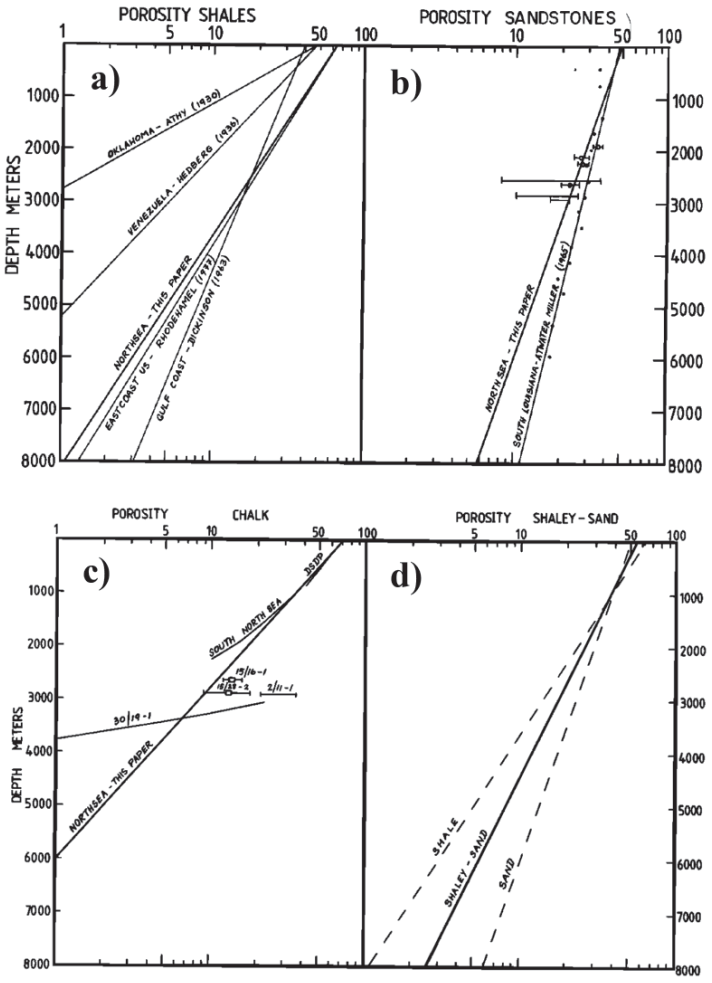

Figure 4-2 - Simplified plots of log porosity versus depth for a) shales and b) sandstones. Plots of log porosity versus depth for c) chalks and d) shaly sands in the North Sea (Sclater and Christie, 1980).

Porosity loss during deposition can be also a result of chemical reactions, termed as 'chemical compaction' or 'pressure solution', in which mineral framework of the rock dissolves into the pore fluid. According to the thermodynamic principles, this occurs along a gradient in chemical potential between the site of dissolution (the grain contact) and the pore fluid (Sheldon et al.,

2003a). In such active chemical environments, particle dissolution and precipitation of dissolved minerals (cementation) simultaneously take place. In terms of overpressure generation, quartz dissolution and precipitation in quartz-rich reservoirs can only generate narrow overpressure ranging from 0.05 to 1.3 MPa (Swarbrick et al., 2002). On the other hand, overpressure can potentially inhibit pressure solution by decreasing the effective stress on the grain surface (Porter and James, 1986). Chemical compaction also appears to be primarily temperature dependant, and not solely controlled by pressure, (Walderhaug, 1994) and yet to be further understood. More details of chemical compaction and porosity evolution in carbonate rocks are provided in Chapter 7.

Compaction, and thus associated overpressure development, can also be influenced by tectonic compression, particularly in regions that have undergone recent thrust faulting, compressional faulting or significant inversion. Indeed, regions of high tectonic stress often contain extremely high magnitude overpressures, approaching the lithostatic gradient, such as in deepwater Sabah (Couzens-Schultz et al.), Cooper Basin (Australia; van Ruth et al.), Niger Delta deepwater fold-thrust belt (Goodwyne, 2012) and Azerbaijan (Feyzullayev and Lerche, 2009). Extremely high magnitude overpressured systems in high stress regions are observed both via direct measurements from drilling and by the existence of highly overpressured geological features such as shale diapirs and mud volcanoes (Morley et al., 2011). Stresses in a region are at their maximum level just before active thrust faulting, and this may induce overpressure. In the foreland basins of active mountain-building thrust belts, the horizontal stresses can reach twice the overburden before faulting occurs, and any stress acting directly on sealed pore fluids would be expected to cause excess pressure, potentially equal to, or even slightly in excess of, the lithostatic gradient. The Qum oilfield in Iran is one of the best examples of extreme high pore pressure at the base of a thrust (Baker Hughes INTEQ, 1993). However, in the case of secondary porosity as a result of tectonic evolution (or salt doming (Osborne and Swarbrick, 1997b)), overpressure can be released by additional pore space (fracturing) or escape through newly created faults in a geologically short period of time (Giles, 1987).

Due to the complexity of tectonic evolution, combined with the fact that tectonic forces act on a large area, while reservoir or basin analyses are usually conducted on a much smaller scale or at shallower depths, the exact mechanism of tectonically induced overpressure is poorly understood. Recent advances in 3D geomechanical modelling provide some insight into the

influences of tectonic forces on compaction and overpressure generation. Li et al. (2010), based on numerical modelling in continental collision zones, suggested that the overpressure that can possibly affect high pressure and ultra-high pressure rocks is mainly related to the forces exerted in accretionary wedges at subduction zones. Another example of tectonically-induced overpressure is reported by Luo et al. (2007) in northwest China, where extremely high pore pressure in the present day is a result of superimposed allogenically transmitted pressure along faults and dipping permeable sandstone on existing mild overpressure. In that basin, the background overpressure is thought to be generated by compaction and tectonic compression. The Himalayan orogeny is one of the biggest and most favourable settings for tectonically-induced overpressures, and it is a good example of active tectonic evolution. Tectonic activities connected to the Himalayan orogeny have created the majority of overpressure in that basin, with additional contributions proposed to come from disequilibrium compaction and clay diagenesis (Sahay, 1999). Indeed, regions of extremely high horizontal stress magnitudes are the only locations in which 'supra-lithostatic' overpressures (pore pressure gradients in excess of the overburden gradient) have been reported (Gressier et al., 2010; Hurai et al., 2015), although I have not ever seen direct reliable measurements of supra-lithostatic overpressures.

4.2.2. Fluid Expansion Mechanisms

Contrary to disequilibrium compaction, which is a result of increasing external load on an effectively sealed pore volume, fluid expansion overpressure mechanisms occur due to a relative increase in the pore fluid volume required to be contained within a confined pore volume (Mouchet and Mitchell, 1989; Osborne and Swarbrick, 1997b). Since compaction in a sedimentary rock is generally known as an irreversible process (Magara, 1980), any increase in fluid volume within a confined pore system will increase the pore pressure (Mouchet and Mitchell, 1989). Unlike DC overpressuring that inhibits compaction during burial, fluid expansion overpressures are not associated with porosity anomalies and are more difficult to identify (Gutierrez et al., 2006; Miller et al., 2002). The theoretical fluid expansion mechanisms include aquathermal expansion, smectite, kaolinite or gypsum digenesis, load transfer, vertical transfer, and gas generation (Lahann and Swarbrick, 2011; Mouchet and Mitchell, 1989; Neuzil, 1995; Osborne and Swarbrick, 1997b; Swarbrick and Osborne, 1998; Tingay et al., 2007). However, not all of these mechanisms are capable of generating high magnitude of overpressure (Lahann and Swarbrick, 2011; Swarbrick et al., 2002; Tingay et al., 2007). Below, a brief explanation of those mechanisms is provided.

4.2.2.1. Kerogen to Hydrocarbon Transformation

Natural gas generation associated with deposition has been already identified as a potential source of overpressure in the sedimentary basins (Hedberg, 1974, 1978, 1980; Momper, 1980). Theoretically, the cracking of only 1% of an oil volume in a confined rock can generate overpressures close to the lithostatic gradient (Barker, 1990). Chilingar et al. (2002) explained the mechanism behind diagenesis of solid kerogen to be acting in two ways: a) by increasing the pore pressure; and b) by further impeding the expulsion of interstitial pore water through the development of a second gas-fluid phase. Meissner (1984) evaluated the potential of volume expansion of solid kerogen, via catagenesis, into liquid hydrocarbons, gas, residue, and other by-products as high as 25% of initial volume. As an example, maturation of a 3-6% of kerogen into gas in the Paris Basin in France was found capable of generating up to 50% fluid volume increase in the type-2 Toarcian black shales (Ungerer et al., 1981). The magnitude of fluid expansion in such processes depends on several factors, such as the kerogen type, abundance of organic matter and temperature history. However, these processes may be self-limiting in a sealed system because the build-up of pressure could inhibit further organic metamorphism (Osborne and Swarbrick, 1997b). Swarbrick et al. (2002) evaluated overpressure potential by kerogen-to-hydrocarbon transformation to vary between 70 and 6000 psi.

In several occasions, such as the Williston Basin, some areas in the northern and central North Sea, and some basins in the Rocky Mountains, the onset of overpressure (or significant increase in pore pressure) were coincident with the occurrence of hydrocarbons (Burrus, 1998; Fall et al., 2012; Spencer, 1987). Indeed, hydrocarbons require a significant overpressure to be released through micropores and microfractures (Tingay et al., 2013), which implies that high fluid pressure must have been generated within the source rock to initiate primary hydrocarbon migration (England et al., 1987; Fall et al., 2012). However, if the source rock is not mature, thick enough, aerially extensive and inclusive of high total organic content, then gas generation wouldn't be able to cause extensive overpressure across a basin and may be confined locally within the source rock (Osborne and Swarbrick, 1997b; Swarbrick and Osborne, 1998). The amount of organic matter in the source rock seems essential to generate high magnitude overpressures by kerogen to gas transformation, as it's been evident only within rich source rocks such as the Alum shales of the southern Norwegian Caledonides (Morley, 1992), the

Bakken Formation of the Williston Basin (Burrus et al., 1996), the Dunkirk shales of western New York state (Lash and Engelder, 2005), and the Middle Miocene shales and coals of the northern Malay Basin (Tingay et al., 2013). It is also known that kerogen maturation can increase the pore space (by 'destruction' of kerogen macerals and the expulsion of hydrocarbon from the source rock) which is known as the reduction in solid/fluid ratio (Osborne and Swarbrick, 1997b). In such case, a very rich source rock with an average porosity of 13% at the depth of peak maturation could contain a 20 vol.% kerogen that can transform into liquid hydrocarbons (Figure 4-3). Additional pore space causes 18 vol.% increase in the total effective stress to which is equivalent to shallower depths (Osborne and Swarbrick, 1997b). However, the rock is then subjected to a greater overburden load which can significantly decrease the porosity of already weakened framework. This is the conditions of disequilibrium compaction whereas resulted anomalies will be regarded as a DC overpressure.

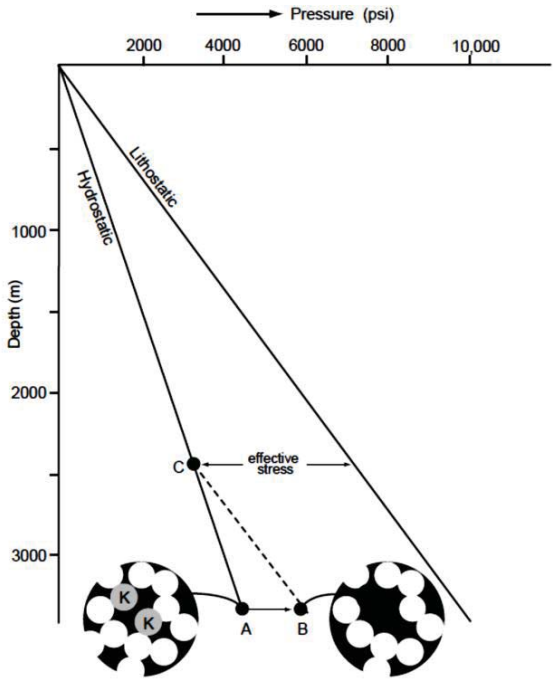

Figure 4-3 - Estimate of the overpressure created by disequilibrium compaction in a maturing source rock (Osborne and Swarbrick, 1997b). If the initial kerogen (K) is transformed into liquid products (A to B), the porosity of the rock would increase. The rock would now have the same porosity as a rock buried to point C. If the effective stress remains constant, the rock would be overpressured.

Despite the hypothetical capacity of overpressure generation, kerogen to gas transformation hasn't been widely referred to as a common factor in the development of overpressure. This might be due to the poor understanding of kerogen maturation and difficulties to identify and assess the phenomenon. In particular, the role of this mechanism in the geological setting of the Abadan Plain Basin hasn't been widely investigated yet, and due to unavailability of geochemical data, it can't be directly assessed. However, indirect analysis such as sonic velocity-vertical effective stress cross plots (presented in Chapter 5) will later be used to examine whether this mechanism is observed in the Abadan Plain Basin.

4.2.2.2. Clay Diagenesis

Dewatering of some types of clays during the deposition process has the potential of generating overpressure in a confined porous media (Lahann, 2000; Luo et al., 2007; Osborne and Swarbrick, 1997b; Tingay et al., 2007). Among several clay compounds, smectite is one of the most commonly found detrital minerals in the shales and contains remarkable amount of water in its crystal structure which is denser than ordinary water (Burst, 1969; Osborne and Swarbrick, 1997b). Expelled water expands when becomes pore water and increases pore pressure when confined (Lahann, 2000). A chemical reaction which expels water as a by-product of such transformation provided below (HOWER et al., 1976):

$$\text{Smectite} + Al^{+3} + K^{+} = \text{Illite} + Si^{+4} \qquad \text{Equation 4-2}$$

Smectite dehydration involves three stages of dewatering according to Swarbrick et al. (2002). The first two stages occur at depths of 0.5- 1.5 km, which generally have hydrostatic connection to the surface and, thus, overpressure is unlikely to be generated. The third stage occurs at depths of 3- 5 km and has the capability of generating overpressure ranging from approximately mild overpressures. In the clay-rich deposits of Gulf of Mexico, top of overpressure has been coincided with a rapid decrease in the ratio of smectite to illite which is then interpreted as the role of clay diagenesis in overpressures (Lahann, 2000). However, quantitative models of overpressure suggest that clay diagenesis can only be a secondary contributor to the overpressuring (Osborne and Swarbrick, 1997b; Swarbrick et al., 2002). Under favourable conditions, a significant amount of clays undergo dehydration that

can result in fluid increase of 15.5% of the smectite volume (Perry Jr and Hower, 1972). That is because smectite minerals can contain interlayer water up to 20-25% of their volume which has the potential of becoming pore water after dehydration (Burst, 1969; Perry Jr and Hower, 1972). It must be also noted that feldspar dissolution has been reported during the subsurface and core analysis that controls the formation of kaolinite or illite if temperature conditions are less than 120 °C (Meunier et al., 2004). Based on laboratory experiments, clay diagenesis is very time sensitive and much less temperature sensitive than many previous estimates (Velde and Vasseur, 1992) and it is highly controlled by the potassium content (Boles and Franks, 1979; HOWER et al., 1976). Under an ideal condition (Figure 4-4), the smectite to illite transformation in an entirely smectite rock can produce only 4% volume increase which is not enough to generate high or even mild overpressure (Osborne and Swarbrick, 1997b). However, clay diagenesis and associated rock volume change could improve sealing attributes of formation which can aid overpressure generation by disequilibrium compaction or other mechanisms (Lahann, 2000; Swarbrick et al., 2002).

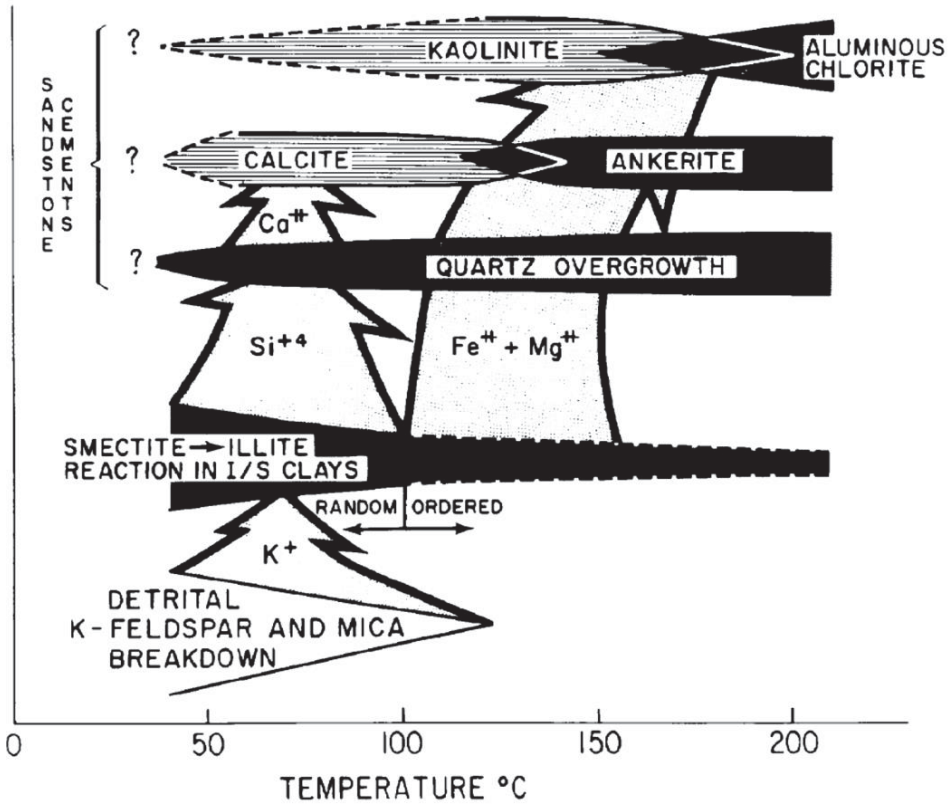

Figure 4-4 - Schematic diagram of influence of illite/smectite clay reactions on Wilcox sandstone cements (Boles and Franks, 1979). Vertical arrows depict ion transfer between I/S clay reactions and phases in sandstones. No sample control at temperatures less than 60°C

4.2.3. Pressure Transfer (Load Transfer)

Overpressure, as an active hydrodynamic system, is inherently unstable and tends to equilibrium conditions, which stabilize at the hydrostatic pressure (Borge, 2002; Neuzil, 1995). Therefore, overpressure can be transferred laterally or vertically to compartments other than where it is generated (Swarbrick and Osborne, 1998). Overpressure is transferred laterally in sealed interconnected porous rock (Mann and Mackenzie, 1990) in such a way that it diffuses along extensive, inclined permeable aquifers until a hydrostatic-parallel gradient is reached (Traugott, 1997). This process enhances the pore pressure at structural crest and is called lateral transfer (Yardley and Swarbrick, 2000). As a pre-existing condition for overpressure transfer, surrounding seal and high permeability inside the isolated aquifer are required.

In an inclined isolated porous media, pore pressure in the centroid is in equilibrium with the pore pressure of the surrounding shale. Within the isolated media, the fluids are in communication and will therefore equilibrate to fall along a hydrostatic parallel gradient inside the isolated reservoir (Figure 4-5). The different pressure gradients in the reservoir and surrounding shales result in reservoir pressures above the shale pressures in sections shallower than the centroid, and reservoir pressure lower than shale pressures when deeper than the centroid depth (Bowers, 2001; Finkbeiner et al., 2001; Traugott, 1997). The pressure in this condition follows a hydrostatic parallel pressure gradient trend. The term 'structure of reservoir' has been associated with this mechanism by Fertl (1976) and Dickinson (1953). Chilingar et al. (2002), based on the work by Hospers (1971), described how growth faulting can be a significant influence on overpressures in the Niger Delta. Lateral transfer has been identified as the main over-pressure generation mechanism in Papua New Guinea by Henning et al. (2002) and in North Sea by Yardley and Swarbrick (2000).

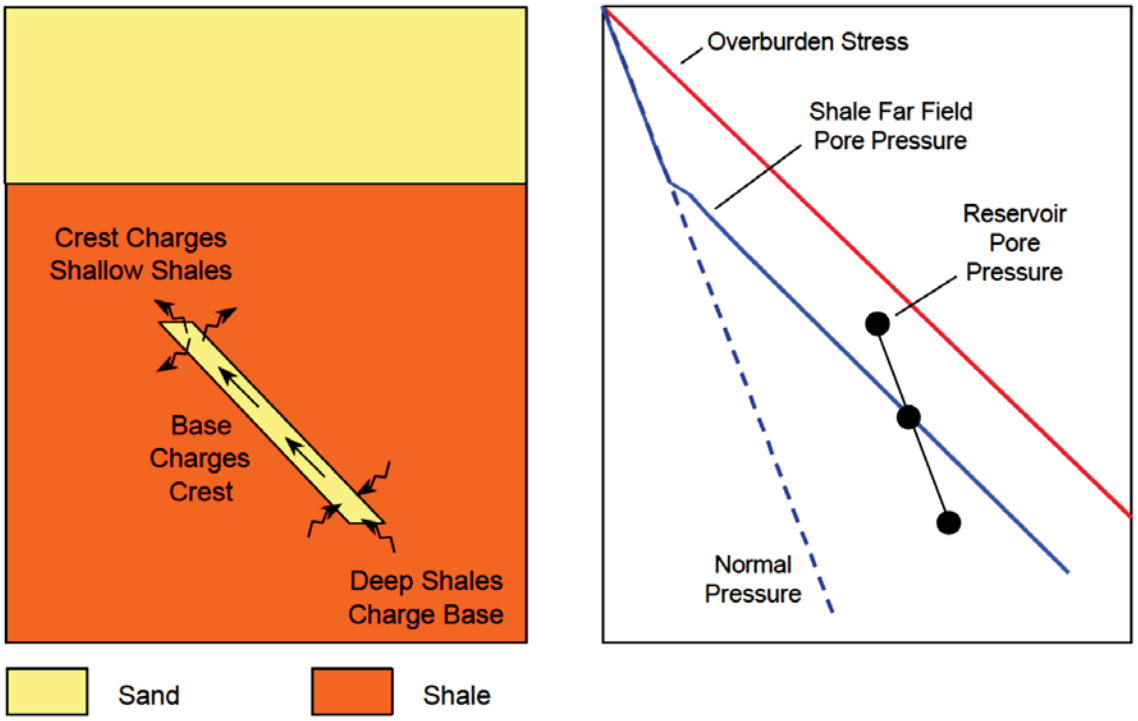

Figure 4-5 - The 'Centroid' effect – Up-dip transfer of reservoir pressures (Bowers, 2001).

Overpressure can also be transferred vertically between an overpressured compartment connected with a shallower normally pressured or less overpressured compartment (Burley et al., 1989; Grauls and Cassignol, 1993; Swarbrick and Osborne, 1998). This type of fluid flow between these two compartments, also known as inflationary, continues until equilibrium is reached. The rate of pressure transfer depends on the permeability of the connecting pathway (such as faults, fractures, or through capillary leakage of top seal (Grauls and Baleix, 1994; Grauls and Cassignol, 1993)) and timing of the phenomenon. In ideal conditions, overpressure can be completely depleted and the compartment becomes normally pressured. In such cases, generally, porosity remains intact in the initially normally pressured compartment and the magnitude of overpressure is a function of fluid flow between two parts of the hydrodynamic system (Tingay, 2003).

Faults, as a mean of pressure transfer, can be either impermeable seal in the interseismic phase, or highly permeable fluid pathway as a result of inherent roughness of natural rupture surfaces after the seismic failure (Sibson, 1990). The fluctuations in transient rotations of near-filed principal stresses may lead to fault sliding (activation) that creates different fluid migration patterns around the fault (Cox, 1995; Finkbeiner et al., 2001; Grauls and Baleix, 1994). Similar to pressure solution, the degree of overpressure is at its maximum when differential stress is low (Sibson, 2003). This is known as fault-valve activity (Sibson, 1990) which acts like a heart and tends to pump fluid from one location to another. In a tectonically active and extensively folded environment such as the Zagros Deformation Zone, fault reactivation is a commonly plausible feature, but the strata are normally thick (several hundreds of metres) and a consistently permeable fault is very rare. Therefore, fault-valve activity can be favourable feature only within various compartments of a thick formation (isolated sub-layers) that distribute the pore pressure across the reservoir.

4.2.4. Other Proposed Mechanisms of Overpressure Generation

4.2.4.1. Aquathermal Expansion

Aquathermal expansion is another proposed fluid expansion process, in which overpressure is proposed to be generated by the increase in the volume of saturating fluid in a sediment that is buried and heated. The volume of a fluid will increase when temperature rises, the degree of

which is a function of water composition (i.e. the amount of dissolved solids). Ideally, pure aquathermal pressuring occurs when the formation is heated at a certain depth (Gretener, 1981), which is not the case in a depositional process where there is a continuous process of deposition and rising temperature together. Like other mechanisms, sealing is essential for the creation and retention of overpressure through this mechanism (Osborne and Swarbrick, 1997b). In fact, the pore fluid needs to be retained within the rock porosity while being heated and therefore, thermal evolution of sequences containing migrated hydrocarbons from other strata, can't be considered as a main source of pressure generation. Bethke (1985) modelled the fluid flow in various permeable mediums and declared that both excess potentials and fluid velocities were found to scale linearly with sedimentation rate, and that aquathermal pressuring accounts for <1% of excess potentials. This could be due to the expansion of fluid with increasing temperature gradient as the viscosity of the fluid decreases, which affects the diffusion of overpressure. According to Swarbrick et al. (2002), the rate of volume change caused by aquathermal expansion, produces a maximum of approximately 100 psi overpressure under a typical range of basin conditions. Hence, the pressuring effect of aquathermal expansion seems to be a non-affecting parameter in practical geopressure studies and is largely neglected (Luo and Vasseur, 1992).

4.2.4.1. Artesian Hydrostatic Pressure (Hydraulic Head)

Hydraulic head and buoyancy force are two phenomena that can impose extra pressure onto pore fluid in confined conditions. Hydraulic head is also known as piezometric head, which is a specific measurement of water level and equivalent pressure above a datum (Chanson, 1999). The main controlling parameters in the artesian head are the piezometric level or water table elevation and sealing (Figure 4-6). In unconfined aquifers, pressure would easily dissipate through the pore spaces and the hydraulic head would be equivalent to the sea level or elevated free water table altered by the soil capillary. This mechanism is liekly to take place in shallow acuifers where they are in a hydrodynamic connection to the free water. Other overpressures as a result of hydraulic head in a tilted confined acuifer is discussed under pressure transfer (4.2.3).

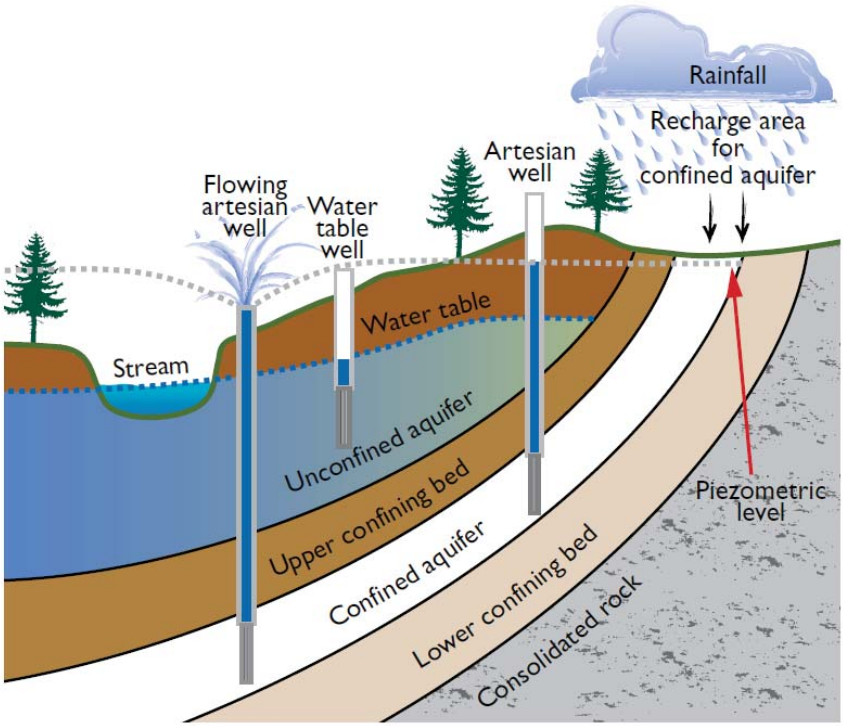

Figure 4-6 - Geological and topographical controls affecting artesian and flowing artesian wells (Ministry of Environment Office British Columbia, 2010)

4.2.4.2. Uplift

In sedimentary environments, burial is often disturbed by tectonic forces, which cause the formation to uplift and be exhumed to a shallower depth (Figure 4-7). If the formation has been fully sealed, and the normal pore pressure inside it is retained during the uplifting process, then the formation may, conceptually, have a higher pore pressure than the surrounding strata. Nevertheless, perfect sealing does not exist in most of depositional environments and therefore, uplifting a perfectly sealed formation to a poorly sealed condition may relieve the overpressure and decrease the magnitude of overpressure. In ideal conditions, lowering the load on a sealed stratum has less implication for pore fluid than gas, and unlikely to generate overpressure (except there is gas in the pore space). Gas has an undrained pore-pressure build-up coefficient (Skempton's coefficient, B) of 0.1-0.2 whereas water has values close to 1, and oil anything between gas and water (Katahara and Corrigan, 2001). That means pore pressure tends to be independent of overburden if B is much less than 1 (gas) and consequently, uplifting of an isolated gas reservoir can result in significant overpressure. In the case of oil or water with higher B value close to 1, uplifting would be offset by volume expansion of the rock frame due to unloading, and unlikely generate overpressure. Meanwhile, uplifting usually occurs in the

range of few hundreds of metres where aquathermal pressuring doesn't have much influence on the pore pressure. Uplift has been proposed a contributing mechanism to overpressure in Assara-Arakan basin of North East India (Bhagwan et al., 1998) as well as Greater Green River basin of southwest Wyoming (Shanley et al., 2004), the Delaware Basin (Lee and Williams, 2000) and the Rocky Mountain basin (Devine, 2014).

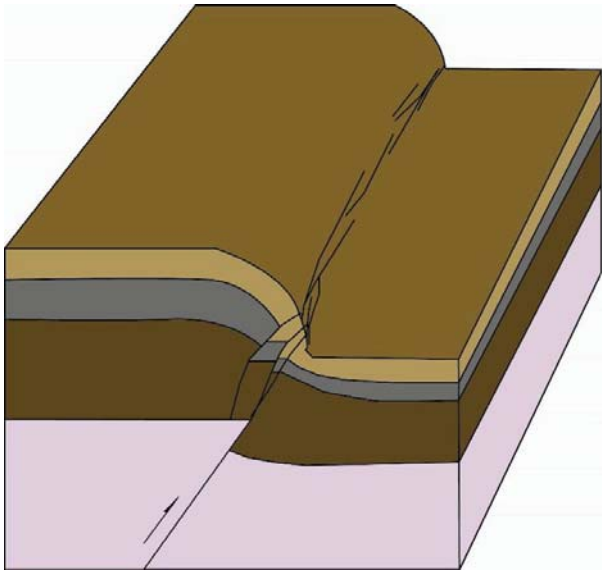

Figure 4-7 – Schematic block of uplifted formations. Uplift is very common in the faulted zones.

4.2.4.3. Hydrodynamic Buoyancy

Fluids within any sealed reservoir rock will requilibriate so as to lie along a pressure gradient related to the fluid density. Hydrocarbons, and especially gases, have lower density than water, and thus hydrocarbon columns will fall along a steeper gradient, and have fluid pressures greater than the hydrostatic or water pressure. These bouyancy pressures are routinely observed with direct pressure tests in hydrocarbon columns, and the slope of the pressures can be used to estimate fluid type (e.g. oil, condensate, gas) as well as the contacts between different fluids (e.g. the oil-water contact). Bouyancy pressures associated with hydrocarbons are a function of the hydrocarbon column height (larger columns create more bouyancy pressures), and the density of hydrocarbon (lower density fluids are associated with greater bouyancy pressures). Bouyancy pressures are important concerns when planning wells that may encounter hydrocarbons, especially near structural crests, as well as hydrocarbons encountered at shallow

depths in deepwater environments. The resulted excess pressure can be as high as several hundred psi (1-6 MPa). An observation of this kind of abnormal pressure in the North Sea is discussed by Osborne and Swarbrick (1997b) who predicted 4 MPa (607 psi) overpressure resulting from the differences between the densities of water, oil and gas. The potential buoyancy force on the Fahliyan formation in one of the oilfields in the Zagros Deformation Zone is estimated as 0.6 MPa (90 psi) over a 250 m oil column above the water-oil contact (Figure 4-8; Atashbari and Tingay, 2012).

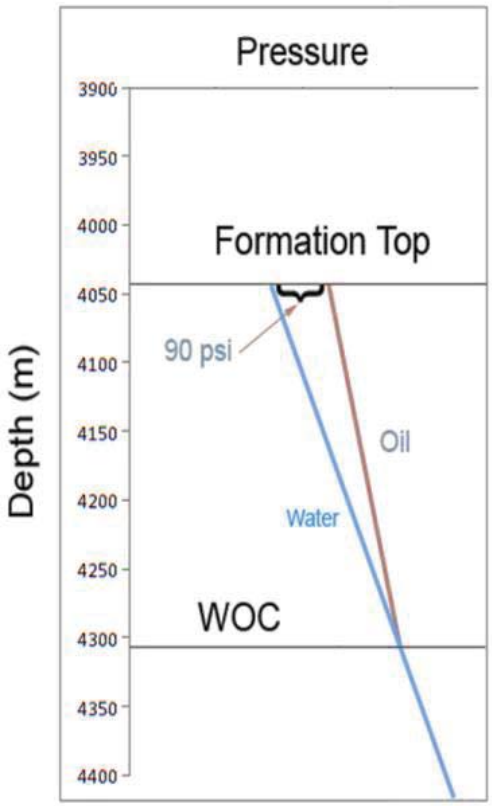

Figure 4-8 - Diagram illustrating the maximum pressures that could be generated by hydrocarbon buoyancy in a field in the Zagros Deformation Zone (Atashbari and Tingay, 2012b).

On the other hand, gas bubbles in the oil could transport the pore pressure from the deeper parts of the reservoir (i.e. water-oil contact) to the top of the oil column. This process is also distinguished as a potential source of overpressure and named 'advective overpressure' by Sahagian and Proussevitch (1992). It is a very complex multi-phase fluid flow behaviour which

requires knowledge of gas compressibility, gas solubility in liquid and the attributes of fluid flow in porous media. To date, it has not been explained in simple terms and due to the dynamic nature of reservoirs, it needs further investigation in order to accurately predict associated overpressure.

4.2.4.4. Gypsum to Anhydrite Transformation

As the temperature of a NaCl saturated solution rises, the nature of the salt changes from gypsum to anhydrite. The chemical reaction has the following form in atmospheric conditions:

$$CaSO_4.2H_2O=CaSo_4+2H_2O$$ **Equation 4-3**

This process results in the expulsion of bound water from gypsum, which is potentially an important overpressure generation mechanism in evaporite sections (Osborne and Swarbrick, 1997b). Depending on the geothermal gradient of the basin, this could happen at various depths, but it normally takes place when the temperature exceeds approximately 40 °C (Figure 4-9). There have been also similar trends for the activity of H_2O based on empirical data (Hardie, 1967). This process is very much depth and temperature sensitive, and each mineral becomes stable in very specific conditions. Testa and Lugli (2000) empirically evaluated relationship between depth and the gypsum–anhydrite reaction temperature for different hydrostatic and lithostatic fluid-pressure regimes and below different sediments (Figure 4-10). Different trends for every rock type indicate differing responses to the pressure-temperature conditions in sedimentary rocks.

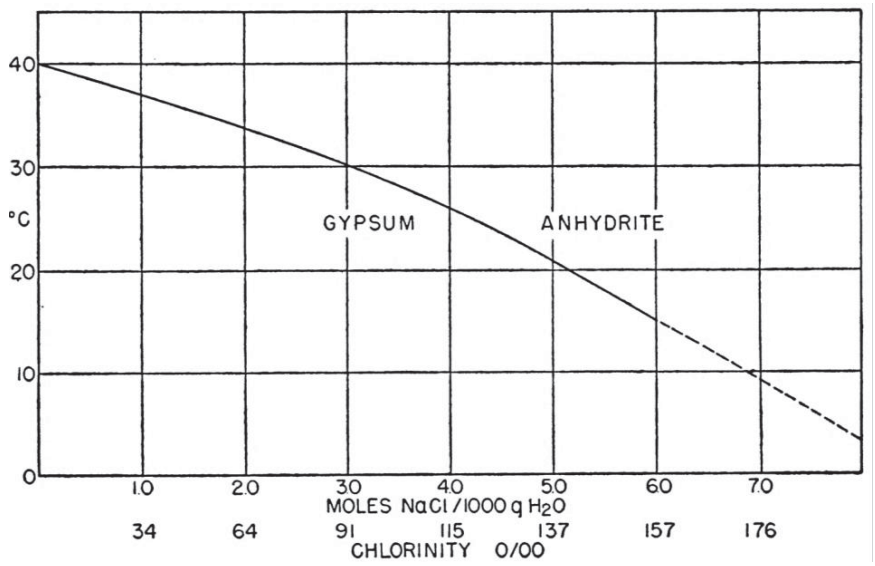

Figure 4-9 – Relationship between gypsum dehydration temperature and concentration of NaCl in solution at one bar pressure (Macdonald, 1953). The data are based on experimental calculations.

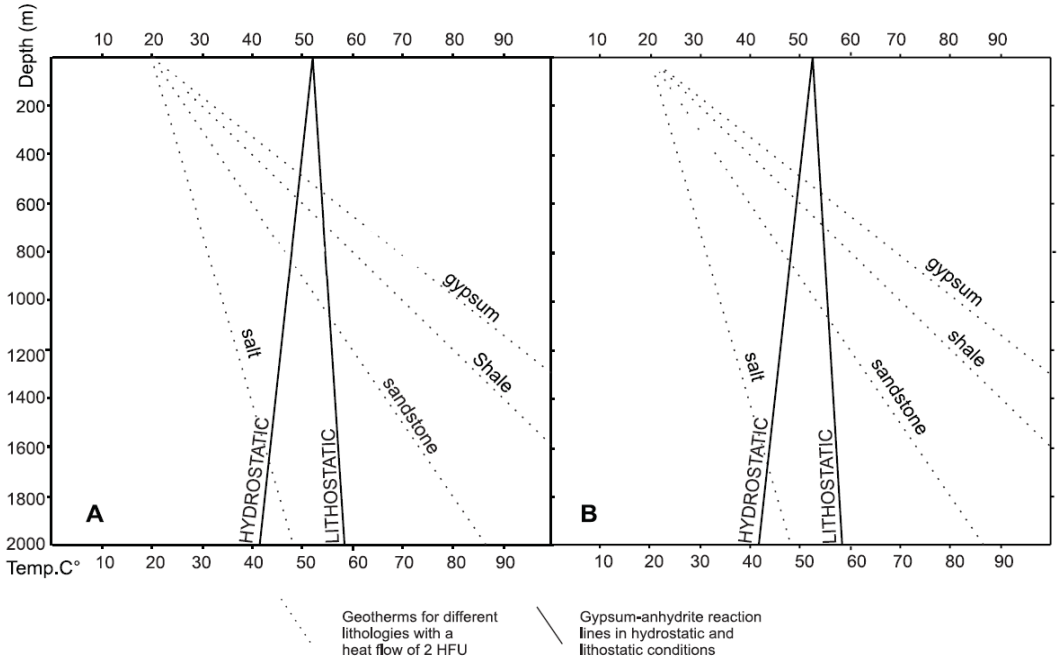

Figure 4-10 - Depth relationship of gypsum–anhydrite reaction temperature for hydrostatic and lithostatic fluid-pressure regimes and below different sediments. a_{H2O} D 0:93, $\_{sediment}$ D 2:4 g=cm3, heat flow D 2 HFU. Conversion to anhydrite occurs where the reaction T line intersects the geothermal gradient in the overlying rock. Modified after (Hanshaw and Bredehoeft, 1968; Jowett et al., 1993; Macdonald, 1953; Testa and Lugli, 2000)

In a very classic explanation of this reaction, Posnjak (1940) investigated the solubilities of anhydrite and gypsum in a salt solution in a similar salt composition of sea water. He then determined 30°C as the temperature in which gypsum is the stable phase whereas anhydrite becomes essentially stable in the temperatures above 30°C. Jowett et al. (1993) based on modelled results, indicated that gypsum-anhydrite transformation takes place in shallow depths (~400 m) in the case of formation overlain by poor conductors like shale in a rift environment. According to their analysis, at greater depths (such as depths greater than 4 km) this transition only happens if the formation is overlain by a good conductor, like salt, in a stable cratonic region. Some observations of gypsum or anhydrite co-existing are listed in Table 4-1.

Table 4-1 – Data on solutions co-existing with gypsum or anhydrite in natural evaporite deposits (Hardie, 1967)

Locality	Mineral Assemblage	Solution			Investigator
		T°C	Chlorinity °/∞	aH_2O	
Trucial Coast, Persian Gulf	Gypsum	27-34	50-110	0.95-0.85	(Bramkamp and Powers, 1955)
	Gypsum, Carbonate	24 To 39	64 91 96	0.93 0.88 0.87	(Kinsman, 1965) (written communication between Lawrence A. Hardie and D. J. J. Kinsman in 1964)
	Anhydrite, Carbonate		134 * 152 * 159 166	0.8 0.77 0.75 0.73	
Boccana de Virrila, Peru	Gypsum	27	108 **	0.85	(Morris and Dickey, 1957)
Saline Valley, Calif.	Gypsum	9-39	16-50	0.99-0.95	(Hardie, 1965)
Salina fm., Mich. (Silurian)	Anhydrite, Halite ***	32-48	Satd. NaCl	≤ 0.75	(DELLWIG, 1955)

* Anhydrite in the zone of capillary draw. Chlorinities as given are for the underlying groundwaters. Actual solutions in which anhydrite formed were presumably more concentrated.

** Precise location in Boccana where gypsum is precipitating is difficult to read from Morris and Dickey's descriptions. The value given here is taken from their data for location C, which may be incorrectly interpreted by the present author as the gypsum site.

*** Delicately preserved 'hopper' crystals which have clearly not suffered alteration since their formation. The same argument must apply to the intimately associated anhydrite. Temperatures of formation of the hopper halite were determined by fluid inclusion studies.

The process of gypsum to anhydrite transformation happens within a certain temperature window, mostly between 40-60 °C, which is the average temperature in shallow formations (Osborne and Swarbrick, 1997a, b). Hence, the excess water expelled from the gypsum to anhydrite transformation could escape from most sediments, as it is unlikely to have a perfect seal at that depth. Thus gypsum to anhydrite transformation is unlikely to be a key overpressure generation mechanism in conventional oil and gas reservoirs lying in depths beyond 2000 m.

4.2.4.5. Coal Dewatering

Sedimentary rocks are significantly enriched with organic matter over average sediments and are so called carbonaceous sedimentary rocks (Sam Boggs and Boggs, 2009). In such deposits, coalification is normally associated with release of relatively fresh water from interbedded coal and carbonaceous sequences (Law et al., 1983). Thus, coal dewatering has the potential to generate excess pressure either in coal beds or carbonaceous rocks if perfect sealing is available. The effectiveness of this mechanism is obviously dependant on the following factors (Law et al., 1983):

- the amount and stratigraphic occurrence of coal
- stage of coalification
- degree of hydrologic isolation

Coal dewatering could generate mild overpressure in unconventional oil and gas reserves while due to low presence of such minerals in the marine depositional environment, its effectiveness in conventional reservoirs (i.e. carbonates) hasn't been investigated yet.

4.2.4.6. Osmosis

Osmosis is the process by which molecules of water or another solvent are able to pass through a semi-permeable membrane into a region of greater solute concentration, so as to make the concentrations on the two sides of the membrane approach equilibrium (Oxford English Dictionary, 2015). The concentration of soluble particles and the capacity of the membrane to exchange ions are the main factors that control the osmotic process (Figure 4-11). In sedimentary reservoirs, the passage of cations and anions through the pores of the compacted clay membrane could be inhibited as the positive and negative layers interact with each other (Marine and Fritz, 1981). According to that study, osmotic pressure at both sides of a shale semi-permeable membrane is postulated to be able to reach 6-20 MPa. However, the theoretical potential of osmotic pressure in a shale deposit in the North Sea has been estimated by Osborne and Swarbrick (1997b) as being 3 MPa (435 psi). The maximum overpressure potential as a

result of the equilibrium osmotic pressures within small porosities, and with large amounts of total dissolved solid (TDS), was estimated to be as high as 20 MPa in a shale formation of central South Dakota, USA (Neuzil, 2000). In this case there must have been a huge difference in the salinity (or TDS) between two sides of the membrane. This condition is plausible in shallow deposits where the underground interstitial pore water is more saline than surface or shallow depth fresh water. But, the required conditions for a higher magnitude of overpressure by osmosis are very unlikely in the deeper depositional environments. Laboratory tests on the siltstone and shales from Lower Cretaceous Viking Formation in central Alberta, Canada showed a few psi excess pressure associated with the osmosis force within the cores (Young and Low, 1965) because effective membranes are absent in shales (Bradley, 1975). Osborne and Swarbrick (1997b) explained Bradley's (1975) results of osmotic pressure direct measurement in shale cores and found that osmotic pressure could only generate a negligible 0.01 – 0.03 MPa of overpressure.

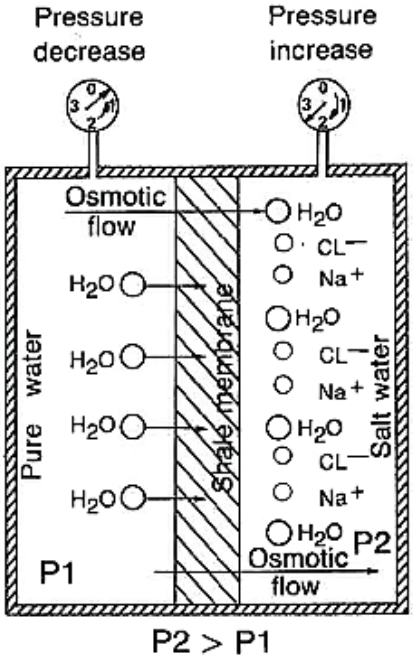

Figure 4-11 – Illustration of the osmotic process (Mouchet and Mitchell, 1989). P1 and P2 are pressure at the both sides of the membrane.

4.3. Potential Mechanisms of Overpressure Generation in the Abadan Plain Basin

Each of overpressure generation mechanisms act in specific circumstances such as depth and overburden load, chemical composition of the rock and pore fluid, tectonic settings, etc. (Figure 4-6). Overpressures in the Abadan Plain Basin are generally observed within carbonate assemblages of the Gachsaran and Fahliyan formations (Chapter 3). Overpressures are then occasionally percolated through the bottommost section of top seals (the Gadvan Formation overlying the Fahliyan Formation). According to the geological background of the Abadan Plain Basin (Chapter 2), the distribution of overpressure across this basin (Chapter 3), and above overview of probable overpressure generation mechanisms, three main mechanisms have the potential to generate overpressure in the Abadan Plain Basin:

- Disequilibrium Compaction
- Kerogen Maturation
- Clay Diagenesis

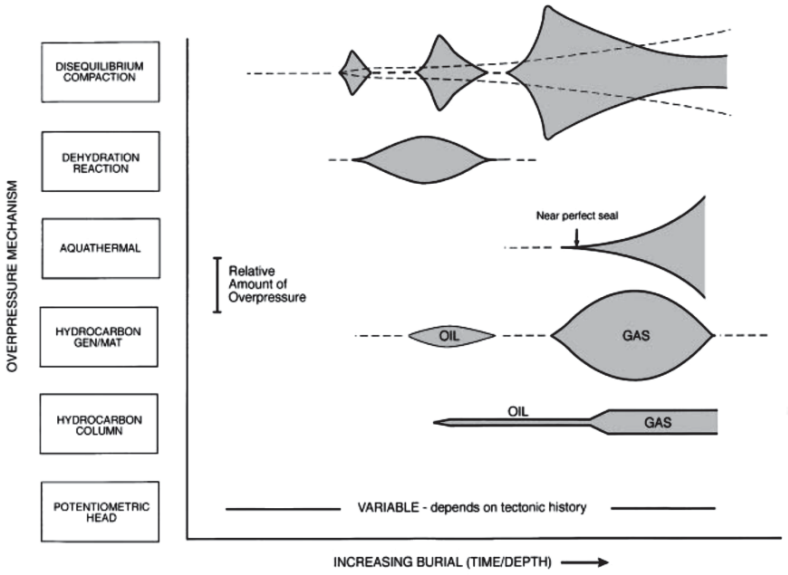

- **Figure 4-12 – Schematic representation of overpressure development through time during progressive burial for each of the principal mechanisms of overpressure generation (Swarbrick, 1995). Disequilibrium compaction is shown for both constant burial rate (dashed line) and variable burial rate (solid line shows overpressure buildup with rapid burial and dissipation of excess pressure during slow rate of burial). GEN/MAT = generation/maturation.**

The water bearing Gachsaran Formation is typically an evaporite deposit which hosts overpressure only in the northern part of the basin. Among the major overpressure generation mechanisms, none seems to be the primary origin in this formation except disequilibrium compaction. The bottommost section of the Gachsaran Formation is a perfect seal for underlying Asmari Formation (Allahkarampour Dill et al., 2010; Gill and Ala, 1972; Soleimani and Bahadori, 2014) and it seems that the pore water in the isolated pores of the formation are confined with the extremely low permeable fabric of the rock itself. Gypsum is frequently evident in the shallow sediments of the Aghajari Formation while it is absent in the Gachsaran Formation and instead, anhydrite exists. Therefore, gypsum to anhydrite conversion has definitely taken place and might have contributed to overpressure generation in this formation. Addition to evaporites, there is noticeable amount of marl and calcareous claystone in this formation (Bahadori et al., 2011; Bahroudi and Koyi, 2004; Gill and Ala, 1972), which might have been undergone clay dewatering process. However, exact clay mineralogy of this formation is unknown to author. On the other hand, Fluid expansion due to lack of hydrocarbon accumulation hasn't been occurring and so has other mechanisms due to shallow depth and mineralogy of the formation.

In southeast and west of Iran, the Gadvan Formation is currently in the oil expulsion phase whose hydrocarbons were migrated through thin shallow-water limestone of the Khalij Member towards the platform facies of the Khami Group (the Dariyan Formation) which is capped by the organic-rich Kazhdumi Formation (Leturmy and Robin, 2010). Such system doesn't exist in the Abadan Plain Basin and the Dariyan Formation hasn't been characterised as commercial oil reservoir in this basin. It seems that such hydrocarbon was not accumulated due to regional extent of the formations. However, the Gadvan Formation is identified as a host to mild to moderate overpressures in the entire basin. Generally, overpressure is essentially generated within the Gavdan Formation pressure transfer from the underlying Fahliyan Formation hasn't contributed to the overpressure development. It is because the shales of this formation are low permeable and even if there is any conductive pathway between the Fahliyan and Gadvan formations, overpressure was unlikely to be distributed across the formation and therefore, overpressure in this formation is autochthonous. During the deposition, loading induced pore pressure hasn't been balanced with the hydrostatic pressure due to low permeability of the Gadvan Formation, which seems the main mechanism of the overpressure generation in this basin. Given the petrology of the Gadvan Formation which consists of dark

shale and argillaceous limestone, kerogen maturation is also a plausible source of overpressure in this basin where the shale layers are capable of providing a pressure barrier within the formation. On the other hand, clay diagenesis could have taken place in the Gadvan Formation. Clay minerals are identified as kaolinite, illite, smectite, and traces of mixed layer clays (Research Institute of Petroleum Industry, 2005a). However, Clay diagenesis is not a major overpressure origin, and since illite abundance hasn't been observed in this formation, smectite-illite transformation doesn't seem to contribute to the overpressure generation or development.

In the Fahliyan Formation of the Abadan Plain Basin, overpressure is evident all over the basin. Thick carbonate deposits are mildly to moderately overpressured and frequently hold hydrocarbon accumulations that are sealed by the Lower Gadvan Shale. Fluid retention depth of the Fahliyan Formation of this basin is at 1200-1300 m (~20 Ma, will be discussed in further chapters) and hence, a 110 Ma per year of undrained loading during the deposition. As a Consequence, disequilibrium compaction is the primary overpressure generation mechanism in this formation. Meanwhile, clay minerals of the Fahliyan Formation could have undergone diagenetic evolution and generated excess pore pressure. Although, the existence of depositional circumstances required for this mechanism are not evident (will be discussed in the next chapter). Indeed, kerogen maturation is unlikely to be an overpressure origin because the hydrocarbon accumulations in this formation are believed to be migrated from deeper Garau source rock (Zeinalzadeh et al., 2015). Unfortunately, no pressure data from the Garau Formation is available and the possibility of pressure transfer remains unclear. Finally, lateral pressure transfer inside the Fahliyan Formation towards the structural crest may contribute to the overpressure development in the fields of this basin. Contingency of abovementioned mechanisms are summarized in the Table 4-2, but require detail analysis of the geology and hydrodynamics of the fields in the Abadan Plain Basin.

Table 4-2 – Potential overpressure generation processes in the Gachsaran, Gadvan and Fahliyan formation.

Process	Influence on porosity	Influence on pore pressure (UC/FE)	Can it be predicted?	Can it occur?		
				Gachsaran Fm.	Gadvan Fm.	Fahliyan Fm.
Pressure solution	Due to shallow depth of the formation, can't	UC	Yes, if pressure and temperature history is known.	-	-	Yes
Dolomite cement precipitation	Hasn't been identified.	UC	No, unless a pore scale model for the precipitation of dolomite rhombs is developed.	-	-	Yes
fracturing	Hasn't been identified.	-	Yes, but detailed facies models are required.	-	??	Yes
Smectite to illite transformation	-	FE	Yes, if the mineral composition and temperature history of the well is known.	Yes	Yes	Yes
Kerogen to oil transformation	-	FE	Yes, if the composition of organic matter and pressure/temperature history is known.	-	Yes	-
Gas generation	-	FE	Yes, if the composition of organic matter and pressure/temperature history is known.	-	Yes	Yes
Gypsum to anhydrite transformation	-	FE	No, unless a model for the water and evaporite mineralization is developed.	Yes	-	-
Pressure transfer	-	-	Yes, if the petrology of the seal and porous pathway are known.	-	-	??

UC: Undercompaction
FE: Fluid expansion
??: Probable, but not confirmed

4.4. Conclusions

Overpressures in the Gachsaran, Gadvan and Fahliyan formations are common in the oil fields of the Abadan Plain Basin, and can potentially be generated by several mechanisms. Based on the geological structure and depositional environment, disequilibrium compaction is found as the primary origin of overpressure in this basin. Moderate to high overpressures in the Gachsaran Formation are mainly a result of undrained loading which pressurized the entrapped pore water in the isolated pore space, as well as partly gypsum to Anhydrite transformation. Whilst there is a high contingency of kerogen maturation, and clay diagenesis in the Gadvan Formation, the magnitudes of these mechanisms aren't comparable to DC, which is a result of undrained compaction of very low permeable deposits. The most probable overpressure origin in the Fahliyan Formation is DC, while minor contribution of clay diagenesis is also plausible. In the next chapter, likelihood of the key overpressure generation mechanisms will be investigated further using petrophysical evaluations of the formations.

CHAPTER 5- Origin of Overpressure in the Abadan Plain Basin

5.1. Introduction

Overpressure and its origins are identifiable through a set of tools including seismic data (Ahmed et al., 2011; Bhagwan et al., 1998; Chatterjee et al., 2012; Fillippone, 1982; Green and Wang, 1986; Katahara, 2003; Pennebaker, 1968; Sayers and Woodward, 2001; van Ruth et al., 2004) as well as petrophysical information such as sonic and resistivity logs (Anderson et al., 1973; Bhagwan et al., 1998; Devine, 2014; Haugland et al., 2013; Katahara, 2003; Ransom, 1986; Teige et al., 1999; Tingay, 2014; Tingay et al., 2003). The basis of the majority of these methods is examining the observed values of the parameters with respect to what can be expected for a given condition (i.e. depth or overburden). Some of the most commonly used techniques to identify the origin of overpressure are sonic velocity-vertical effective stress (VES) plots (Bowers, 1994; Bowers, 1995) as well as sonic velocity-density (Hoesni, 2004; Katahara, 2003; Lahann et al., 2001) and resistivity-density plots (Ramdhan and Goulty, 2010), in which any departure from the loading curve is interpreted as the effect of overpressure.

In this chapter I examine the petrophysical properties of overpressure in the Abadan Basin, and identify that overpressure is primarily caused by disequilibrium compaction and has developed across multiple reservoirs. I will undertake a petrophysical analysis of overpressure generation mechanisms for 10 wells in 6 fields, and highlight that disequilibrium compaction occasionally acts at the shallow deposits of the Gachsaran Formation and throughout all the deeper reservoirs of Gadvan and Fahliyan formations. Finally, I will briefly examine the implications of the generation mechanisms on pore pressure prediction and field development, as an introduction to the detailed examination of pore pressure prediction, and testing of new methods, presented in chapters 7 and 9.

5.2. Sonic Velocity – Vertical Effective Stress Relationships

5.2.1. Introduction

Different overpressure mechanisms, which result from various geological or diagenetic processes, can be identified by their effects on the petrophysical attributes of overpressured sequences (Hermanrud et al., 1998; Lahann and Swarbrick, 2011; Tingay et al., 2009; van Ruth et al., 2004). Plots of porosity, or a petrophysical proxy to porosity (e.g. sonic velocity, density, resistivity), versus vertical effective stress (VES) are a common method for distinguishing between overpressures generated by disequilibrium compaction and overpressures due to fluid expansion type mechanisms, such as kerogen-to-gas maturation or clay diagenesis (Bowers, 1994; van Ruth et al., 2004; Tingay et al., 2009).

In aquifers that are hydraulically-connected to the surface, pore pressure always remains equal to the weight of the fluid column at the depth of measurement and is known as hydrostatic pressure. In these normally-pressured sequences, the porosity of shale decreases with increasing depth as a result of increasing vertical effective stress imposed on the rock. Hence, normally pressured shales will experience increasing vertical effective stress with depth and a decrease in porosity (and associated increase in acoustic velocity, density and resistivity). The burial depth and the implied acoustic velocity follows a trend that is the same for a certain rock type. This is known as a loading curve (LC) or normal compaction trend (NCT) (Dobrynin and Serebryakov, 1978; Pennebaker, 1968; Serebryakov et al., 1995). Such a relation with stress does not exist in carbonates rocks that have undergone diagenetic processes (will be discussed in Chapter 8).

According to Terzaghi and Peck (1967), in a confined or semi-confined pore space, a part of the pressure on the rock will be carried out by the fluid and, the effective pressure on the rock frame will decrease. Disequilibrium compaction overpressure is generated by an imbalance between loading that attempts to porosity loss through mechanical compaction and the ability for fluid to be expelled from pore spaces (permeability). Porosity loss in an undercompacted sediment is inhibited due to the resistance of pore fluid and consequently, pore pressure rises according to a mean stress parallel or approximately lithostatic-parallel trend (Figure 5-1b).

Similarly, pore pressure due to fluid expansion overpressure follows a hydrostatic-parallel trend (Figure 5-1b). In a porous media, compaction is driven by increases in the effective stress which is defined by Terzaghi and Peck (1967) in Equation 5-1.

$$\sigma' = \sigma - P \qquad \text{Equation 5-1}$$

Where σ' is effective stress, σ is total stress, and P is pore pressure. In an abnormally pressured rock, if overpressured is generated by DC, the sediments are at their maximum effective stress (Bowers, 2001). According to that, effective stress in sediments with fluid expansion overpressure has been maximum in the past. If disequilibrium compaction is the origin for overpressure, effective stress remains the same for the entire overpressure zone. Consequently, compacted sediments remain on the loading curve on velocity-vertical effective stress cross plots (Figure 5-1c; Bowers, 1995). Alternatively, sediments with overpressure due to fluid expansion or vertical transfer follow a different trend, called an unloading curve (Figure 5-1c). It is because compaction is commonly an irreversible process (Issler, 1992; Magara, 1980) and overpressures generated by fluid expansion are only associated with a small porosity change against effective stress and thus, follow a path away from the loading curve (Tingay et al., 2013). This is one of the commonly used methods to distinguish between the type of overpressure origin, and specifically, whether it is created by disequilibrium compaction or fluid expansion.

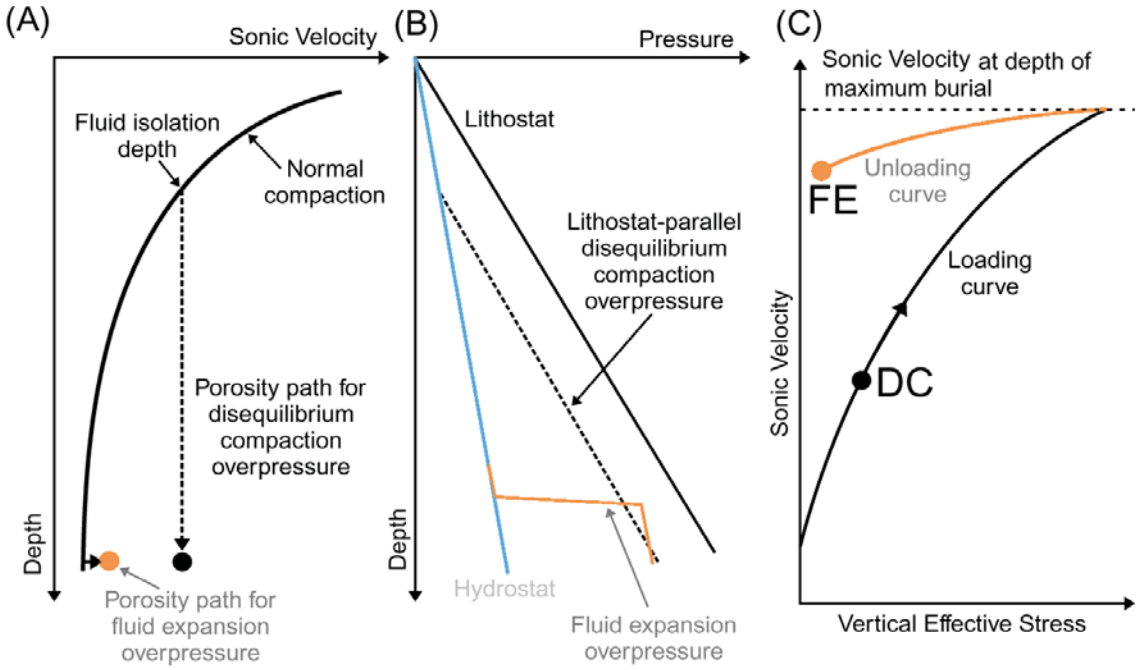

Figure 5-1 - (A) Schematic sonic velocity-depth and (B) pressure-depth paths for overpressure generated by disequilibrium compaction (DC) and fluid expansion (FE) or vertical transfer. (C) sonic velocity–effective stress schematic of overpressured sediments where overpressure is generated by DC, where sediments plot on the loading curve, and FE or vertical transfer during which sediments follow an unloading curve, modified from Bowers (1995) and Tingay et al. (2007).

5.2.2. Methodology

Loading and unloading curves in the velocity-vertical effective stress plots vary by rock properties and they can be only defined for a single lithology. Carbonate rocks of the Sarvak, Jahrum, and Fahliyan formations in the Abadan Plain Basin have different attributes and none has vertical extension to the surface in this region. Given that the porosity loss in the carbonates are not solely mechanical (as will be discussed in the further chapters), Bowers' (1995) method of overpressure origin identification can't be performed on carbonate samples. Contrary to this, shales have been long known as a mechanically compactable sediments (Chierici et al., 1978; Hedberg, 1936; Krushin, 2013; Weller, 1959) and interbedded shale deposits can be a representative of the mechanical deformation in the surrounding formation (Huffman, 2013; Huffman et al., 2011; Weakley, 1990). The deposition environment of the Abadan Plain Basin, as discussed in Chapter 2, was mainly a marine environment and normally, relatively small amounts of clay minerals, and thus shales, were deposited. The thickness of observed shale layers is in the order of few meters and could be as thin as one meter. To consider all available data and remove data peaks to avoid data acquisition errors, a minimum 2 metres thickness is

defined for the data gridding and all log attributes over this interval was averaged. This 2m range was determined as the best compromise between shale discrimination accuracy, logging zone of investigation and amount of available shale data. Then a shale discrimination scheme was applied to the data to pick only shale deposits.

5.2.2.1. Shale Discrimination

Sonic velocity versus vertical effective stress plots are designed to work with shales, and require a method for isolating the shale petrophysical properties associated with measured or inferred pore pressures (and vertical effective stresses). V_{shale}, based on gamma ray data, has been used to discriminate between shales and other rock types. Shale is defined herein as having a V_{shale} greater than 80%. V_{shale} in this research is calculated using the standard liner interpolation equation:

$$V_{shale} = \frac{GR_{log} - GR_{min}}{GR_{max} - GR_{min}} \qquad \text{Equation 5-2}$$

Where GR_{log} is the log measured gamma ray value, GR_{min} is the gamma ray value of clean sand, and GR_{max} is the gamma ray value of a 100% shale deposit (Western Atlas International Inc, 1992). GR_{min} and GR_{max} have been determined separately for each formation to obtain the precise value of V_{shale} (Values for each well and formation are provided in Appendix A). Wherever clean sand or shale was not available, the values of surrounding sediments have been considered.

Concurrently, another filter was applied to the data utilising the neutron porosity and density porosity. This method was introduced by Katahara (2007) on a dataset in the Gulf of Mexico and examined further in that area (Katahara, 2008). In this method, porosity values obtained from Neutron (NPHI) and Density logs (DPHI) are compared, and sediments within a certain range of NPHI-DPHI are identified as shale. This filter was also implemented on data from the Lower Kutai Basin, Indonesia by Ramdhan (2010) and Ramdhan and Goulty (2010), and then by Goodwyne (2012) in the Niger Delta. Katahara (2007) who defined an arbitrary cut-off value of 0.15, while in his other research, an NPHI-DPHI equal to 0.18 has been used. Meanwhile, in the Kutai Basin of Indonesia, Ramdhan (2010) defined a cut-off value of 0.22 to distinguish between grain-supported sand and clay-supported shale. I have used 0.18 as the shale cut-off in the Abadan Plain Basin (Figure 5-2).

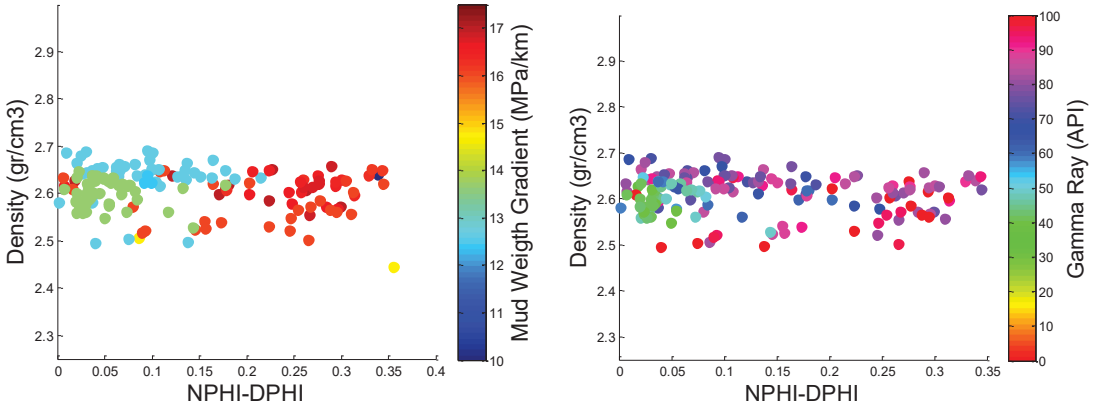

Figure 5-2 –Cross plot of density against the difference between neutron and density porosities estimated from wireline logs. Data are colour-coded by mud pressure (left) and gamma ray (right). An arbitrary cut-off value of NPHI-DPHI=0.18 was used for shales.

After running all shale discrimination schemes, a new dataset with 2 metres resolution has been constructed. As noted earlier, all attributes of the rock such as gamma ray, sonic velocity, and resistivity are averaged over the smoothing interval and used for further analysis. Then, sonic velocity-vertical effective stress trends of this database are plotted and further analysed.

5.2.2.2. Sonic velocity-vertical effective stress evaluation

All well log data of shales in 10 wells of the Abadan Plain Basin are collected to comprise the dataset of this research. Then the petrophysical analyses are applied to examine the possible origin of overpressure in the Abadan Basin. Among the commonly used techniques is Bowers' (1995) method. The core of this technique is identifying the loading curve to investigate the position of overpressured data with respect to it. Ideally, the LC is a collection of data points where the directly measured pore pressure is hydrostatic. However, due to unavailability of direct pressure measurements in the normally pressured interval of the wells, mud weight has been used as a proxy to the pore pressure (discussed in Chapter 3). It is noted that pore pressure could be more than mud weight and consequently, wells could have been drilled in underbalance conditions. Thus, drilling and completion reports are coupled with the geology of the wells to ensure that data points used for LC are from normally pressured formations and adequately set for this purpose. In overpressured intervals, two set of analysis are provided: one uses the mud weight (as a proxy to pore pressure) and the other one considers direct

pressure measurements. Not all of the RFT/MDT intervals contained log data to be included in the dataset. Where possible, sonic velocity data at the close vicinity of the RFT/MDT measurement location is used to represent that data point. Albeit, lithological attributes are carefully considered to verify this kind of approximation and it is valid only in the same lithologies as to where the RFT/MDT data collected.

Vertical effective stress is calculated by extracting pore pressure from the vertical stress. Vertical stress in each point is the force resulted from the weight of overlying deposits. It can be calculated by integrating the rock density over the intended depth interval. The distribution of vertical stress and variation of its magnitude in the Abadan Plain Basin is discussed in Chapter 6. The database is not populous enough to have individual plot for each well, especially for LC evaluation. Thus, all sonic velocity and VES data of all wells are combined as a single cross plot for the entire basin. However, individual cross plots are provided where required and data are inclusive.

5.2.3. Results of Sonic Velocity – Vertical Effective Stress Analysis in the Abadan Plain Basin

The data from 10 wells from 6 oil fields of the Abadan Plain Basin are combined into a single cross plot to investigate the origin of overpressure in this basin using sonic velocity-VES cross plots. A total of 310 data points of interbedded shale are obtained from the shale discrimination scheme whilst 117 normally pressured data points comprise the loading curve. Although the majority of formations in this basin are normally pressured, the loading curve is still comprised of few data points due to lack of well log data in non-reservoir formations. The loading zone is in the form of a polygon that is narrow at left and expands to the right (Figure 5-3). Tingay (2003) has attributed the wide scatter of a loading curve to the following causes:

- lithology variation;
- uplift or chemical compaction, and/or
- differences between the pore pressure measured in sands and adjacent shales. Since the data in this study was filtered only in favour of shales, this may not be the case here.

However, a solid loading curve is essential to conduct appropriate sonic velocity–vertical effective stress analysis. Since shale interbeds, are surrounded by different rock types, rock properties of the shale that represent those deposits could vary by the depositional environment. This can be a reason for wide range of variation in loading zone. A unique loading curve can be obtained by eliminating the effect of depositional environment by defining loading curve for each rock type. Three main rock types have been identified within the normally pressured formations which are: clastics, carbonates, and sandstone (other minor rock types such as evaporates were neglected). Only the clastics (clay rich sediments) were extended to shallow depths that enabled elaborating a loading curve. So loading curve has been defined based on clastics, which is already consistent with other rock types (Figure 5-3). Best fit for the loading curve is provided below with coefficient of determination as 0.36.

$$V=2.0483(\sigma'^{0.1785}) \qquad \text{Equation 5-3}$$

Where V is sonic velocity, and σ' is effective stress.

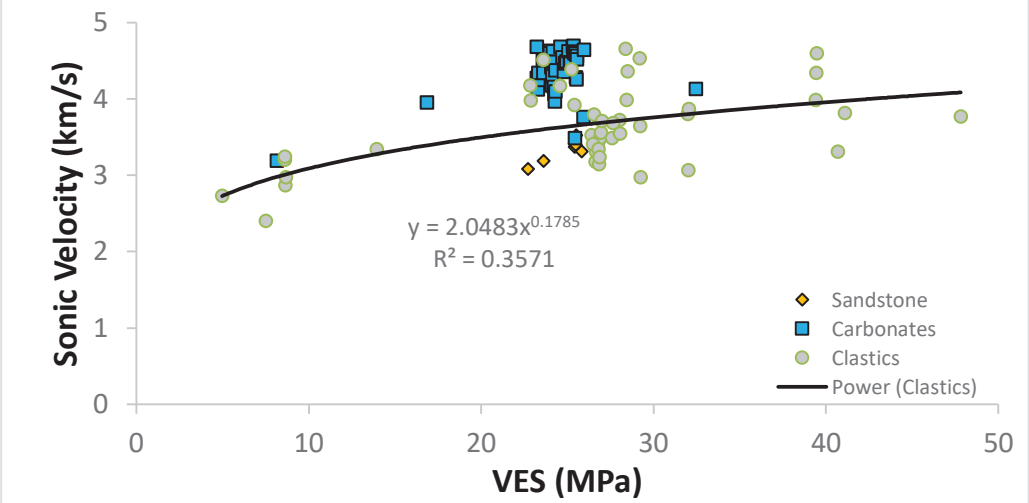

Figure 5-3 – Loading Curve of the Abadan Plain Basin. The loading zone is narrow at left and expands to its right. The power trend of loading curve is also presented.

In the overpressured intervals, 115 data points are mildly overpressured, and 78 data points are moderately overpressured (Figure 5-4). High overpressures were observed in the Gachsaran Formation of northern fields where no wireline log was run and therefore, not presented here. The rest of overpressures that presented in the proceeding figures are formations are either normally pressured, mildly or moderately overpressured. While all overpressured data points lie on the loading curve, right-to-left rollback from the mildly overpressure towards moderately overpressure is observed (Figure 5-4).

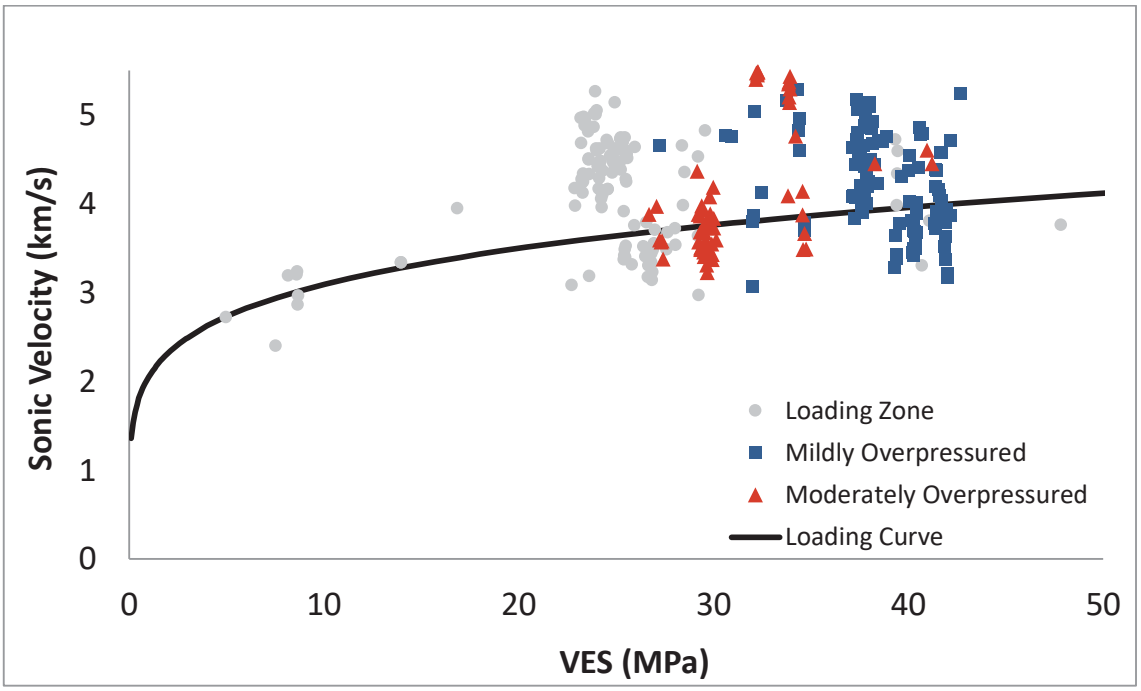

Figure 5-4 – Sonic velocity-VES plot for the Abadan Plain Basin. The pore pressure values are divided into normally pressured (grey circles), mildly overpressured (blue squares; 13.2-15.2 MPa/km), and moderately overpressured (red triangles; 15.2-17.5 MPa/km). Although the Gachsaran formation is highly overpressured in some fields, due to the absence of log data from that section of those wells, no highly overpressured data point is presented. Overpressured points lie on the loading curve, suggesting that a significant component of overpressure in this basin has been generated by disequilibrium compaction.

Directly measured pore pressure data are also plotted in

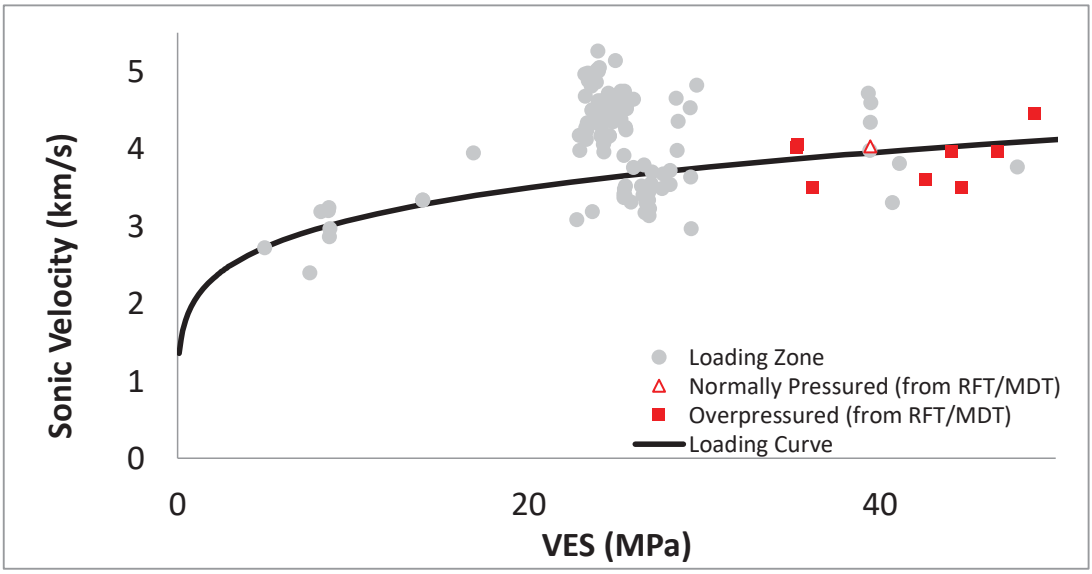

Figure 5-5. As discussed in Chapter 3, the equivalent pressure to mud weight is approximately 10% higher than formation pore pressure. Hence, to justify the normally-pressured data points

from mud weight with the data points from direct measurements, vertical effective stress values are placed at 10% higher than their original values. Overpressures still lie on the loading curve.

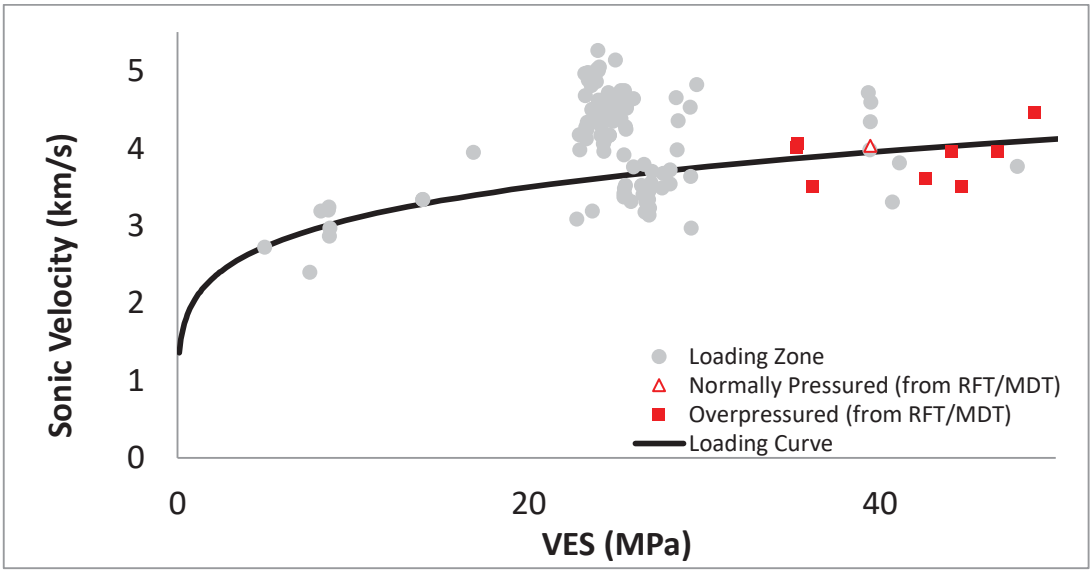

Figure 5-5 - Sonic velocity-vertical effective stress plot using the direct pressure measurement in the Abadan Plain. The normal compaction trend is defined by the zone of grey circles. Overpressured data are from direct pressure measurements. Since the mud weight is normally 10% above the pore pressure, vertical effective stress (VES) is justified to offset the difference between the two pore pressure values of RFT/MDT and mud weight. Similar to Figure 5-4, overpressured points lie on the loading curve, suggesting that overpressures have been generated by disequilibrium compaction.

Sonic velocity–vertical effective stress analysis has also been conducted individually on each of the overpressured Gadvan, Fahliyan, and the rest of shallower mildly overpressured formations using all data within the Abadan Plain Basin (Figure 5-6). Shallow mildly overpressured formations lie on the right end of the loading curve and, the data points from Gadvan and Fahliyan formations exhibit a reversal on the loading curve.

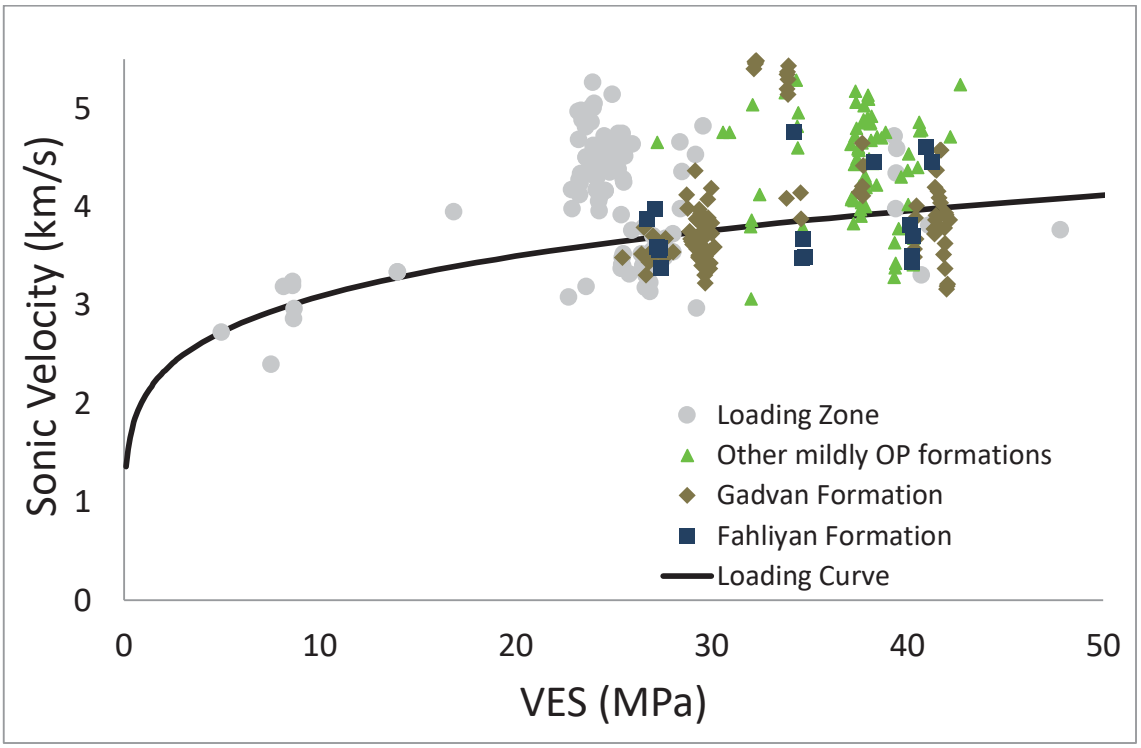

Figure 5-6 - Sonic velocity–vertical effective stress plots for the Gadvan, Fahliyan and rest of shallower mildly overpressured formations.

In a well scale overview, the majority of wells exhibited DC trend. Mildly overpressured data points 'off the loading curve' belong to wells A-6, J-4 and D-5 whereas moderately overpressured data points 'off the loading curve' are from wells D-5 and D-15 (Figure 5-7). As a regional trend, the fields at the southern part of the basin (field D and H) lie on the right end of the loading curve whilst the northern fields (field J and Y) typically lie on the middle of the loading curve, indicating higher overpressure magnitudes. Meanwhile, data of well A-6 seems to be more scattered and found in both areas.

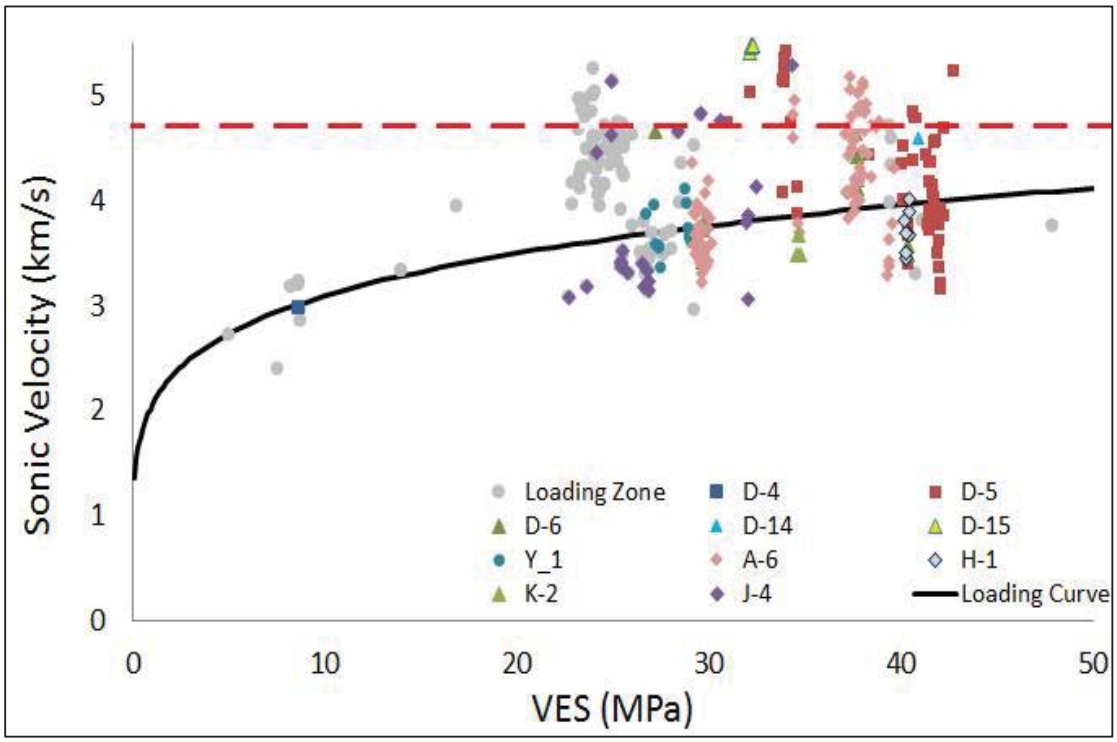

Figure 5-7 – The sonic velocity-VES cross plot of the mildly and moderately overpressured data points. Normally pressured data points are in grey circles and the envisaged maximum velocity of normally pressured shales are set to the maximum velocity in the Fahliyan Formation (Figure 5-6) shown with dashed line. The points which lie above the loading zone are most likely the data with higher velocities and could be marl, argillaceous limestone or other types of denser deposits with similar attributes to shales.

5.2.1. Discussion on Sonic Velocity – Vertical Effective Stress Analysis in the Abadan Plain Basin

The majority of the overpressured data points lie on the loading curve, which suggests a disequilibrium compaction overpressure mechanism in this basin. Some overpressured data points slightly lie 'off the loading curve', which could indicate an additional component of fluid expansion or transfer related mechanisms. However, it should be noted that these 'off the loading curve' points are not displaying a VES-sonic 'path' that is consistent with fluid expansion overpressure, as they are not 'shifting to the left' of the loading curve, which would indicate increasing pore pressure with little change in porosity. Rather, the 'off the loading curve' overpressured points appear to be simply sections of anomalously high sonic velocity, but with little change in pore pressure, and are essentially moving 'upwards' away from the loading curve. Hence, these 'off the loading curve' data points are interpreted to be due to stiffer/faster rock section, such as argillaceous limestones or marls that simply display similarly high GR values to 'cleaner'

shales. The inclusion of anomalously fast velocity zones within the VES-sonic dataset, and the resulting 'false positive' fluid expansion overpressure signature, is a consequence of the shale discrimination methods and 2m sample interval used. However, as discussed previously, this sample interval provides the best compromise herein between data robustness and having a statistically meaningful dataset. Moreover, 'off the loading curve' data points are restricted to a few wells (D-5, D-15, A-6) and it cannot be decisively a sign of FE overpressure generation in the entire basin. It must also be noted that left and upward path might indicate overpressure due to fluid expansion in those wells and therefore, other techniques are utilized in the proceeding section of this chapter to assess the possibility of such mechanisms. The maximum sonic velocity in the abnormally pressured Fahliyan Formation is 4.7 km/s (Figure 5-6), represented by a dashed line in Figure 5-7. Hence, for the purposes of this overpressure origin analysis, I have considered this velocity to represent the uppermost 'pure shale' velocity, and used this to discriminate between pure shales and other likely fast lithologies, such as argillaceous limestones. This process is not uncommon, and represents the V_{max} point used in the Bowers' (1994) pore pressure prediction methodology.

It should also be noted that normal loading is in the form of an expanded polygon which expands towards the right. This pattern of the velocity-density cross plots is a common attribute of LC. While in some areas it may form a line, in most areas it is in the form of an interval or polygon. The polygon seems to be a little wider than in other areas studied in the literature (Tingay et al., 2009; Tingay et al., 2013), which is one main reason that I attribute it to varying acoustic velocity in the shales. Some high velocity layers might have been considered as shale deposits in this investigation which has made the loading polygon a little bit wider than in previously published investigations. This study is the first work performed on thick carbonate strata interbedded with thin shale deposits and given the different size/length of investigation, and thus resolution, of sonic and GR logs (GR resolution>sonic resolution), there is an increased potential of the sonic log to be measuring both shales and surrounding carbonates, whilst GR is measuring properties of just a shale interbed. This has made the shale attributes different from those found in thick shale formations such in Brunei, Sumatra and East Java basins SE Asia (Jenkins et al., 2012; Tingay, 2003) or Baton Rouge in Louisiana and the East Delaware basin in Texas, North America (Cox et al., 2007; Luo et al., 1994).

Northern fields of the Abadan Plain Basin generally exhibit higher magnitudes of overpressure (Figure 5-7; data points at the middle of the loading curve, indicating low VES) than southern fields (data points at the far end of the loading curve and thus, higher VES). The high magnitude of overpressure in the northern fields, which is closer to the Zagros Deformation Front is most likely controlled by the tectonic activities of the Zagros Orogeny. As discussed in Chapter 4, tectonic forces cause mechanical compaction in the rock and hence, provides another evidence of DC overpressure generation in this basin. However, a general cross section of the pressure in all wells, presented in Figure 5-8, hasn't provided any clear link between the well positions with respect to the Zagros Deformation Front and overpressures in the Gadvan and Fahliyan formations. As discussed in Chapter 3, there is a side influence of Zagros Orogeny on the overpressures in the Gachsaran formation. Although the degree of influence of tectonic forces on the overpressure generation/development in the Gadvan/Fahliyan horizon hasn't been certainly evaluated, it is probable that it has contributed to the overpressure generation by putting additional load on the formation. The potential of providing structural seal or conductive faults by tectonic forces hasn't been examined research due to unavailability of seismic and other required data.

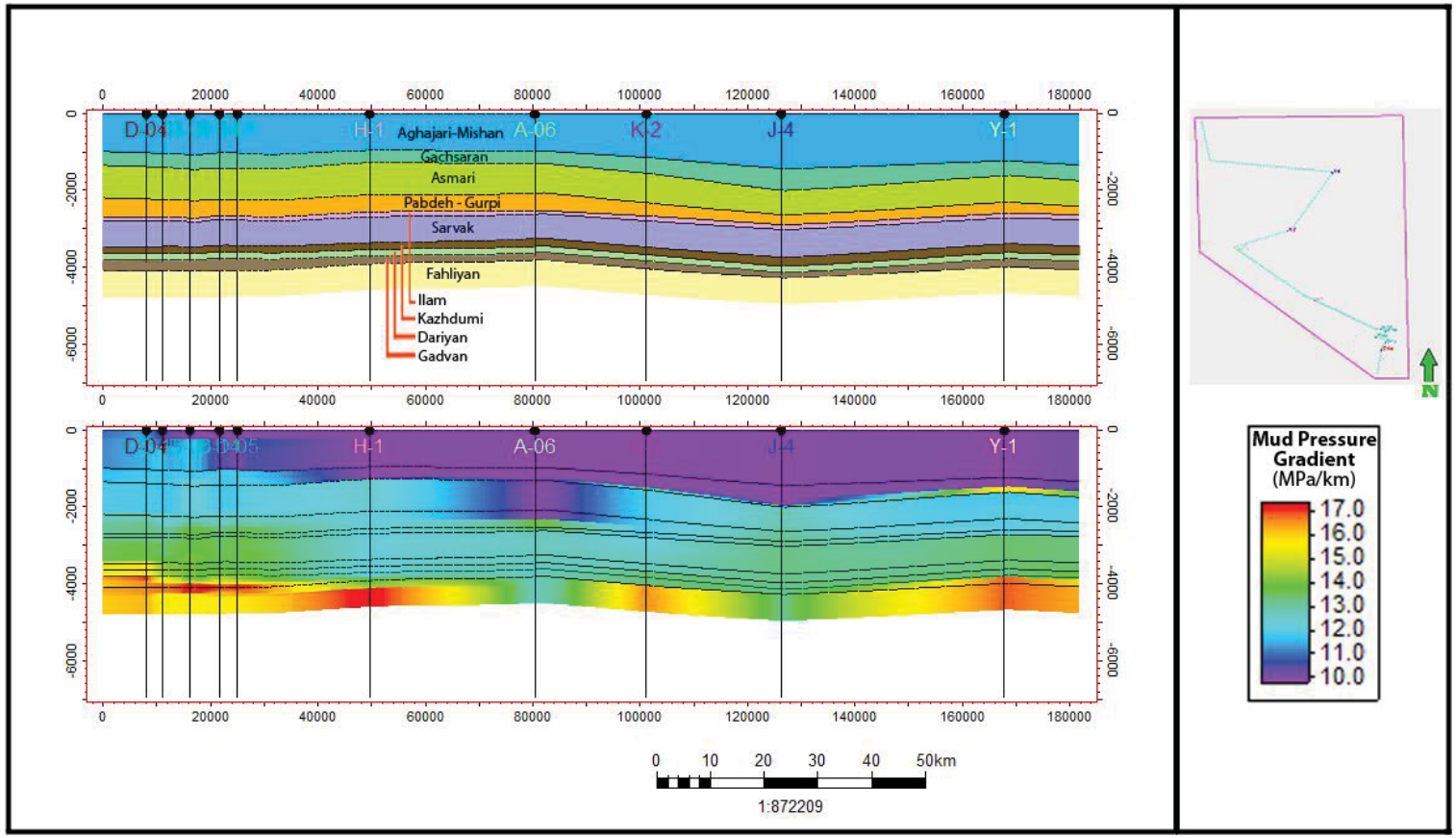

Figure 5-8 – Pore pressure profiles of the general cross section passing all wells studied in the Abadan Plain Basin. Pore pressure is represented by mud weight. The overall trend of layers is dip towards the Zagros Fold-Thrust Belt at north-west. The variation of mud weight by depth is shown and this differs between the fields. A low pressure gradient in A-6 in the formations above Sarvak is due to a lack of data which is shown as hydrostatic gradient.

5.2.4. Conclusion of Sonic Velocity – Vertical Effective Stress Analysis in the Abadan Plain Basin

Pore pressure in the Abadan Plain Basin deviates from the hydrostatic gradient at varying depths in each of the wells studied here. To identify the overpressure origin, a set of discrimination criteria has been applied on the dataset to filter clastic deposits and then, a comparative method of sonic velocity-vertical effective stress cross plot of Bowers (1995) was performed on the filtered shale data. Clastic deposits such as shales were frequently observed in the deeper formations, such as Kazhdumi and Gadvan while few traces of shales were observed in the shallower overpressured horizon of the Gachsaran formation. Nevertheless, the loading curve was successfully defined using the available data points from normally pressured strata and then, overpressures were analysed with respect to it. As a result, disequilibrium compaction has been identified as the main overpressure generation mechanism in this the Abadan Plain Basin. A few cases of upward 'off the loading curve' trend were also observed, which is believed to be due to the inclusion of stiffer deposits such as argillaceous limestone or marls into the dataset. Yet, these findings require further support from the other analyses to identify the most likely origin of overpressure in this basin. In the next section, velocity-density cross plots will be analysed to investigate the possibility of other mechanisms contributing to overpressure generation.

5.3. Sonic Velocity-Density and Resistivity-Density Log Response to Overpressures in the Abadan Plain Basin

5.3.1. Introduction

Cross plots of sonic velocity and density in shales are a relatively recently proposed method for helping to identify overpressure generation mechanisms (Bowers, 2001; Hoesni, 2004; Katahara, 2003, 2006, 2007; Lahann et al., 2001). Whilst these plots are sometimes used in isolation (Ramdhan and Goulty, 2011), they are particularly useful when compiled in conjunction with porosity-VES plots, and when used in comparison with local geology (Katahara, 2003, 2007; Lahann et al., 2001; Tingay et al., 2013). However, unlike porosity-VES or sonic velocity-VES cross plots that only help to identify the overpressures generated by DC, fluid expansion or transfer mechanisms, sonic-density cross plots have the additional benefit to being able to potentially distinguish between different fluid expansion or transfer overpressure mechanisms (Hoesni, 2004; Lahann et al., 2001).

In normally compacted rocks, such as fine grained mud rocks, porosity is primarily controlled by the mechanical compaction (Dickinson, 1953; Hedberg, 1926; King Hubbert and Rubey, 1959). The burial rate in the rocks undergoing normal compaction is slow enough to let the pore fluid to discharge the pore space. In such conditions, density and sonic velocity, which are both related to porosity, exhibit a proportional response to compaction that is referred to as the loading curve. However, transport properties such as sonic velocity, permeability and resistivity are more responsive to the elastic attributes of rock than bulk properties like porosity and density. Bulk properties are dependent only on net pore volume, while transport properties are sensitive to pore geometry as well as pore network (Bowers and Katsube, 2001). The pore system in a rock is a combination of relatively large, high aspect ratio ‘storage pores’ connected together through smaller, lower aspect ratio ‘connecting pores’, and each exhibit different responses to confining load (Figure 5-9).

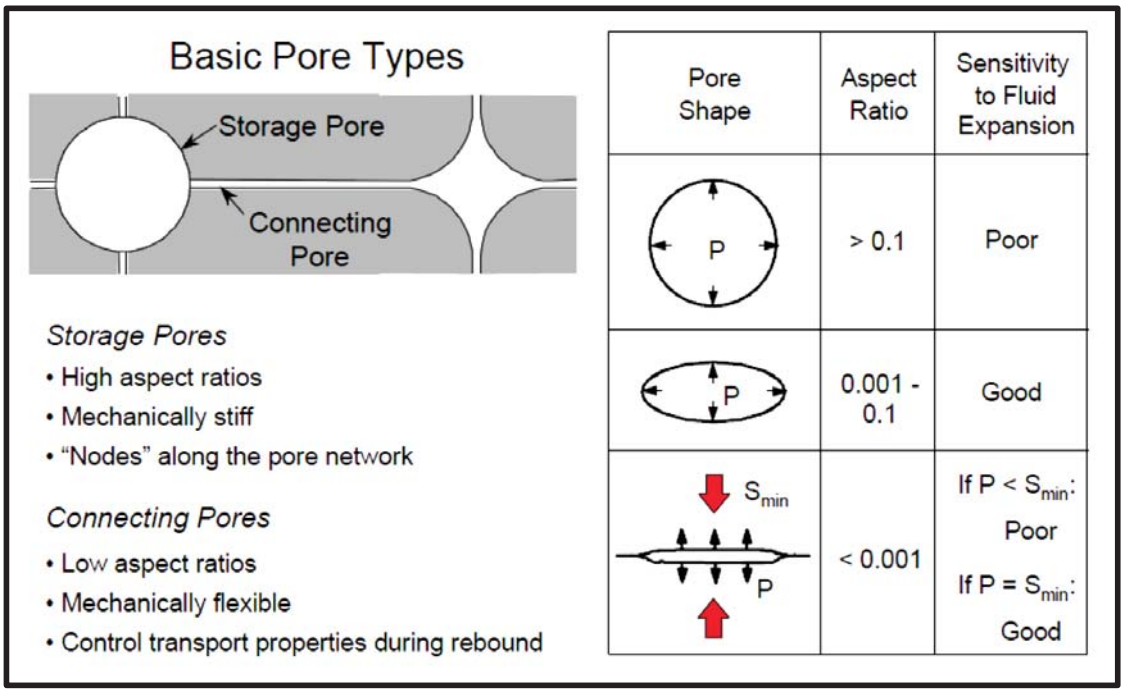

Figure 5-9 - Pore structure models used to characterize the deformation behaviour (Goodwyne, 2012), after Bowers and Katsube (2001).

Compaction of a rock during burial has a great degree of irreversible deformation component (Hedberg, 1926; Skempton, 1969; Weller, 1959) which is associated with grain rearrangements. The inelastic component of compaction is mainly due to closure of storage pores which cannot be reopen after removing the load. In contrast, connecting pores with small aspect ratio widen during the load reduction (Cheng and Toksöz, 1979; Toksöz et al., 1976). An undercpmpacted rock is at their maximum effective stress in present time and thus, both of storage and connecting pores have undergone deformation at the same way. When the load decreases (unloading), the width of connecting pores increase which leads to a change in the number of intergranular contacts for transmitting sound and consequently, altering the flow path size for fluid and electrical current (Bowers, 2001). Consequently, the response to unloading is much greater in sonic velocity and resistivity (transport properties) than density and porosity (bulk properties). This can be observed when transport properties and bulk properties are plotted versus each other (i.e. sonic velocity vs. density) whereas both parameters will be on a single path (loading curve) if the pores are pressurized with loading curve (Figure 5-10). Any departure from the LC is interpreted as a signature of unloading where

elastic rebound occurs until the past maximum effective stress is reached and inelastic deformation resumes (Bowers, 2001).

In a normally compaction, as well as DC overpressuring, both of transport and bulk properties change according to the compaction of the rock. Therefore, lower values of VES in overpressured zone are proportional to the lower velocity/resistivity and density and thus, a reversal on the loading curve. Contrary to this, fluid expansion unloading is associated with a decrease in velocity while density exhibits minor decrease (Figure 5-10a). In a clay diagenesis process, excess pore water is released into the confined pore space and from that point, velocity-density plot shifts from smectitic trend towards illitic trend (Figure 5-10b). Indeed, this process is a natural diagenetic evolution of clay-rich minerals and can happen even when there is no simultaneous/consequential increase in overpressure

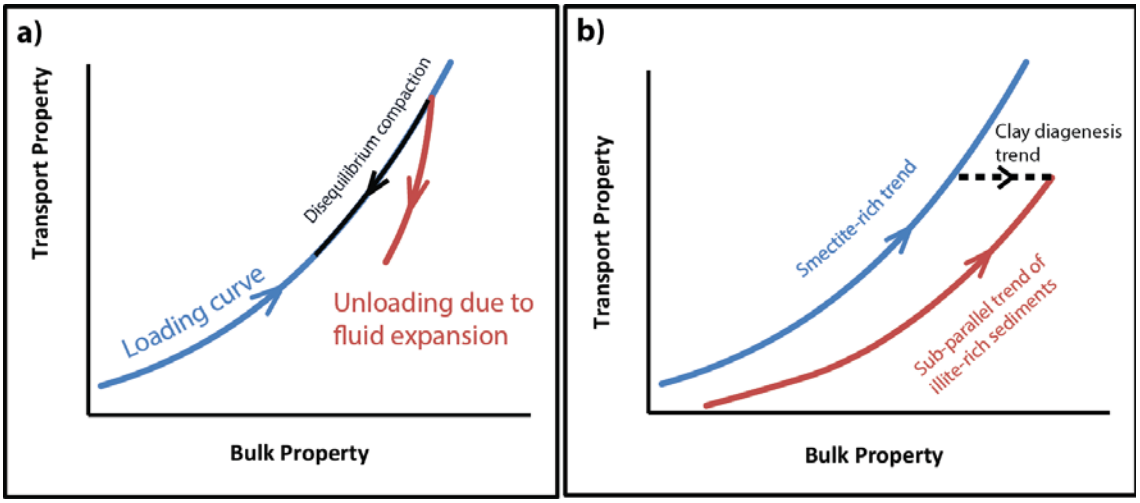

Figure 5-10 – Influence of fluid expansion on the transport property-bulk property cross plot. The blue curve is the loading curve and unloading departure due to kerogen maturation (a) and clay diagenesis (b) is illustrated.

For example, the impact of smectite/illite proposition in some basins in the Gulf of Mexico shelf, with different shale mineralogy, revealed vanishing trend from the loading curve (Katahara, 2003; Lahann et al., 2001). A different (basically slower) sonic velocities in illitized shales than those with a higher smectite content and hence, unloading path for smectite-illite transformation was identified. Clay diagenesis is associated with increased density which shifts from the loading curve towards right (Hoesni, 2004, Figure 5-11). Alternatively, kerogen

maturation and aquathermal fluid expansion decrease the density, making them distinguishable from clay diagenesis (Lahann et al., 2001). This is noticeable as a downward trend in the cross plot (Figure 5-11). A combination of such overpressure origins would allow a minor density increase and right-downward departure from loading curve. Analyses based on potential departures from loading curve in sonic velocity-density plots have been widely used in several geological settings such as shales of the Gulf of Mexico (Bowers, 2001; Katahara, 2003; Lahann et al., 2001), mudrocks of the Kutai Basin, Indonesia (Ramdhan, 2010; Ramdhan and Goulty, 2010; Ramdhan and Goulty, 2011), and the Northern Malay Basin, SE Asia (Tingay et al., 2013).

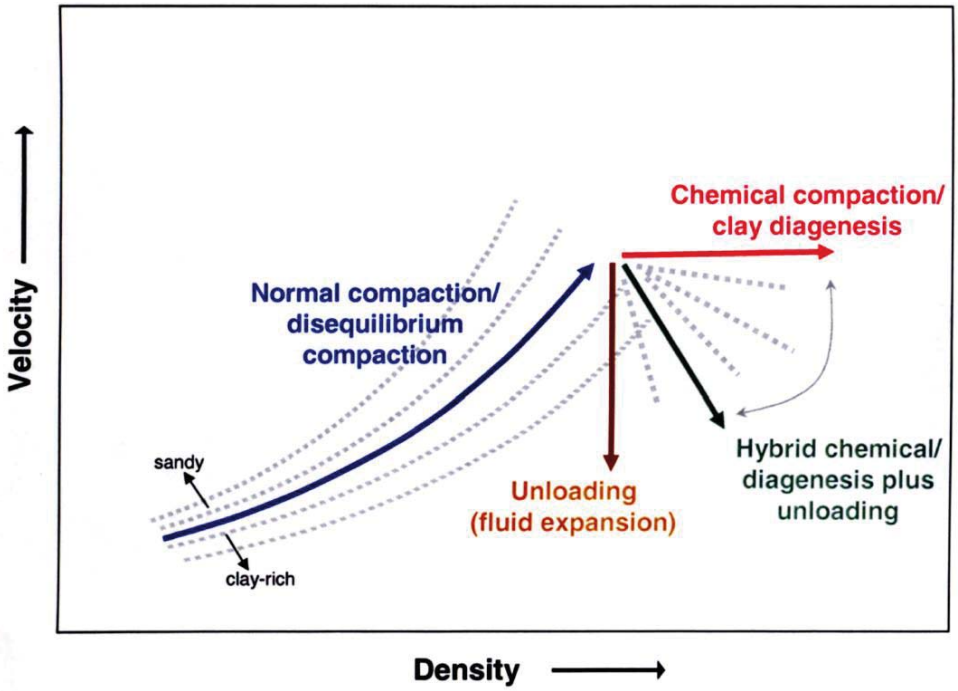

Figure 5-11 - Typical velocity vs. density cross plot and the signature of causal overpressure generation mechanisms (Hoesni, 2004).

Similar trends for resistivity-density plots can be expected. However, despite having the same concept as sonic velocity-density analysis, resistivity-density cross plots were rarely utilized for identifying overpressure origin and, to the best of my knowledge, was only tested in the Lower Kutai Basin, Indonesia (Ramdhan and Goulty, 2010). To date, this method was mainly used to determine the possibility of unloading mechanism, and was not explained in detail as

to whether it can distinguish between several unloading processes or not. In this research, it is used for the unloading identification too.

5.3.2. Methodology

Sonic velocity-density and resistivity-density plots are constructed to determine the origin of overpressure in the Abadan Plain Basin. The discriminated shale dataset used in the sonic velocity-VES analysis is used here. All data from 10 wells were combined together to construct a single cross plot. Although each well, field or basin may have its own loading curve, due to limited number of shale data points, I have first examined the data of entire basin, then, further analyses in individual wells are also provided where required. As discussed earlier, the data is a bit widely scattered in this study than usual analysis and hence, difficult to suggest a single loading curve. Instead, loading curve consisted of data from normally pressured formations is in the form of a polygon (Figure 5-12). A best fitting trend line crossing these points is in the form of Equation 5-4. Alternatively, I assumed that all data can be anywhere between the upper and lower bound of sonic velocity-density trend in normally pressured sediments (will be explained later). However, it seems the loading curve of individual wells comprising their own normally pressured data are generally steeper than the upper and lower bound, but within that interval.

$$velocity = 0.29e^{1.03density} \qquad \text{Equation 5-4}$$

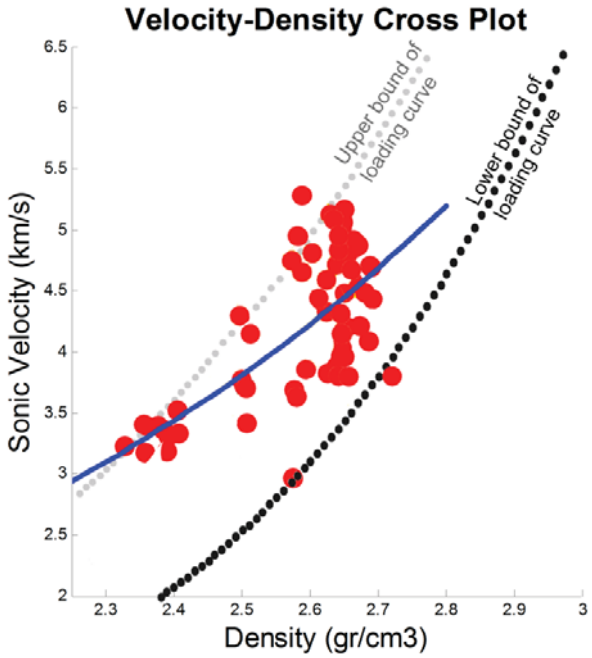

Figure 5-12 – Normally pressured data and loading curve for the data from the Abadan Plain Basin. Best fitting trend line is presented as a blue solid line. The grey and black dashed lines are the upper and lower bound for the loading zone.

Several empirical relationships between sediment velocity and density have been published (Bowers, 2001; Brocher, 2005; Christensen and Mooney, 1995; Dutta, 2002; Gardner et al., 1974; Ludwig et al., 1970) and can be used to compare and contrast against the velocity and density data in the Abadan Plain basin. These relationships are particularly useful for evaluating expected sonic-density loading curve trends and how to distinguish overpressure origins where observed data points deviate from it. Some of the published and commonly used relationships are presented in Figure 5-13.

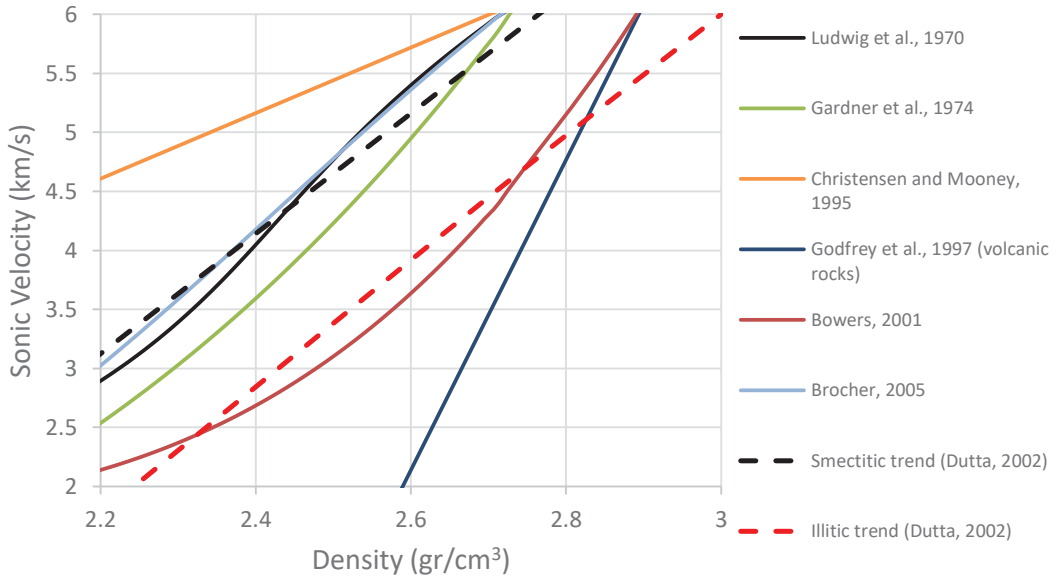

Figure 5-13 – Comparison of published velocity-density relationships. The equations are plotted for an interval where most of the data from the Abadan Plain Basin observed. Equations are from Ludwig et al. (1970), Gardner et al. (1974), Christensen and Mooney (1995), Godfrey et al. (1997), Bowers (2001), Dutta (2002) and Brocher (2005).

Among these equations, the most appropriate relationship for the area of study has been identified, after a short overview of published bounds. I attempted to define the upper and lower bound of a loading zone by two of the aforementioned relationships. Consequently, any unusual data point placement or trend with respect to the loading zone may indicate fluid expansion or pressure transfer mechanism of overpressure generation. One upper and lower bound compaction trend has been introduced by Dutta (2002) in the Gulf Coast shales of the Miocene deposits. Dutta (2002) proposed that diagenesis causes different incremental trends in bulk density for a given sonic velocity in eodiagenesis (smectitic) and telodiagenesis (illitic) deposits (Figure 5-14).

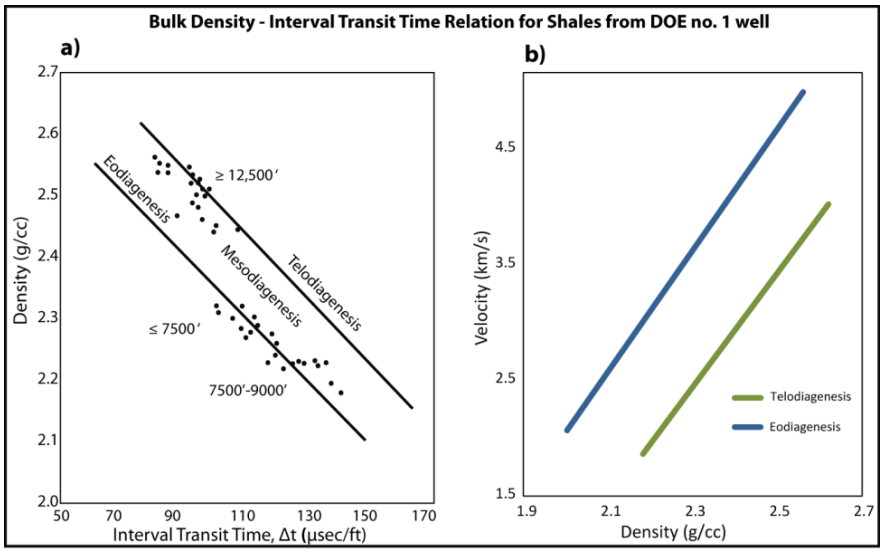

Figure 5-14 – a) Density-interval transit time (slowness) of shales in the Gulf Coast obtained from well log data (Dutta, 2002) and b) schematic velocity-density cross plot based on that data. Ramdhan (2010) believes that the eodiagenesis trend is the compaction of smectite while the telodiagenesis trend represents the illitic compaction.

The majority of data points in this basin lie between these two boundaries. However, the clay diagenesis of the basin hasn't been well examined yet and, therefore, instead of such linear trends, I have herein attempted to define alternative boundaries in close proximity to smectitic/illitic trends. Once again, it must be noted that the basin-wide boundaries are just peripheral tools that help identifying 'off the loading curve' data points and albeit, each field may have different loading curves. Gardner et al.'s (1974) equation is one of the frequently used velocity-density relationships and given by:

$$\rho = \eta V^{\beta} \qquad \text{Equation 5-5}$$

Where ρ is density, V is sonic velocity, and η and β are empirically derived constants. The best fitting commonly used values are η= 0.23 and β=0.25 for density in (g/cm^3) and velocity in (ft/m), but they are also often locally varied. The equation with best fitting parameters, turns into the following form for velocity in (m/s) and is considered to be the upper bound for density as a function of shale velocity:

$$\rho = (0.31V)^{0.25} \qquad \text{Equation 5-6}$$

Bowers (2001) introduced another relationship which defined the lower bound for shale velocity of his data as a function of density:

$$V = 4790 + 2953\,(\rho - 1.3)^{3.57} \qquad \text{Equation 5-7}$$

Equation 5-7 uses the same abbreviations as Equation 5-6 and velocity in feet per second (ft/s). Equation 5-7 turns into the following form for velocity in meters per second (m/s) using a 3rd order polynomial regression:

$$V = 2779.7\rho^3 - 14950\rho^2 + 27357\rho - 15286 \qquad \text{Equation 5-8}$$

Whilst the data points are limitted to the upper bound, the abovementioned lower bound doesn't seem inclusive of all normally pressured data in this basin. The lower bound of the loading zone in the Abadan Plain Basin is defined by a modification to the Bowers' (2001) Equation 5-7 and becomes as follows:

$$V = 2700 + 2953\,(\rho - 1.3)^{3.57} \qquad \text{Equation 5-9}$$

Unlike sonic velocity, no empirical relationship of resistivity and density exists. The loading zone of the resistivity-density cross plot is defined by the boundaries of an area that is comprised of normally pressured data points. The loading zone can't be practically defined in well-scale as the data from normally pressured formations is not available in all wells. But the data trend of individual wells with respect to the loading zone of the basin is provided in where required. Any departing trend from the LC in such cross plots can be a signature of unloading (fluid expansion or pressure transfer). In the upcoming section, the velocity-density and resistivity-density cross plots of the shales interbeds in the Abadan Plain Basin will be displayed and discussed.

5.3.3. Results of Sonic Velocity–Density and Resistivity-Density Cross plot Analysis in the Abadan Plain Basin

Velocity-density and resistivity-density cross plots of 10 wells in 6 fields in the Abadan Plain Basin have been constructed to examine the origins of overpressure, and to subsequently help guide selection of proper pore pressure prediction methods. The equations of Gardner et al. (1974) and modified Bowers (2001) set the upper and lower bound of the loading curve respectively. In Figure 5-15, the data points from all wells are plotted in a single chart that is colour-coded by pore pressure gradient (a) and effective stress gradient (b). Although it seems that the deeper sediments are shifted towards the bottom right of the loading curve, they are still within the loading zone, and there are shallower data underlying these, as can be more clearly seen in Figure 5-16 where the data points are colour-coded by depth of burial.

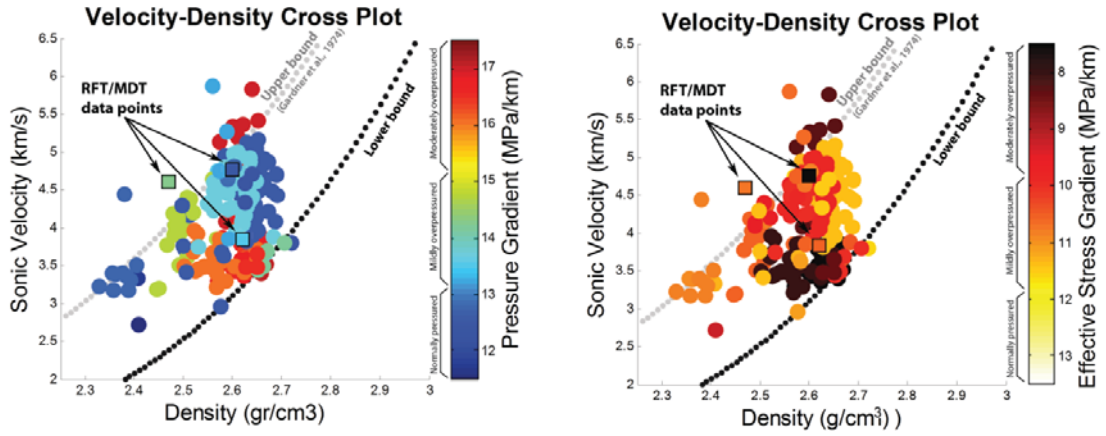

Figure 5-15 – Sonic velocity-density cross plot of 10 wells studied in the Abadan Plain Basin. Grey and black dotted lines are the upper and lower bound for shale loading zone respectively. The data points are colour-coded by a) pressure gradient and b) effective stress gradient. The majority of data points lie between or within areas around the upper and lower bounds which indicates disequilibrium compaction as the primary origin of overpressure in this basin. The data are divided into three areas of normally pressured, mildly overpressured and moderately overpressured. A few RFT/MDT measurements in mudrocks are also indicated by squares.

In the Abadan Plain Basin, both of the normally-pressured and overpressured data points on the velocity-density cross-plot lie between the upper and lower bound for shale. The pore pressure is estimated from mud weight and classified into three areas of normally-pressured (below 13.2 MPa/km), mildly overpressured (13.2 – 15.2 MPa/km) and moderately overpressured (15.2 - 17.5 MPa/km).

The density of sediments is supposed to be higher in deeper sequences, but the pore pressure is also observed abnormally higher in some of the deeper units. Although plotting sonic-density with respect to depth (Figure 5-16) does not, on its own, highlight any specific overpressure origin, it does help illustrating that a few data points that lie outside the loading zone are not necessarily from the deep Fahliyan Formation, but also shallower deposits such as the Dariyan Formation. It also highlights some of the attributes of the loading 'path' which seems steeper than loading bounds.

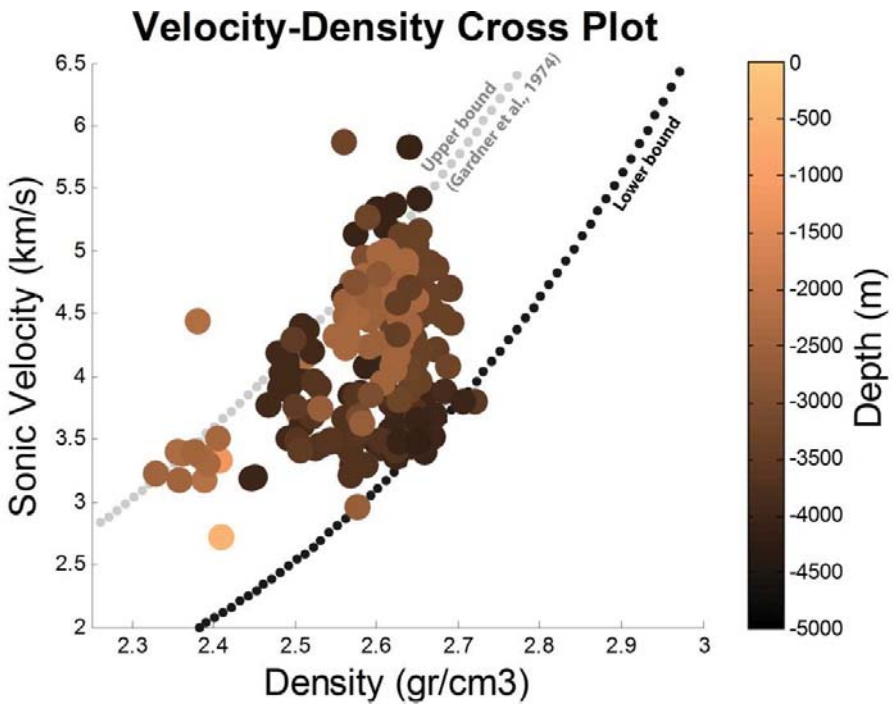

Figure 5-16 - velocity-density cross plot of the data from all wells studied in the Abadan Plain Basin color-coded by depth of burial. Grey and black dotted lines are the upper and lower bound for shale loading zone respectively. The majority of data points lie between or within areas around the upper and lower bounds which indicates that overpressure origin in this basin is most likely disequilibrium compaction.

However, it should be noted that some overpressured data points do appear to fall at the bottommost part of the normally pressured loading zone, and thus may indicate a non-disequilibrium compaction component of overpressure. The majority of these data points are from wells A-6 and D-6, the sonic-density cross plots for which are displayed in Figure 5-17 and Figure 5-18 respectively. The combined analysis with sonic velocity-VES doesn't provide a clear signature of unloading in these two wells.

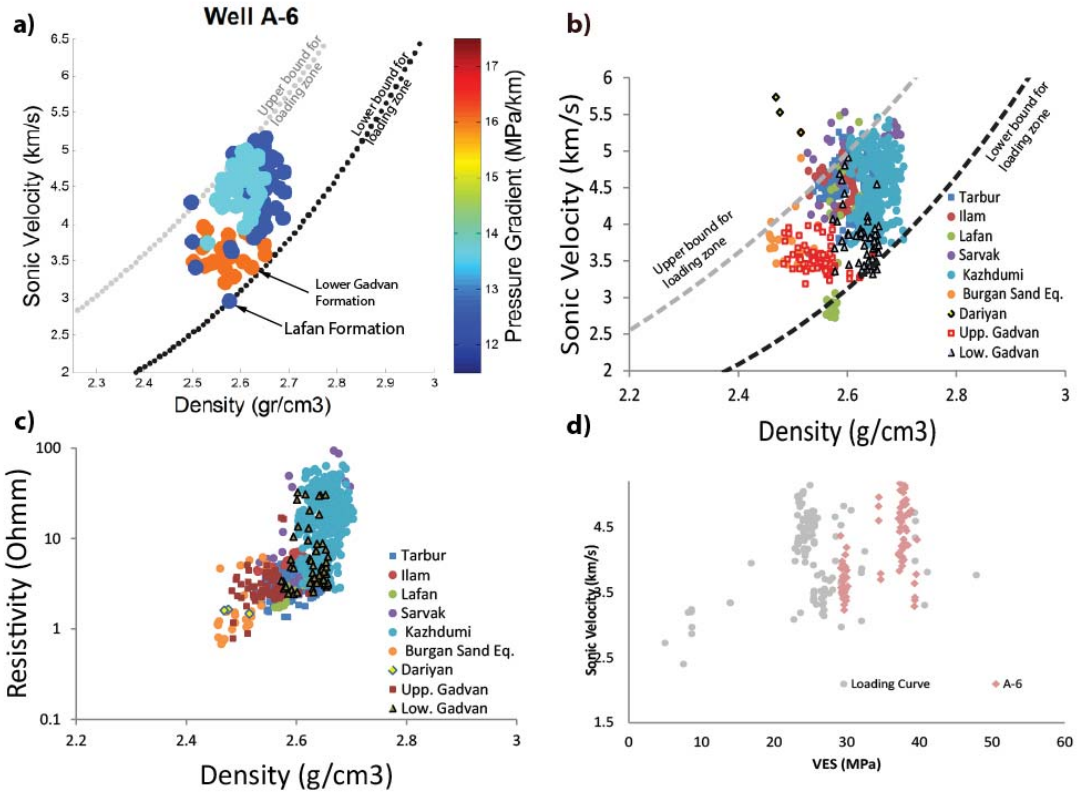

Figure 5-17 - a) Velocity-density cross plot of the data in well A-6 colour-coded by pressure gradient. Near the lower bound data points of the overpressured Gadvan and normally pressured Lafan formations are indicated. b) Velocity-density cross plot of the data in well A-6 classified according to formations. In this plot, the data were not averaged and all shale data are plotted. c) Resistivity-density cross plot of well A-6 suggests DC compaction as the origin of overpressure. d) Sonic velocity-VES cross plot in well A-6 which also indicates the DC component of overpressure.

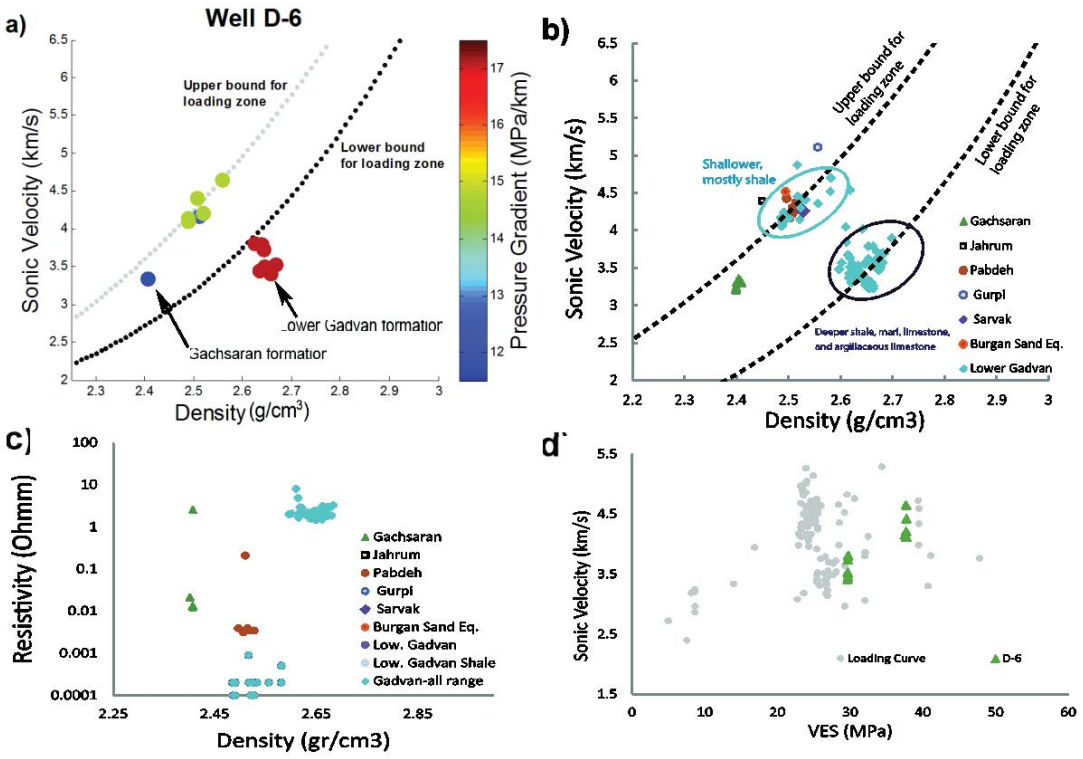

Figure 5-18 - a) Velocity-density cross plot of the data in well D-6 colour-coded by pressure gradient. b) Velocity-density cross plot of the data in well A-6 classified according to formations. In this plot, the data were not averaged and all shale data are plotted. The possible signature of unloading in the Gadvan Formation is indicated. c) Resistivity-density cross plot of well A-6 has more discrepancy. d) Sonic velocity-VES cross plot in well A-6 which also indicates the DC component of overpressure.

Similar to sonic velocity, the variation of resistivity, as another transport property of the rock, with respect to density was also investigated. The resistivity-density cross plot was constructed for all wells of the Abadan Plain Basin (Figure 5-19). The loading zone has been defined using the normally pressured data points shown as a dashed line in Figure 5-19. Almost all data points lie on the loading zone, confirming disequilibrium compaction as the origin of overpressure in this region. There are a few data points beyond the loading zone in the Lower Gadvan Formation of well Y-1 and D-6 which doesn't show a trend, but some very low resistivity readings. This will be discussed in further section.

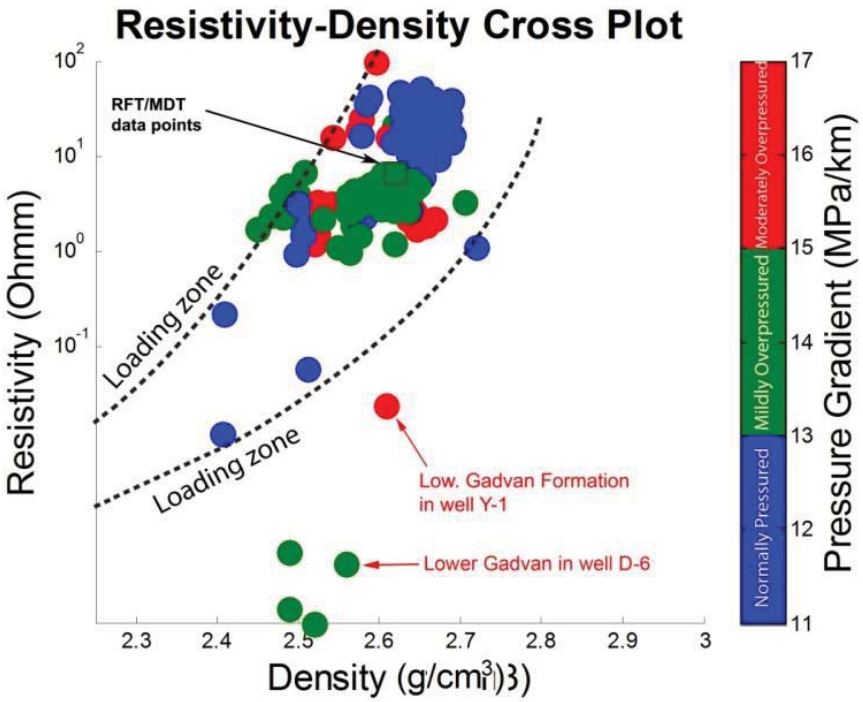

Figure 5-19 – Resistivity-density cross plot of the wells in the Abadan Plain. The off the loading curve data belongs to the Lower Gadvan Formation in wells Y-1 and D-6. Such departure from the loading zone hasn't been observed in the other wells. Since this behaviour is seen only in this well and the rest of wells follow a loading curve, it could be due to a very conductive (saline) fluid in the pores which probably is a result of drilling fluid intrusion into the formation. RFT/MDT measurements are also indicated. There were few direct pressure measurements in the mudrocks.

Collective cross plots of the rest of the wells are provided below. They include all available data that are not perfectly inclusive of all formations. However, they provide a more comprehensive knowledge of the possible overpressure origins.

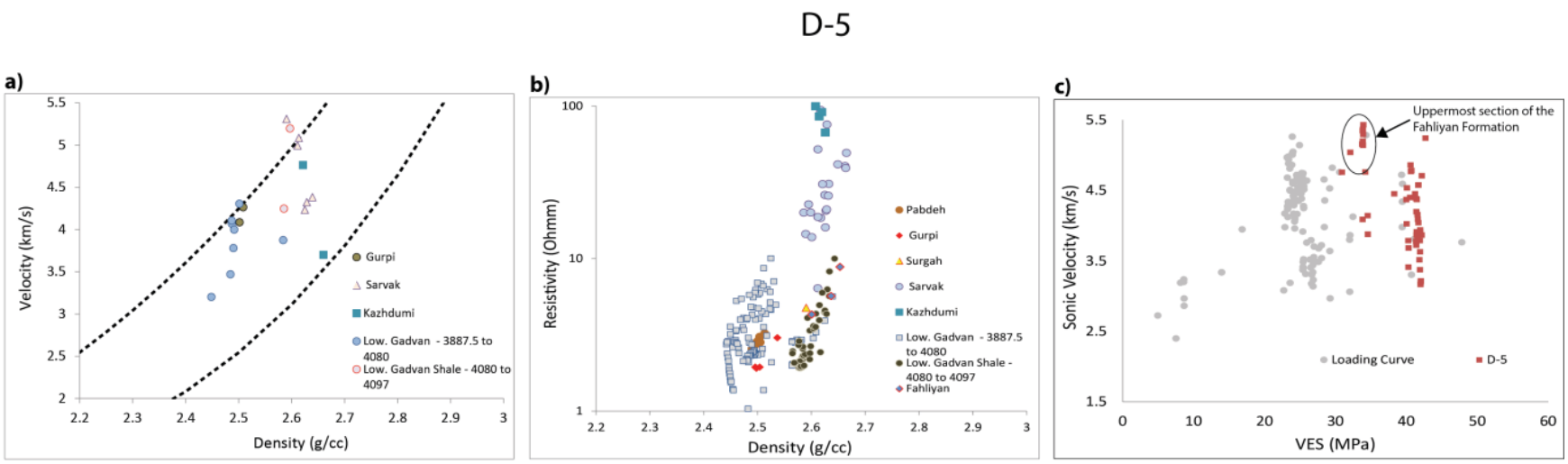

Figure 5-20 - a) Velocity-density cross plot of the data in well D-5 classified according to formations. All data lie on the loading curve suggesting DC as the overpressure origin. b) Resistivity-density cross plot of well D-5 in which the data of overpressured formations general follow the loading curve. However, shale deposits of the Lower Gadvan and Fahliyan formations are slightly shifted towards right of the normally pressured formations which can suggest a minor contribution of fluid expansion to overpressure. c) Sonic velocity-VES cross plot in well D-5 also indicates the DC component of overpressure. The plausible 'off the loading curve' cloud at the top of this plot belong to the carbonate deposits of the Fahliyan Formation.

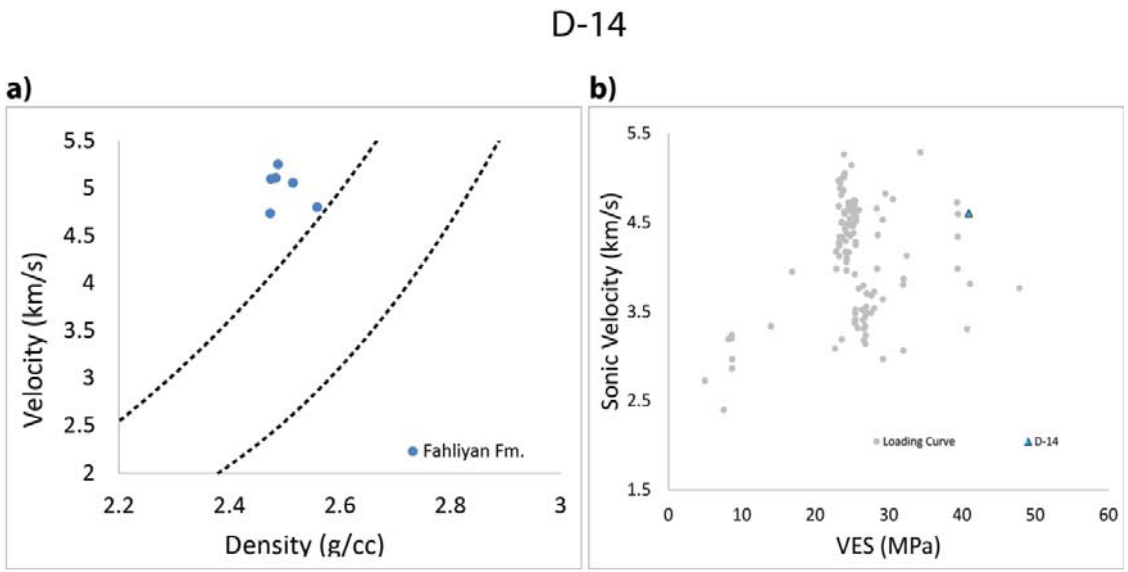

Figure 5-21 – a) sonic velocity-density cross plot of well D-14. b) Sonic velocity-VES cross plot of the same well. It suggests DC as the primary origin of overpressure in this well.

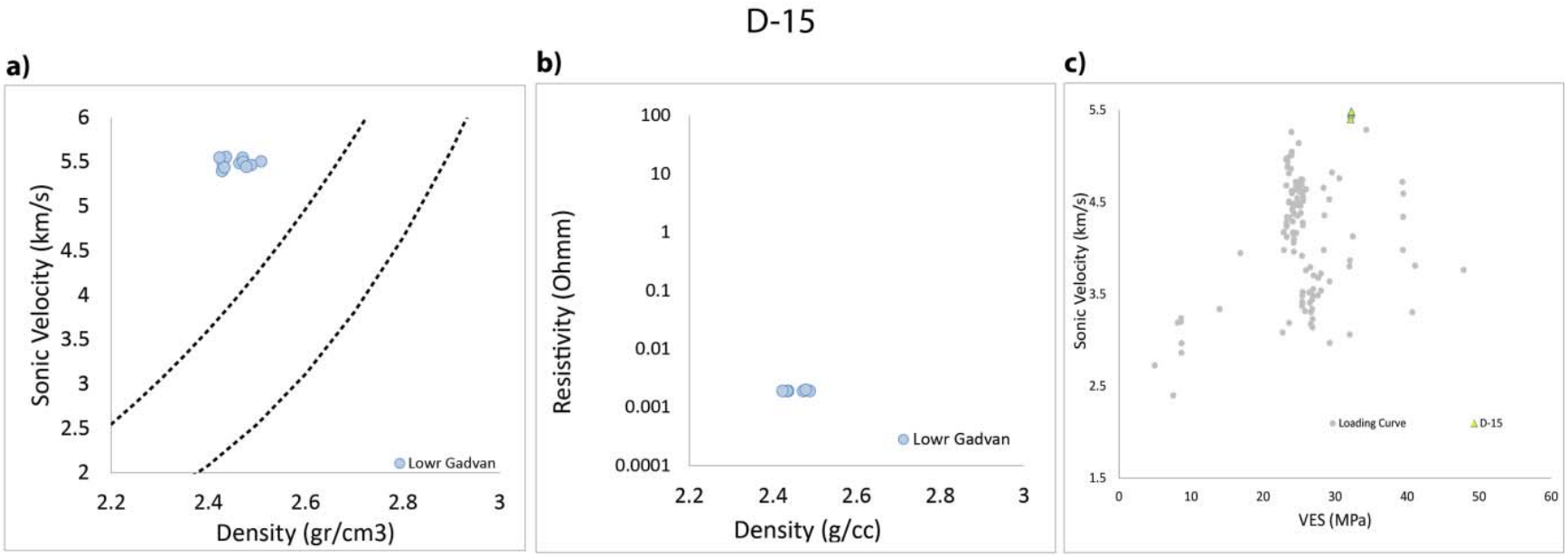

Figure 5-22 - a) sonic velocity-density cross plot of well D-15. b) Resistivity-density cross plot of the same well. c) Sonic velocity-VES cross plot of the same well.

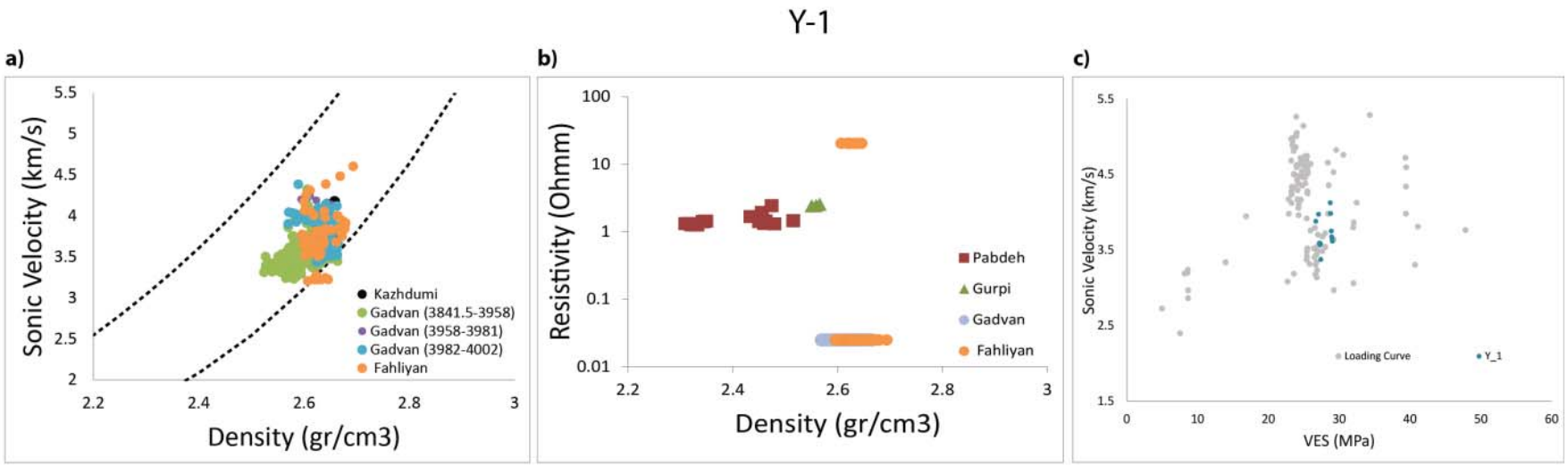

Figure 5-23 - a) Velocity-density cross plot of the data in well Y-1 classified according to formations. All data lie on the loading curve suggesting DC as the overpressure origin. b) Resistivity-density cross plot of well Y-1 in which the data of overpressured formations general follow the loading curve. However, there are some of the range data points that are result of highly conductive pore fluid, most likely the drilling mud intrusion into the formation. c) Sonic velocity-VES cross plot in well D-5 also indicates the DC component of overpressure.

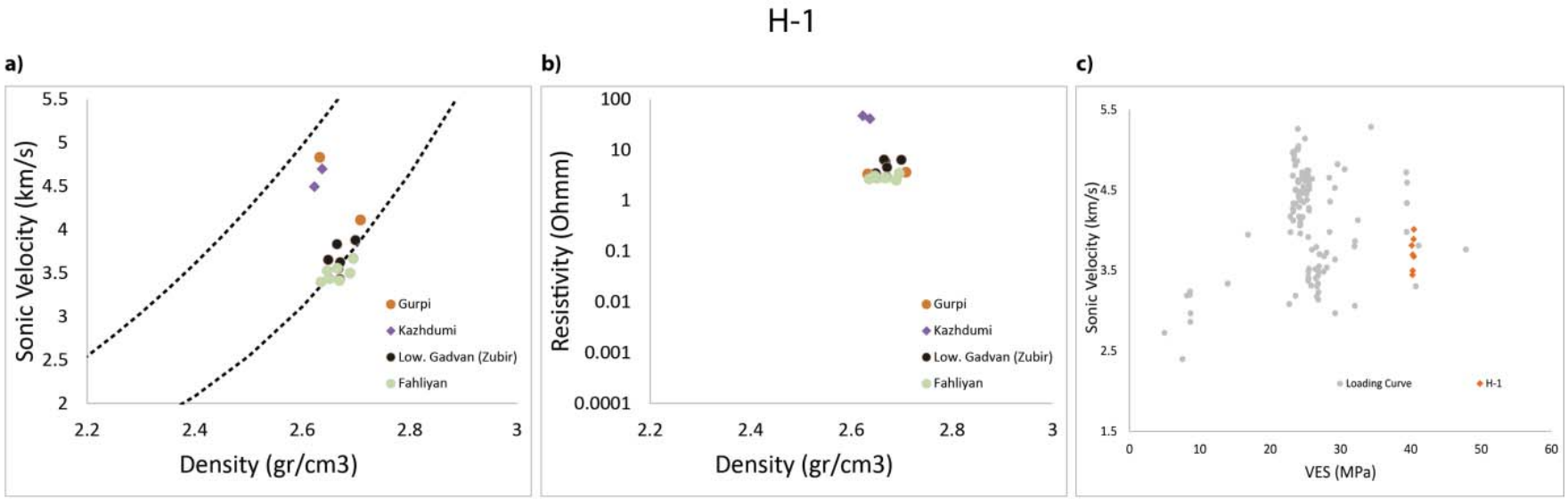

Figure 5-24 - a) sonic velocity-density cross plot of well H-1. The Gadvan and Fahliyan formations are at the right end of the loading zone where a few data points from the normally pressured Gurpi Formation observed. But most of the normally pressured data points are at the left end of the loading zone which may indicate a minor unloading behaviour. b) Resistivity-density cross plot of the same well. c) Sonic velocity-VES cross plot of the same well. All plots suggest DC as the primary origin of overpressure in this well.

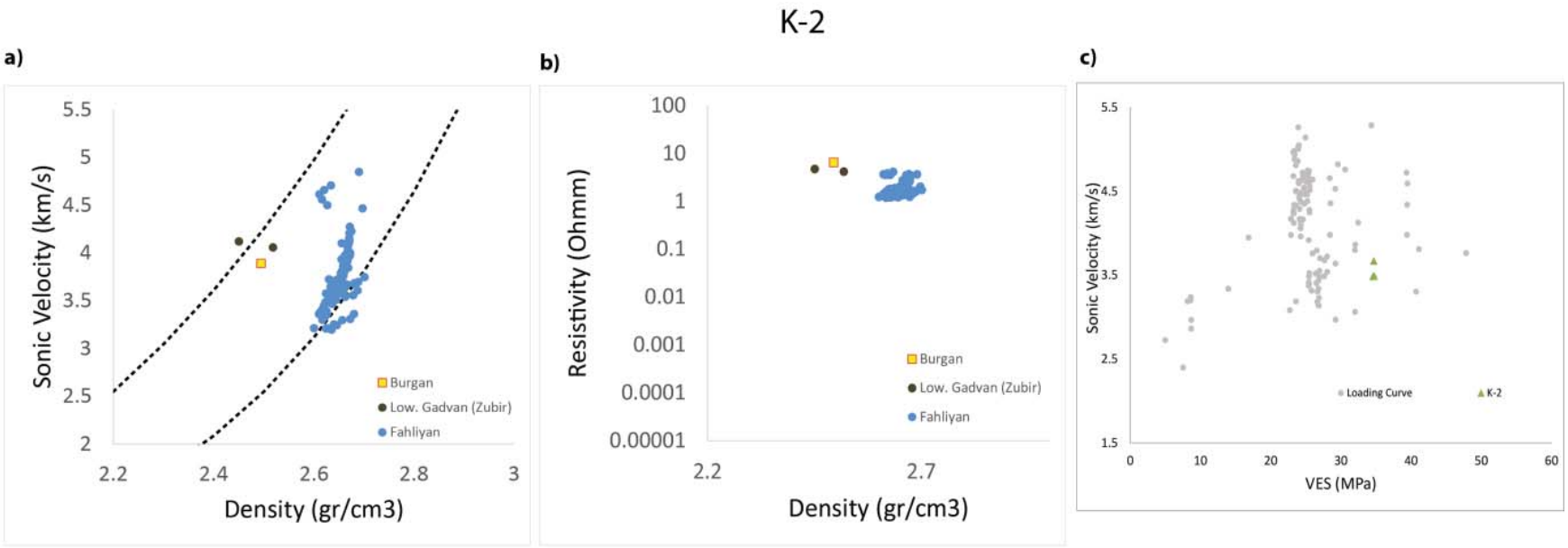

Figure 5-25 - a) sonic velocity-density cross plot of well K-2. The data points of the Fahliyan Formation seem to be shifted to the right of other data points, but due to lack of adequate number of data points in the shallower formations, it is hard to say whether or not it is 'off the loading' departure. Those data points still lie on the loading zone. b) Resistivity-density cross plot of the same well. Similar to the velocity-density plot, the Fahliyan Formation in this cross plot is also found to have been shifted to the right of the other data points. But the shortage of data points doesn't provide a proper basis for unloading. c) Sonic velocity-VES cross plot of the same well. DC is suggested as the main overpressure origin by this plot.

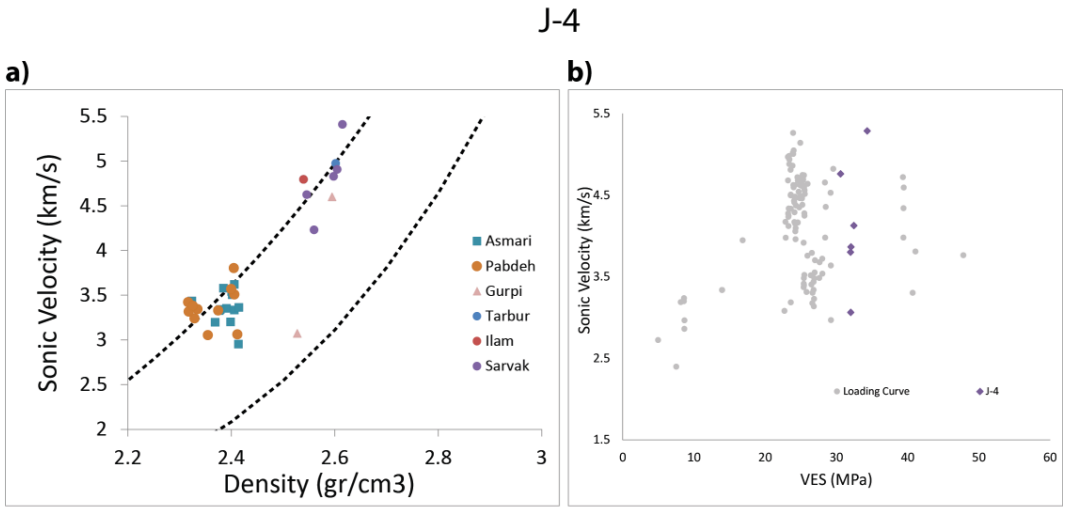

Figure 5-26 - a) sonic velocity-density cross plot of well J-4. b) Sonic velocity-VES cross plot of the same well. Both plots suggest DC as the primary origin of overpressure in this well.

5.3.4. Discussion on Sonic Velocity–Density and Resistivity-Density Cross plot Analysis in the Abadan Plain Basin

The velocity-density and resistivity-density cross plots provide a high degree of confidence for identifying the origin of overpressure, especially when they are aligned with the sonic velocity-VES cross plots and knowledge of local geology. To examine the normal and abnormal behaviour of such formations, sonic velocity-density and resistivity-density cross plots of the entire basin have been constructed to study the trends of the variation in the shales. This leads to identifying the overpressure generation mechanism(s) in this basin. To assess the observations, whether they lie on the loading curve indicating DC or not, the loading curve zone was plotted based on the published velocity-density relationships, as well as a zone of normally-pressured resistivity data points. All attempted methods in this research indicate disequilibrium compaction to be the main mechanism for generating overpressure with minor contribution of fluid expansion.

There is a bit of a data point cloud down towards the lower bound of the loading zone in the velocity-density cross plot which may induce speculations about the unloading. Most of those data belong to special cases of wells A-6 and D-6 (Figure 5-17 and Figure 5-18), which suggest a potential unloading overpressure mechanism in the Lower Gadvan formation in these two wells. In well A-6, there are some data points from the normally pressured Lafan Formation at the bottom of the cloud, which indicates that the overpressures are on reversal trend on the loading zone of its own. No signature of unloading in the resistivity-density plot has been observed where the data points of the overpressured Gadvan Formation lie on the shallower normally pressured formations (Figure 5-17c). The sonic velocity-VES cross plot (Figure 5-17d) suggests that overpressure in well A-6 is still generated by disequilibrium compaction, and that the reason for some sonic-density data apparently lying at the bottom of the loading curve zone is likely due to lithological effects of the rock rather than an influence of pore pressure. It would be a more reliable analysis if there were available data from any other well in this field; but the only accessible data was from one well and hence, the conclusion is left with some degrees of uncertainty.

The downward data point cloud in well D-6 occurs in several interbedded clastics among a sequence of limestone and marl from 4053m to 4101m at the lowermost section of the Lower Gadvan formation (Figure 5-18). This interval is right above the shale layer, which separates the Gadvan from the Fahliyan Formation. To investigate this issue, lithological attributes and well logs of the Lower Gadvan and upper section of the Fahliyan formations are highlighted and presented in Figure 5-27. The anomaly happened only in a specific interval in well D-6 where the data point cloud in the sonic velocity-density cross plot of well D-6 (Figure 5-18b) looks like unloading rollback. Although, such data points are slightly departing from the loading curve, but still on the loading zone, that suggests fluid expansion as a secondary mechanism while the evidence for DC compaction is greatly confirmed by resistivity-density (Figure 5-18c) and sonic velocity-VES cross plot (Figure 5-18d). There are a few 'off the loading curve' resistivity data points which don't follow any trend and just appeared at the bottom of the Figure 5-18c. As discussed earlier, such very low resistivity data points are due to high conductive pore fluid (probably due to intrusion of saline mud into the formation) and thus, can't be considered as any reliable evidence of unloading. Fluid expansion requires further investigation and can be confirmed if similar trends are observed in the other well of this field.

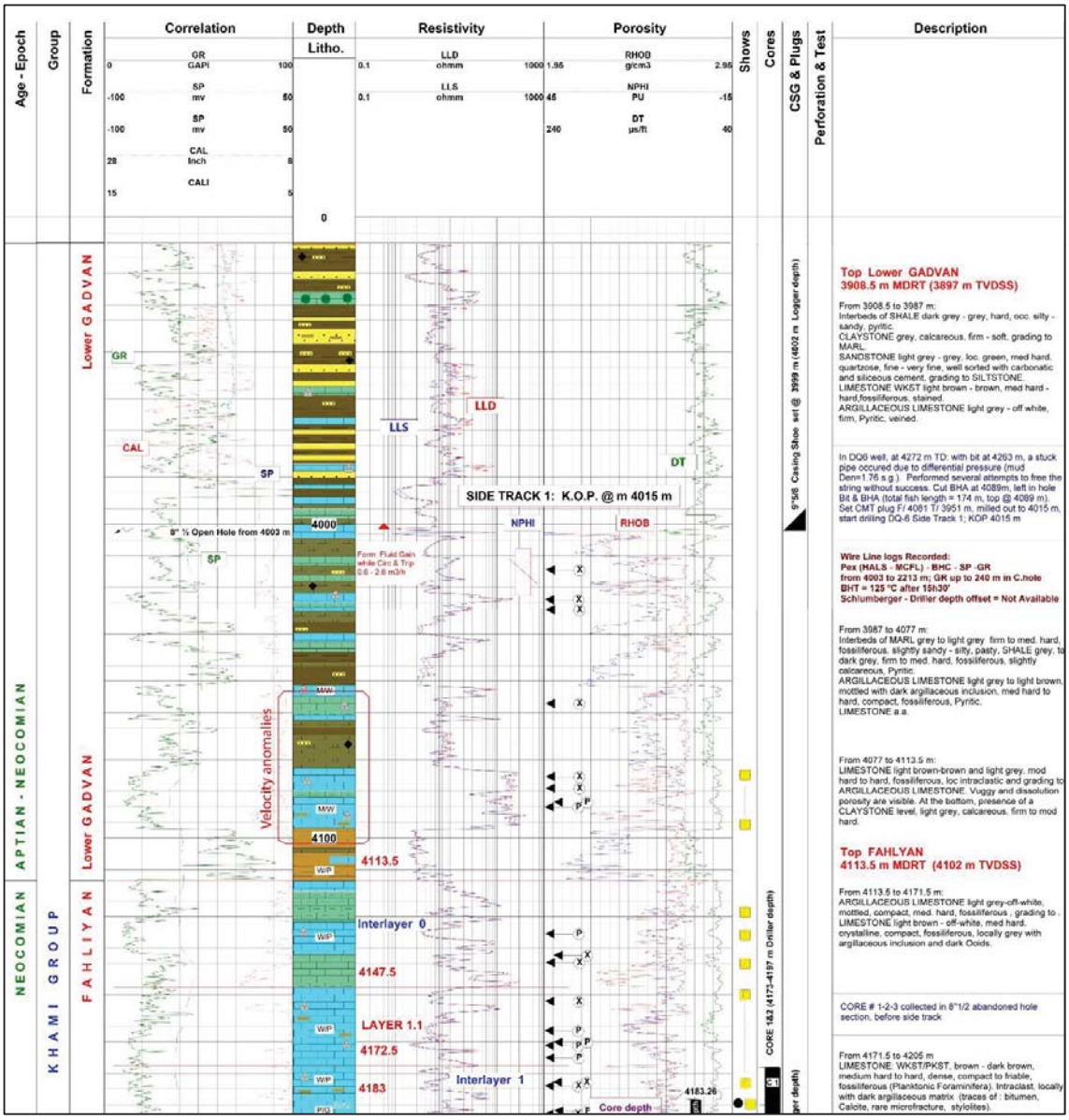

Figure 5-27 – Composite well log of the Lower Gadvan and Upper Fahliyan formation in well D-6. The velocity anomaly is indicated by a red square. Well logs and formation tops are noted.

In well D-5, still a suspicious behaviour of unloading can be spotted in the resistivity-density plot (Figure 5-20b). However, the degree of departure from the loading curve is narrow. The shales of the Lower Gadvan and carbonate deposits of the Fahliyan formations are found to exhibit a degree of unloading where the data points are placed to the right of the normally pressured deposits. A small 'off the loading curve' cloud in the sonic velocity-VES plot is pertinent to such minor unloading and belongs to the uppermost section of the Fahliyan Formation (Figure 5-20b). As discussed in Chapter 4, buoyancy force is capable of generating

~350 psi (2.5 MPa) overpressure in this field at top of the Fahliyan Formation. That overpressure could have been percolated through the low permeability of the Lower Gadvan shales making them overpressure too. The magnitudes of overpressure as well as the degree of departure from the loading curve in these two formations are the same. Therefore, hydrocarbon buoyancy is the most probable secondary mechanism of overpressure in this case as kerogen maturation (while seems probable in the Gadvan source rock) doesn't take place in the Fahliyan Formation.

The rest of the wells in field D have data only from one formation (Gadvan or Fahliyan) and thus, are not discussed here (Figure 5-21 and Figure 5-22). In well Y-1, despite a few 'off the range' data points in the resistivity-density cross plot which are neglected, DC is identified as the only origin of overpressure in the Gadvan and Fahliyan formations of this well (Figure 5-23). Well H-1 and K-2 are close to each other and suspicious of having hydrodynamic connections. The Fahliyan Formation of these two wells exhibited same behaviour which lies on the lowermost part of the loading zone (Figure 5-24 and Figure 5-25). In both wells, overpressured formations are placed at the right of the normally pressured formations, but still on the loading zone. This may suggest a minor effect of fluid expansion in these formations, but due to lack of required data points from shallower normally pressured formations, can't be assertively confirmed. Finally, the data in well J-4 perfectly follow the loading curve, which is purely indicative of DC origin of overpressure (Figure 5-26). Resistivity data was not available at this well, so the analysis was conducted based on sonic velocity and resistivity versus density, which exhibited a loading curve compliant behaviour.

Another important finding of this analysis will be determined when the fields are spatially located at the basin geometry with respect to the Zagros Deformation Front. The wells of field D at the southern part of the basin exhibited clearer signature of unloading while the northern fields (fields Y and J) are solely overpressured by DC. It highlights the role of high stresses in the areas close to the Zagros Orogeny on the pore pressure. As discussed in Chapter 2, the structures in such areas are more folded than the low-stressed areas of the southern fields. It is most likely that the Zagros Orogeny has induced additional load on the confined overpressured deposits of Gadvan and Fahliyan formations in northern fields and made them exclusively overpressured by DC.

It is now clear that there is only, at best, minor additional supporting evidence to propose a fluid expansion (unloading) overpressure mechanisms for the sequences of Gadvan and Fahliyan formations in some of wells. Hence, I conclude that disequilibrium compaction is likely to be the primary overpressure generation mechanism in the studied wells in the Abadan Plain Basin whilst minor contribution of fluid expansion is possibly observed in the middle and southern fields of the basin.

5.3.5. Conclusions of Sonic Velocity–Density and Resistivity-Density Cross plot Analysis in the Abadan Plain Basin

Different response of bulk and transport properties of rock to any change in pore pressure has been considered as a guide to identifying the origin of overpressure in the Abadan Plain Basin. Sonic velocity and resistivity, two measures of a rock's 'transport properties', were plotted versus density as a 'bulk property' of the rock. Most of the overpressured data points lied on the loading curve of normally pressured horizons, which was defined specifically for this basin. Thereupon, disequilibrium compaction is identified to be the primary overpressure generation mechanism in all of the wells investigated in this basin. However, a few 'off the loading curve' trends in wells D-5, D-6 and A-6 were further investigated which revealed a minor effect of fluid expansion in the southern fields of the basin. Namely, the fields closer to the Zagros Deformation Front are solely overpressured by DC whilst southern fields are evident with minor contribution of fluid expansion (unloading trend). The rest of off the range data points are attributed to lithological response to the change in the rock properties (non-pore pressure effects).

5.4. Discussion on the overpressure generation in the Abadan Plain Basin

The qualitative analysis performed on shale data from 10 wells in the Abadan Plain Basin indicates that overpressure in the shale deposits of this basin is primarily generated by disequilibrium compaction. This conclusion is supported by both the regional geology (rapid loading of low permeability shales), as well as from sonic velocity-VES analysis, sonic velocity-density and resistivity-density cross-plot analysis. Deposition of the Aghajari Formation in the Miocene-Pliocene period indicates a rapid sedimentation rate in the Abadan Plain Basin where 910-1366 m sediments of the Aghajari Formation were deposited during 11 Ma (Table 5-1). Underlying formations (especially the Gadvan and Fahliyan formations) have also experienced the same burial rate and considering the low permeability of the Gadvan shale, this rapid deposition is the primary origin of overpressure in this basin.

Table 5-1 – Thickness of the Aghajari Formation in the wells studied in the Abadan Plain Basin. The Aghajari Formation has an average thickness of 953 m in the southern fields and 1256 m in the central and northern fields.

Well	Thickness of the Aghajari Formation (m)
D-4	922
D-5	910
D-6	965
Y-1	1245
A-6	994
H-1	974
K-2	1157
J-4	1366

There are very few data points from the overpressured Gachsaran formation that doesn't fulfil the requirements of running the qualitative analysis. But it is believed that disequilibrium compaction of the low permeable evaporites and consequent entrapped fluid in confined condition is the origin of overpressure in this formation (Atashbari and Tingay, 2012; Field Owner, 2002). Mild overpressures were occasionally encountered in the Sarvak, Kazhdumi, and Dariyan formations while moderate overpressured observed in the Gachsaran (only in fields J, H and Y), Gadvan and Fahliyan formations (in all wells). The Gachsaran Formation is also highly overpressured in well J-4. Unlike the Gachsaran Formation, the Gadvan and

Fahliyan formations are often logged in the studied wells and can be properly examined. The Gadvan formation has the overpressure peak at its bottommost shales where it caps the carbonates of the Fahliyan Formation. The pore pressure at the upper parts of the Gadvan formation is remarkably lower than the lower parts of it, which indicates permeability transition in a seal. The overpressure at the top of the Fahliyan formation could be in the hydrodynamic interaction with the lower parts of the Gadvan formation. But due to very low permeability of the shales in this formation, the hydrodynamic connection doesn't seem extensive. Sonic velocity-VES analysis suggests DC origin of overpressure in this basin. In sonic velocity-density and resistivity-density plots, all data lied on the loading zone and confirms the origin of overpressure to be primarily disequilibrium compaction. A few cases of downward cloud of data points such as wells A-6 and D-6 while still on the loading zone, suggests a minor contribution of fluid expansion to the overpressures in those wells. There are also other 'off the loading curve' data points which are attributed to the lithological effects and hence, not suggesting FE or pressure transfer mechanism. The hypothesis of entrapped fluid in the lower Gadvan and Fahliyan formations is reinforced when the temperature gradient is considered (Figure 5-28). Wireline logs have been used to obtain the formation temperature in the majority of wells. It is noted that the static bottom hole temperatures (SBHT), except for wells no. 17 and 18 in field D were extrapolated using Fertl and Wichmann's (1977) method, which regulates that two log runs at the same depth must be present to fulfil the methodology. The formation temperature has almost the same gradient as the formations above the Gadvan formation, then suddenly a different trend occurs at the depth of the Gadvan Formation which extends into the and Fahliyan Formation. Surprisingly, temperature approaches the normally-pressured gradient in the lower parts of the Fahliyan formation towards the Garau Formation.

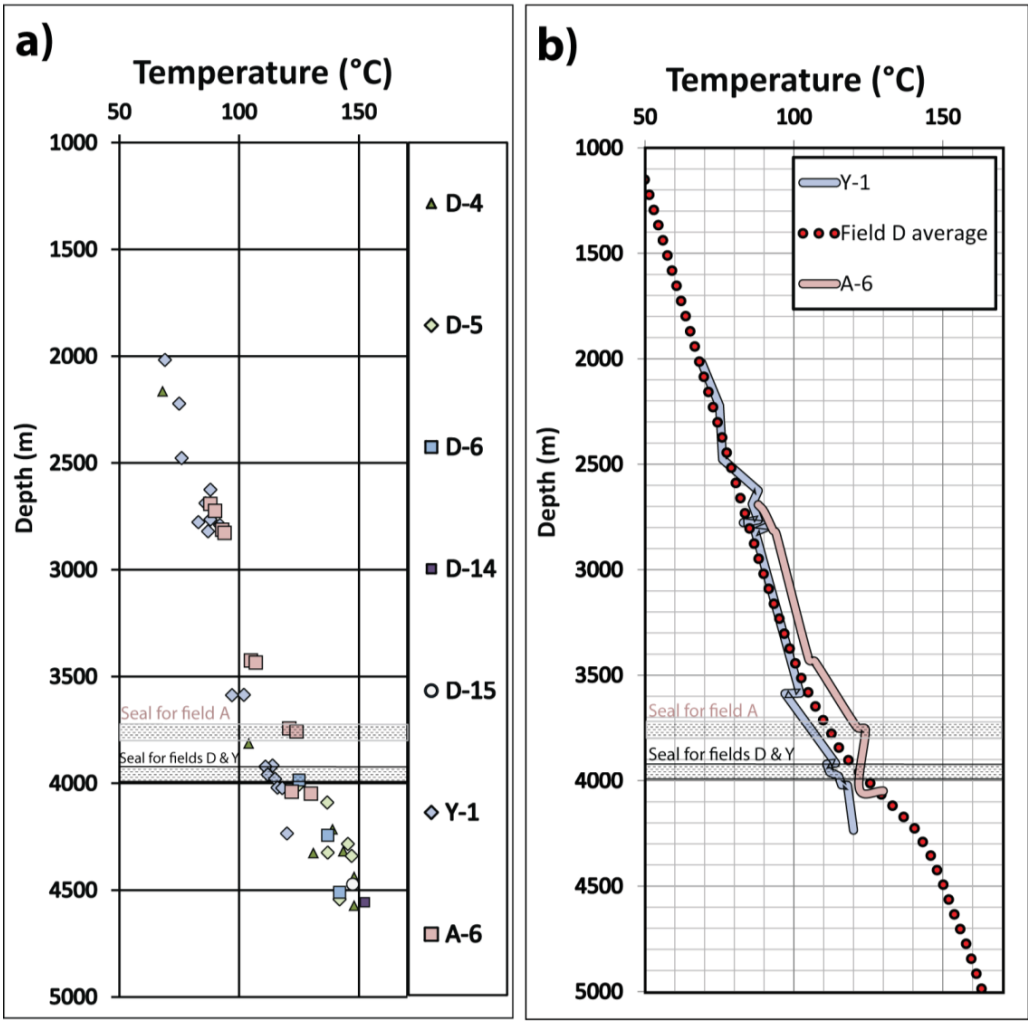

Figure 5-28 - Temperature gradient in the wells in the (a) summarized trends (b). The average temperature in field D is in the dashed red line compared to the trends in fields A and Y. Note the top of the Gadvan formation in field D at depths of around 3800 m and the top of the Gadvan formation at 3900 m. Top of Gadvan formation in fields A and Y is indicated in the graph. The temperature gradient rises at these depths and decreases in the lower parts of the Fahliyan formation which is in good agreement with the pressure measurements, where the fluid pressure tends to hydrostatic gradient.

The Garau Formation is a source rock for oil in the Fahliyan Formation of this basin and had reached hydrocarbon expulsion temperatures, and charged the Fahliyan reservoir by the end of Cretaceous (Leturmy and Robin, 2010; Zeinalzadeh et al., 2015). The Garau Formation source rock is currently at the beginning of gas expulsion. Hydrocarbons have migrated vertically from the deeper Garau source rock and laterally through the reservoir rock in early times (Figure 5-29). In terms of overpressure generation, it seems possible that overpressure has been transferred from the Garau Formation into the Fahliyan Reservoir. However, no pressure data

was available in the Garau Formation to evaluate the potential of transferrable pressure. Furthermore, the Fahliyan Formation is overpressured, but identified as mainly water saturated in fields Y and J, and this further suggests that vertical transfer or hydrocarbon generation are unlikely the overpressure generation mechanisms in the Abadan Plain Basin.

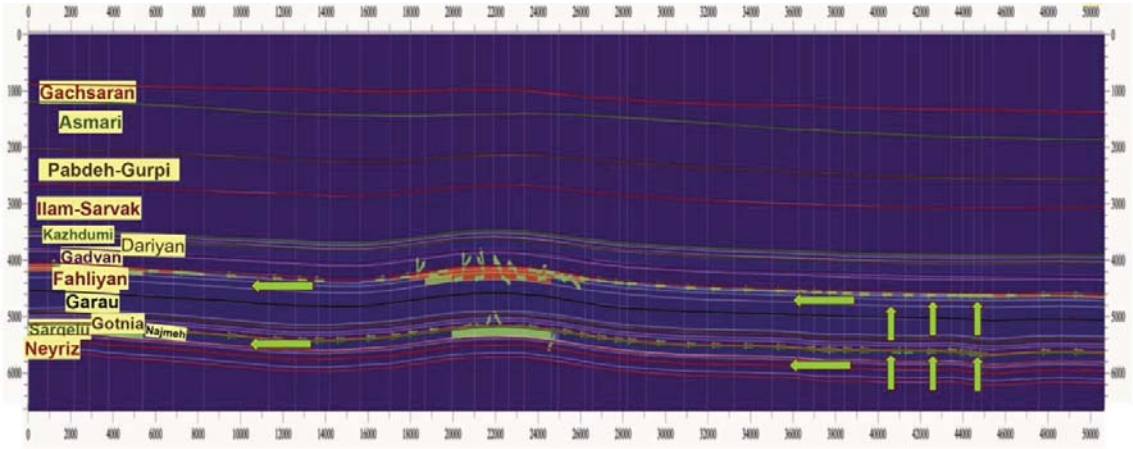

Figure 5-29 - Migration paths in two-dimensional section in field D (Zeinalzadeh et al., 2015). Expelled hydrocarbons migrated vertically to reservoir rocks and lateral migration occurs through reservoirs.

The Fahliyan Formation has several sub-layers that exhibited different pressure gradients in field D. Generally, deeper parts of the formation tend to have lower pore pressure magnitude. The RFT/MDT measurements show that pore pressure slightly decreases in the lower parts of the Fahliyan Formation. This behaviour has also been seen in the temperature gradient (Figure 5-28), which determines two isolated zones within this formation. The Upper Fahliyan, which is already low permeable and capped by the low permeability Gadvan Formation is often more overpressure than the Lower Fahliyan which is a little bit more permeable and several times thicker. There is a very thick oil column in the Fahliyan Formation whose thickness reaches to several tens to hundred meters in some wells. The difference in the density of oil and water imposes an extra pressure of 2.5MPa (~360 psi) at the top of the formation.

The temperatures in field D and Y at the depth of the seal are 120-130°C, while field A, despite having a shallower seal, has a present-day higher temperature of 135°C. This temperature is suitable for a series of potential additional overpressure generation mechanisms, such as clay diagenesis, although there is no evidence to support this hypothesis based on sonic-density

cross-plot analysis. The different temperature above and below the seal layer may also indicate a possible component of overpressure generated by load transfer, though no data is available to test this directly, and the petrophysical data shows no evidence for any additional load transfer overpressuring.

The clay content of the Gadvan and Fahliyan formations has also been examined briefly herein to help identify clay mineralogy, as this will help identify whether a clay diagenesis overpressure mechanism is even plausible for the Abadan Plain Basin. Unfortunately, no X-Ray Diffraction (XRD) analysis is available for the Gadvan and Fahliyan formations of the Abadan Plain Basin shales to properly examine clay mineraology. However, there is a reasonable amount of spectral gamma ray (SGR) data available, and this thus allows for some basic analysis via thorium-potassium cross plots (Schlumberger, 2009). SGR data is available for the Gadvan (a set of limestone, sand and shale) and Fahliyan (a few shale and argillaceous deposits at top and relatively pure limestone in the rest of the formation) formations, but is not available on the evaporitic Gachsaran formation (Figure 5-30). Thorium-potassium cross plot analysis indicates that most Gadvan and Fahliyan clays fall within the 'mixed clay' zone, although some data from wells A-6 and K-2 fall within the 'kaolinite' zone. There are some clay sections with very low potassium content in wells K-2 and Y-1, which suggests the presence of heavy thorium-bearing minerals. Of particular significance, whilst the data suggests a predominate mixed smectite-illite clay content, the data also indicates no significant 'pure' illite content, which would be expected if clay diagenesis was a major contributor to overpressure. This is further supported by well report data, which indicates that illite is the dominant clay mineral in the Ilam and shallower formations, but that illite and montmorillonite is dominante in the Sarvak Formation and carbonate parts of the Kazhdumi Formation, while even deeper (and more overpressured) formations are often rich in smectite (without minor traces of illite). Indeed, the main overpressured Gadvan and Fahliyan formations are dominated by montmorillonite (smectite family) and kaolinite, which indicates that significant clay diagenesis has not happened in these formations. Hence, this clay mineralogy data further supports the evidence from sonic-density and sonic-VES cross plots, which suggest that overpressures in the Abadan Plain Basin are unlikely to have been generated by, or associated with, clay diagenesis (and load transfer). Although minor effects of other mechanisms such as aquathermal and hydrocarbon-water buoyancy are plausible in the Gadvan-Fahliyan horizon, the main mechanism of overpressure is concluded to be disequilibrium compaction.

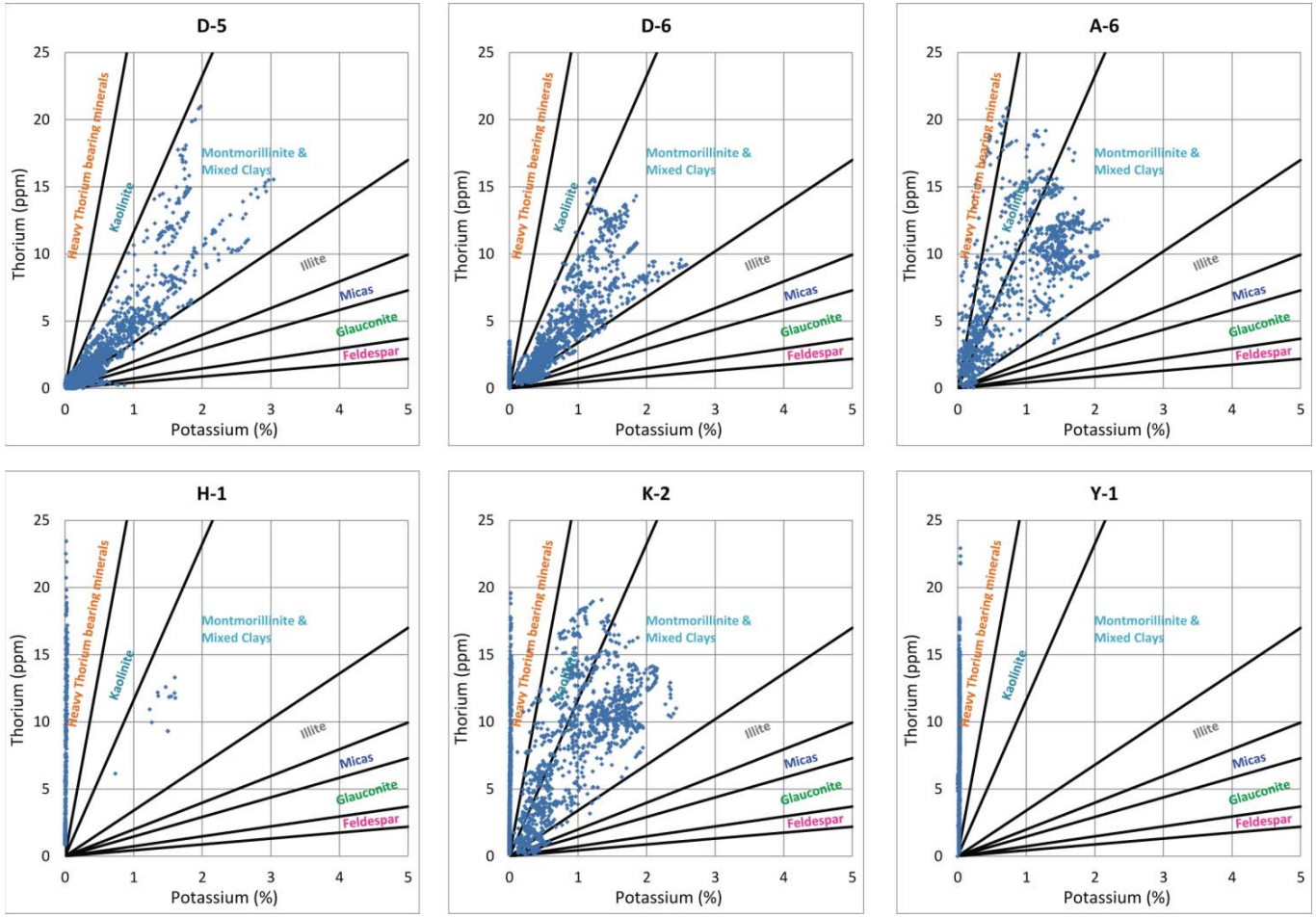

Figure 5-30 – Thorium-potassium cross plot of the Gadvan and Fahliyan formations in six wells of the Abadan Plain Basin. The thresholds are based on Schlumberger (2009) Chart CP-19. The majority of the data fall into the mixed clay area. A part of the data from wells A-6 and K-2 are fall into the kaolinite zone. There are some areas of very low potassium content in wells K-2 and Y-1 which indicates heavy thorium bearing minerals.

Hydrodynamic seal of the Gadvan-Fahliyan horizon is believed to have formed in the late Paleogene period (fluid retention depth, as will be explained in Chapter 8). Since then, lower parts of the Gadvan Formation have undergone a compaction process such a way that they developed a relatively impermeable seal. As a result, fluid pressures within the Gadvan and Fahliyan deposits have had no effective connection to the formations above, and the excess pressure generated by compaction of the sediments has been kept within the formation. This is strongly consistent with the findings from drilling and geophysical data, where Abdollahie Fard et al. (2006a) proposed that the driving forces for structural features in the Abadan Plain Basin are basement faulting and Hormuz salt movement. According to this hypothesis, the structural evolution reached its peak in the Cretaceous and then again in the late Paleogene. This has induced the structural movement along the Arabian trend (north-south), whereas these structures acted as the bounding regime for the Zagros deformation. As an index, porosity-depth graphs reveal a distinct anomaly starting from 3300 m depth (Figure 5-31) which corresponds to the top of the primarily shaly Kazhdumi formation at the peak of structural movement. It has also been found in this study that the northern fields of the Abadan plain Basin which are at the vicinity of the Zagros Deformation Front are solely overpressured by DC, while southern fields have minor contribution from fluid expansion mechanisms such as hydrocarbon buoyancy.

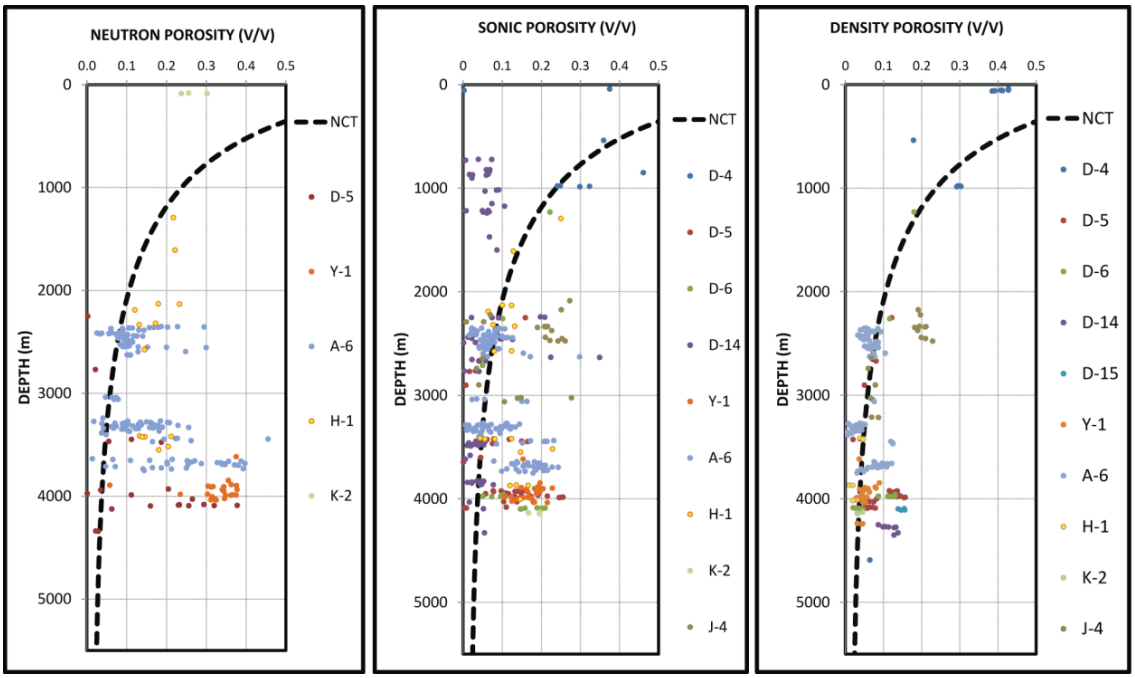

Figure 5-31 – Depth profile of porosity obtained from a) neutron log, b) sonic log, and c) density log. All show an abnormal departure from NCT at the depth of Kazhdumi-Dariyan horizon.

Depth profiles of sonic velocity and resistivity also provide a clear change in the values between shallow depths where the formations are on hydrostatic pressure and the deeper overpressured strata (Figure 5-32). Shallower formations comply with the normal compaction trend while a distinct departure is observed at the depth of the Gadvan and Fahliyan formations. Such departures from the NCT are the basis of some of the most common pore pressure prediction methods, which will be provided in Chapter 6.

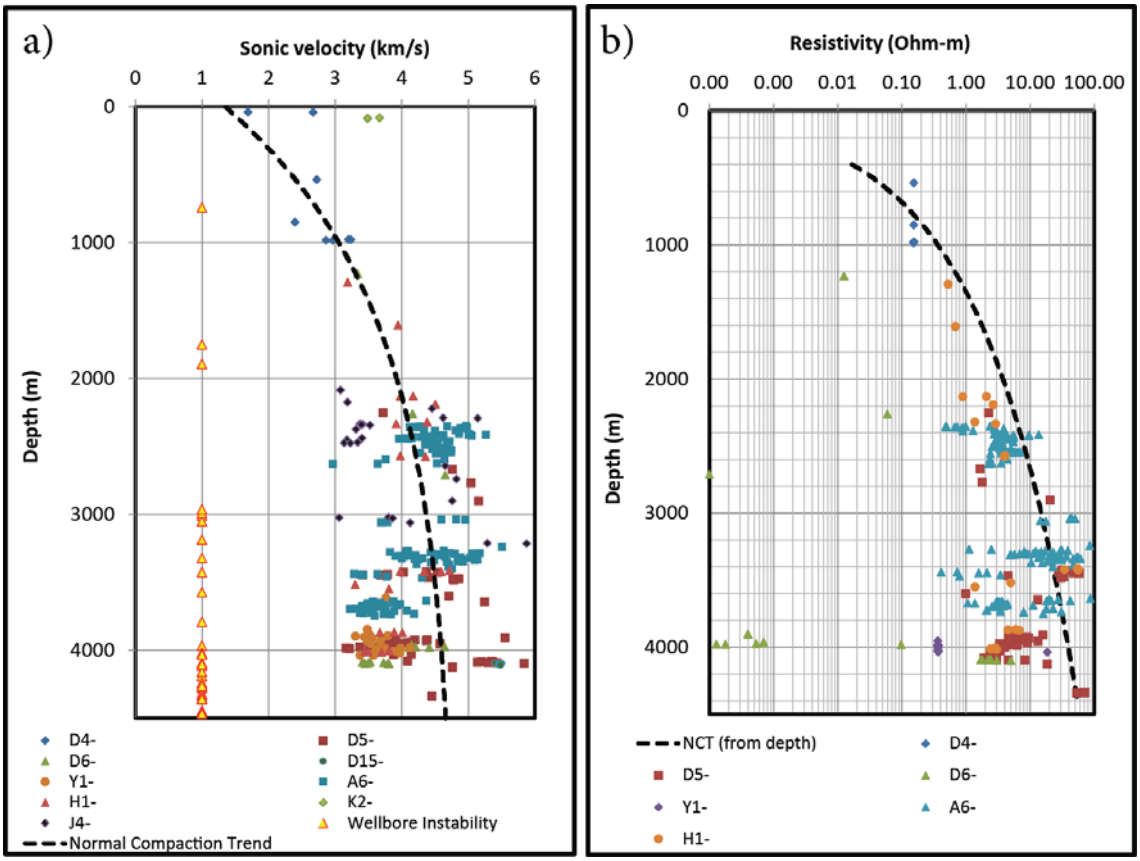

Figure 5-32 – depth profile of sonic velocity and resistivity of the wells studied in this research. The anomalies start from the depth of 3300 m.

5.5. Conclusions

A range of pore pressure, petrophysical and geological data has been used herein to examine the likely origins of overpressure in the Gachsaran and Gadvan-Fahliyan horizons of the Abadan Plain Basin. Examination of the sealing potential of the upper Gachsaran Formation and lower Gadvan formation indicates that these units represent good top seals that are able to maintain and seal overpressure, and thus supports the evidence of these sections being pore pressure transition zones, as discussed in Chapter 3. Analysis of sonic velocity-VES plots (Bowers type plots) was used to first characterise the range of normally pressured 'loading curve' properties, and was then compared with the properties of overpressured sequences. Overpressured sequences plot predominately within the loading curve zone, suggesting disequilibrium compaction as the likely primary cause of overpressure in the region. Analysis of sonic-density and resistivity-density cross plots yielded further support for disequilibrium compaction as being the dominant overpressure generation mechanisms in the basin, and

provided no strong evidence for significant pressure transfer, and occasionally minor evidence to suggest the existence of fluid expansion overpressure generation mechanisms at the basin-scale. Northern fields in this basin are believed to be solely overpressured by DC, whilst southern fields are predominately overpressured by DC but may have a small contribution from fluid expansion, likely as a result of hydrocarbon-water buoyancy force. The results of petrophysical analysis into overpressure origin are still further supported by the geology of the basin, and a brief examination of clay minerology in shale-rich sequences. The geology and minerology of overpressured shale units strongly suggest that typical fluid expansion type overpressuring mechanisms, such as kerogen-to-gas maturation or clay diagenesis (and associated mechanisms, such as load transfer) are unlikely a primary mechanism in the studied sections of the Abadan Plain Basin, though may potentially act at deeper, and yet unexplored, sections of the basin.

The identification of disequilibrium compaction as being the most likely overpressuring mechanisms in shale sequences of the Abadan Plain Basin is extremely useful for pore pressure prediction. Shales overpressured by disequilibrium compaction have a porosity anomaly that can aid in pre-drill, real-time and post-drill pore pressure prediction. However, the pore pressure prediction is highly problematic in the Abadan Plain Basin because the shale units are often quite thin (sub-seismic) and lithologically variable (e.g. shales to marls to shaly carbonates). Furthermore, the neighbouring carbonates are also often overpressured, and the petrophysical properties of these sequences can make it very difficult to isolate shale properties, even in log types that have higher resolutions. However, the overpressure origin in this chapter forms the required and critical foundation for examining pore pressure prediction methods in carbonates and shales of the Abadan Plain Basin throughout the rest of this thesis. Indeed, vertical stress, as one of the critical components of pore pressure prediction, needs to be precisely determined. Vertical stress magnitude across the basin is examined in the next chapter and, subsequently, pore pressure predictions are provided in the following chapters.

CHAPTER 6- Distribution and Determination of Vertical Stress in the Abadan Plain Basin

6.1. Introduction

Vertical stress plays a critical role in petroleum exploration as it relates to pore pressure generation and fracture gradient prediction (Bruce and Bowers, 2002; Eaton, 1972; Traugott, 1997). Since vertical stress affects the rock properties, it is essential to know about rock mechanics for petroleum exploration and well control. In conventional pore pressure prediction methods, such as those described by Eaton (1972) and Bowers (2001), vertical stress is one of the key input parameters. Vertical stress is often assumed to have the average value of 22.6 MPa/km (1.0 psi/ft), primarily after the work done on Gulf Coast pressures by Dickinson (1953), who evaluated the overburden stress using 2.3 g/cm^3 as the mean rock density of Gulf Coast sediments. This average value is correct in some geological settings, but seems invalid for many different conditions (e.g. Bell (1996); Tingay et al. (2003), King et al. (2010)). As rocks may undergo different consolidation and compaction process during the burial, the density of sediments, and subsequent vertical stress, varies with depth. This value may differ from basin to basin, and even from well to well, within the same geological structure (Hasegawa et al., 1985); King et al. (2010). The main factor that controls vertical stress in the Abadan Plain Basin is the compaction attributes of the sediments. Herein, the methods of estimating vertical stress, as well as variation of this parameter across the basin, are discussed. It is shown that different rock types have undergone different process of compaction, which subsequently result in a variation in vertical stress across the basin. Finally, I describe how the variation in vertical stress over the study area has several key implications, and also highlights the overall importance of accurately calculating overburden gradient in pore pressure studies.

6.2. Methodology

Vertical stress is the total overburden pressure on any surface at a certain depth, which can be calculated by integrating rock densities from the surface to the depth of interest (Bell, 1996). It is obtained using the following equation:

$$\sigma_v = \int_0^z \rho(z) g d_z \qquad \text{Equation 6-1}$$

Where z is the depth, ρ(z) is the bulk density of the formation at that depth, and g is the gravitational acceleration constant. As discussed in the previous chapter, rock density and therefore, vertical stress could be also approximated as a function of depth. In this research, density data has been integrated from well log data based on the following criteria (modified from Tingay et al., 2003):

1. Petrophysical data must be corrected for hole inclination to the true vertical depth, and then used as the calculation input
2. Spurious data must be removed from the petrophysical logs
3. For the areas with no data, interpolation between two points above and below the interval is to be applied. Interpolation in the LAS file of the log data was performed using a VB macro in Microsoft Excel by Rockenbach (2006).
4. Where sonic logs are available, the density obtained from the sonic log will be used for the points without density data, with density estimated from sonic velocity by means of an appropriate published relationship (e.g. Ludwig et al. (1970) or Gardner et al. (1974)).
5. In the shallow section of the wells, where a density log is not available, an average density from the surface to the top of the density data will be considered and derived from sonic velocity data.

6.2.1. Removing Spurious Data from the Density Log

It is essential to have direct contact between the logging tool skid and the wellbore to obtain accurate density measurements (Asquith and Gibson, 1982; Western Atlas International Inc, 1992). The density logging tool consists of a radioactive source which emits medium-energy

gamma rays into the surrounding media, where the gamma rays lose some energy as a result of interacting with electrons in the formation (Western Atlas International Inc, 1992). The detectors, at a fixed distance from the source, receive the scattered gamma rays which are then used to reliably measure the electron density of the formation (with electron density then being used to accurately estimate the bulk density). Density logs have quite low depths of investigation, and thus only measure density in close proximity to the logging sensors. As such, rugosity of the wellbore can cause the logging tool to come in contact with the low density wellbore fluid (instead of rock), which leads to an apparent low density reading. These spuriously low density values must be removed from the log dataset. In this research, two associated logs (caliper and DRHO) have been used to filter out poor quality data. The caliper log is a direct indication of cavities or any other kind of rugosities in the wellbore. Any log reading of caliper values ±10% greater than bit size (Caliper > bit size+10%) was assumed to be a bad hole condition and readings were eliminated from the dataset. Concurrently, DRHO was used to filter the poor density readings from log data. According to Asquith and Gibson (1982), density readings associated with DRHO that are greater than ±0.1 g/cm indicate bad hole conditions, hence must be disregarded in the calculations. An example of correlation of the density and caliper logs of a well in the Abadan Plain Basin is illustrated in Figure 6-1, where spurious density readings in the rigorous well conditions are indicated by caliper enlargement.

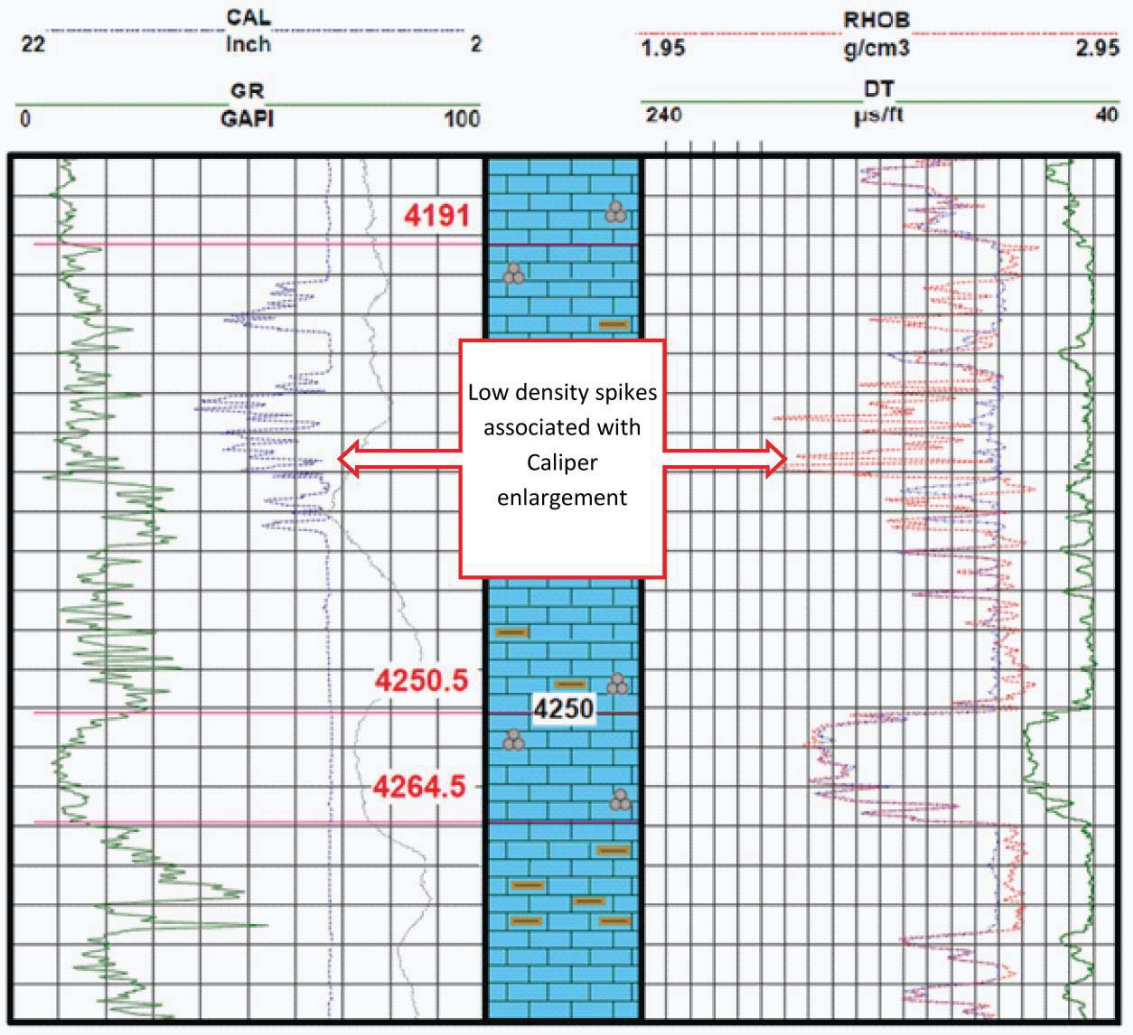

Figure 6-1 – Low density spikes are an indication of spurious data as the caliper indicates very low contact between the logging tool and borehole wall. The data of such rigorous zones are removed from the analysis.

Moreover, spikes in the data have been removed by using a running median filter to lessen the variations. Moreover, spurious data have been manually removed from the dataset wherever mud log data or other well reports noted poor logging recordings. Finally, the data have been smoothed over a constant sampling interval of 2 metres for more consistent results.

6.2.2. Estimating the Density for Areas without Density Log Data

Normally, the uppermost sections of wells are not petrophysically logged. Logging may not be performed because the drilled rocks are shallow unconsolidated sediments, where it is hard to keep the hole open for logging and, therefore, the well is cased immediately after drilling in that area. More commonly, it is not deemed required, nor commercially appropriate to spend time and money logging sections that may be well above the target reservoirs. This unlogged interval could be more than 1000 meters (and occasionally several thousand meters). However, the calculation of vertical stress requires knowledge of density from the surface, and thus, reliable estimation of density at depths above the top of density log recording is necessary. There have been several methods proposed to estimate the average density for the aforementioned depth interval such as:

1. Measuring bulk density from shallow sediment cores (Niemann, 2002)
2. Estimating density though downhole gravimetric data (Niemann, 2002)
3. Estimating density from regional density-depth trends (Traugott, 1997)
4. Estimating density from compressional wave velocity versus density trends (Gardner et al., 1974; Hamilton, 1978; Ludwig et al., 1970)
5. Estimating density from compressional wave velocity to porosity relationships (Dvorkin and Prasad, 2001; Raymer et al., 1980) and porosity to density transformations (Asquith and Gibson, 1982)

Due to a lack of adequate data and published results for the first two methods, a combination of regional density-depth trends and compressional wave velocity-density trends have been used in this research to obtain the most accurate and reliable approximate of the bulk density of formations. Regional density-depth trends from wells with density data from shallower depths wherever available have been considered to obtain an accurate correlation between the wells. Regional trends can be either used as density-depth values in the wells without log data or they can be considered when estimating the density-depth trend of a single well with the same geological characteristics. For example, if the density log starts at 2000 m depth and there is a density-depth trend for 500-2000 m depth interval in nearby wells, that trend could be used

in this particular well to estimate the density in such interval. Shallower deposits are normally associated with unconsolidated sediments and regional trends from available wells represent the density. On the other hand, the compressional wave velocity-density trends are also reliable tool in estimating the density, if utilized carefully. They are based on the strong relationship between bulk density and compressional wave velocity, of which several techniques have been proposed by researchers as follows.

1. The Nafe-Drake sonic velocity to density transformation (Ludwig et al., 1970).
2. The Gardner sonic velocity to density transformation (Gardner et al., 1974).
3. Using sonic velocity to estimate porosity and then converting porosity to bulk density.

The third technique is performed according to the following set of equations. First, porosity is calculated from sonic log (compressional wave velocity or travel time) according to the corrected Wyllie et al.'s (1956) time average equation (Raymer et al., 1980):

$$\varphi_{\Delta t} = (1/cs)(\Delta t-\Delta t_{ma})/(\Delta t_f-\Delta t_{ma}) \qquad \text{Equation 6-2}$$

Where $\varphi_{\Delta t}$ is the porosity calculated from sonic log, cs is an empirical regional correction factor for unconsolidated sediments which is considered 1.0 in this basin, Δt is the travel time of compressional wave, Δt_{ma} is the rock matrix (or grain) sonic wave travel time and Δt_f is the sonic travel time in the pore fluid. Equation 6-2 gives the porosity based on the sonic log readings. Then the following classic equation of density from porosity (Asquith and Gibson, 1982) can be used to calculate the bulk density of the sediments.

$$\varphi_{RHOB} = (\rho_{ma}-\rho_b)/(\rho_{ma}-\rho_f) \qquad \text{Equation 6-3}$$

Where φ_{RHOB} is porosity from density data, ρ_{ma} is the density of the rock matrix (or grain), ρ_b is bulk density and ρ_f is the pore fluid density. Tingay et al. (2003) compared and contrasted the above methods on data from the Baram basin of Brunei and found that the Nafe-Drake sonic velocity to density transformation provided the best overall results when tested in wells that had available shallow density data. In this research, a

combination of the Nafe-Drake and Gardner transforms were used wherever density data is not present. In such approach, an average of density values calculated from Ludwig et al. (1970) and Gardner et al. (1974) for sonic velocity to density relationships is calculated and averaged for vertical density determination (Figure 6-2). The adjustability of the relations to the data vary in wells and a lateral shifting is required in some wells which has been performed individually for well accordingly.

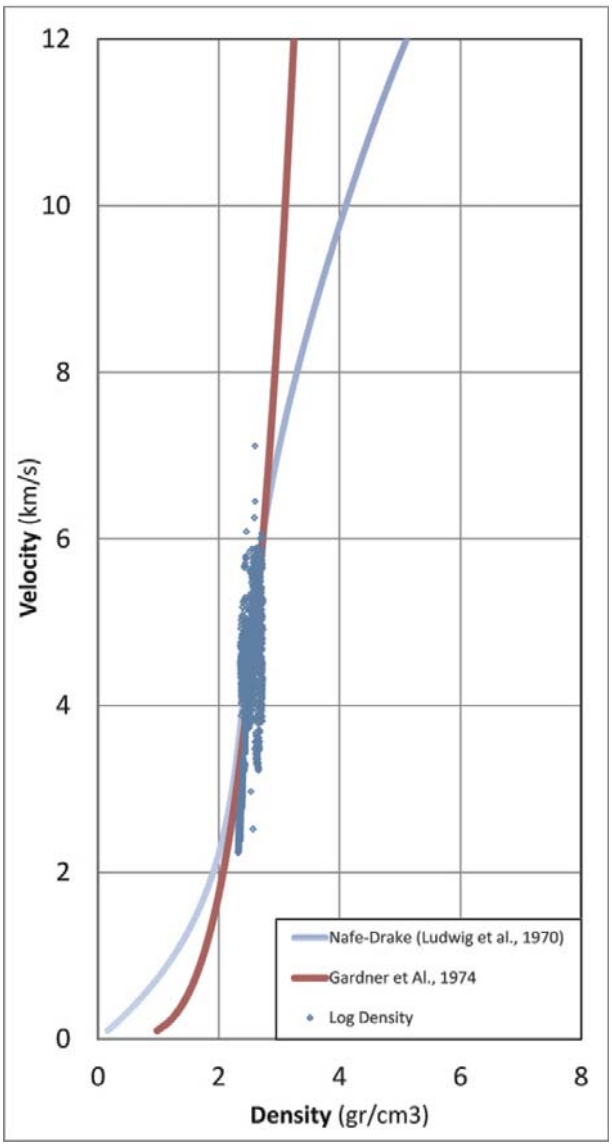

Figure 6-2 – Representation of Nafe-Drake (Ludwig et al., 1970) and Gardner et al.'s (1974) equations for sonic velocity-density relationships. The data are for well D-6 of this study. The curves show the original equations and no modifications were required. Some other well of this basin seemed to needed a slight curve shifting to fit the data.

6.3. Results

The vertical stress of 10 wells within six fields of the Abadan Plain Basin have been calculated and presented as both vertical stress and vertical stress gradients to provide a convenient basis for comparison between the wells. In Figure 6-3, the vertical stresses of all wells were combined in a single figure to analyse possible trends in the variation. Whilst most wells display similar vertical stress profiles, well D-4 displays some notably low magnitudes with respect to other wells in the basin, even the other wells of the same field.

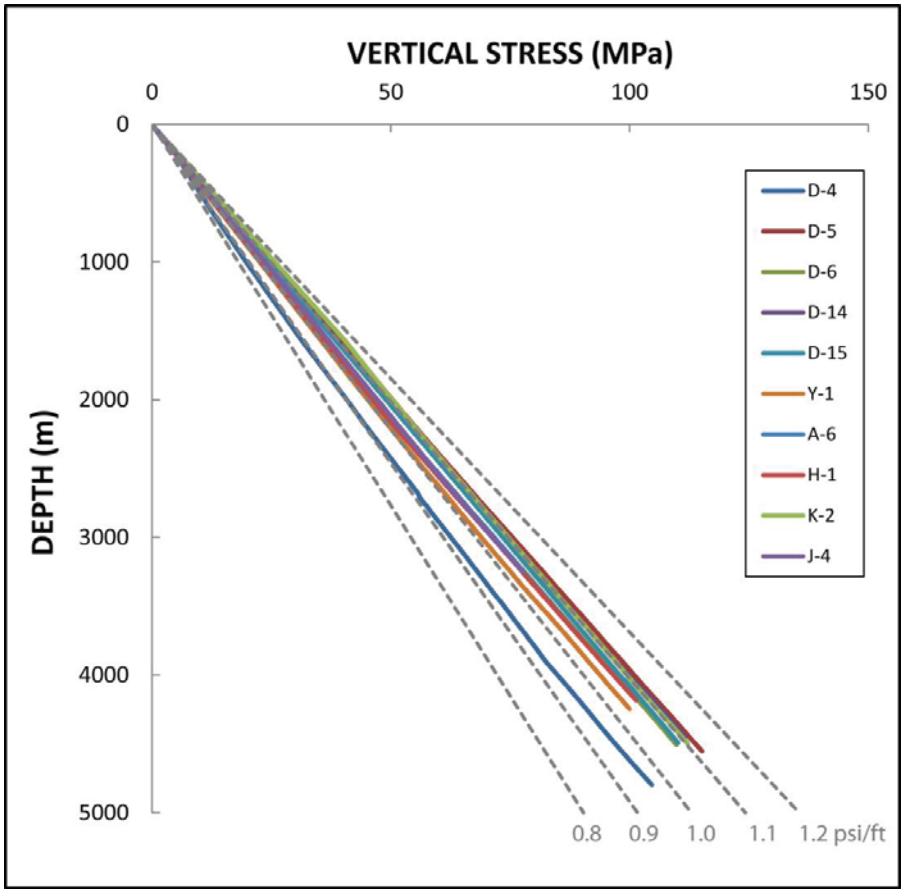

Figure 6-3 - Calculated vertical stress (σ_v) magnitudes over the Abadan Plain Basin. Vertical stress varies with depth and between fields. Well D4 exhibited unusual low σ_v values compared to the other wells of this basin.

It is important to note that the bulk density of the rocks changes over depth whereas it is normal behaviour due to porosity variations in the formations or differences in the rock fabric. Figure 6-4 contains the vertical stress gradient against depth for the wells

presented in Figure 6-3. As discussed earlier, well D-4 exhibits unusually low values. Wells in the northern parts of the basin exhibited lower magnitude of vertical stress than those of southern fields. This might be due to the tectonic controls of impact of the Zagros Orogeny on the entire basin. However, the variations due to spatial placement of wells are of less significance and thus, vertical stress is more likely to be influenced by the lithological attributes than tectonic forces. The variation in σ_v is greatest in the shallower depths, where density is less well constrained and density variations have the greatest impact on vertical stress gradient (Tingay et al., 2003), and the σ_v trends of the wells get closer to each other at such deeper sections. When well D-4 is excluded, the σ_v narrowly varied between 23 MPa/km to 25.3 MPa/km at 4200 m.

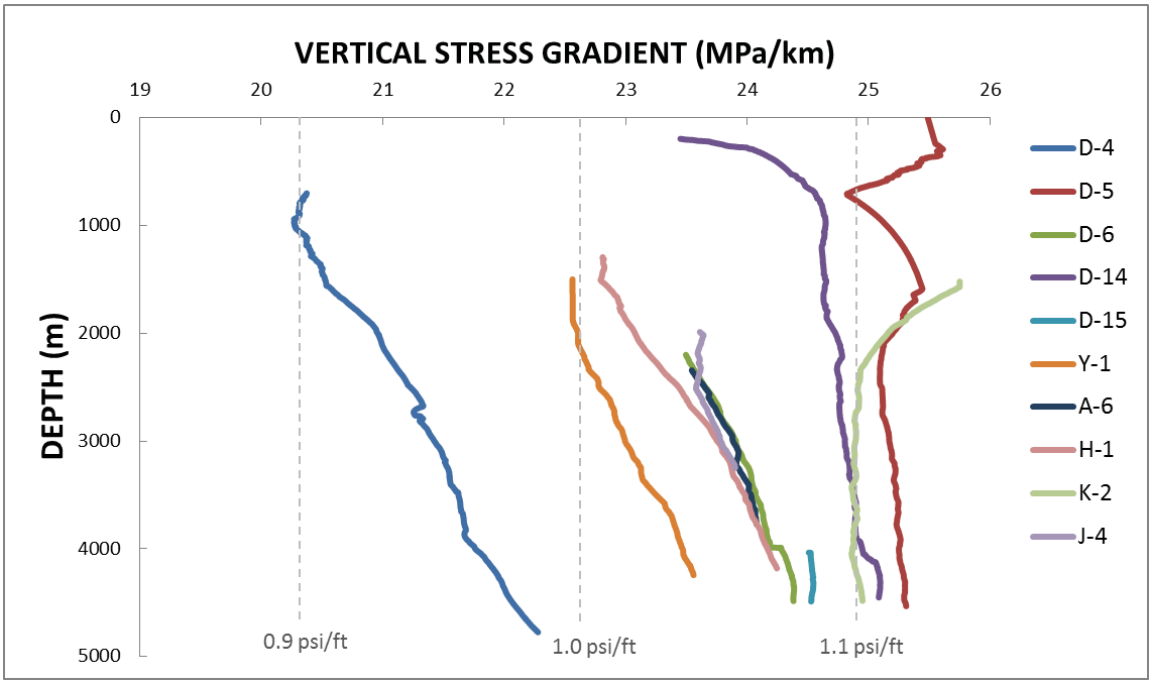

Figure 6-4 - Calculated σ_v gradients of the Abadan Plain Basin. Vertical stress varies with depth and spatially between fields. The low magnitude of σ_v in well D-4 is noted. Northern fields have slightly lower magnitudes of vertical stress gradient than the fields in southern parts of the basin.

6.4. Discussion

6.4.1. Density Estimation from Sonic Log

The frequency of density log is almost the same as sonic log and in the wells studied, these two sets of logs were both collected. Therefore, the density log was used as the basis of

calculations for vertical stress in this basin. However, due to some bad hole or spurious data reading, the density data are filtered occasionally in some areas and instead, density from sonic log estimation was considered. For example, well D-14 had no density log from surface to the depth of the Lower Gadvan Formation, whilst sonic log was available from the depth of 195 m. Therefore, the density is estimated as the average of Gardner and Ludwig correlations from that depth to the top of density log. In well Y-1, sonic log starts from 2862 m while density log is available from 1902 m. Estimated density from sonic log is the average value of Gardner et al. (1974) and Ludwig et al. (1970) which seems to be in a close proximity to the density log as demonstrated in Figure 6-5 and Figure 6-6. The error approaches zero as depth increases and validates the relatively accurate estimations.

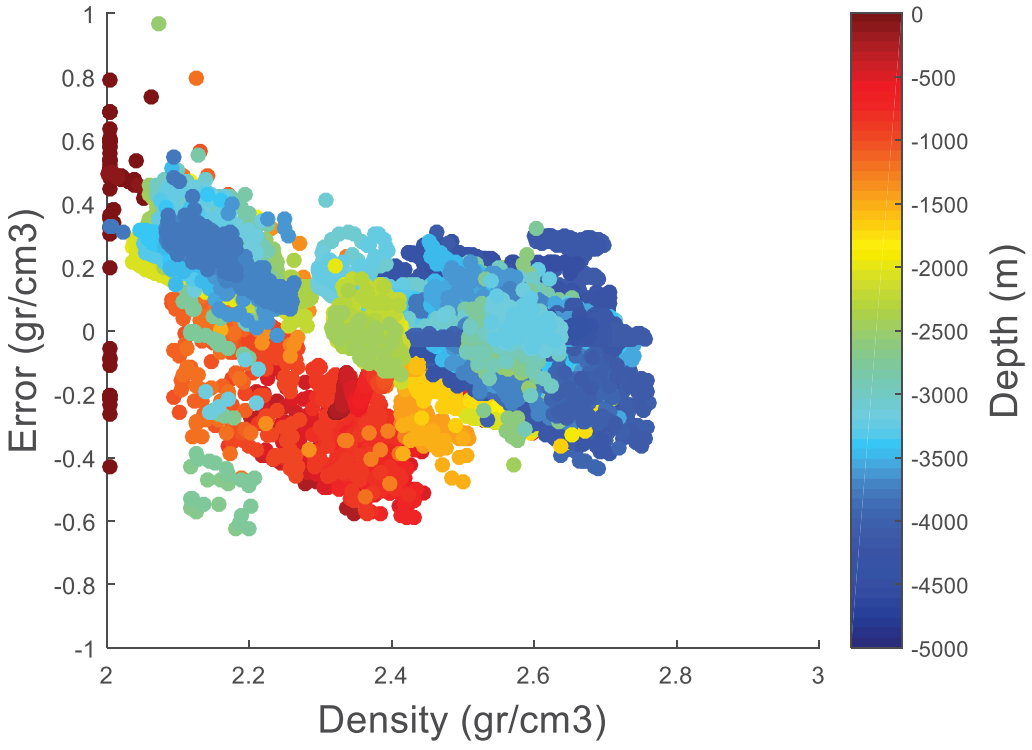

Figure 6-5 – Cross plot of error in the estimated density with respect to density log. Estimated density is the average of calculated density from Gardner et al. (1974) and Ludwig et al. (1970). The data points are color-coded by depth.

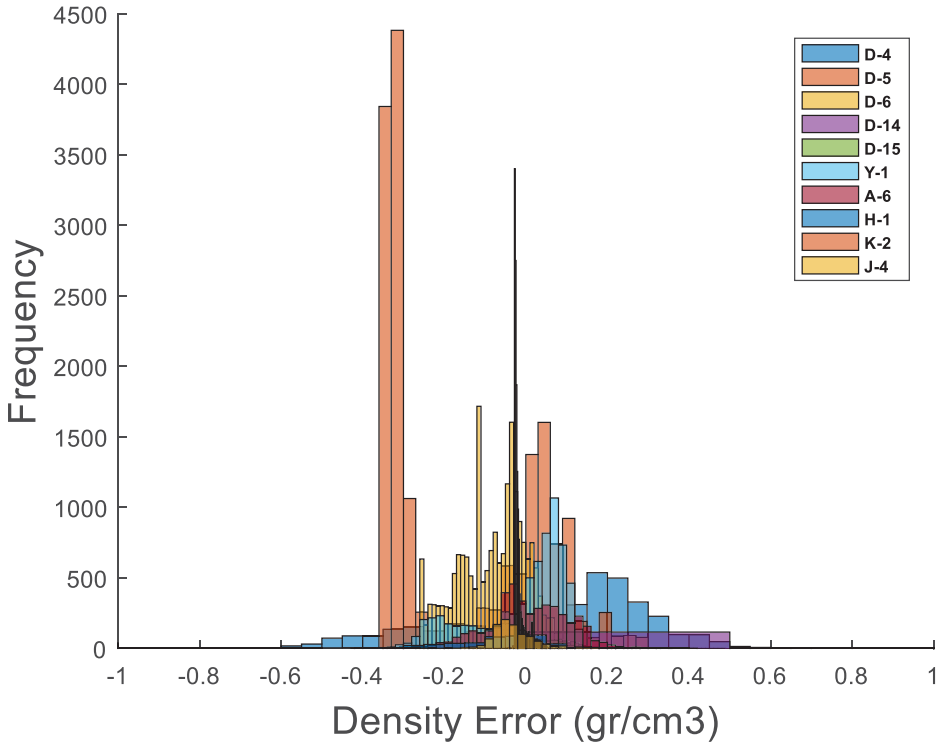

Figure 6-6 – Histogram of error in density calculations with respect to density log. The off the centre columns around 0.3 gr/cm3 is majorly the error of calculation in well K-2.

As stated above, the density and sonic logs are often run together in the wells of this basin and there are few depth intervals without density log where sonic log was recorded and density is estimated from that (Table 6-1). Although, density estimation is in a close approximation to the recorded density. That confirms the accuracy of the vertical stress calculations using the available data.

Table 6-1 – Top of density and sonic log and depth interval where density is estimated from sonic log

Well	Top of Density Log	Top of Sonic Log	Interval where Density is Estimated from Sonic Log
D-4	41	41	
D-5	239	239	
D-6	207	207	
D-14	4050	195	3855
D-15	4048	4034	14
Y-1	1631	2862	
A-6	2345	2345	
H-1	1512	1293	219
K-2	1570	1549	21
J-4	2018	1987	31

6.4.2. Variation of Vertical Stress in the Abadan Plain Basin

Vertical stress gradient of all wells except D-4 varies between 22.5 and 25.5 MPa/Km which doesn't show any particular trend in Figure 6-3 or Figure 6-4. Vertical stress has been calculated at 2500 depth where the majority of wells had correspondent density log at that depth (the Gurpi Formation in most of the wells) and a depth slice passes through those wells (Figure 6-7). Northern fields exhibited lower magnitudes of vertical stress than fields in southern parts of the basin. Such south-to-north trend suggests the effect of the Zagros Orogeny (binding northern border of the basin) on the vertical stress. In this region, Eurasia-Arabia plat collision has resulted in thrust tectonics, the Zagros Orogeny, associated with shortening and thickening of the strata along the direction of collision. The formations of the northern fields under the influence of the Zagros Orogeny are more folded than the southern parts of the basin which are characterised with extensive fractures. A fractured substance has more pore space, hence less density, than the same volume of rigid material. As such, the more fractures a rock has, the lower its density is recorded and hence, lower values of density in northern fields, which resulted in lower magnitude of overburden stress.

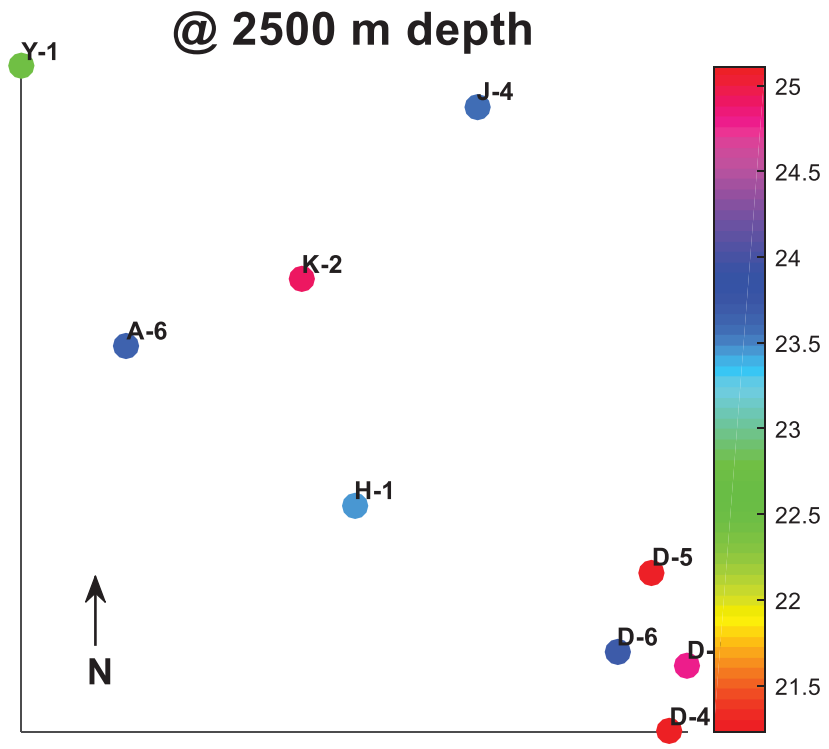

Figure 6-7 – Vertical stress at 2500 m depth in the studied wells. A decreasing trend from south to north and northwest is observed.

Well D-4 exhibited an unusual magnitude of low density (compared to the other wells of this basin) and consequently, lower magnitudes of vertical stress which requires further investigation (Figure 6-8). Although density in well D-4 never goes below 2 g/cc, the density remains around 2.1 in much of the of 2,000 to 3,900 m depth interval. Despite performing the bad hole data filter, the issue is still persistent and thus, the vertical stress estimate for this particular well remains uncertain. Such low values are not only off the range from other fields of the basin, but also off the range of field D average. No explanation is available with the log data, and in spite of all attempts to avoid erroneous data, density measurement in most of this particular well is believed to be a tool malfunction. Density is back to the same range as other wells in the deeper Gadvan and Fahliyan formations.

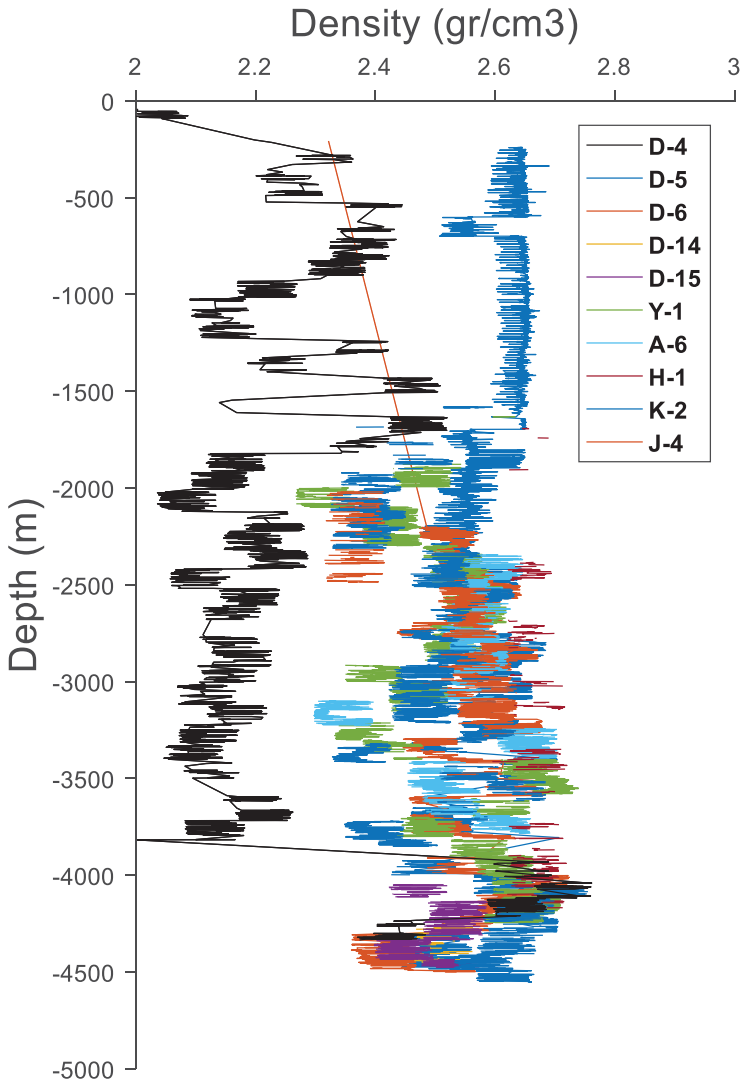

Figure 6-8 – Density logs of the 10 wells in the Abadan Plain Basin. Low density of well D-4 is illustrated with black colour. The density at the Gadvan Formation and beyond is in the range of other wells.

The borehole breakout analysis, presented in Figure 6-9, demonstrates a different fracture attribute in well D-4, on the crest, and D-14, on the flank of the anticline. The large amount of borehole breakout (that indicates a NE-SW maximum horizontal stress by the way) suggests that there may be zones of induced fracturing that could potentially affect the density logs. Fractures, particularly wellbore failure associated with borehole breakout, may potentially result in reduced bulk density measurements. However, the density and

resulted overburden gradient is low even in the shallower depths which are significantly less folded.

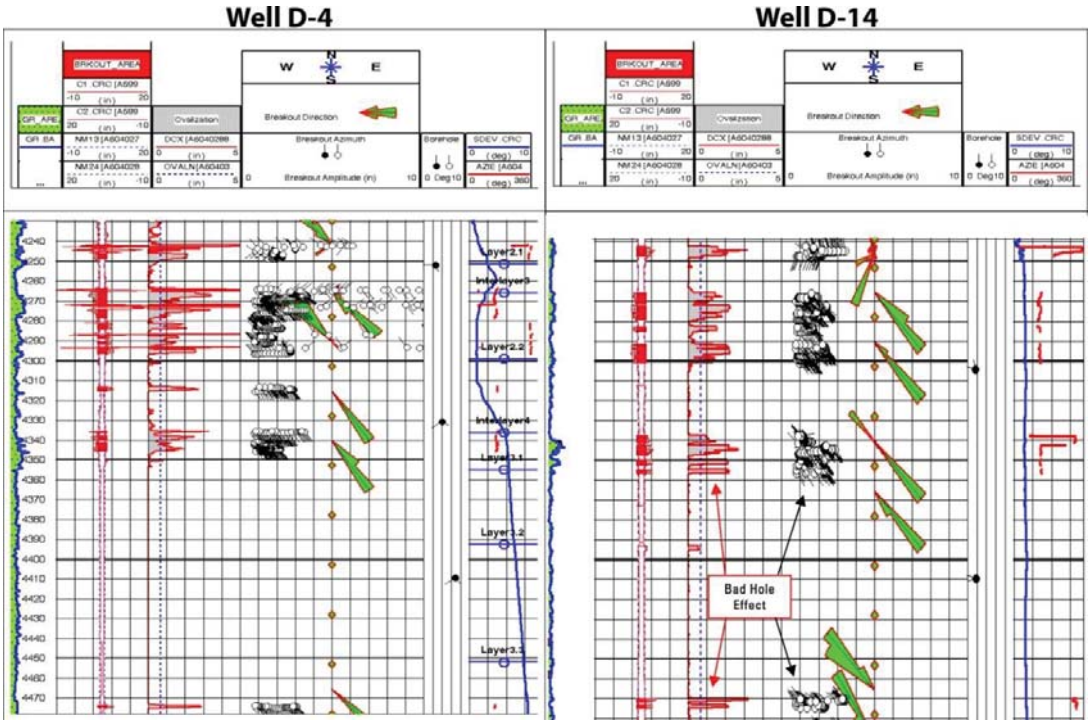

Figure 6-9 - Borehole breakout analysis for in-situ stresses of well D-4 (Field D Owner, 2003) and well D-14 (Field D Owner, 2005). Elongated breakouts are indicated at a number of places. Their longer axes trend dominantly north-west to south-east. According to them the orientation of minimum horizontal stress (σ_{hmin}) is north-west to south-east and the orientation of maximum horizontal stress (σ_{Hmax}) is north-east to south-west.

The reason of abnormally low density values in well D-4 could be due to location, as this well is located at the crest of the field D anticline, where the structure folds (Figure 6-10). That might have caused extensive fracturing which then led to lower density readings in well D-4. It is very odd to see such a shift in density between wells of the same field over a short distance without some major geological reason. The abnormal values belong to the shallower formations whilst the most folded strata, the Gadvan and Fahliyan formations, have same density as other wells of the basin and extensive folding doesn't seem a reason for such low density readings. After all, no geological explanation for lower values of density in the shallow formations of well D-4 was identified (neither by the field owner nor by me based on available data). Therefore, such abnormal density values are considered as false reading of density log.

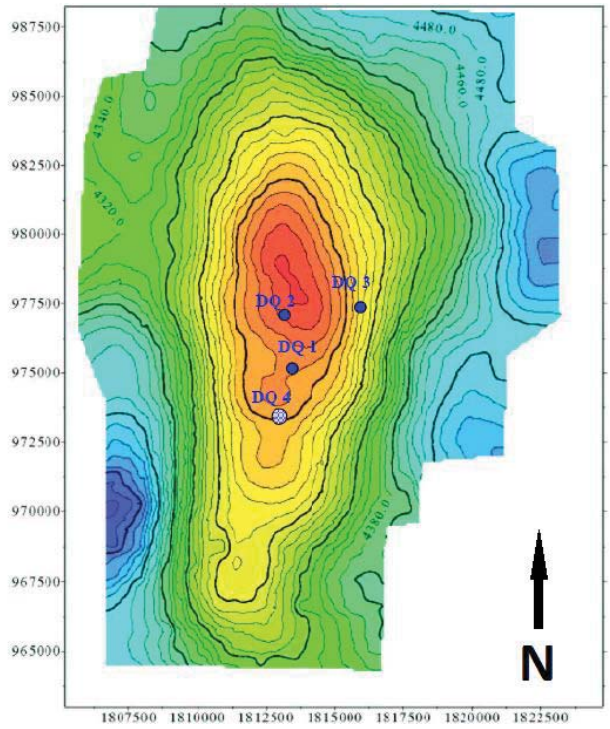

Figure 6-10 - Contour map of Fahliyan Fm. top in field D. Location of well D-4 is indicated on the crest of the anticline.

6.4.3. Implications of Vertical Stress on Pore Pressure Prediction

Several studies after Dickinson (1953), such as Nashaat (1998) and Harrold et al. (1999), used Dickinson's hypothesis to assume that vertical stress could be approximated as 22.6 MPa/km (1.0 psi/ft). This assumption might be valid in some depositional environments, but not in this study as noted above while the average vertical stress gradient in the Abadan Plain Basin is 24 MPa/km. Vertical stress is a key parameter in not only pore pressure prediction, but also in all fracture gradient methods and many other geomechanical analyses that engage the overburden or burial age and rate of deposition in the calculations. Conventional pore pressure prediction methods require σ_v as an input in the equations and therefore, inaccurate values of σ_v will result in erroneous predictions. Due to the varying density of formations and different sedimentation characteristics where each formation undergoes different compaction processes, σ_v varies in wells. Herein, I undertook a sensitivity analysis of the effect of different vertical stress gradients on the predicted pore pressure using typical Eaton (1975) parameters. At 5000m depth, and for the same input parameters other than vertical stress, the predicted pore pressure varied from 12.8 MPa/km to 17.0 MPa/km when vertical stress gradient was increased

from 17.0 MPa/km to 27.0 MPa/km. Hence, a 24% absolute value change in the vertical stress (with respect to the base case of 22.6 MPa/km) potentially results in a 14% variation in the absolute value of predicted pore pressure at 5,000 m depth.

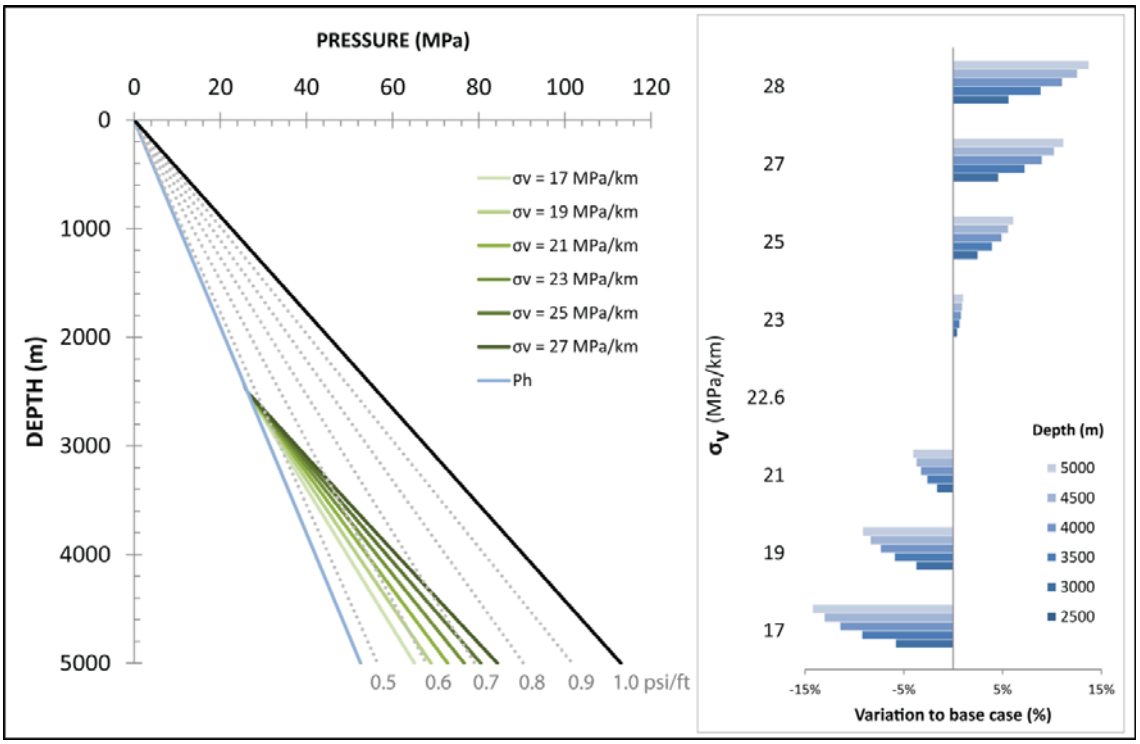

Figure 6-11 – Sensitivity analysis on predicted pore pressure in a conceptual well with varying vertical stress. Vertical stress varies in a range of 17-27 MPa/km which resulted in a greater than 19 MPa difference in predicted pore pressure at 5000 m depth. For the purpose of this analysis, fluid retention depth is at 2600 m.

In this study, all efforts were taken to obtain the most accurate estimation of vertical stress in this basin which is then used in further calculations of pore pressure in upcoming chapter. The special case of well D-4 does not harm the entire analysis as a very few data points were available after performing the shale discrimination scheme on the data of this well; and those points are in shallow deposits of the Aghajari and Mishan formations that are normally pressured.

6.5. Conclusions

Vertical stress is a key parameter in predicting pore pressure in traditional pore pressure prediction analyses, as well as earth's constitutive mechanical models. In the Abadan Plain Basin, vertical stress varies with depth and ranges from 20 MPa/km in well D-4 at the southernmost part of the study area to 25.5 MPa/km in well K-2 in the middle of the basin. The majority of the wells lie in the interval between 22.6 MPa/km (1 psi/ft) and 25.5 MPa/km (1.13 psi/ft). Such a range has been also observed in other sedimentary basins such as Brunei (Tingay, 2003; Tingay et al., 2003). The only well with a substantially lower gradient is well D-4. This abnormal vertical stress in D-4 is attributed to the erroneous density log readings. The rest of the wells exhibited a consistent range of vertical stress gradients. The difference between the vertical stresses is greater at shallower depths and remarkably less at deeper parts of the wells. A south-to-north decreasing trend of σ_v is observed in this basin which suggests the role of the Zagros Deformation on the magnitude of vertical stress in the Abadan Plain Basin. In the light of the narrow range of σ_v variation in this basin, compaction of deposits is identified as the primary cause of the variation in the sediment densities, and associated differences in the vertical stress. Tectonic forces and the structure of the anticlines are secondary phenomena affecting the formation densities. The calculated values of σ_v outlined here will be used in further calculations to predict pore pressure (Chapter 8) after reviewing the diagenesis and porosity evolutions in carbonate rocks in the next chapter to understand pitfalls and regional facts that may result in unreliable pore pressure prediction using conventional methods.

CHAPTER 7- Diagenesis and Porosity Evolution in Carbonate Rocks

7.1. Introduction

Contrary to shales that are highly compressible, carbonates experience a more complex burial process (Choquette and Pray, 1970; Heydari, 2000; Imbt and Ellison, 1946; Lucia and Murray, 1967; Mazzullo, 2004; Moore, 1989, 2001; Murray, 1960; Nurmi et al., 1990; SCHMIDT and MCDONALD, 1979). In addition to purely mechanical compaction processes, carbonate porosity is strongly affected by chemical processes such as pressure solution and dolomisation, which are purely functions of chemical composition of the rock and pore fluid, and implicitly independent of the vertical effective stress (Amthor et al., 1994; Baker et al., 1980; Blount and Moore, 1969; Budd, 2001, 2002; Croizé et al., 2010; Heydari, 2000; Koepnick, 1987; Lucia and Murray, 1967; Melim et al., 2001; Moore and Wade, 2013b; Murray, 1960; Scholle and Halley, 1989; Sheldon et al., 2003b; Stueber and Walter, 1991). Brecciation and fracturing are additional mechanically controlled processes that affect carbonate porosity, but which also act independent of depth and are often independent of vertical effective stress (primarily controlled by tectonic forces) (Brown, 1997; Conybeare and Shaw, 2000; Dravis and Muir, 1993; Longman, 1985; Mohammadlou and Mørk, 2012; Moore and Wade, 2013c; Murray, 1960; Nurmi et al., 1990; Rajabi et al., 2010; Read, 1982; Roehl and Weinbrandt, 1985; Xu et al., 2007). As a result, porosity, in terms of stress dependency, becomes generally unpredictable in carbonate rocks, and, as such, carbonate porosity is often considered to be largely 'stress-insensitive', and thus completely different to shales, in which compaction is primarily 'stress sensitive'. This is a critical distinction, as conventional pore pressure prediction methods (e.g. Eaton, Bowers, etc) all essentially rely on the assumption that porosity (or some proxy for porosity, such as velocity, density, resistivity, etc) is directly related to the vertical effective stress. Indeed, all conventional pore pressure prediction methods, in essence, use a measurably rock property to estimate a vertical effective stress and thus, with the use of the absolute vertical stress, estimate pore pressure. Therefore, applying conventional pore pressure prediction methods is likely to give erroneous results in

carbonates. This chapter undertakes a literature review to examine the diagenesis and porosity evolution of carbonate rocks, and explain in detail why porosity-depth (or porosity-effective stress) relationships in carbonates cannot be easily predicted. First, common classifications of carbonate rocks will be explained before describing the deposition and diagenetic processes of carbonates. Then stress sensitivity of carbonates and implications on determining a normal compaction trend is discussed. Finally, the pore types and evident diagenetic process in the carbonate formations of the Abadan Plain Basin are illustrated and characterized, so as to provide an appropriate foundation for the examination of pore pressure prediction methods in Chapter 8

7.2. Carbonate Rock Classification

As a very common rock type in oil and gas-bearing deposits, the fabric and diagenesis of carbonate rocks have been widely studied and several classification schemes and terminologies have been proposed and developed. In this section, an overview of the various types of carbonate rocks and a brief explanation of the depositional environment and existing classifications of texture and pore space is provided. There are two main types of carbonate rock classifications: the pore space classification and classification based on texture and mineralogy.

7.2.1. Pore Space Classification of Carbonate Rocks

The first attempt to classify carbonate rocks in terms of the porosity was by Howard (1928) and Murray (1930) who categorised the sediments into three main classes: primary porosity, secondary porosity and fractured rocks. The third class, fractured rocks has a secondary post-emergent porosity that might have been developed by the solvent action of mineral salts, carbonic acid and organic acids on calcareous limestones, or on magnesian or dolomitic limestone (Murray, 1930). In the context of my study area and topic, porosity is classified into primary and secondary types only, and fractures are considered as secondary porosity. From that perspective, carbonate rocks frequently show evidence of both primary and secondary porosity. In this research, secondary

porosity is attributed to the various types of pore space changes that have occurred after final deposition. The term final deposition was introduced by Choquette and Pray (1970) for clastic accumulation or accretionary precipitation. This consideration may conflict with definitions that relate primary porosity to the lithification process, but includes broader diagenetic processes as well. Howard and David (1936) developed a classification scheme with more explanations of fractures, and further sub-classified limestone reservoirs. Imbt and Ellison (1946) proposed that classification schemes of carbonate porosities could also be based on the:

- size of openings;
- shape of openings, and;
- origin of openings.

Waldschmidt et al. (1956) expanded this scheme, but with more emphasis on classification of fractures into four major groups of 'open', 'partly filled', 'filled', and 'closed fractures', and provided five subclasses for the positioning of pores as follows.

A. Random.
B. Vertical.
C. Horizontal.
D. Inclined.
E. Intersecting.

Subclasses A and E were further sub-divided into several geometries. A comprehensive classification for the petrophysical rock properties of carbonate rocks was provided by Archie (1952), and is still in wide usage in the petroleum industry. Archie (1952) divided pore space into visible porosity and matrix porosity (porosity which is not visible under a
10-power microscope, or where pore size is less than about 0.01 mm in diameter). He also provided a classification of matrix porosity, including three types of texture: compact

(crystalline), chalky, and granular (saccharoidal), then defined four classes of visible porosity depending on the amount of visible pore space as follows.

Class A: no visible porosity.
Class B: visible porosity, greater than 0.01 mm but less than 0.1 mm.
Class C: visible porosity, greater than 0.1 mm, but less than size of cuttings.
Class D: visible porosity as evident from secondary crystal growth on the faces of cuttings or weathered-appearing faces showing evidence of fracturing or solution channels; where pore size is greater than size of cutting.

Archie's classification is widely used in petrophysical evaluations, but it does not allow any scope for highlighting the influence of depositional environment or diagenetic fabrics, which are also very important factors in carbonate sedimentology (Choquette and Pray, 1970; Lucia, 1983; Murray, 1960). In further attempts to classify the carbonate rocks, pore geometry was broadly investigated to classify their size and shape. Choquette and Pray (1970) classified carbonate porosity types into two major types of 'fabric selective' and 'not fabric selective', with seven and four subclasses in each group respectively. Fabric selective pores are dependent on the 'fabric elements' of the rock, while 'not fabric selective' denotes pore space without any such a relationship. Fabric elements refer to the primary and secondary solid constituents of the carbonate rocks, including their textural and smaller structural features. Choquette and Pray (1970) also attempted to provide a basis for pore size classification by grouping the regular-shaped pores into three classes based on the average diameter of equal or tubular pores and the width of platy pores as follows:

- micro-cracks- less than 1/16 mm
- meso-pores- 1/16 - 4 mm
- mega-pores- 4 - 256 mm

Lucia (1983) provided another classification of based on porosity, dividing the pore space into two categories: 'interparticle' pores and 'vuggy' pores. In his definition, the term

particle has a broader meaning than that of Choquette and Pray (1970) and includes grains (multicrystalline particles) and crystals (single crystal particles). According to this concept, interparticle porosity is the pore space located between the particles of the rock that is not significantly larger than the size of particles. In further classification levels, interparticle pore space was divided into three subclasses based on the particle size. Concurrently, the vuggy pore space was divided into two groups of separate and touching vugs. A summary and comparison of the major classifications explained above is presented in Table 7-1.

Table 7-1 – Main petrophysical classification of pore space in carbonates

Archie (1952)															
Matrix pore space							Visible pore size								
Type I (compact crystalline)	Type II (chalky)	Type III (granular or saccharoidal)					Class A: not visible by x10 microscope	Class B: 0.01mm - 0.1 mm	Class C: 0.1mm to size of cuttings	Class D: > size of cuttings					
Lucia (1983)															
Interparticle							Vuggy								
Particle size							separate			touching					
fine (<20 μ)			medium (20 - 100 μ)			large (>100 μ)									
Choquette and Pray (1970)															
Fabric selective							Not fabric selective				Fabric selective or not				
interparticle	intraparticle	intercrystal	moldic	fenestral	shelter	growth-framework	fracture	channel	vug	cavern	breccia	boring	burrow	shrinkage	

None of the previously explained classifications was capable of covering all common and rare facies. Therefore, an integrated classification was developed by Lucia (1999), according to the two major divisions of interparticle and vuggy pore spaces (Lucia, 1983). It includes the basics of the previous classifications, highlighting the role of fabric on the petrophysical properties (Figure 7-1).

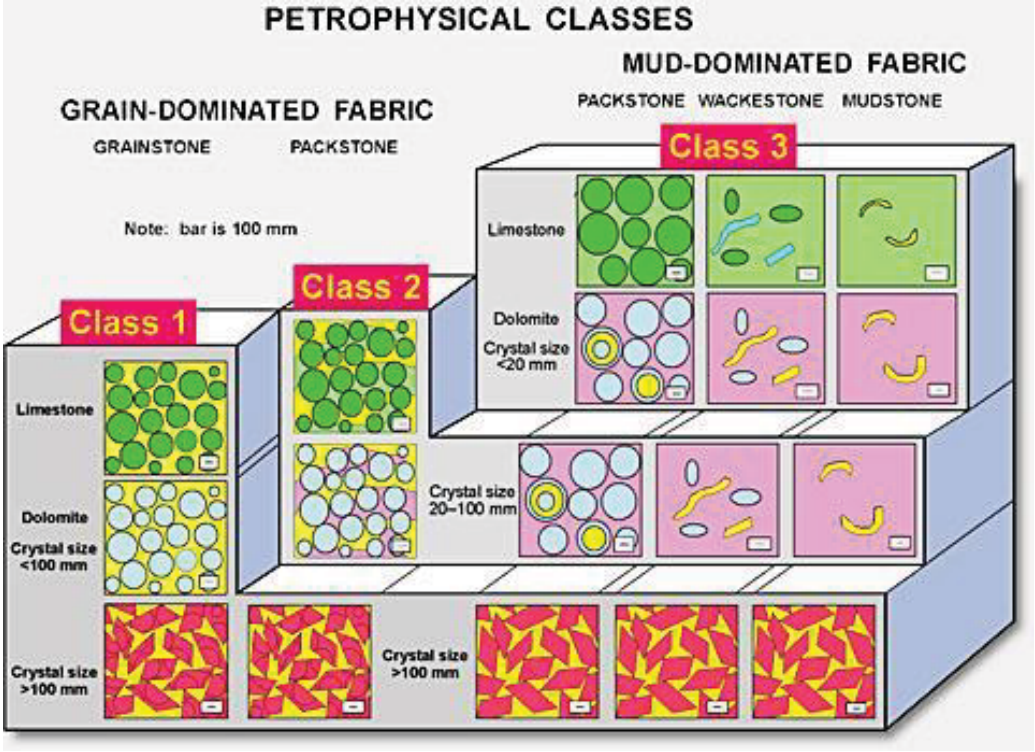

Figure 7-1 - A block diagram illustrating the relationship between rock fabrics and petrophysical classes based on similar capillary properties and inter-particle porosity/permeability transforms (Lucia, 1999). Class 1 includes grainstone, dolo-grainstone, and large crystalline dolostones. Class 2 is composed of grain-dominated packstones, fine and medium crystalline grain-dominated dolo-packstones, and medium crystalline mud-dominated dolostones. Class 3 comprises mud-dominated limestones and fine crystalline mud-dominated dolostones.

7.2.2. Textural Classification of Carbonate Rocks

Carbonate rocks do not only vary based on pore space, but also in terms of the matrix (mostly known as cement) that binds the grains together. Therefore, other classification schemes, focussing on texture and mineralogy, have been developed to alternatively describe carbonate rocks. These first require the origin of carbonate minerals to be properly identified. Carbonate sediments, as a result of deposition in sea water, are

mainly formed either by the precipitation of carbonate minerals from sea water or the extraction of calcium carbonate by the organisms present in the sea water, which forms skeletal material. The vast diversity of biological organisms in sea water leads to various types of sediment fabrics. Harder and larger skeletal species create larger particles, such as sand and gravel-sized particles, while mud-sized particles are formed by planktons. Consequently, inter-particle porosity and related permeability is a function of pore geometry, which is strongly controlled by the amount of cementation. For example, mud-dominated textures compact faster than grain-dominated textures (Figure 7-2).

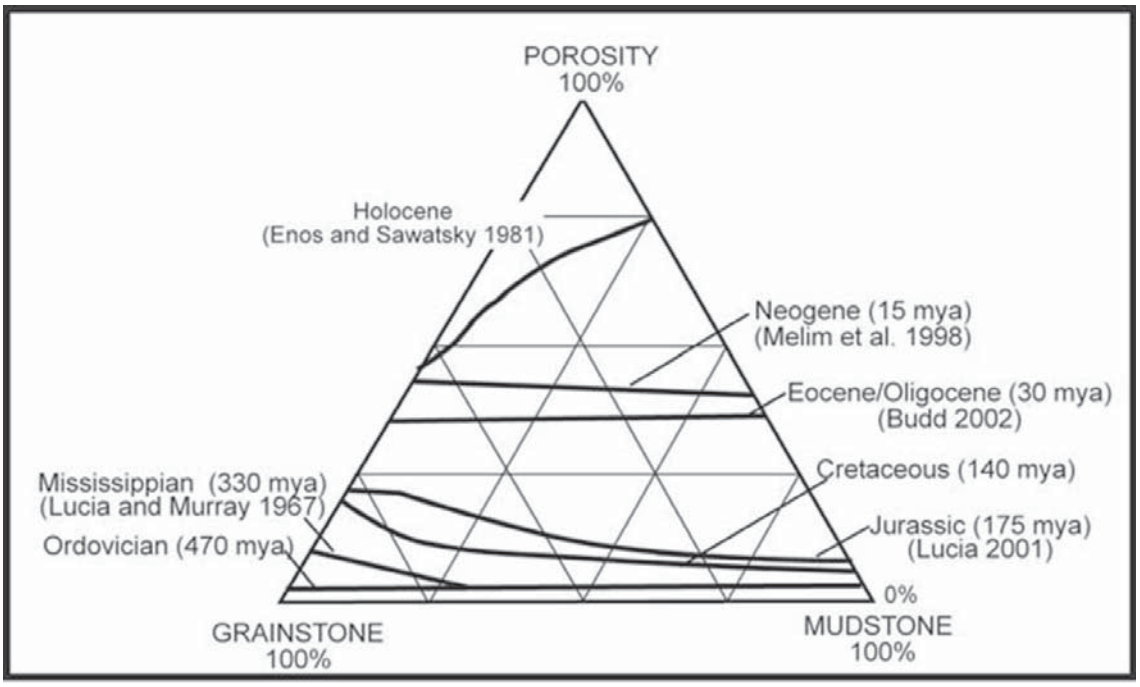

Figure 7-2 - The relationship between porosity, depositional texture, and geologic time modified from Lucia (2007). The referenced articles are: Enos and Sawatsky (1981), Lucia and Murray (1967), Melim et al. (2001), Budd (2002) and Lucia et al. (2001). The porosity loss in the mud-dominated texture is faster than the grain-dominated texture.

Cement is another textural attribute of carbonate rocks and must be considered within classification of carbonates. Generally, precipitation of cement in the pores starts from the pore wall and propagates towards the centre of the pore (Lucia, 1999). Several processes of dissolved precipitation invoke different textures in cement. The type of the precipitation and associated texture depends on the dominant chemical environment within the pore space (Figure 7-3). According to Folk (1974), micritic or fibrous

aragonite and magnesian calcite are created in the pores saturated with sea water, while fresh water produces micritic or sparry calcite. Sparry calcite is also precipitated under deep subsurface conditions.

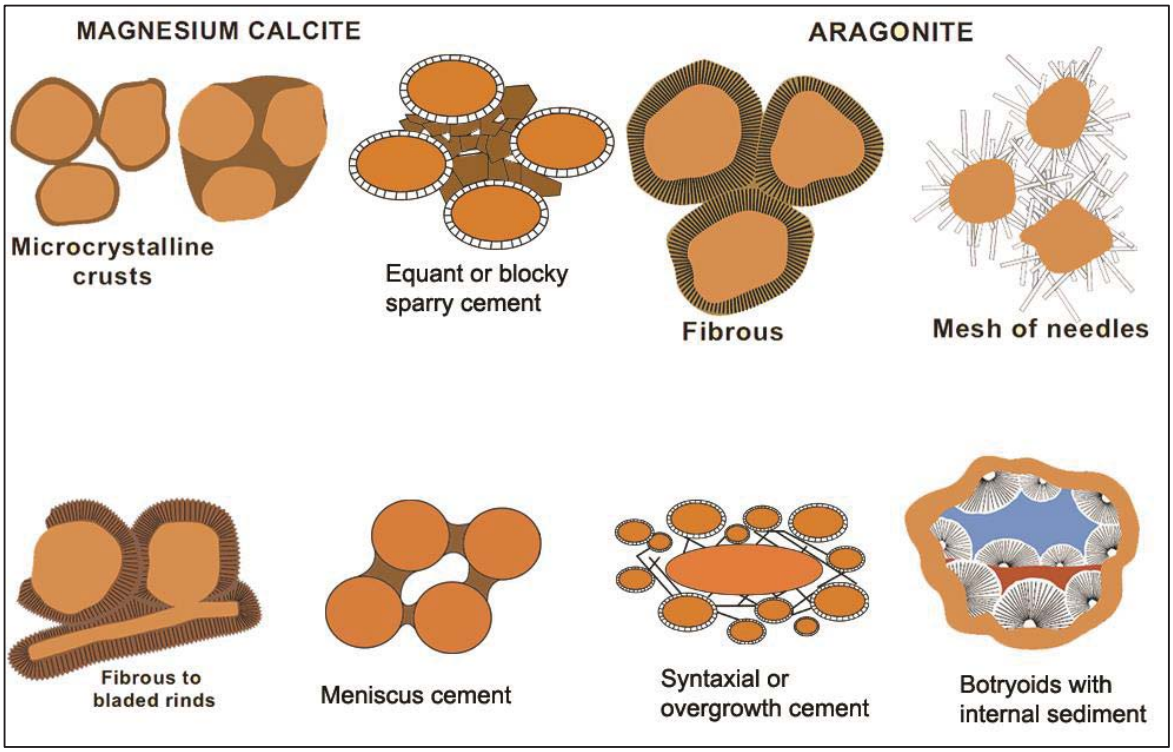

Figure 7-3 - Common calcite cement texture modified from Cui (2012), James and Choquette (1983) and Lucia (1999).

In a further attempt to understand the fabric of carbonate rocks, Archie (1952) classified the matrix texture into three types: compact crystalline, chalky, and granular or saccharoidal. Folk (1959) provided a more detailed classification dividing the dolomitised limestones and primary dolomites into two main groups of terrigenous and allochemical constituents. Then he classified allochthonous dolomites based on their particle size and type. Dunham (1962) provided another classification scheme, based on depositional texture, that first discriminates allochthonous and autochthonous limestones, and then dividing the allochthonous limestone into three sub-classes based on the grain-to-matrix relationship. He signified the role of coarse material (mud) with respect to size, abundance, and condition, as well as its ability to remain at the site of

deposition. Dunham's (1962) classification was simpler and more flexible than that of Folk's (1959), but both seem oversimplified for autochthonous limestones, which are grouped under one term: biolithite by Folk and boundstone by Dunham. A gap in such classifications was size discrimination, which was filled by Ashton and Klovan (1971). They took the idea of previous classifications and introduced new distinction criteria. Their classification identifies six rock types based on particle size and the grain-to-matrix relationship in allochthonous rocks, and three rock types in autochthonous rocks with respect to the way that organisms bind sediments. However, Dunham's classification (Table 7-2) is still the most commonly used tool in sedimentology analysis within the petroleum industry.

Table 7-2 - Classification of carbonate rocks according to depositional texture (Dunham, 1962).

<table>
<tr><td colspan="4">Depositional texture recognisable</td><td rowspan="4">Original components were bound together during deposition:

boundstone</td><td rowspan="5">Depositional texture not recognisable:

crystalline carbonate

(Subdivided according to classifications designed to bear on physical texture or diagenesis.)</td></tr>
<tr><td colspan="3">Original components not bound together during deposition</td><td rowspan="3">Lacks mud and is grain-supported:

grainstone</td></tr>
<tr><td colspan="2">Contains mud</td><td rowspan="2">Grain-supported:

packstone</td></tr>
<tr><td colspan="2">Mud-supported</td></tr>
<tr><td>less than 10 percent grains:
mudstone</td><td>more than 10 percent grains:
wackestone</td><td></td><td></td></tr>
</table>

7.2.3. Carbonate Rock Assessment

Several tools have been introduced with the aim of understanding diagenetic environment and porosity evolution of carbonate rocks. According to a classification by Moore (2001), available techniques are categorized in three groups, namely:

- petrography/geologic setting;
- trace element and stable isotope geochemistry of cements and dolomites, and;
- assessing two-phase fluid inclusions.

Petrography provides a reliable framework for porosity evaluation, with focus on the analysis of cement morphology, cement distribution patterns and grain-cement relationships relative to compaction. The second group of techniques takes into account the type of water involved in the diagenetic environments and includes studying the geochemistry of calcite cements and dolomites, stable isotopes and strontium isotopes. Third group, fluid inclusion techniques, assess the temperature in which cement or dolomite is formed, and also provide essential information about the composition of the precipitating or dolomitising fluid.

Regarding the particular circumstances and level of details required for a reservoir study, either one or a combination of the above mentioned classifications may be used. Apart from their diagenetic nature, rocks are also evaluated with respect to their response to structural load, tectonic forces, or other factors present in the depositional environment. Due to the specific characteristics of carbonate rocks, as is briefly explained in the next section, their response to the overburden and tectonic stresses is not as closely related, or even necessarily directly linked to, carbonate porosity or petrophysical properties.

7.3. Carbonate Rock Deposition, Sedimentation and Lithification

The sedimentation regime of carbonate rocks is a combination of mechanical and chemical compaction that varies with burial depth, temperature, mineral composition, and type of pore fluid. Porosity, and some other rock properties, is modified in three environments known as diagenesis regimes (Cui, 2012; Moore, 2001) (Figure 7-4)

1- Marine environment: characterised by supersaturated sediments with normal or modified pore fluid (Moore, 1989).
2- Meteoric environment: occurs in the vadose zone associated with precipitation of calcite (needle fibres, meniscus cements, and micritic networks), neomorphism and dissolution (Sherman et al., 1999). This zone is characterised by fresh water or very low salt saturation with respect to most carbonate mineral species (Moore, 2001).

3- Subsurface environment: where the pore fluid is either marine or meteoric water (Connolly et al., 1990; Cui, 2012) or there is a mixture of water-rock interactions (Stoessell and Moore, 1983; Stueber and Walter, 1991).

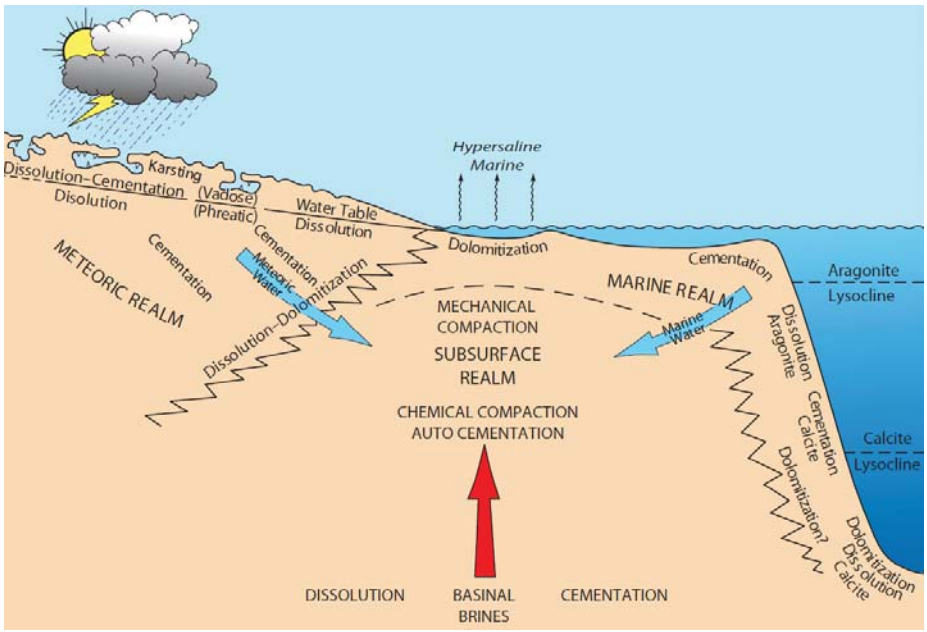

Figure 7-4 – Schematic illustration of diagenetic regimes in a carbonate deposition environment (Moore and Wade, 2013a). Active diagenetic processes are identified in each of the three realms.

In each of the above mentioned environments, different types of burial process takes place. The first stage of burial in shallower depths is mainly dominated by a mechanical compaction and results in de-watering (Figure 7-5). First, a set of grain rearrangements takes place to reach the most stable packing geometry (Moore, 2001). This phase is generally associated with rock fracturing or plastic deformation (Bhattacharyya and Friedman, 1979; Coogan, 1970) and since allochems in unlithified sediments are in a mud context, the deformation is less homogenous because the load is applied on both the mud and grain. The force on the grain surface would vary in different parts of the deposit depending on the grain/mud proportion, mud strength and magnitude of the load. To put it simply, compaction in post-lithified sediments exhibits more homogeneity as the load is uniformly applied on the rigid substance. Therefore, co-existence of deformed and undeformed allochems is essential for distinguishing the relative time of compaction with respect to lithification (Bhattacharyya and Friedman, 1979).

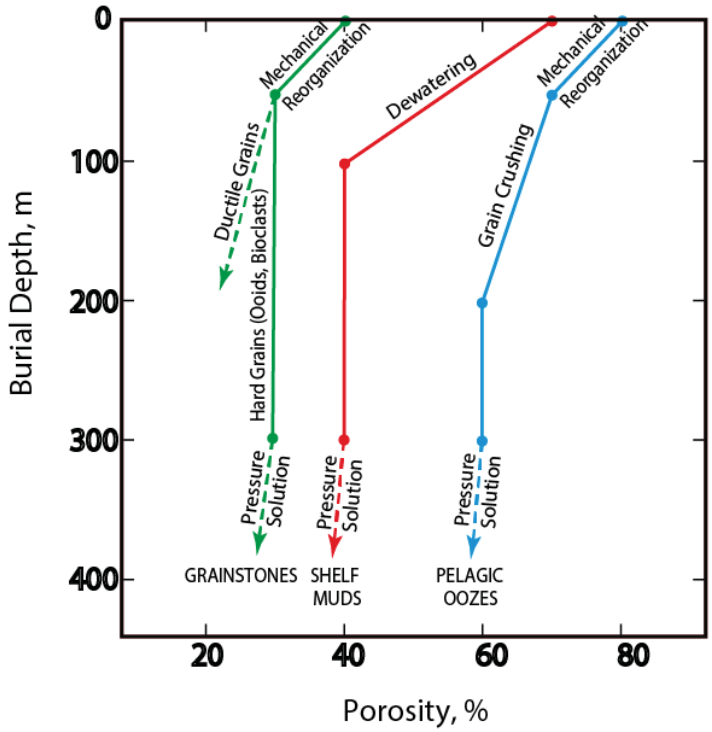

Figure 7-5 - Schematic diagram showing the porosity evolution of shelf grainstones and mud versus pelagic oozes during the first 400m of burial, modified from Moore (1989) and Moore (2001). Curves are created based on data from Neugebauer (1973), Scholle (1977), Garrison (1981) and Enos and Sawatsky (1981).

It is important to notice that mechanical compaction would be different in grain-dominated deposits (such as carbonate sands) and mud-dominated sediments (Moore, 2001) and therefore, clay plays a critical role in controlling a variety of mechanical and chemical responses to the applied load. Clay in the rock fabric could enhance force diffusion or, at the same time, impede cementation (Sibley and Blatt, 1976).

Mechanical compaction influenced by the mineralogy of the sediments (controlled by depositional environment) creates the rock frame with the primary porosity. After that, several processes are applied to the carbonate rocks which modify the existing porosity, either by creating more pore space or reducing pore space by filling them. Additional

porosity created by post-depositional events is known as secondary porosity and could form from either of the following processes:

1- dissolution
2- dolomitization
3- brecciation
4- fracturing.

Similar to this classification, Lucia (1999) grouped diagenetic processes according to their conformance to depositional patterns in order to study the petrophysical rock fabric. The first group involved cementation, compaction, and selective dissolution. The second group consisted of reflux dolomitization and evaporite mineralisation, while massive dissolution, collapse brecciation, and fracturing formed the third group. The dissolution process is occasionally followed by mineral precipitation and the resultant porosity is discussed herein under the title of chemical compaction.

7.3.1. Chemical Compaction

Once carbonate sediments become stiffer and lithified, increasing load results in greater elastic strain at the individual grain contact points. The increased strain leads to a high potential for chemical reactions, such as solubility at grain contact points (Moore, 2001). Under such conditions, as a crystal is immersed in its saturated solution, the contact points of the grains under stress may be dissolved (Bathurst, 1972). This phenomenon is known as the 'pressure solution' which is attributed to the dissolution of minerals under non-hydrostatic stress (Durney, 1972). Indeed, the original mineralogy of the sediment and the pore-filling fluid properties are key controlling factors over the whole process of 'chemical compaction', which involves one or more cycles of pressure solution and cementation (Moore, 2001). As a result, the dissolution of rock mass into the pore fluid creates several textural features (Figure 7-6). A numerical model for rock deformation and mass transfer by pressure solution is provided by Rutter and Elliott (1976) as a function of pressure and temperature. Meanwhile, Sibley and Blatt (1976) observed less

pressure solution in the well-cemented samples of the Tuscarora Orthoquartzite samples than was seen in more friable samples, but with more cemented samples also displaying greater amounts of pore fill mineralisation. They pointed to four factors that control the amount of pressure solution: proximity to folds; grain size; sorting; and clay content.

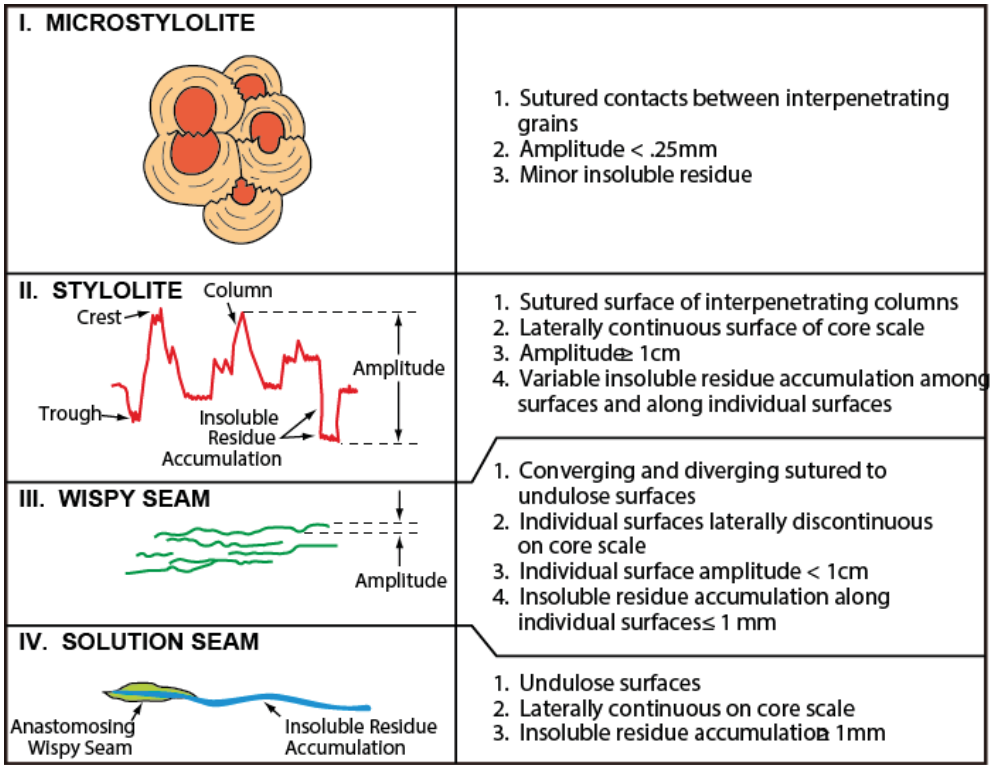

Figure 7-6 – Types and characteristics of pressure solution features that develop in underground conditions based on Koepnick (1984), modified from Moore (2001).

In carbonate sequences, massive dissolution can be either carried out by near surface water (Lucia, 1999) or deep burial fluid (Dravis and Muir, 1993) and leads to substantial secondary porosity. Several major oil and gas reservoirs in the Middle East, such as the Ghawar supergiant field in Saudi Arabia, are enhanced by this type of diagenetic process. Pressure solution also creates stylolites, which can be filled by several chemicals and minerals such as dead oil in the Dariyan Formation and sparry calcite, pyrite, black organic matter and rare dark grey argillaceous matter in the Fahliyan Formation of the Abadan Plain Basin (Figure 7-15). Aharonov and Katsman (2009) suggested that stylolites propagate only when both the pressure solution and clay-enhanced dissolution take

place in unison. A list of key parameters influencing pressure-solution/recrystallisation reactions in carbonate rocks is provided in Table 7-3.

Table 7-3 - Mechanisms and controls of pressure-solution/recrystallisation reactions in carbonate rocks (Baker et al., 1980).

Porosity (permeability)		
low porosity	**high porosity**	
transport control	**surface area**	
	low	**high**
	rate of dissolution control; stress concentration is an important predictor	rate of dissolution and crystal growth, about equal magnitude inhibition is important; low super-saturation (high silicates content cause inhibition)

Dissolution can be accelerated by high stress at grain-to-grain contact points and the dissolved particles may precipitate in the adjacent pore space where the regional stress is lower. Precipitation is found in the form of 'calcite cement', which is composed of calcite,

high-magnesium calcite, or aragonite (Lucia, 1999). The porosity loss by cementation is equal to the proportion of total inter-granular cement to total pore space (Heydari, 2000). After, or during, matrix texture precipitation, grains could undergo partial leaching which creates porosity. On some occasions during meteoric diagenesis, grains are leached out completely by selective dissolution while the matrix remains unaltered. In such cases, the main porosity is ex-grain and the rock framework consists of phreatic cement. In this research, I follow the definition of cement by Bathurst (1972) to include all passively precipitated, space-filling carbonate crystals that grow attached to a free surface. Meanwhile, it is briefly noted here that there are three main requirements for calcium and carbonate ions to undergo continuous cementation (Lucia, 1999).

1- Grain dissolution associated with chemical compaction.
2- Dissolution of unstable minerals, such as aragonite.

3- Long distance transport of ions by ground water flow.

As another control on chemical compaction, thermal degradation of hydrocarbons in carbonate environments at temperatures higher than 150°C generate CO_2, H_2S, methane and solid pyro-bitumen (Sassen and Moore, 1988). Although the combination of CO_2 and H_2S in an aqueous environment could accelerate dissolution and enhance porosity, solid pyro-bitumen precipitation can significantly degrade formation porosity (Moore, 2001). Therefore, cementation will not proceed in pores filled by hydrocarbon, and any further dissolution (without cementation and in the absence of compaction) may create additional secondary porosity.

7.3.2. Dolomitization

Hypersaline evaporated sea water accumulated in hypersaline tidal flat environments and associated hypersaline ponds, lakes, and lagoons could reflux from the surface down into underlying strata, replacing seawater and interacting with ground-water (Lucia, 1999). Sea water flows down towards the sea by a hydrodynamic force due to the higher density of sea water and the higher elevation of tidal flats. As a result of hypersaline sea water and groundwater interaction, dolomites are produced, and gypsum and anhydrites are precipitated. Chemical reactions forming dolomite are in two forms of replacement and cementation (Lucia, 2007).

$$2CaCO_3 + Mg^{++} = CaMg(CO_3)^2 + Ca^{++} \quad \text{(replacement)} \qquad \text{Equation 7-1}$$

$$Mg^{++} + Ca^{++} + 2CO_3 = CaMg(CO_3)^2 \quad \text{(cementation)} \qquad \text{Equation 7-2}$$

The role of magnesium, and the need for fluid flow to introduce the magnesium to the system, is obvious from the above chemical reactions. Murray (1960) provided an interesting relationship between dolomite content and porosity in the Midale beds (lime muds) of the Charles Formation, Midale field, in Saskatchewan, Canada. Floating dolomite rhombs occupy available pore spaces as long as the mud is consists of up to 50% dolomite. From this point, dolomite rhombs provide a rigid framework for the sediment and

prevent further compaction. Therefore, porosity increases with increasing dolomite percentage (Figure 7-7). Lucia (2007) reported a porosity increase by dolomitization in mud-dominated carbonates, but with no significant effect on pore size distribution in grainstones. Saller and Henderson (1998) observed a varying effect of dolomitization on the porosity in the Permian platform dolomites of west Texas. Saller and Henderson (1998) also investigated the role of differential compaction in the formation of platform-margin dolomites over structural highs, and platform-interior dolomites in down-dip and basin-ward structures. Differential compaction provided the best reservoir quality on the basin-ward flanks of the structure, while the reservoir quality was the worst on the crest of the structure.

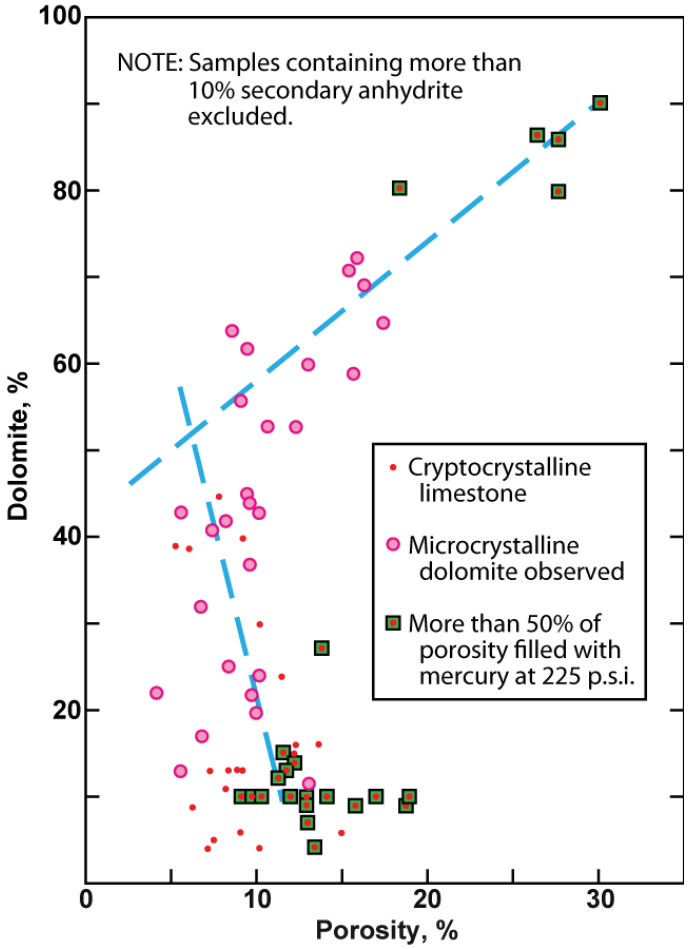

Figure 7-7 – Relationship of porosity to fraction of dolomite in the Midale beds of the Charles formation, Midale field, Saskatchewan, Canada, modified from Moore (2001) and Murray (1960).

There is another process that occurs in dolomites, similar to differential compaction, that is known as 'evaporite mineralization' (Lucia, 1999). Evaporite mineralisation was previously which was explained in detail under gypsum to anhydrite transformation in Chapter 4. The controlling factors in this reaction are temperature and water activity. Hardie (1967) provided a relationship between these parameters (Figure 7-8), which showed a reasonable compatibility to the recent supertidal flat sediments of the Trucial Coast in the Persian Gulf.

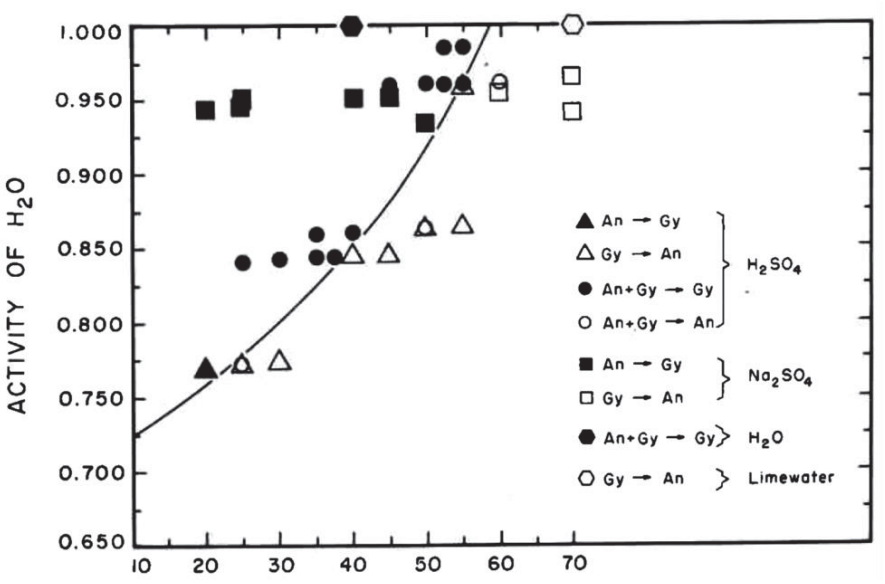

Figure 7-8 - The stability of gypsum and anhydrite determined experimentally as a function of temperature and activity of water at atmospheric pressure (Hardie, 1967).

Lucia (1999) classified anhydrite and gypsum textures in carbonate rocks, and their effect on the formation porosity and permeability, as follows (Figure 7-9).

1. Poikilotopic anhydrite crystals are formed by a combination of replacement and pore-filling mechanisms that reduce porosity. Since poikilotopic anhydrite is typically scattered across the rock, the matrix between crystals remains constant and permeability is not affected while pore size remains constant.
2. Nodular anhydrite is a form of diagenetic texture that does not reflect the depositional environment conditions. It is formed within the sediments by

displacement as either anhydrite or gypsum in the shape of microcrystalline masses. While it locally reduces porosity, total rock porosity and permeability does not change as these nodules only make up a small percentage of the bulk volume.

3. Pore-filling anhydrites are pervasive, evenly distributed in the rock, and occlude the inter-grain, inter-crystal, and vuggy pore space. They have a destructive impact on porosity and permeability.
4. Bedded anhydrite is deposited out of hypersaline water as gypsum, which converts to anhydrite later in the form of laminated or coalesced nodules. It is formed either by precipitation out of water or by displacement and replacement of near surface sediments as gypsum or anhydrite. This type of anhydrite is laterally continuous and provides an impermeable barrier and seal for reservoirs.

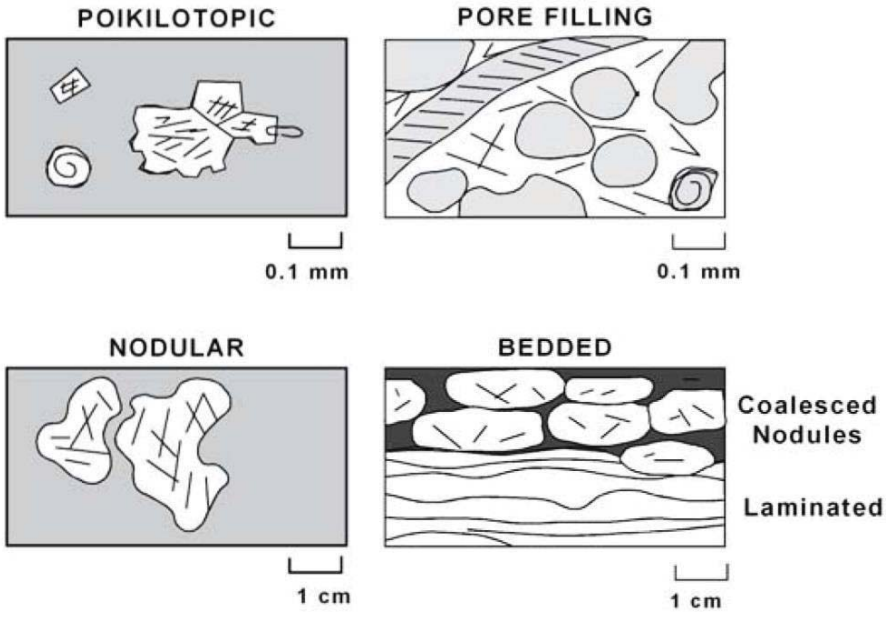

Figure 7-9 - Anhydrite and gypsum textures in carbonate rocks (Lucia, 1999).

7.3.3. Brecciation

Several conditions in carbonate rocks lead to massive dissolution that can cause large scale collapse and brecciation (Lucia, 1999). This phenomenon happens in situations such as limestone solution collapse, evaporite solution collapse, faulting and soil formation (Blount and Moore, 1969). Four types of brecciation were classified by Kerans (1990) as: fracture breccia, mosaic breccia, chaotic breccia (siliclastic-matric supported), and chaotic breccia (carbonate-clast supported). A schematic diagram (Figure 7-10) shows that several facies may be formed during massive dissolution, with several mineralisation processes. The additional pore space created in such conditions provides improved reservoir conditions, and can host hydrocarbons under some circumstances, such as those of the Mississippian Northwest Lisbon field, Utah (Miller, 1985) and the Permian Yates field (Craig, 1988). Additional evidence of karstic limestone collapse associated with unconformities was provided by Kerans (1993) in west Texas, and which improved reservoir quality.

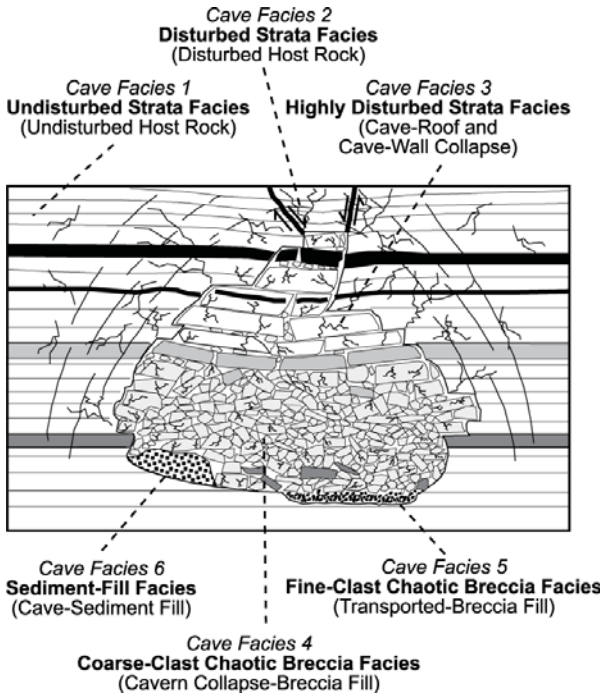

Figure 7-10 – Schematic diagram of burial evolution of cave-related breccia (Loucks and Mescher, 2001; Loucks et al., 2004).

7.3.4. Fracturing

A fracture is a discontinuity or parting in material caused by brittle failure (Narr et al., 2006). According to this definition, joints and faults are types of naturally occurring fractures. Fractures are the deformation strain of a rock body against stress, and can form from many processes. A natural fracture system can play a significant role in reservoir performance during primary, secondary, and tertiary recovery. Despite the low intrinsic porosity and permeability of carbonate grain and matrix, a remarkable amount of hydrocarbon is produced from fractured carbonate formations. As an example, the Asmari limestone (Oligocene-Miocene) of the Gachsaran field in Iran (which has been producing 80000 barrels of oil per day) has a total porosity of 25% porosity and greater than 100 md permeability, even though the matrix porosity is only 5-9% (McQuillan, 1985; Nairn and Alsharhan, 1997). Fractures are particularly common in carbonate rocks due to their brittle nature when compared with fine-grained siliclastics. Since naturally occurring fractures originate as a result of various mechanisms, fracture patterns vary in their attributes and are primarily related to stress conditions at the time of fracturing. Though, some fracture systems tend to be simplified when the paleo-stratigraphical model is constructed (Zahm et al., 2010).

Three common driving forces that create fractures are tectonic stresses, pore fluid overpressure, and the formation of large voids (Lucia, 1999). Tectonic stresses are explained in terms of stress analysis (Zoback (2007)), and are typically considered to result in three different types of fractures: shear fractures, extensional fractures, and tensile fractures. However, Nelson (2001), classified naturally occurring fractures in four types, based on the nature of causing effects.

1- Tectonic fractures (due to surface forces)
    a. Fault-related fractures
    b. Fold-related fractures
    c. Other tectonic fractures (such as piercement and impact structures).
2- Regional fractures (due to surface forces or body forces), a result of:
    a. desiccation

   b. syneresis
   c. thermal gradients
   d. mineral phase changes.

3- Contractional fractures (due to body forces).
4- Surface-related fractures (due to body forces).

According to this classification, tectonic fractures are those created, or attributed to, tectonic events and are associated with the folds and faults. Nelson (2001) stated that the majority of tectonic fractures in outcrops tend to be shear fractures. Regional fractures are those that are developed over large areas of the earth's crust with relatively little change in orientation. Desiccation fractures are like mud cracks, which result due to shrinkage upon loss of water in subaerial drying. Syneresis fractures are the result of chemical processes during subaqueous or subsurface dewatering which cause volume reduction. Thermal contractional fractures are created when a hot rock cools due to different thermal gradients (Turcotte, 1974). Mineral phase change fractures are those created due to the mineral phase change in carbonate or clay constituents where the substances have different molar volumes before and after a mineral transformation (Kulander et al., 1990). Under proper conditions, mineral phase changes can create a 'chicken wire pattern' of fractures. Contractional fractures can be due to tension or extension and result in a general bulk volume reduction in the rock. Finally, surface-related fractures are the result of body forces during unloading (Fertl, 1980). The most common feature of this type is observed in quarrying operations when a piece of rock body is removed from the quarry. The rock relaxes due to reduced surface load, and spalls or fractures on a plane parallel to the newly developed free space. Extensive fracturing creates a brecciation pattern in rocks. Indeed, the characteristics of fold-related fractures, such as opening, propagation and distribution, are generally predictable from numerical modelling of the bedding curvature (Calladine, 1986; Fischer and Wilkerson, 2000; Lisle, 1995; Ramsay, 1967).

7.4. Stress Sensitivity of Carbonates

The compaction of carbonate rocks is a more complex process than in siliciclastic deposits, because post-deposition petrophysical attributes of the rock are not controlled by mechanical factors. Compaction in carbonate rocks is often not clearly related to effective vertical stress, as several diagenetic processes create or destroy porosity after burial and, therefore, porosity-depth relationships cannot be defined as a function of overburden stress. The prior review of carbonates and their classification schemes highlights that it is critical to know the conditions under which a rock was deposited in order to develop any understanding of a carbonate's mechanical attributes. The composition of carbonate rocks can reflect depositional environment because of two reasons: lack of transport in carbonate regimes and the direct tie to the biological components of the environment (Moore, 2001). Due to the vast variety of organic and chemical parameters in the marine environment, where the majority of carbonate rock is deposited (Kendall and Schlager, 1981; Milliman, 1974; Wilson, 1975), a wide variety of petrophysical properties are observed. There is strong evidence that carbonate porosity decreases exponentially with depth (Heydari, 2000; Schmoker and Halley, 1982). However, predicting compaction trend as a function of depth or overburden stress is still generally an invalid approach. Furthermore, it is also noted that carbonates are not the only rocks to often exhibit a lack of any robust porosity-depth relationship, as this is also observed in shales of the North Sea due to diagenetic phenomena occurring along with mechanical compaction (Carstens and Dypvik, 1981; Teige et al., 1999).

As noted earlier, carbonate rocks mainly consist of the grain and inter-particle cement, which binds the grains together. Any stress on the rock is carried by both the grain and cement, and the rock can deform in different ways depending on the strength of either part. On the other hand, carbonate rock burial history consists of two mechanical and chemical compactions. At shallow depth, non-cemented rocks undergo a mainly mechanical compaction, which rearranges the position of grains with respect to each other as well as cement. This configuration and the grain-to-grain contact is, in turn, linked to chemical compaction in deeper sediments. Chemical compaction is dependent on the rock's petrophysical properties as well as pore fluid. Another controlling

parameter in the extension of the chemical compaction processes is the diffusion of solids into the pore fluid, which is also a time dependent variable of mineral and fluid interactions.

The complexity of porosity in the carbonate pore system is due to a variety of reasons related to diagenesis, which converts a carbonate rock from a shallow porous sediment to a low porosity rock (Choquette and Pray, 1970; Heydari, 2000) and from an unstable mineral combination to a stable assemblage of low-magnesium calcite, etc. (Choquette and Pray, 1970; Land, 1967; Runnegar, 1985). Geological structures also control the occurrence and frequency of the petrophysical features, such as dissolution and karstification, associated with subaerial exposures that occur over the depositional high and crest of structures. A brief explanation of the diagenetic processes in carbonate rocks was provided earlier whilst remarkable work has been done on this subject to understand the whole phenomenon, which is available in the literature (Bathurst, 1972; Garrison, 1981; James and Choquette, 1983; Koepnick, 1987; Land, 1967; Moore, 1989; Neugebauer, 1973; Schmoker and Halley, 1982; Scholle, 1977; Sherman et al., 1999). In the context of diagenetic processes, the complexity of pore shape and size in carbonates is attributed to the wide range of particle sizes and shapes of the rock. The skeletal organs that form the grain, or primary hard framework, also exist in a wide range of textures, shapes and sizes. Initial pores are, therefore, expected to be highly varied as a result of particle positioning. Additionally, pore-filling cement also varies extensively in nature and size. In Choquette and Pray's (1970) classification, the grain and pore-filling fluid interactions have been considered as a fabric-selective attribute of the rock, which takes into account the porosity enhancement potential of the mineral dissolution into the fluid phase. In many limestones, the volume of pore-filling cement is almost the same as, or even exceeds, that of the initial sediment, and additional porosity as a result of dolomitization is quantitatively minor compared to the porosity loss that happened in the subsurface (Pray and Choquette, 1966).

In terms of the chemical reactions taking place in carbonate depositional environments, it is noted that pressure solution and calcium carbonate precipitation are two concurrent processes that have different impacts on rock porosity, and make porosity-depth

predictions problematic (Choquette and Pray, 1970; Harris and Matthews, 1968). In carbonates, chemical compaction is also strongly affected by pre-existing fracture patterns and vadose/phreatic contact (Lucia, 1999). Dissolution is partially affected by the depositional texture, where the soluble minerals, such as evaporites, are selectively dissolved in groundwater and create karstic porosity. This means that the existence of fractures filled with various minerals, including calcite, dolomite, anhydrite, galena, sphalerite, celestite, strontianite, and fluorite, is another source of carbonate rock complexity (Moore, 2001). This causes increased heterogeneities in the petrophysical properties of these sediments and makes them less predictable.

Fractures are created under different conditions and they add huge uncertainty to geological models by their complex distribution in non-homogenous rock types. Fractures are dependent not only on stresses, but also on rock fabric and mechanical strength, which varies spatially over depth and width within a specific formation. Different fracture attributes, such as opening and length, make the rock properties highly variable, even whilst the fractures significantly improve porosity and permeability of the reservoir. Alternatively, by increasing the load on carbonate rocks, cracks may originate and develop along the matrix (by-passing the harder grains and developing fissures in the fine-grained mud) or across the grain and matrix together. Fractures can develop perpendicular to the direction of least stress in the environment (Ingraffea, 1987; Nordgren, 1972; Salz, 1977; Zoback, 2007). But the matrix and particles would have different response to the stresses. A test done by Shinn et al. (1977) on carbonate rocks revealed a surprising result of compressive behaviour of the rock particles. While there is a measurable bulk compressibility, the shells, foraminifera and other fossils remained uncrushed under compressive stress up to 7900 psi, confirming the selective creation of primary cracks in the matrix. In the folded structures, the highest intensity of fractures exists at the crest while there is a preferred orientation in the lowermost section of the layer that improves the vertical permeability parallel to the formation's structural axis. Precise drilling is needed in such anisotropy to intersect those fractures and thereby improve the rate of reservoir drainage through the well.

It must be noted that diagenesis is not limited to compaction and, in many carbonate sediments, it involves tectonism and post-tectonism events. Therefore, recent diagenetic processes could also alter pre-existing porosities by a large amount, as pore fluid may flow through high permeability conduits and cause excess pore space. This may place formation porosity and permeability in complete opposition to Saller and Henderson's (1998) findings, where they showed a destructive effect of dolomitization on porosity. However, the mineralogical modifications occur when the metastable minerals such as magnesian calcite and aragonite, as the main parts of the carbonate sediment, are exposed to the meteoric waters over the geological time leading to dissolution and then stable mineral precipitation, in the form of calcite and dolomite (Moore, 1989, 2001). A schematic of the varying relationship between porosity and depth in a carbonate rock (Figure 7-11) shows several stages of porosity evolution over time.

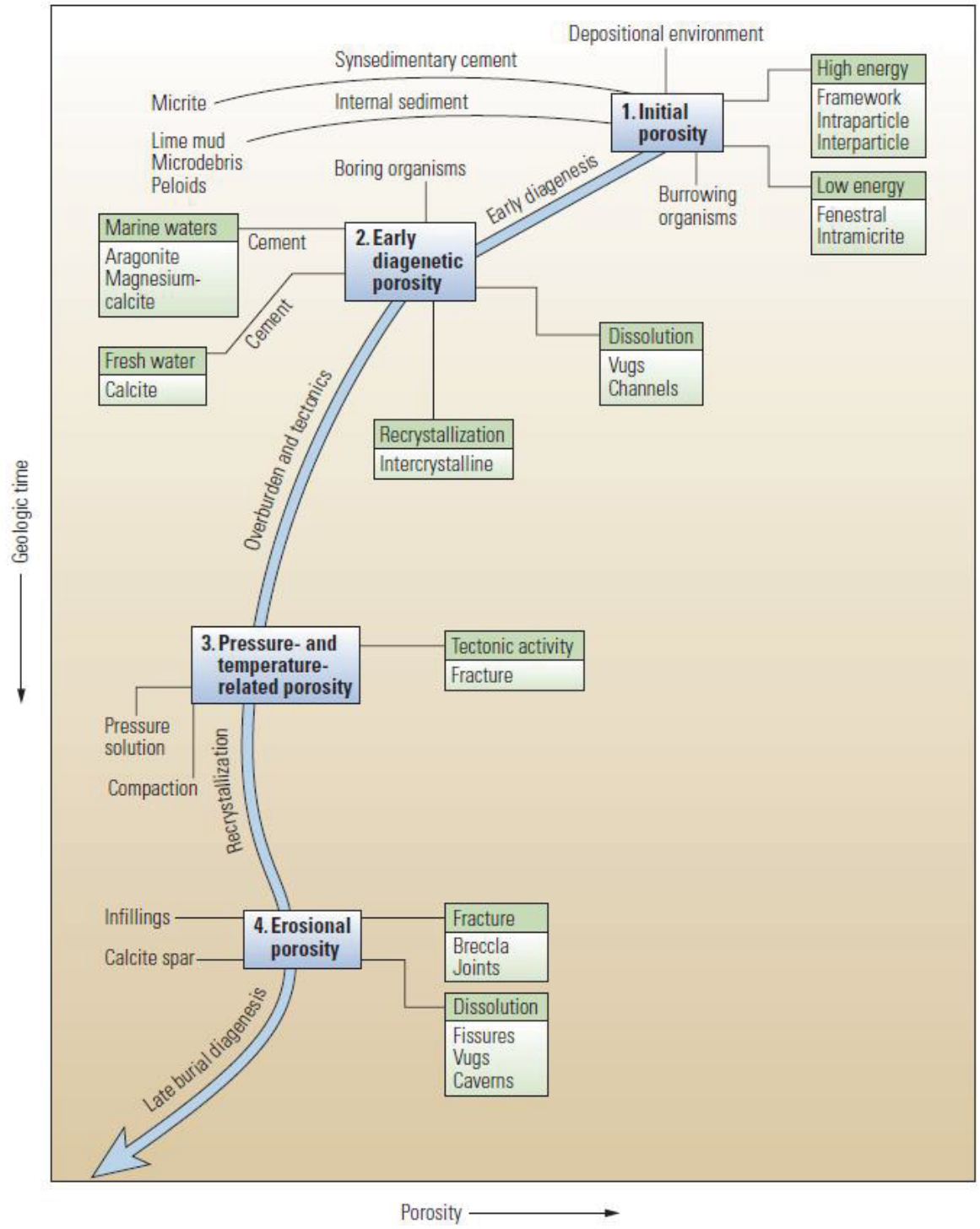

Figure 7-11 – Carbonate porosity (Ali et al., 2010 which is adopted from Aquitaine et al., 1982 and Derby, 1984). Porosity generally decreases during early diagenesis and further burial until the onset of pressure solution and/or fracturing that creates additional pore space. Further crystallization inhibits the porosity rise until another stage of porosity rise due to recent erosion that creates fissures, vugs and caverns.

Although porosity normally decreases with depth, obtaining a function that relates compaction to just a single parameter, and specificallya function of effective stress, simply is not plausible for most carbonate rocks. As such, all existing pore pressure prediction methods struggle to provide reliable and accurate estimates in many carbonates. Several other important factors directly or indirectly control the porosity in the carbonate rocks. For example, Swarbrick (2012) outlined the effect of temperature and its effect on cementation and seal development (and, consequently, overpressure generation) . From that point of view, there are four aspects of traditional pore pressure prediction that are affected by temperature include:

- rocks become stiffer in higher temperature, which accelerates cementation;
- higher temperature augments dissolution, and further rock body collapse reduces pore space;
- higher temperature makes grains more ductile and weakens the rock framework, and;
- mineral transformations (e.g., clay diagenesis) will be accelerated in higher temperatures.

Due to the large diversity in trends, there is no unique porosity-depth relationship that can be used to relate porosity to depth of burial and estimate porosity in present day. A list of rock body compaction models on chronological order has been presented by Chilingar et al. (2002), though all are based on porosity variation of clay versus depth of burial. Figure 7-12 shows the different depth-porosity relationships for rocks in several geographical locations.

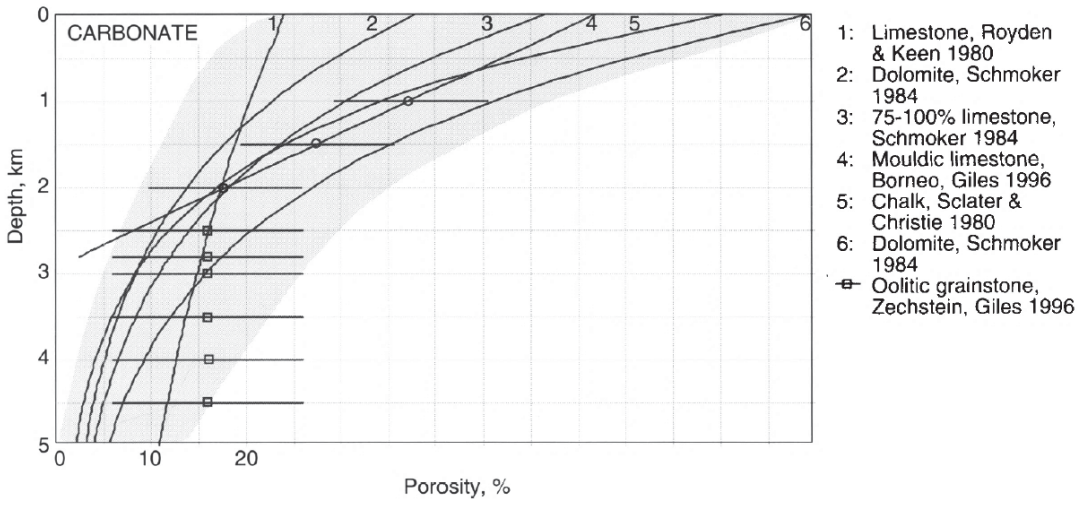

Figure 7-12 – Porosity versus depth trends for carbonates (Giles et al., 1998). Curves are from Royden and Keen (1980), Schmoker (1984), Giles (1997) (noted as 1996 in the figure), and Sclater and Christie (1980).

Since the nature and fabric of carbonates varies, petrophysical characterisation also requires a specific set of empirical relationships. Permeability–porosity relationships in carbonates, as a characteristic of the formation, also exhibita wide range, as illustrated in Figure 7-13. Wackestones and mudstones exhibit the lowest porosity and permeability while reefal rocks provide the highest value of permeability, and grainstone as well as cocolith chalk provide the highest porosity. According to Lun et al. (2013), stress sensitivity of porosity is lower than that of permeability in a carbonate environment. They analysed porosity and permeability in four types of core samples with different fracture attributes, including matrix cores and cores with non-packed, semi-packed and fully-packed fractures in the littoral Caspian Basin (Figure 7-14). As a result, the packing degree of fractures had a great impact on the stress sensitivity due to the closure of fractures under the overburden load.

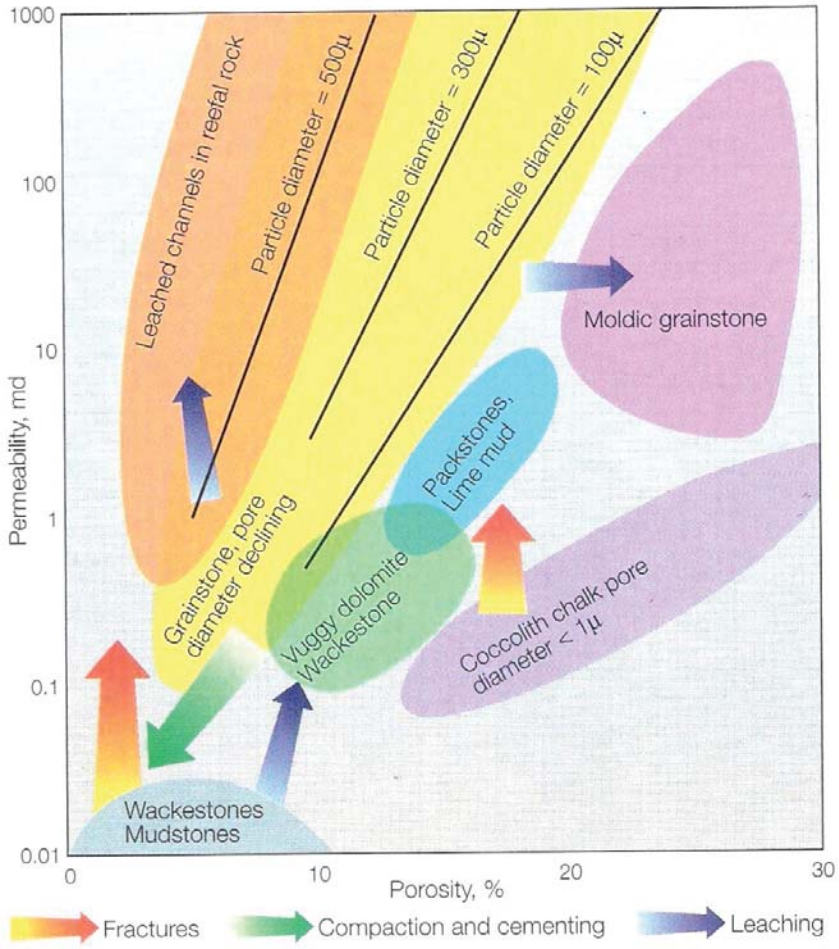

Figure 7-13 - Porosity, pore type, and permeability in carbonates (Delhomme, 2007). Fractures are associated with great permeability improvement whilst they create less porosity compared to other processes. Note the porosity reversal trend of cementation at the bottom left part of the figure.

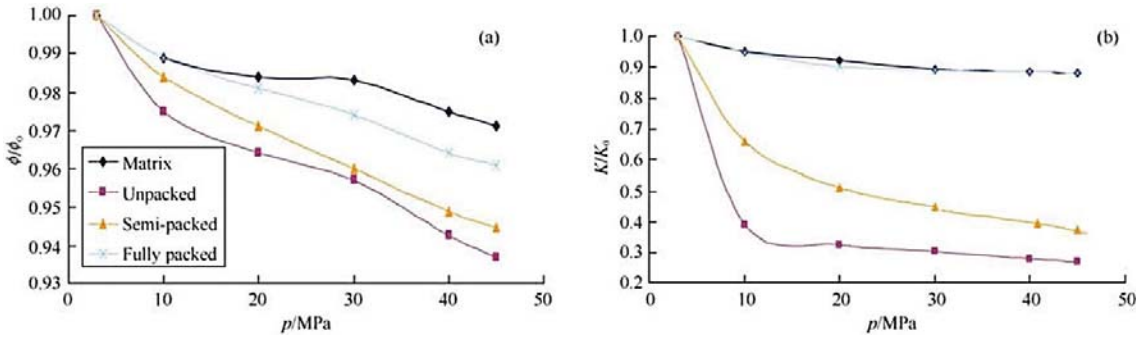

Figure 7-14 - Comparison curves of the variation in (a) porosity and (b) permeability of cores with different packing degrees (Lun et al., 2013)

In the tabulation of data gathered from various types of rock and reservoirs in several locations within the United States of America (Magner, 1963), carbonate rocks showed a narrower range of variation in porosity and bulk density in relation to depth of burial, age, degree of tectonic disturbance, and departure from homogeneous texture. Pure shale formations had the highest relationship between porosity and increase in bulk density (stress sensitivity) with depth of burial and degree of tectonic disturbance, while sandstone generally, but not invariably, had good dependencies. However, such relationship is not a single-parameter function in carbonates. Changes in carbonate rock properties, including those due to burial are caused by different physicochemical processes occurring in the pore spaces of sediments and rocks (Bagrintseva, 1977; Chilingar et al., 1979; Pavlova, 1975; Proshlyakov, 1974). Putting all of this information together, the influence of gravitational compaction plays a secondary role in a carbonate rock evolution (Buryakovskiy et al., 1991) and most carbonates are classified as non-stress-sensitive deposits. This invalidates the application of conventional pore pressure prediction methods on this type of rock and stresses the necessity of introducing purely new or complementary techniques to the conventional methods.

7.5. Diagenetic Processes in the Carbonate Rocks of the Abadan Plain Basin

In the Abadan Plain Basin, fracturing and pressure solution are common features that account for most reservoir micro-porosity. This is because the matrix is deeply reorganised, but the crystals are not perfectly euhedral (Field D Owner, 2004). Furthermore, the matrix is poorly microporous and connectivity is high due to micro-fracturing (Figure 7-15).

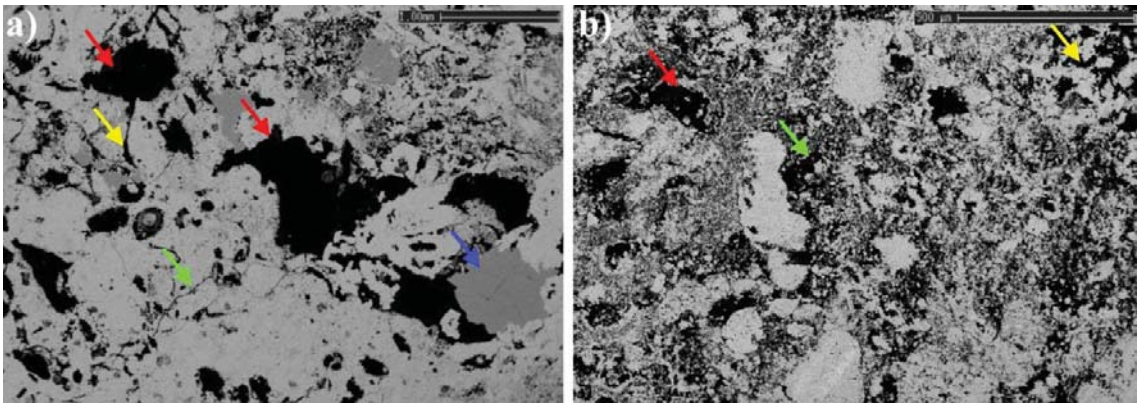

Figure 7-15 – a) High efficiency, complex pore network with vugs (red arrows), microfractures (green arrow) and open stylolites (yellow arrow), partly filled by dolomite (blue arrow) in a core sample from a depth of 4458.48 m. b)This sample is highly porous with vugs (red arrows), a zone of deep dissolution of the matrix (green arrow) and irregular shaped pores (yellow arrow) in a core sample from 4190.25 m deep in well D-6. Modified from Field D Owner (2004).

Brecciation is abundant in the Abadan Plain Basin (Figure 7-17) and its frequency, along with conglomerates, iron bearing sediments and a disconformity in the upper part of the Sarvak Formation in the Abadan Plain Basin as well as Dezful Embayment and Fars region, suggest local uplift in the Cenomanian-Turonian period (Motiei, 1993). The nodular limestone fabric and channel breccia of the Sarvak Formation are filled with clay deposits (Figure 7-17). In the carbonate formations of this region, most observed stylolites and solution seams are planar and parallel to the rock bedding (Figure 7-15 and Figure 7-18). In this region, the Fahliyan Formation is comprised of massive, oolitic and peloidal limestone with contemporaneous brecciation in the lower part. In that formation, the dolomitization process, when all limestone transformed into dolomite, has created a bland secondary intercrystalline porosity (Figure 7-19). Meanwhile, dolomite cementation has partially reduced the total porosity whilst dolomite cements only locally form cementation zones with total plugging of pores. Calcite cements are often observed embedding echinoderm fragments after dissolution (Figure 7-20). Abundance and widespread extension of secondary diagenetic processes in carbonate rocks of the Abadan Plain Basin suggests a multi-variable phenomenon of compaction in such deposits, and explicitly puts them into the non-stress-sensitive category of sedimentary rocks.

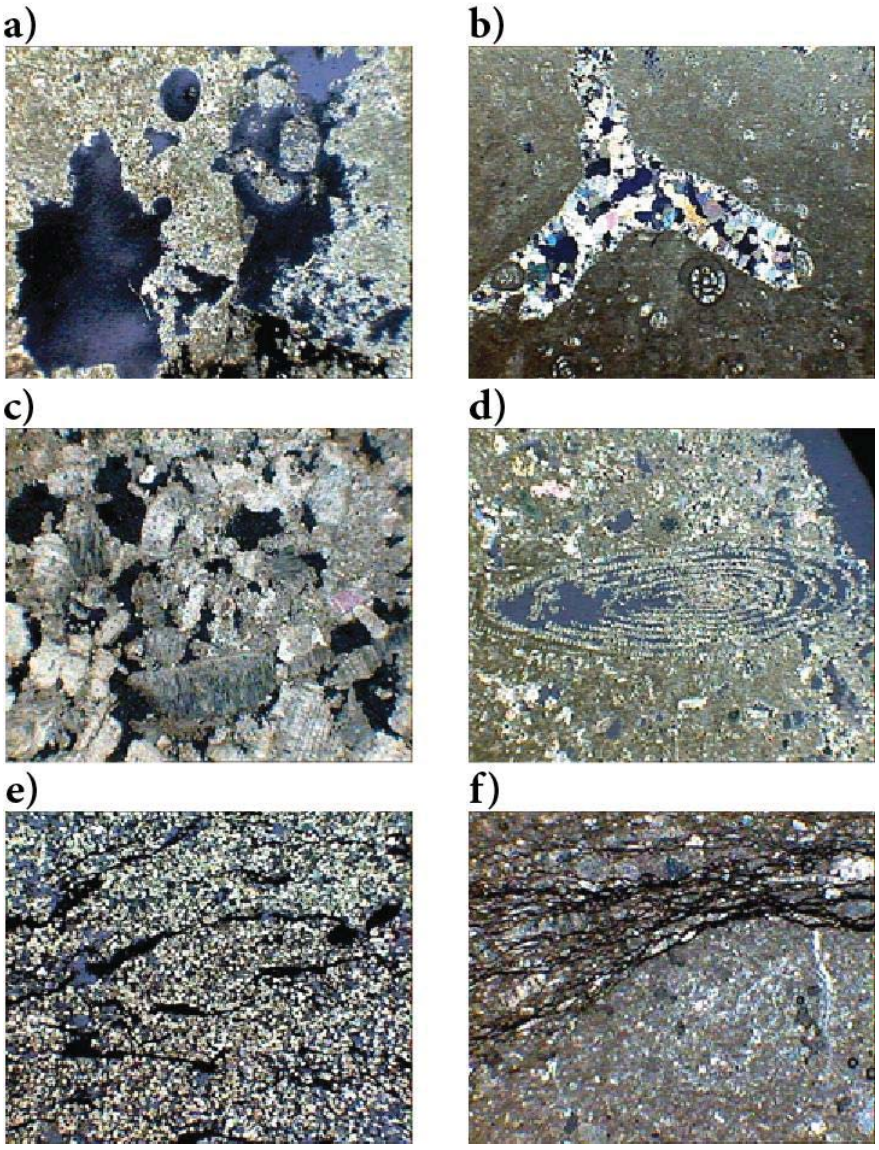

Figure 7-16 - Thin section photomicrographs showing a) improved vuggy porosity in limestone, which is not replaced with cement under polarized light, X23. b) Bioturbated wackestone; Wackestone shows is replaced with calcite cement, X26. c) Grainstone; Echinoid fragments dominated with obviously interparticle porosity type under polarized light, X23. d) Limestone represents dissolution of skeletal grains (Praealveolina cretacea), which make sufficiently intraparticle porosity type under polarized light, X47. e) Dolostone, which depends on intercrystaline and less vuggy porosity make it to contain good reservoir properties under polarized light, X23.6. f) Limestone that represents solution seams plane with obviously pathway to flow conduction according to the observation of oil staining under polarized light, X60. Also it accompanied with concentration of non-soluble material indicates development of pressure solution by time. Photos are adopted from Research Institute of Petroleum Industry (2005b).

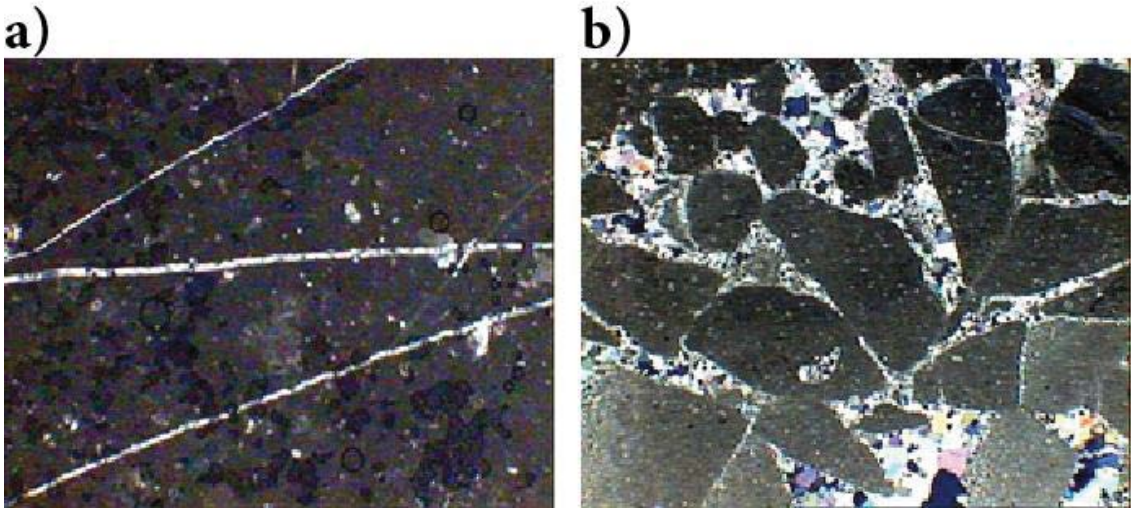

Figure 7-17 – a) Carbonate Photomicrographs in one of the wells of field A, X23; Mudstone with crossed filled (with calcite) fractures. b) Brecciaed limestone from one of the wells of field A, X23. Intraclast grains (with mudstone texture) dominated with calcite cement, which represents unstable substrate. Photos are adopted from Research Institute of Petroleum Industry (2005).

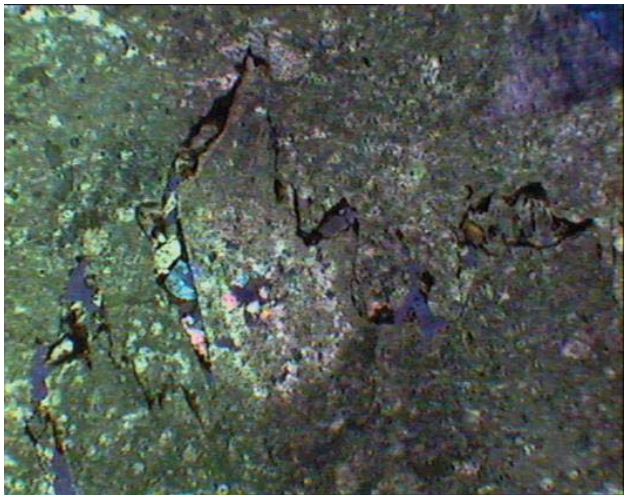

Figure 7-18 - Sutured stylolite, which is the result of high compaction by the time during diagenesis stages under polarized light, X23. Photos are adopted from Research Institute of Petroleum Industry (2005).

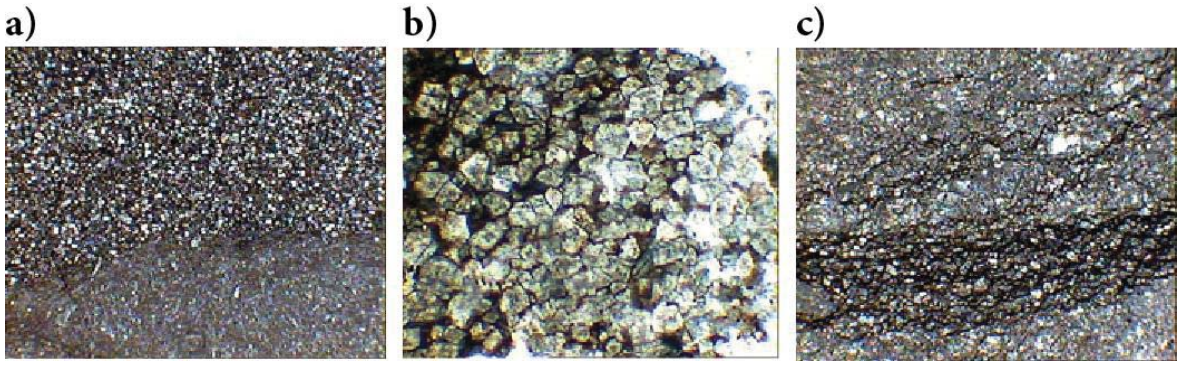

Figure 7-19 - Thin section Photomicrographs in one of the wells of field A shows a) partly dolomitization after limestone, X23. b) Xenotopic subhedral dolomite crystals. It represents dolomitization after lime in burial diagenesis stages, X95. c) Solution seams surfaces accompanied with dolomite rhombs; Represents late dolomitization and relationship between rich organic matters in these surfaces, X65. Photos are adopted from Research Institute of Petroleum Industry (2005).

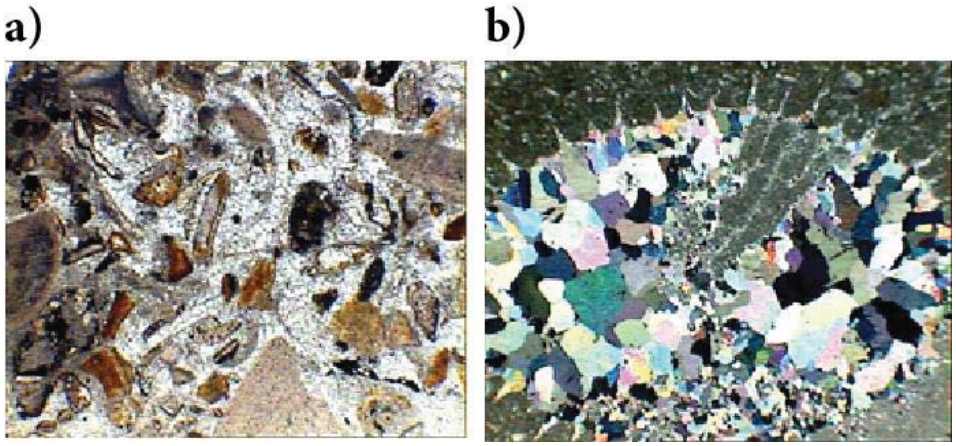

Figure 7-20 – a) Grainstone; echinoderm fragments embedded in coarse sparry calcite cement, X40. b) Replacing sparry calcite cement after dissolution the coral fragment under polarized light, X23. Photos are adopted from Research Institute of Petroleum Industry (2005).

7.6. Conclusions

Porosity is controlled by several depositional and diagenetic processes in carbonate rocks, such as pressure solution, cementation, dolomitization, brecciation and fracturing. Some of these processes create additional pore space while some diminish the existing porosity. Any of them can occur in specific conditions regardless of burial depth. Carbonate deposits of the Sarvak and Fahliyan formations of the Abadan Plain Basin are associated with extensive fracturing, which further creates brecciation patterns in the rocks. Pressure solution and stylolites filled with calcite and dolomite cements are also frequently evident in these formations. Although in-situ stresses significantly affect some of those processes, the overall porosity evolution isn't entirely controlled by stress. Therefore, carbonate rocks are classified as non-stress-sensitive and hence, hard to attribute a normal compaction trend for the purpose of predicting pore pressure. This invalidates the use of conventional pore pressure prediction applications in carbonates which is tackled with some specified methods in the next two chapters.

CHAPTER 8- Shale vs carbonates Pore Pressure Prediction (PPP) in the Abadan Plain Basin

8.1. Introduction

Overpressure has a detectable signature on the petrophysical attributes of shales (Bhagwan et al., 1998; Bowers, 2001; Bowers and Katsube, 2001; Eaton, 1972; Fertl and Chilingarian, 1987; Haugland et al., 2013; Katahara, 2003; Ransom, 1986; Sayers et al., 2002). Variations in observed rock properties with respect to the expected values (NCT) are central to almost all pore pressure prediction methods (Bowers, 1995; Eaton, 1972; Lindberg et al., 1980). However, as discussed briefly in the previous chapter, petrophysical-based pore pressure prediction is only valid if the formation undergoes certain mechanical change; such as responses to compaction by Eaton (1972) and mechanical compaction and/or fluid expansion by Bowers (1995). Carbonate rocks have exhibited other kinds of porosity evolution such as 'chemical compaction' (Croizé et al., 2010; Goldhammer, 1997; Shinn and Robbin, 1983), which is also termed as 'pressure solution' (Aharonov and Katsman, 2009; Baker et al., 1980; Neugebauer, 1973; Rutter and Elliott, 1976), 'fracturing' (Brown, 1997; Conybeare and Shaw, 2000; Longman, 1985; Moore and Wade, 2013c; Murray, 1960; Nurmi et al., 1990), 'dolomitization' (Kinsman, 1965; Lucia, 1995; Moore, 1988), and 'brecciation' (Dravis and Muir, 1993). This makes many carbonate rocks non-stress-sensitive, which means that porosity isn't only a function of effective overburden stress, but also the diagenetic processes during burial. Lack of relationship between effective stress and porosity/velocity in carbonates make conventional methods of pore pressure prediction inaccurate, if not inapplicable, in such deposits (O'Connor et al., 2010; Wang et al., 2013).

The pore structure and carbonate types in the overpressured horizons of the Gadvan and Fahliyan formations show a wide variety of pore systems, including vugs, micro-fractures and open stylolites partly filled with dolomite. The porosity and permeability vary

significantly throughout the formation and, the petrophysical properties are also highly non-uniform. Moreover, chemical compaction is frequently encountered in the carbonate formations of this basin and, therefore, a normal compaction trend as a result of effective overburden load can't be obtained. Hence, conventional pore pressure prediction methods cannot be reliably used on carbonate sequences in this basin. However, these carbonate sequences do contain a range of interbedded shales, and as seen in chapters 5 and 7, these shales do display petrophysical signatures relating primarily to overpressures generated by disequilibrium compaction. Hence, there is the possibility of applying standard shale-based pore pressure prediction methods to these thin interbedded shales, and using this to then infer the pore pressure in adjacent carbonates. Indeed, to date, this is the most common approach that has been successfully applied for pore pressure prediction in stress-insensitive carbonates (Azadpour and Shad Manaman, 2015; Couzens-Schultz and Azbel, 2014; Weakley, 1990). Thus, in this chapter I will examine whether conventional pore pressure prediction methods can be successfully applied to shale interbedded sequences of the Abadan Plain Basin. I will first review and explain conventional pore pressure prediction methods. I will then apply these methods to shales, and discuss the advantages of this approach, but also describe some of the significant issues with this method, as a foundation for the alternative method proposed and tested in Chapter 9.

8.2. Conventional Shale-based Pore Pressure Prediction

One of the first attempts to recognise overpressure was taken by Hottmann and Johnson (1965) by plotting acoustic velocity and resistivity data for the shales of Texas and Louisiana, USA. The sonic wave travel time in the normally pressured interval of the well had a logarithmic relationship with depth, whilst resistivity exhibited another kind of trend. Such relationships are called a 'normal compaction trend' or NCT (Fertl and Chilingarian, 1987; Serebryakov et al., 1995; Shaker, 2007). Top of overpressure is commonly identified as the depth where the shale petrophysical properties diverged from the NCT. Pennebaker (1968) applied the same idea to seismic data and tried to relate the degree of overpressure to the observed travel time departure from the NCT.

Eaton (1972) introduced an equation to predict pore pressure in terms of the difference (ratio) between NCT and observed acoustic sonic wave travel time, taking overburden stress and hydrostatic pore pressure into account. A similar equation, using resistivity data instead of sonic wave travel time, was also incorporated (and, subsequently, these equations have been modified for use with other properties, such as conductivity, drilling-exponent, density and shear-wave velocity). Eaton's equation considers a single NCT for the entire depth interval of the well and implicitly assumes one overpressure origin (usually disequilibrium compaction, but sometimes empirically modified to account for multiple mechanisms).

Two decades after Eaton, Bowers (1995) provided a new method that considers disequilibrium compaction and fluid expansion together, introducing an unloading curve in addition to a standard loading curve. The standard loading curve is used in zones of normal pressure or disequilibrium compaction overpressure to relate porosity to vertical effective stress. The unloading curve, constructed using an effective stress vs. velocity cross plot, is essentially a second relationship between porosity (or a petrophysical proxy for porosity, such as sonic velocity) and vertical effective stress that is only applied in zones that contain fluid expansion overpressure. Bowers (1995) tested this method in several types of formations in the Deepwater Gulf of Mexico and central North Sea.

The Eaton and Bowers methods are based on the basic hypothesis that porosity decreases by burial depth in normally pressured formations. Overpressure often reduces the ability for porous rock to compact, resulting in a detectable porosity anomaly, as discussed in detail in Chapters 5 and 6. However, there are a number of potential pitfalls for porosity-based pore pressure predictions, which are nicely summarized by Swarbrick (2001), such as: lateral transfer, tilted reservoirs, shallow top overpressures, mixed lithology, vertical versus mean effective stress, overpressure mechanisms other than disequilibrium compaction, and non-mechanical compaction. However, in the Abadan Plain Basin, overpressure is found to be largely generated by disequilibrium compaction with minor contribution of fluid expansion mechanism. Therefore, Eaton's (1972) method is expected to provide reasonable pore pressure prediction in shales in this basin.

8.3. Applying Shale-based Pore Pressure Prediction in the Abadan Plain Basin

In this chapter I have applied the Eaton (1972) pore pressure prediction method, using petrophysical log data, to the shale interbeds observed within the carbonate formations of the Abadan Plain Basin. The main assumption here is that this method assumes that interbedded shales are in complete hydrodynamic equilibrium with surrounding carbonates. Since the shale deposits of this basin are mainly thin interbedded layers of a few metres thickness (except a few thick shale deposits in the Kazhdumi and Gadvan formations), a hydrodynamic link between the shale and surrounding rocks seems reasonable.

The porosity of shale (clay) at the surface can be more than 60%, and can decrease to less than 5% at 4 km depth (Hermanrud et al., 1998; Teige et al., 1999). It is this large variation in porosity with depth that makes shales so useful for pore pressure prediction, as such a large porosity change means that anomalous porosities (undercompaction) associated with overpressure is easier to detect. Weakley (1990) was the first person who applied a filter on a database of some carbonate deposits, then used the Eaton method to predict pore pressure with promising results. His method was validated based on a geological hypothesis which says: "in all sands there is some shale, in all shales there is some sand, in all carbonates there is some sand and shale and so forth". Weakley (1990) used gamma ray to determine shaliness within the rock matrix and applied the Eaton method selectively to just these zones. Additional similar approaches have been used by Couzens-Schultz and Azbel (2014) and Azadpour and Shad Manaman (2015). This same concept is used herein to test pore pressure prediction from sonic, resistivity and density log data. Shale discrimination, and compilation of associated sonic, density and resistivity values has already been done and fully described in Chapter 5, and was previously used to examine overpressure origin. Herein, this same data will be applied with the Eaton and Bowers methods to predict pore pressure. As previously described, all well log data were averaged over a 2 metres interval to avoid the Spurious data errors, and shales identified from gamma ray data.

8.3.1. The Application of the Eaton Method

Eaton (1972) proposed an equation to predict pore pressure based on the ratio of acoustic travel time in mechanically (normally) compacted sediments as follows:

$$P_p = \sigma_v - (\sigma_v - P_h)\left(\frac{\Delta t_{normal}}{\Delta t}\right)^x \qquad \text{Equation 8-1}$$

Where x is an exponent, σ_v is vertical effective stress, P_h is hydrostatic pressure, Δt_{normal} is acoustic travel time in the normally compacted sediments and Δt is the observed acoustic travel time from sonic log. Δt_{normal} is obtained from the normal compaction trend (NCT) at the depth of investigation. This method of pore pressure prediction is applied on shales as they undergo mechanical compaction in response to the overburden load. Eaton (1972) also provided a similar equation for pore pressure prediction using the resistivity data. Borrowing the same terminology from the previous equation, it is formulated as:

$$P_p = \sigma_v - (\sigma_v - P_h)\left(\frac{R_{shale}}{R_{normal}}\right)^x \qquad \text{Equation 8-2}$$

Where x, σ_v and P_h are same as the previous equation. R_{shale} is the observed resistivity of the shale and R_{normal} is the resistivity obtained from normal compaction trend. It is important to note that the validity of Eaton's method depends on the homogeneity of the formations, and it must be applied to the same lithology with the same mechanical properties. Every rock type may exhibit a different path of compaction and thus using a single NCT for a number of different shale formations might be (and often is) incorrect. Therefore, depositional environment and physical properties of the formations need to be examined. As discussed in Chapter 2, the depositional environment of the Abadan Plain Basin is shallow marine conditions and, except for short periods of sea degradation, there has been continuous deposition from Permian to Pliocene. Hence, a single NCT is used in this study, though it is also noted (as was discussed in Chapters 2 and 5) that

shales do vary throughout the sedimentary sequence, particularly with regards to carbonate content (ranging from almost 'pure' shales to marls).

Although it wasn't proposed by Eaton, the same method can be performed using density data. Density is actually a better reflection of changing porosity (a bulk measurement, and not affected by textural effects, like sonic and resistivity log data), and thus is particularly applicable to pore pressure prediction in disequilibrium compaction overpressures (Swarbrick, 2001) However, most pore pressure predictions have utilized sonic or resistivity data and to my knowledge, density hasn't been explicitly used for this purpose (It must be noted that density has been implicitly used with other methods, such as the equivalent depth method). In this research, I conduct the pore pressure prediction using the density data (Equation 8-4) as well as sonic and resistivity.

$$P_p = \sigma_v - (\sigma_v - P_h)\left(\frac{\rho_{shale}}{\rho_{normal}}\right)^x \qquad \text{Equation 8-3}$$

8.3.2. NCT analysis in the Abadan Plain Basin

A normal compaction trend (NCT) is an indicator line of certain petrophysical measurements for a given normally-compacted rock (Tang et al., 2011). In a normal compaction process, the pore pressure remains hydrostatic while the rock undergoes burial processes and consequently compacts. A NCT is obtained from porosity-depth or porosity-vertical stress profiles for the interval of a well or basin where the pore pressure is hydrostatic (and then extrapolated into overpressured zones, or derived from equivalent normally pressured formations in offset wells). The simplest normal compaction trend was defined by Slotnick (1936) as a linear relationship between seismic wave velocity and depth. It was after Hedberg (1926) identified curved trends of differential compaction attributes in the sedimentary rocks of Texas, Kansas and Arkansas states of America. Logarithmic and power trends for NCT were then proposed in numerous locations, beginning with the seminal work by Athy, and these are still the main NCT types used in pore pressure prediction today (Athy, 1930a, b; Devine, 2014; Hall, 1953a; Serebryakov et al., 1995; Zhang, 2011, 2013).

In the wells of this study, formations above the Sarvak formation are normally compacted with an exception in the Gachsaran Formation in some wells. However, very few shale data points are available in the Gachsaran Formation, and so this doesn't alter the trend of normally pressured formations developed herein. Therefore, the NCT is evaluated for the shales from the surface to the depth of the Sarvak Formation. The data points were interpolated as a single curve using CurveExpert software (Hyams, 2009) in the form of an exponential equation with the following best fit:

$$V_{normal} = 3.48(1.45 - e^{-0.027\sigma_v}) \qquad \text{Equation 8-4}$$

where V_{normal} is velocity of sonic wave in shale (in km/s) and σ_v is the overburden stress in MPa. This NCT is used in the pore pressure prediction and porosity evaluations by comparing sonic-porosity with neutron-porosity and density-porosity evaluations. The NCT determined for resistivity data is also an exponential relationship, and is given by:

$$R_{normal} = 0.000007\sigma_v^{3.38} \qquad \text{Equation 8-5}$$

Where R_{normal} is the resistivity obtained from NCT in the shales in Ohmm and σ_v is the overburden stress in MPa. The NCT of density log data in the normally pressured formations is also determined as:

$$\rho_{normal} = 1.9986\sigma_v^{0.016} \qquad \text{Equation 8-6}$$

All available data of the wells studied in this research were put together and illustrated in Figure 8-1, which also includes the NCT. The last remaining constant to be determined is the Eaton exponent, which is defined and determined in the following section.

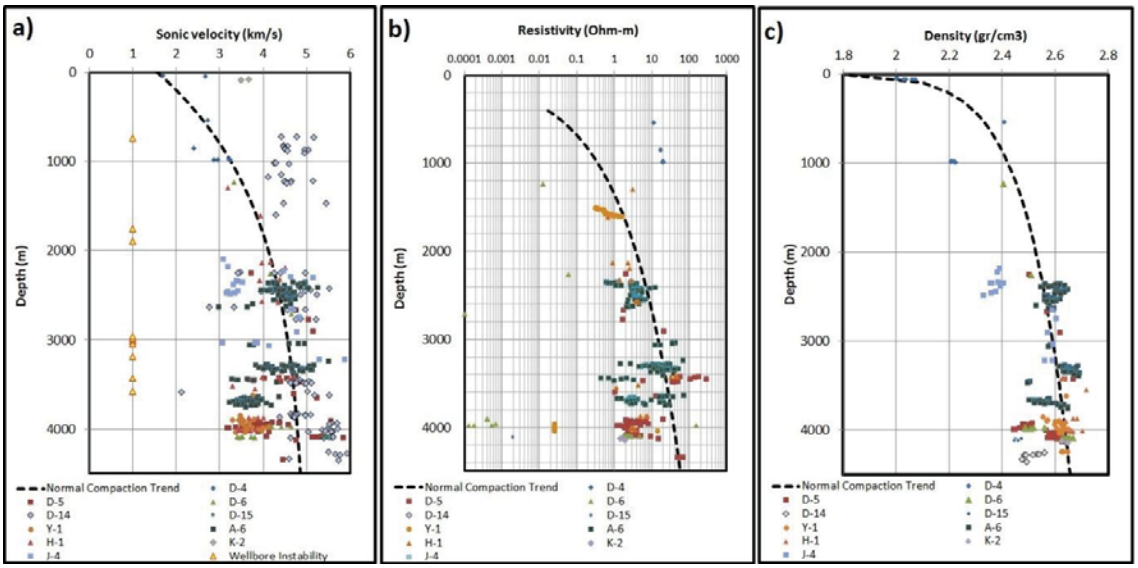

Figure 8-1 - a) Sonic velocity-depth profile; b) resistivity-depth profile and c) density-depth profile of the wells studied in the Abadan Plain Basin. The normal compaction trend and wellbore instability issues are also indicated.

8.3.3. The Eaton (1972) Exponent

The Eaton's (1972) equation contains an exponent which calibrates the method for pore pressure estimation with the observed field data. Typically, this exponent is considered to be 3 for the sonic travel time, and 1.5 for the resistivity of shale sediments hosting overpressure (Eaton, 1975; Hermanrud et al., 1998; Mouchet and Mitchell, 1989). In different geological settings, the process of overpressure generation as well as the petrophysical attributes of the rock may differ, which requires a different exponent to reflect (amplify or curtail the response) of the difference in observed and normally-predicted acoustic velocity or resistivity. The Eaton Exponent for PPP used with sonic log data has been reported as being as low as 0.1-0.3 in a West Kazakhstan Dolomite field (Kadyrov and Tutuncu, 2012) and as high as 6.5 in Brunei (Tingay, 2003). In this study, a total of 106 RFT/MDT measurements are available for the wells studied, mainly at the depth of Gadvan and Fahliyan formations. Sonic velocity, resistivity and density are not known for those points, but there are data points in close proximity to the RFT/MDT points. The Eaton (1972) exponent for accurate pore pressure prediction can be determined by re-arranging Equation 8-1, Equation 8-2 and Equation 8-3 to substitute Equation 8-4, Equation 8-5 and Equation 8-6 respectively. Normally, an iterative curve matching or data fitting process is applied to find the best matching exponent for the

shallow depth interval of a well with normal pore pressure. An average Eaton exponent of 1.0 for sonic pore pressure prediction was determined herein from the direct pressure measurements, as well as from pore pressure evaluation from mud weight. Accordingly, data analysis for resistivity pore pressure prediction yields an average Eaton exponent of 1.0 for sonic velocity, 0.1 for resistivity, and 5 for density data. Eaton pore pressure prediction is compared with Bowers (1995) and can be verified with field data.

8.3.4. Bowers Pore Prediction Method

Bowers (1995) primarily proposed an empirically determined method for pore pressure prediction in the conditions where disequilibrium compaction is the overpressure origin. This method is a relationship between effective stress and sonic velocity as:

$$\sigma = \left(\frac{V - V_0}{A}\right)^{\frac{1}{B}} \qquad \text{Equation 8-7}$$

where V is sonic velocity at a given depth, V_0 is the sonic velocity at the surface and σ is the vertical effective stress. A and B are regional parameters obtained from regional sonic velocity-effective stress cross plots. Where the overpressure is generated by the fluid expansion, Bowers (1995) introduced the following equation to account for the effect of unloading:

$$V = V_0 + A\left(\sigma_{max}\left(\frac{\sigma}{\sigma_{max}}\right)^{\frac{1}{U}}\right)^{B} \qquad \text{Equation 8-8}$$

where

$$\sigma_{max} = \left(\frac{V_{max} - V_0}{A}\right)^{\frac{1}{B}} \qquad \text{Equation 8-9}$$

where σ is the overburden stress, σ_{max} and V_{max} are effective stress and sonic velocity at the onset of unloading respectively and, U is unloading parameter as a proxy to the sediment plasticity so that U=1 indicates no permanent deformation as the unloading curve reduces to the loading curve. U=∞ implies completely irreversible deformation because velocity becomes equal to V_{max} for all values of effective stress less than σ_{max}. V_{max} is simply considered as 1.5 km/s for the weathered sediments at the surface. Similar to Eaton, Bowers' method also relies on the accurate estimation of the loading curve. Bowers tested this method in several types of formations in the deep water Gulf of Mexico and central North Sea.

8.3.5. Bowers' Normal Compaction Trend

In the case of existing measured pore pressured, Bowers's Equation 8-7 can be calibrated at measurement points to obtain parameters A and B (Figure 8-2). Parameters A and B are the coefficients of the V-V0 versus effective stress cross plot. This gives the values of A=0.0214 and B=1.2036 in the Abadan Plain Basin. Putting these values in Equation 8-7 and Equation 8-8 should, ideally, accurately yield the magnitude of effective stress. However, R2 (~ 0.21) in the cross plot of velocity versus calculated effective pressure at measured points is quite low, and it is highly likely that the Bowers prediction method may exhibit substantial errors due to low accuracy of A and B parameters.

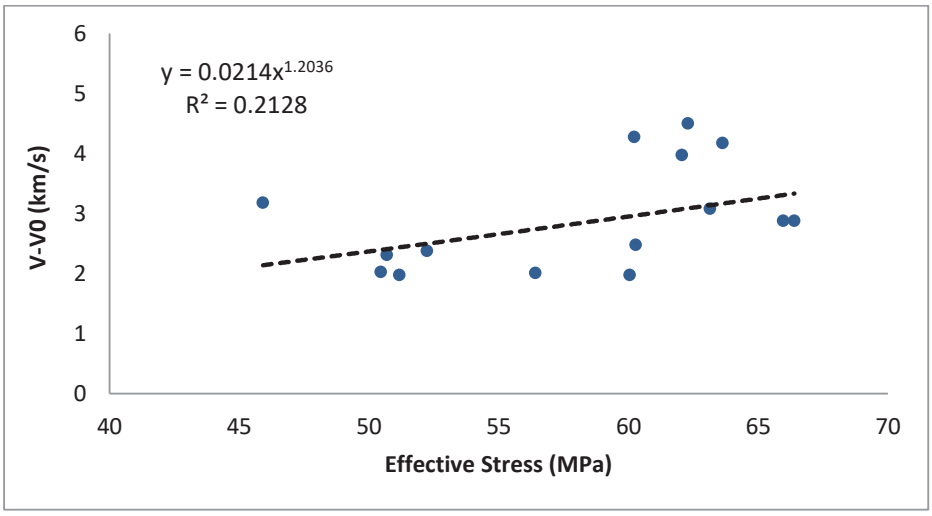

Figure 8-2 – Cross plot of V-V_0 versus effective stress in the Abadan Plain Basin. Data points are for pressure measurement depths.

8.4. Results of Pore Pressure Prediction

The Eaton (1972) and Bowers (1995) pore pressure prediction methods were tested in 10 wells in 6 fields of the Abadan Plain Basin. Pore pressure was predicted using an Eaton exponent of 1 for sonic velocity, 0.1 for resistivity and, 5 for density data (Figure 8-3 to Figure 8-13). Bowers' (1995) method was also tested here, but found to underestimate pore pressure in shallow sections. This inaccuracy in using the Bowers' method in the Abadan Plain Basin is due to inaccurate estimation of loading curve as discussed in the previous section.

Direct pressure measurements are limited to only the Gadvan and Fahliyan formations in the most of wells studied herein. These two formations are overpressured and provide the best data to examine the reliability of shale-based PPP methods in the basin. Where direct pressure measurements (RFT/MDT, well test, etc.) were unavailable, mud weight was the only available proxy to pore pressure, such as in well H-1 (Figure 8-11) in which no direct pressure measurements are available. This is also the case for the Aghajari, Gachsaran and Asmari formations, in which only mud weight data is available. On the other hand, log data is limited to the deeper sections of the wells where hydrocarbon accumulations were anticipated (i.e. Asmari, Sarvak and Fahliyan formations). As an

exception, sonic velocity data was provided from the Gachsaran to Fahliyan interval of well D-14, which unfortunately, seems to have very different petrophysical signatures to the other wells in Field D (e.g. the different vertical stress as discussed in Chapter 6). Sonic log data of well D-14 is widely scattered and hence, must be disregarded in this study. However, density data were available in the Gadvan and Fahliyan formations of this well, which are considered for the PPP analysis (Figure 8-7). A short description of the prediction results in each well is provided after the figures.

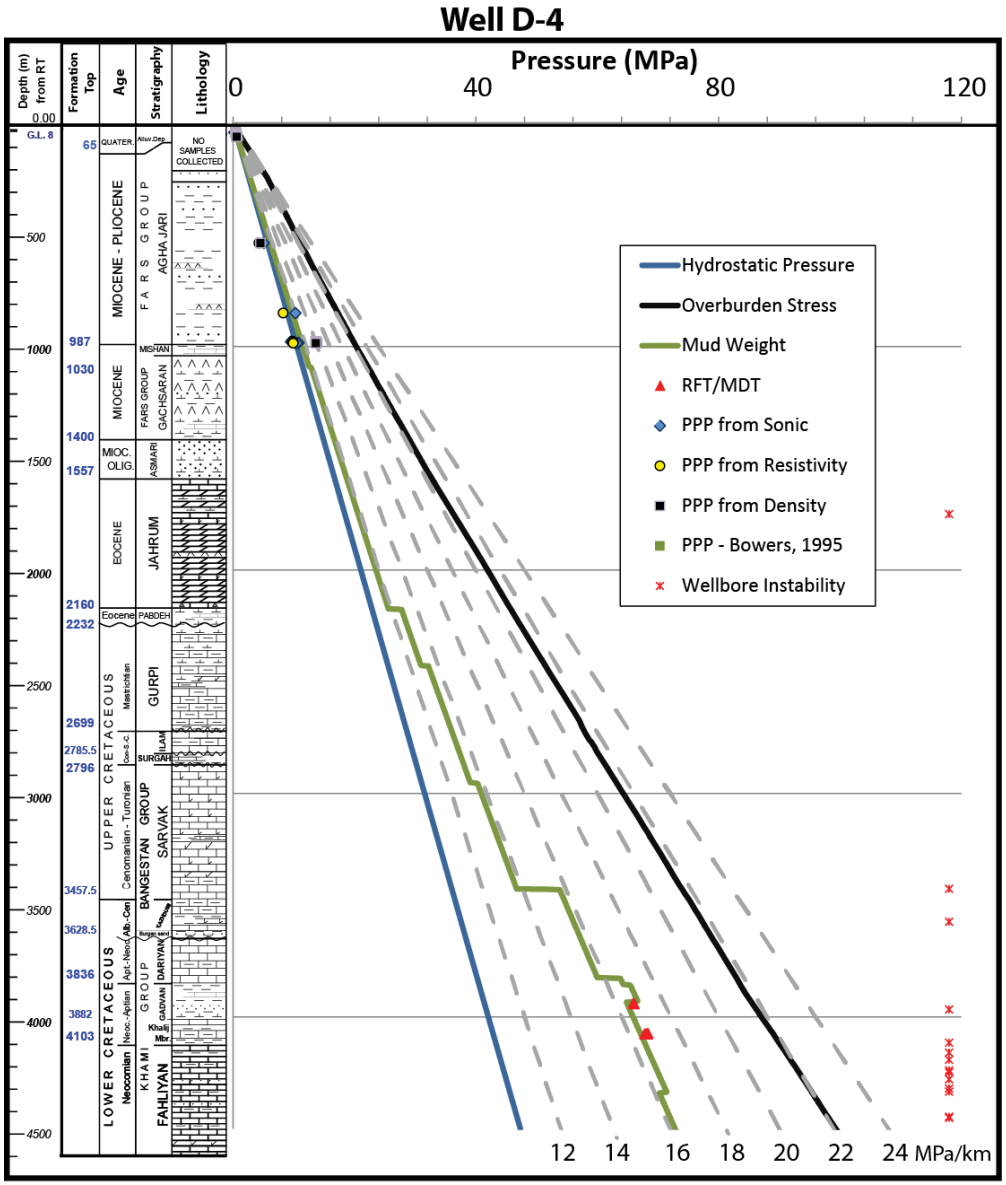

Figure 8-3 – Predicted pore pressure in well D-4.

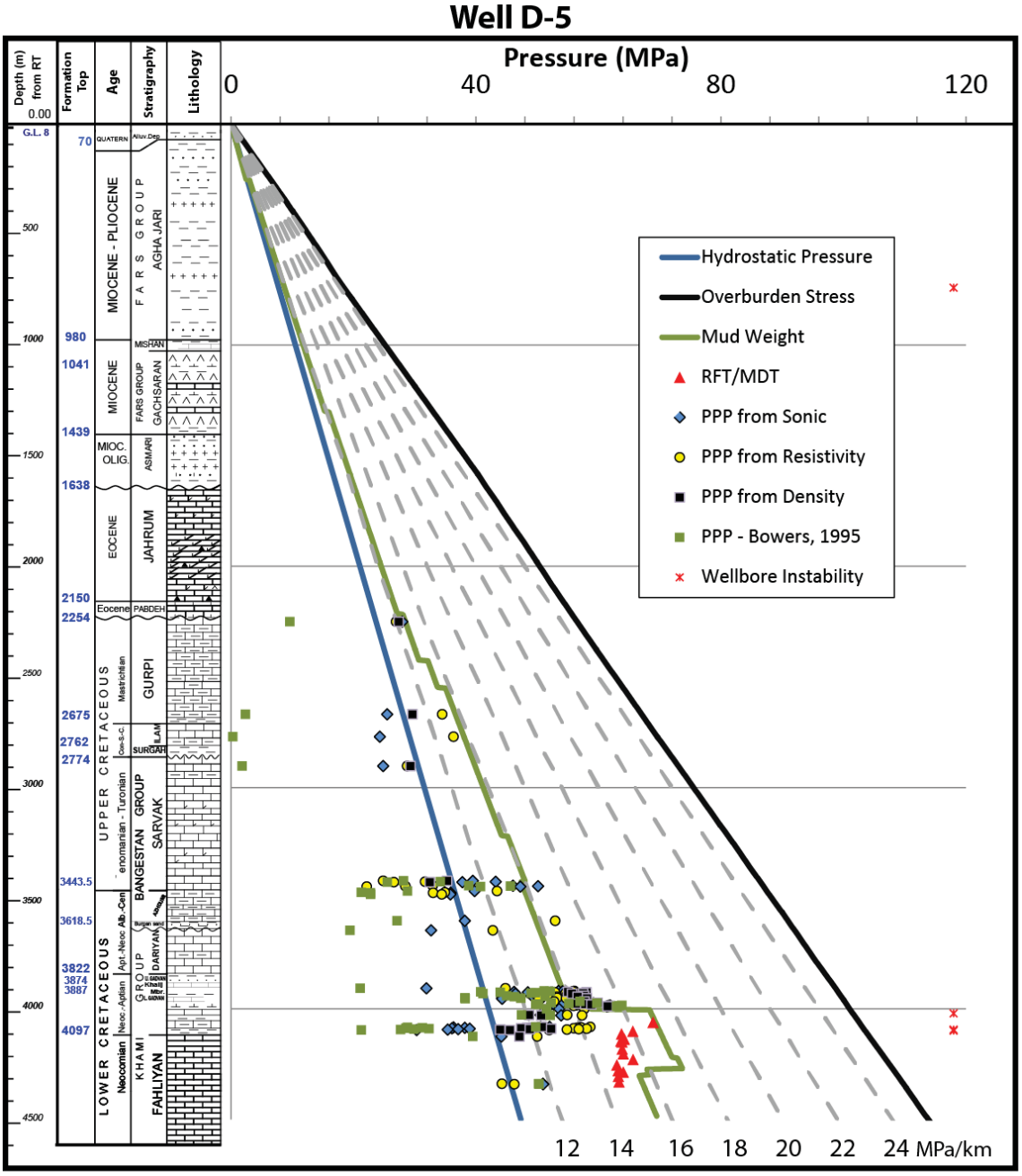

Figure 8-4 - Predicted pore pressure in well D-5.

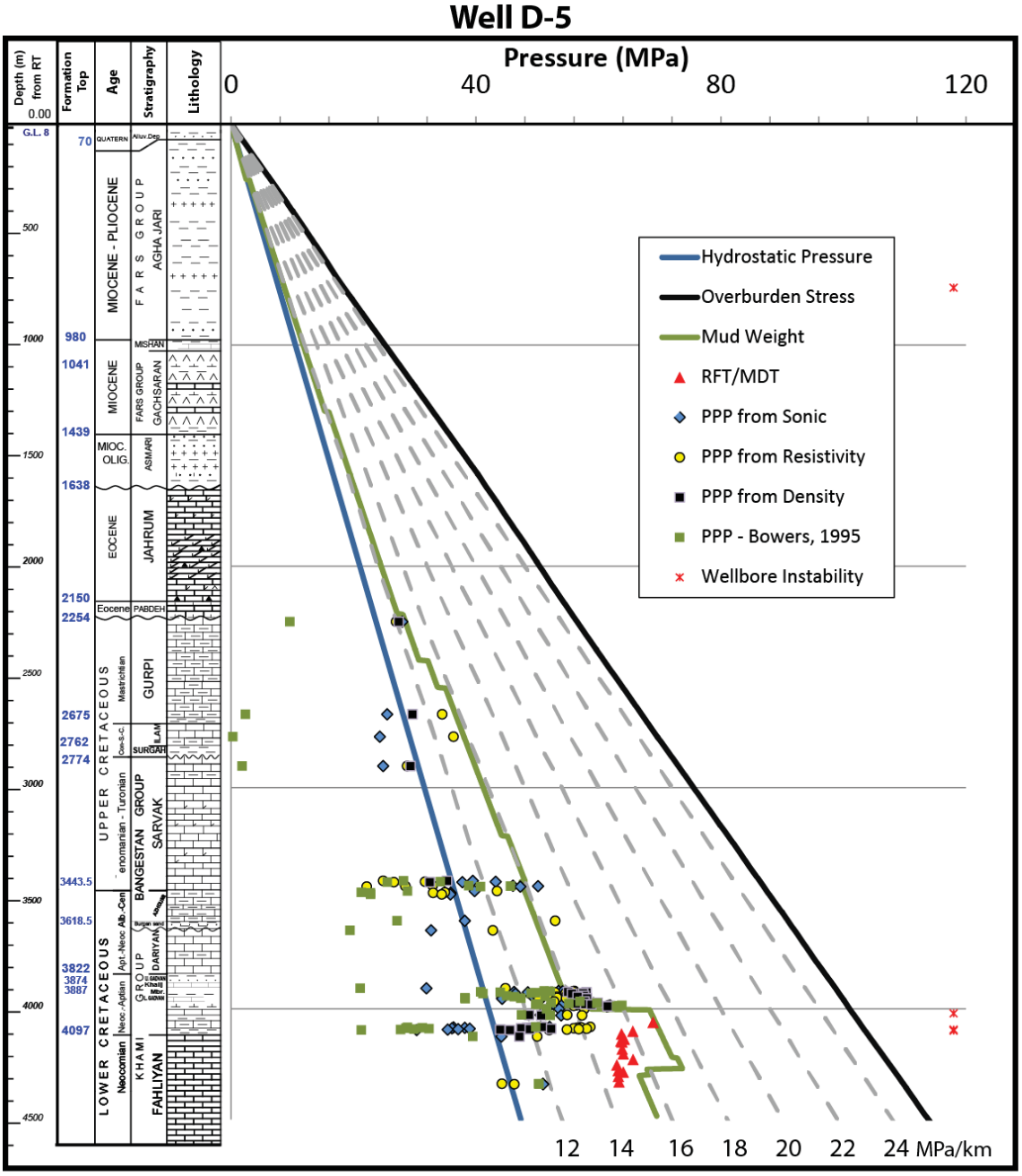

Figure 8-5 - Predicted

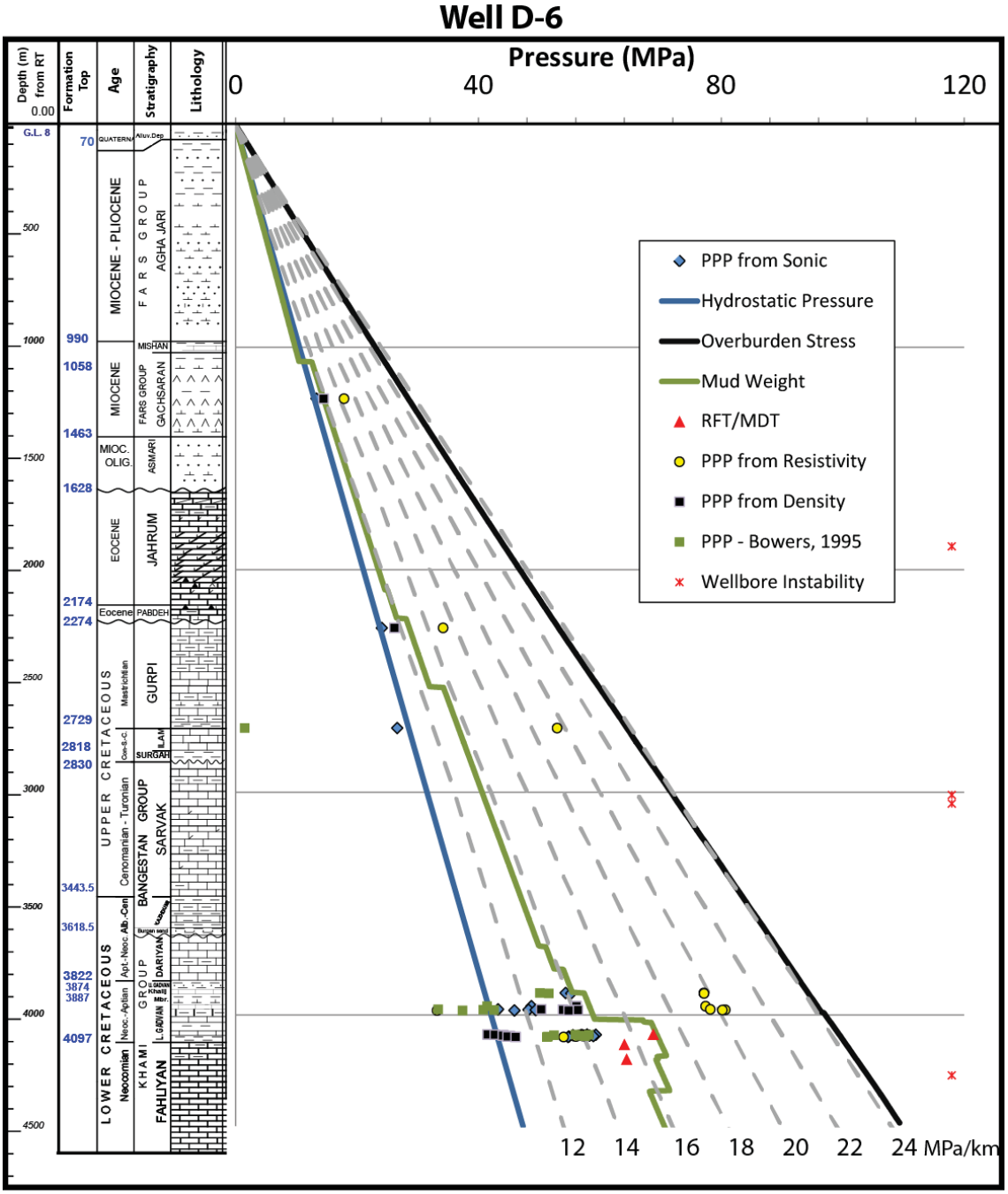

Figure 8-6 - Predicted pore pressure in well D-6.

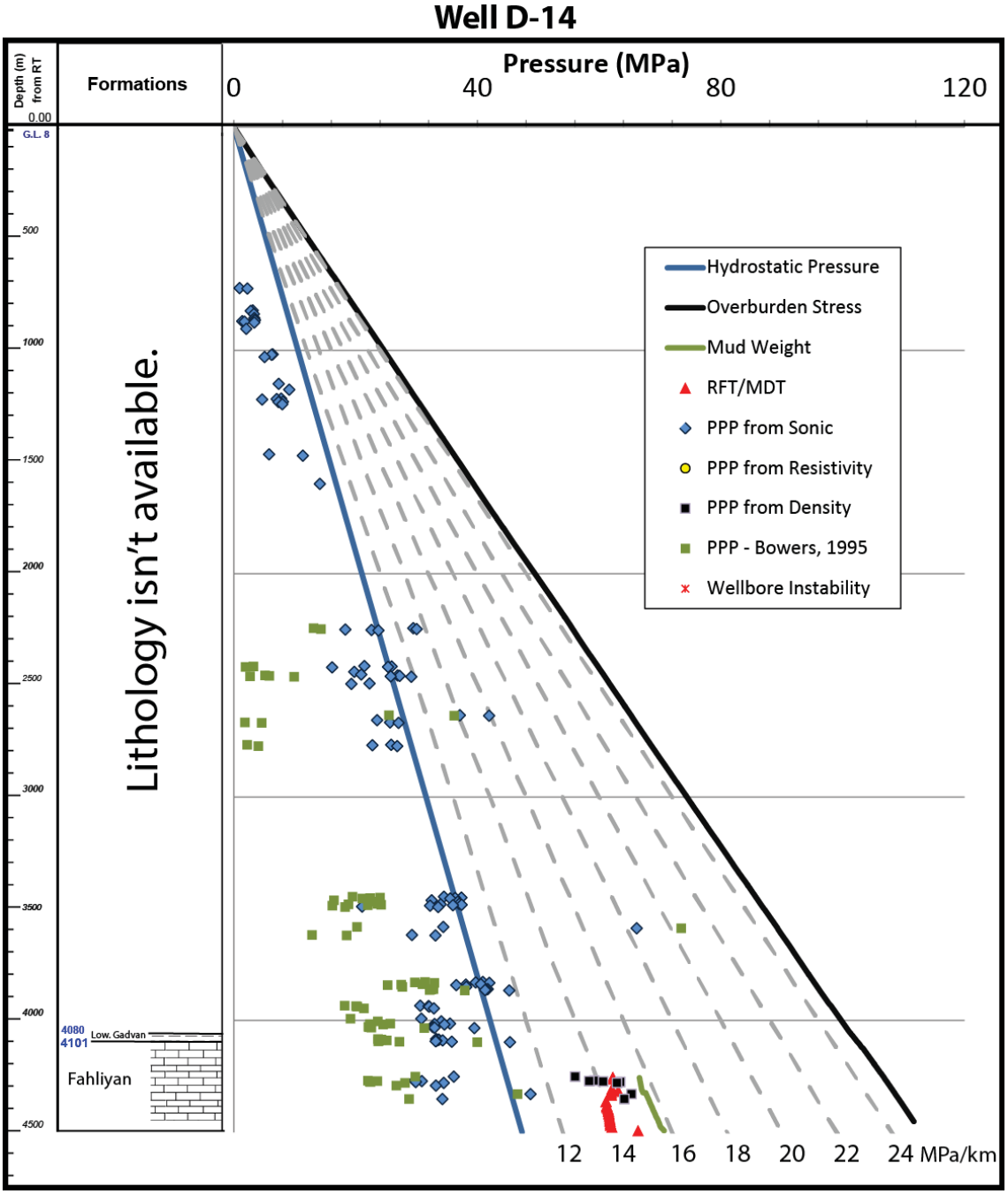

Figure 8-7 - Predicted pore pressure in well D-14.

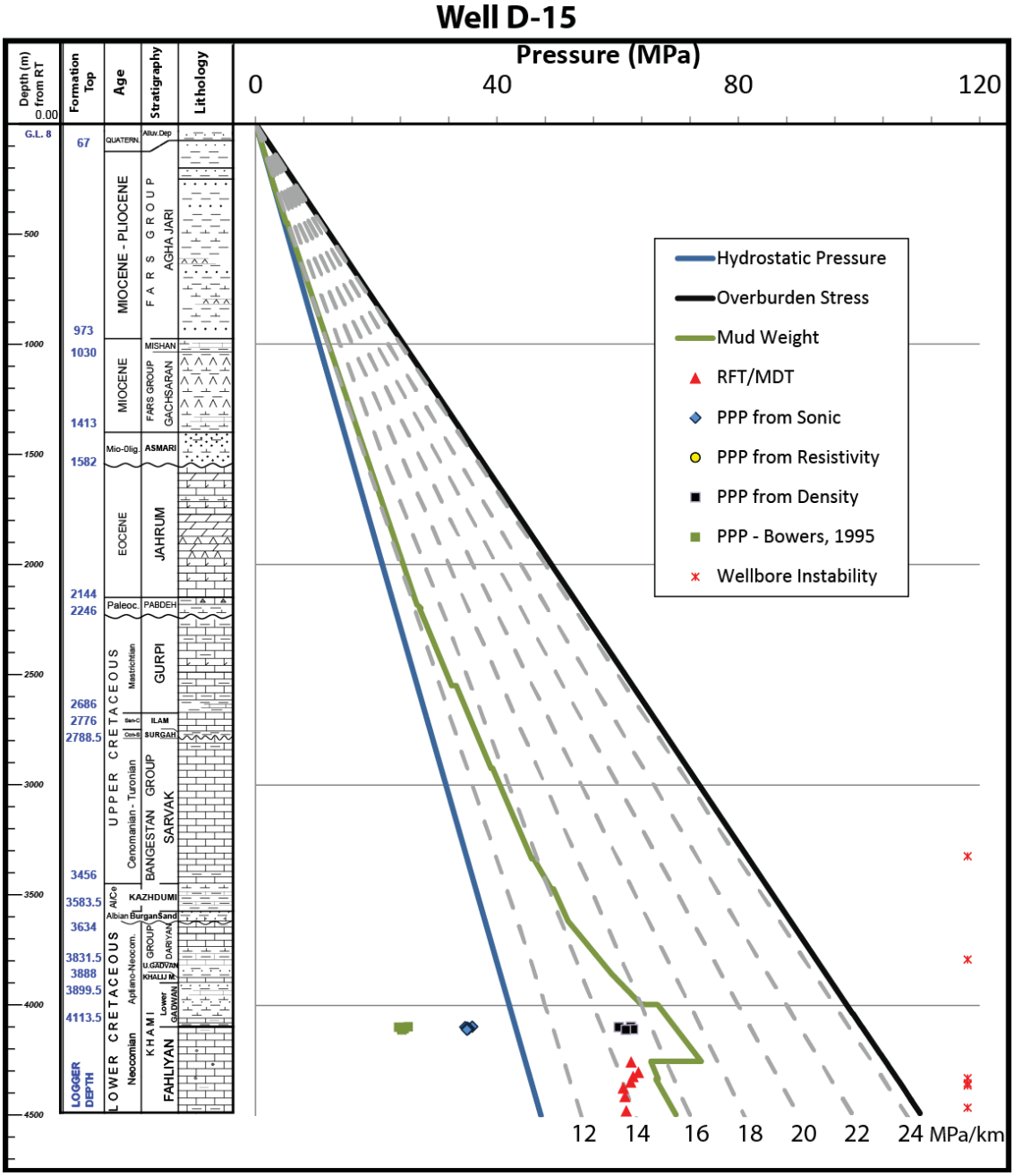

Figure 8-8 - Predicted pore pressure in well D-15.

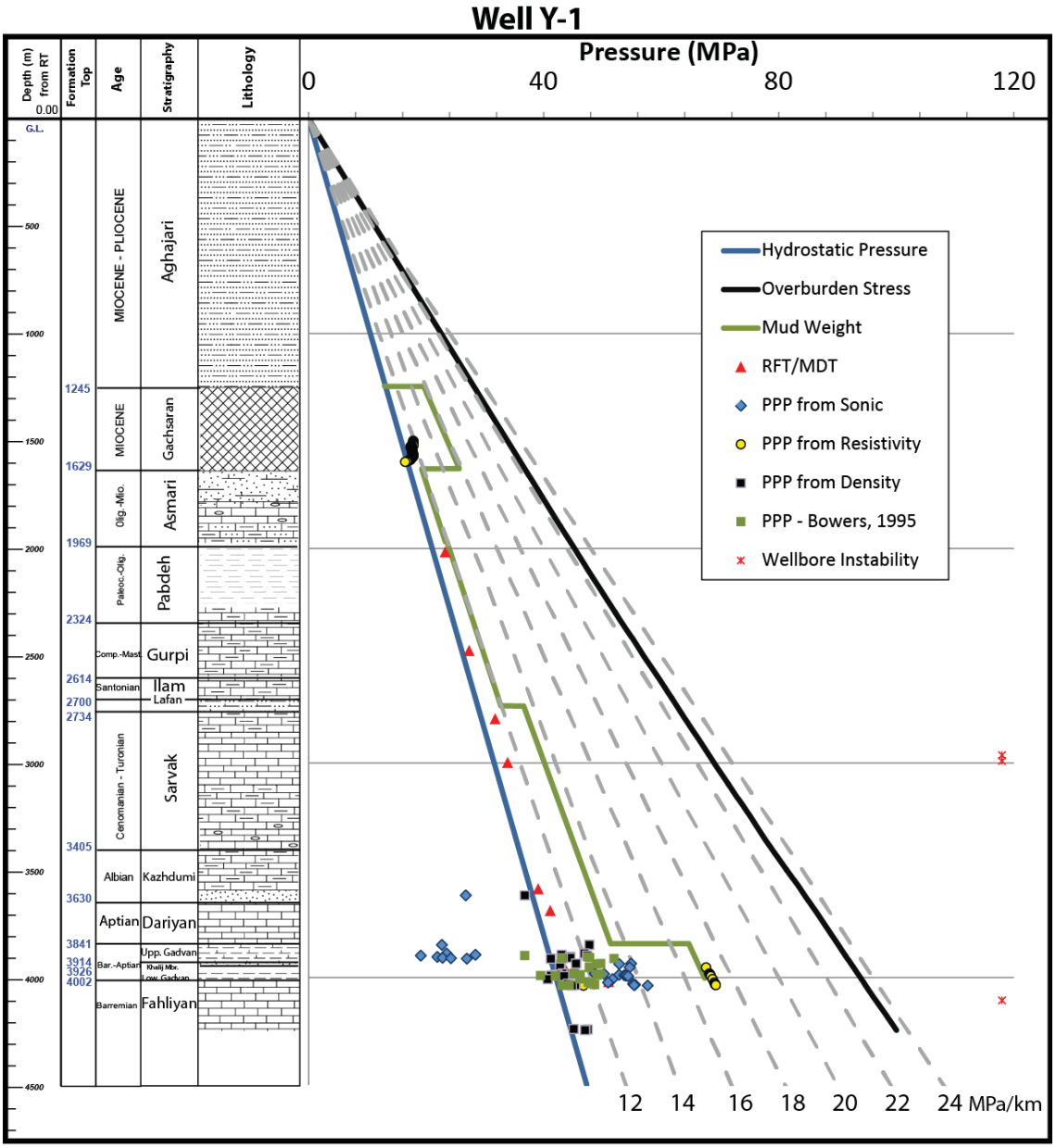

Figure 8-9 - Predicted pore pressure in well Y-1.

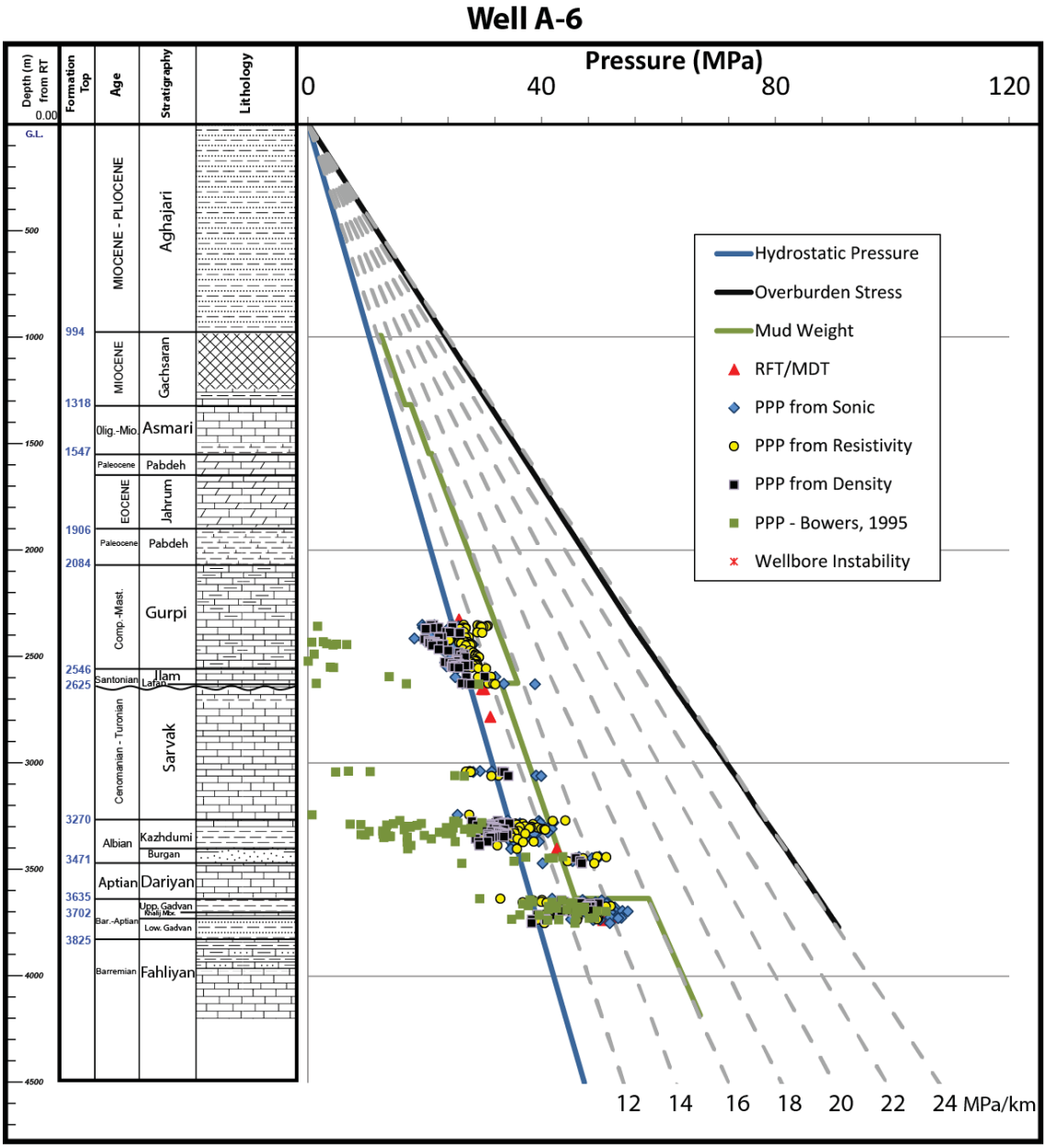

Figure 8-10 - Predicted pore pressure in well A-6.

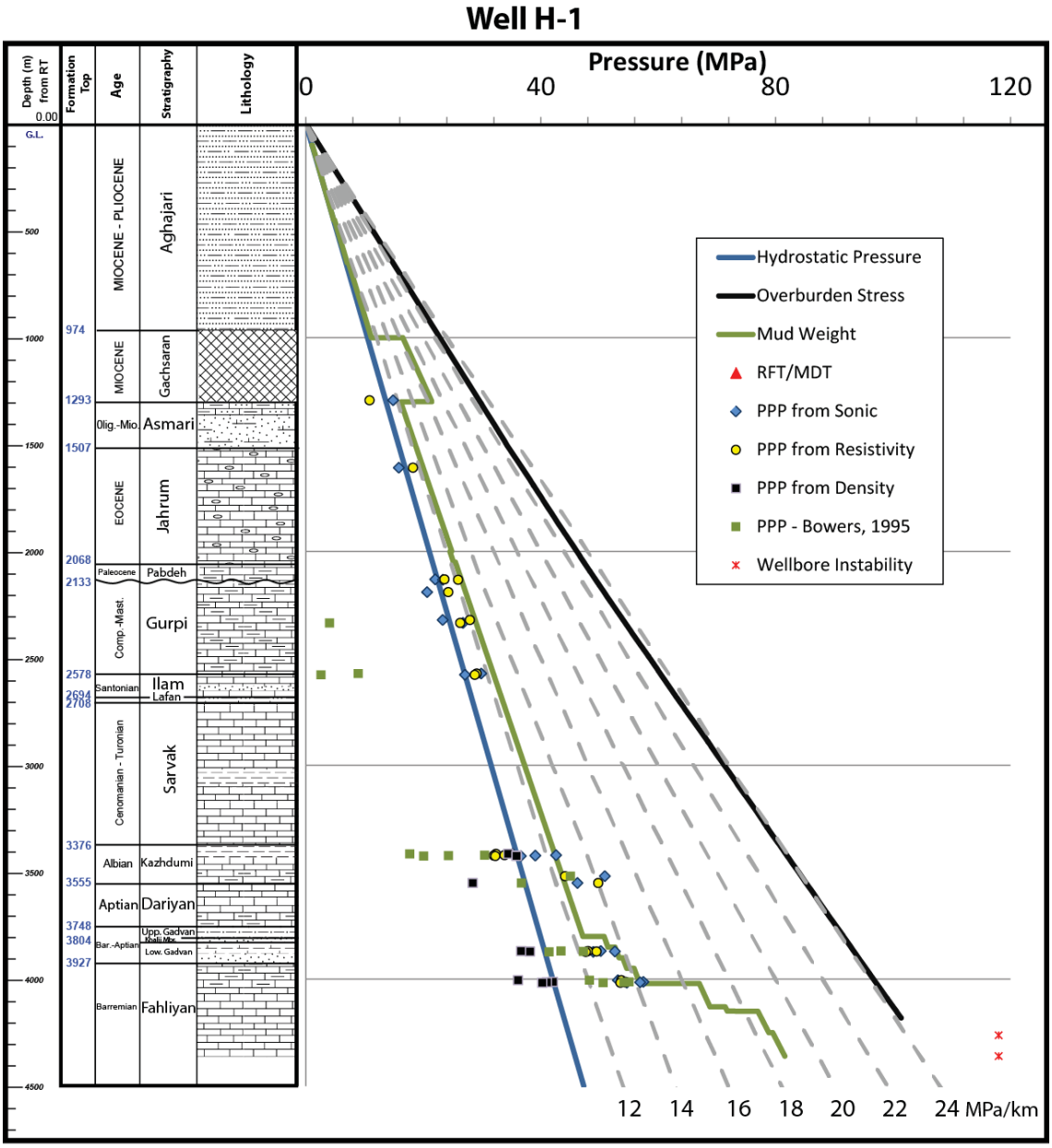

Figure 8-11 - Predicted pore pressure in well H-1.

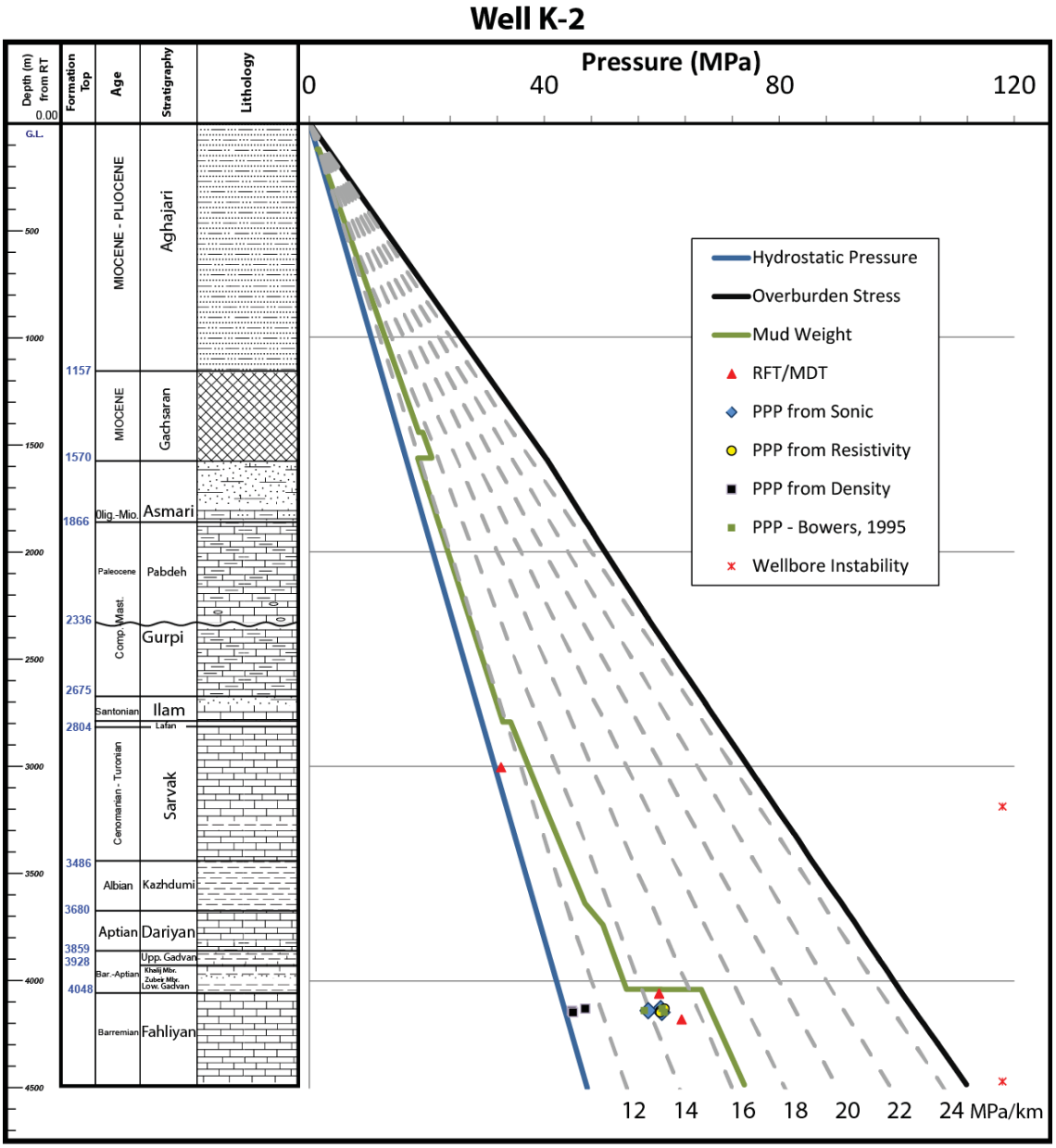

Figure 8-12 - Predicted pore pressure in well K-2.

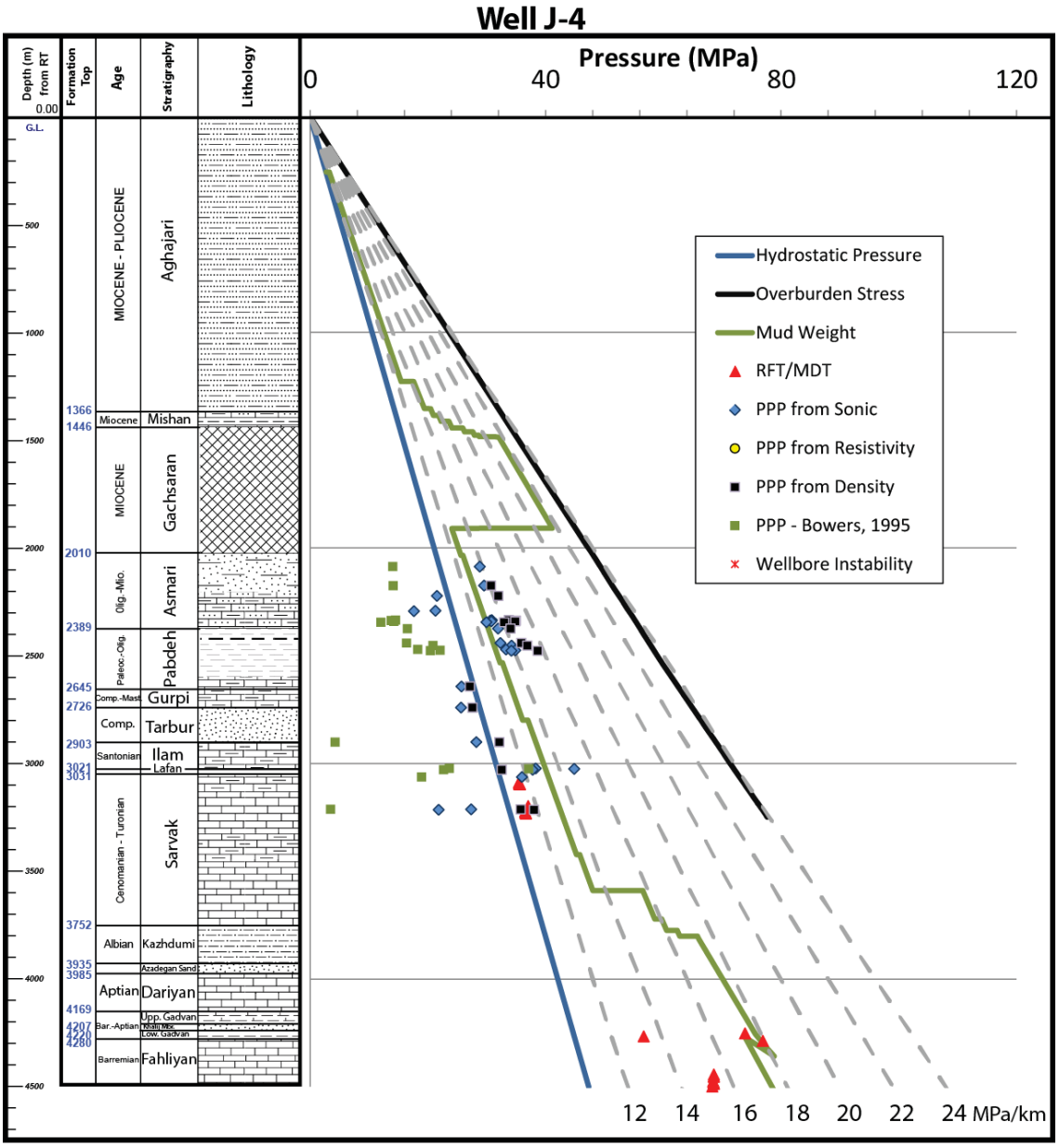

Figure 8-13 - Predicted pore pressure in well J-4.

After running the standard 2m smoothing and shale discrimination scheme on the data of well D-4, no data points remained in formations below the Aghajari Formation. The predicted pore pressure in this formation suggests a hydrostatic pore pressure, which is in agreement with the mud weight data. However, calculations based on density data predicted slightly higher pore pressure (~13.3 MPa/km) at the bottommost section of this formation (Figure 9-4).

In well D-5, mud weight slightly deviates from the hydrostatic gradient at 2200 m depth and sharply at 4000 m in the Lower Gadvan Formation, which then extends into the Fahliyan Formation (Figure 9-4). Sonic log slightly underestimates pore pressure in Ilam-Sarvak interval whilst prediction from the resistivity log overestimate pore pressure in the Ilam Formation. In this well, Bower's PPP underestimated pore pressure in the formations above the Gadvan Formation. Density calculations provide the best match in this normally pressured interval, as well as the rest of the well D-5. There seems to be an overpressure transition zone at the onset of the Kazhdumi Formation, where sonic and resistivity-based predicted pore pressure sharply increases, while mud weight is also mildly above hydrostatic gradient. The predictions in the Gadvan and Fahliyan formations exhibit a promising similarity with mud weight, RFT/MDT measurements and are as expected from the geology of these formations. Despite a few data scattering in the Bowers' PPP at this interval, there is a cluster of Bowers' as well as Eaton's PPP data points shifting from the hydrostatic gradient towards the elevated mud weight which reflects the overpressure.

Mud weight in well D-6 follows the same trend as D-5 with a mild pore pressure rise at the Gurpi Formation and a sharp rise at the Gadvan and Fahliyan formations. A few Wellbore instability issues were also reported in the Jahrum, Sarvak and Fahliyan formations where, unfortunately, no log data was available. The issues in the Jahrum Formation are due to a failure in the surface facilities, but those of the Sarvak and Fahliyan formations were during the drilling operation. But unfortunately, no log data was available at those depths to assess the predictions. In this well, Eaton's PPP using sonic and density logs, as well as Bowers' prediction using sonic log, perfectly match the field data (Figure 8-6). However, despite the good match in the Fahliyan Formation, resistivity PPP overestimates the pore pressure in the shallower formations.

In well D-14, mud weight and direct pore pressure measurements are limited to the Fahliyan Formation (Figure 8-7). Although sonic log was available from shallower depths, it is scattered around NCT and doesn't reflect the overpressure (Figure 8-1 a). As a result, Eaton's pore pressure prediction falls within -20% ~ +10% range around the hydrostatic gradient and does not provide an accountable match with the pressure data. Bowers' PPP

is even poorer in terms of matching the field data. However, the pore pressure predicted from density log data within the Fahliyan Formation exhibited a good match with RFTs. Resistivity log data was not available in this well to test PPP based on resistivity data.

In well D-15, only a few data points at depth interval of 4097m-4110m (the lowermost section of the Lower Gadvan Formation) are available. Both of the Eaton and Bowers sonic PPP estimate a sub-hydrostatic value, while the density data provides a more reasonable prediction with respect to MDTs (Figure 8-8). In this well, the Fahliyan, Sarvak and Dariyan formations encountered several wellbore instability issues. Mud weight is already above the hydrostatic gradient in those formations, but no log data or pressure measurement was available in the Sarvak and Dariyan formations to investigate the possible contribution of overpressure to wellbore instabilities. Similar to well D-14, resistivity log was not available and, thus, resistivity PPP hasn't been performed in this well.

MDTs in well Y-1 cover a wide range of the well's depth profile, starting from the Pabdeh Formation and continuing to the Fahliyan Formation (Figure 8-9). A few resistivity and density data points exist from the Gachsaran Formation whose pore pressure predictions predicted a hydrostatic gradient in that formation, despite the elevated mud weight. Direct pressure measurements from the Gurpi to the Upper Gadvan formations, where there is a data point cloud predicted by Eaton sonic PPP, indicate a hydrostatic gradient and then vanishes at the Lower Gadvan Formation. All of sonic log based calculations accurately predicted pore pressure in the Lower Gadvan and Fahliyan formations. The resistivity log yields proportionally higher predictions at the edge of mud weight, which is a significant overprediction, as the mud weight is roughly 4 MPa/km higher than measured pore pressure at that depth in well Y-1. In this well, wellbore instabilities were observed in the Sarvak and Fahliyan formations, while the overpressured Gachsaran Formation of this field did not exhibit any drilling/completion issues.

Well A-6 has been tested in the Gurpi, Sarvak, Burgan Sand, and Gadvan formations and pore pressure is hydrostatic until the Burgan Sand above the Dariyan Formation. Eaton's

pore pressure predictions yielded accurate values for these zones. This method also accurately predicted overpressure in the Gadvan and Fahliyan formations. Bowers' PPP underestimated pore pressure at shallower deposits, while its results get closer to the other predictions in deeper formations, and exactly matches them in the Gadvan and Fahliyan formations.

In well H-1, the Gachsaran Formation is overpressured (based on mud weight data), while all other formations, except the Gadvan and Fahliyan, are normally pressured (Figure 8-11). Wellbore instability incidents were observed in the Fahliyan Formation of this well, whilst the overpressured Gachsaran Formation was drilled without any issues. In the absence of RFT/MDT measurements, predicted pore pressures are compared with mud data. Eaton's sonic and resistivity predictions fully comply with the mud weight trends in both normally pressured and overpressured formations. However, Bowers' PPP underestimates the pressure at shallower depths and gets closer to the other predictions in the Burgan Sand and the Dariyan Formation, where density PPP agrees with the mud weight as well as other PP prediction methods. Bowers method also accurately predicts pore pressure in the Gadvan and Fahliyan Formations. However, predictions from the density log doesn't provide satisfactory predictions in these formations and underpredicts, wrongly suggesting normal pressures.

In the Gachsaran Formation of well K-2, mud weight has been slightly raised and then, returns back to the hydrostatic gradient until the top of the Sarvak Formation, where it is again increased (Figure 8-12). However, measured pressure shows no overpressure at this depth and mud weight seems to be increased as the driller's conservative attempt to confront the potential challenges of wellbore instability in the Sarvak Formation. Both resistivity and sonic velocity predictions are good matches with the RFT data. However, a few density data points in the Fahliyan Formation lie on the NCT and thus, doesn't appear to be responding to overpressure.

In well J-4, sonic, resistivity and density data were only available in the depth interval of the Asmari to the upper section of the Sarvak Formation (Figure 8-13). Above this

interval, the Gachsaran Formation seems to be highly overpressured (according to mud weight). At the bottom of The Gachsaran Formation, mud weight reduces to slightly above the hydrostatic gradient and remains constant until the bottom section of the Sarvak Formation. The Asmari to Sarvak interval is normally pressured. The mud weight sharply increases from the bottom section of the Sarvak Formation and into the underlying formations, though there is no evidence of overpressure seen in direct pressure measurements (RFT/MDTs). However, direct pressure measurements in the Fahliyan Formation confirm that high magnitude overpressures exist in this formation. Unfortunately, well log from the formations beyond the Sarvak Formation is not available in this well and pore pressure prediction could only be attempted in the upper sections of the well. No resistivity log data was available either, and thus pore pressure predictions are based only on sonic data. Eaton's sonic and density PPP suggests underbalanced drilling in the Asmari-Pabdeh formations while Bowers' PPP underestimated pore pressure in the same interval. However, without direct pressure measurements, nor reported wellbore instabilities, it is hard to confirm the accuracy of these predictions. Sonic and density log based PP prediction suggest the lowermost Pabdeh-Sarvak formations are normally pressured, while the Bowers prediction suggests PP below hydrostatic and is considered unreliable in this well.

Broadly speaking, the pore pressures predicted from density data are less scattered but more accurate than those of the sonic velocity and resistivity. This indicates that the density-based pore pressure prediction is a more reliable method in this basin. In addition to a better performance, density PPP also better reflects pore pressure variations in both of normally pressured and overpressured areas. Data interpretation and further implications of the results are provided and further discussed in the next section.

8.5. Discussion on Shale-based Pore Pressure Prediction in the Abadan Plain Basin

As discussed in the previous chapter, the response of carbonate rocks to stress is not solely mechanical and, considering the existence of chemical processes taking place during deposition, carbonates in the Abadan Plain Basin (and many other parts of the world) are classified as non-stress sensitive. In this section I have tested the only currently available 'solution' to undertaking PP prediction in carbonates, in which only interbedded shales are used, in combination with conventional shale-based prediction methods, with the assumption that carbonates and interbedded shales are in pressure equilibrium. Eaton's (1972) method has been applied on this set of data and pore pressures were predicted using an Eaton (1972) exponent of 1.0 for sonic velocity, 0.1 for resistivity data and 5 for density data. Before starting the results discussion, it is important to note that the pore pressure predictions are compared to two different sets of identifiers: direct pore pressure measurement, which are primarily only available in the Gadvan and Fahliyan hydrocarbon reservoir formations, and mud weight. This may have specific implications for the comparison in different formations, as the mud weight is only a proxy for pore pressure, and is generally slightly higher than pore pressure but can be significantly overbalanced and even potentially underbalanced in impermeable formations. As an example, in well H-1 (Figure 8-11), no pore pressure measurements were available and thus, predicted pore pressure is entirely compared with the mud weight. This is also the case for the Aghajari, Gachsaran and Asmari formations in this study. Wherever possible, a mud weight to RFT/MDT calibration is also discussed.

During the data analysis for shale-based PPP, there were several instances where the predicted pore pressures fail to match direct pore pressure measurements, as noted in the prior section. These mismatches between prediction and observation likely arise from a number of issues. For example, data smoothing is undertaken to remove spurious data and to obtain an 'average' petrophysical value for a specific lithology (herein, shales). However, the used 2m smoothing window is still large enough to potentially include a range of lithologies, such as carbonates, even if the predominant lithology is shale. Furthermore, the shales of the Abadan Plain Basin vary in clay and carbonate volume

from almost 'pure' shales to marls. The possibility of smoothed data containing a 'mixture of shales and other lithologies' was discussed previously in Chapter 5. One example is seen in the Gadvan/Fahliyan zone of well D-14, which appears to have shale velocities that are as fast as the matrix velocities of clay minerals (Figure 8-1a), implying that either the shale has zero porosity (not realistic) or that the velocity is anomalously fast due to the presence of another lithology within the sample window. Another limitation of the shale-based PP method herein is the shale data point constraint. Shales are relatively infrequent within the sedimentary succession of the basin, and are also not often covered by petrophysical logging data. As such, there are often significant depth and data gaps in the shale-based predictions, and an overall lack of 'connected' prediction data, particularly in shallow formations (which are so critical for developing a NCT). Indeed, data coverage varies in each well and therefore, except the Gadvan and Fahliyan formations, which are well logged and associated with good quality data, a basin wide correlation can't be fully implemented. Hence, pore pressure predictions are individually examined in each well, and discussed as a well-scale analysis, rather than a more beneficial (and originally envisaged) field and basin scale analysis. Though, it is also worth noting the usefulness of background gas, connection or trip gas, and wellbore instability incidents, which were used when available, and which can also indicate underbalanced drilling and implicitly determine the pressure at which wellbore and the formation equilibrate. The majority of wellbore instability issues in this field have occurred in the Fahliyan Formation whilst a few reported in the Aghajari (1 case) Jahrum (2 cases), Sarvak (3 cases), Kazhdumi (1 case), and Gadvan (2 cases) formations. They mainly occurred during Run in Hole (RIH) or Pull Out of Hole (POOH) operations in shallower formations than the Gadvan formation and, given almost the same mud weight trend in all studied wells of this field, none of the wellbore instability issues can be attributed to the underbalanced drilling conditions. In an overpressured horizon, several causes of wellbore instability can be outlined, such as shale swelling of the Gadvan Shale and, most importantly, the overpressure in both of the Gadvan and Fahliyan formations. These cases, as well as background gas and connection gas implications, are individually discussed in each well as follows.

In field D, mud weight in all studied wells was usually increased in the Gurpi Formation prior to penetrating the carbonate, even though the Ilam Formation appears to be normally pressured. In the absence of direct pressure measurements, overpressure can't be confirmed in the strata below this depth until the Gadvan Shale. Therefore, pore pressure prediction can't be accurately assessed in the units between the Ilam and Gadvan formations. On the other hand, well D-4 has very few data points, which are limited only to shallow deposits of the Aghajari Formation where pore pressure is hydrostatic (Figure 9-4). As a consequence, PPPs are better performed in the Gadvan and Fahliyan formation of field D. In well D-4, Eaton's sonic and resistivity PPP indicates good compliance with mud weight. Density PPP has slight offset to observed data, but is still accordance reasonable fit with the field data. However, Bowers' PPP suggests unrealistic (negative) values for pore pressure, and not shown on the plot. In well D-5, mud weight has been raised from 14 MPa/km to 17 MPa/km in the bottommost section of the Gadvan Formation due to a gas and oil inflow (Figure 9-4). Under such conditions, wellbore fluid pressure is increased to create a slight overbalance with the formation pressure and can be an accurate estimation of pore pressure if direct measurement isn't available. Fortunately, several tests were conducted at this depth, in the overpressured Fahliyan Formation, and confirms that mud weight is an accurate indicator of pore pressure in this section of the well. Gas shows and mud gains were also observed at 4003 m depth in well D-6, which was controlled by increasing mud weight from 1.5 to 1.63 kg/l (Figure 8-6). In well D-15, high total gas values were detected at 4472 m, a few meters above the well's total depth, though this section was not petrophysically logged (Figure 8-8). This increase in mud weight within the bottom section of the Gadvan Formation, which extends into the Fahliyan Formation, is a general trend observed throughout all of Field D, and thus likely represents a field-wide overpressured zone, or a zone in which overpressures are anticipated (and previously observed) by drillers.

Predicted pore pressure in field D is consistent with the mud weight and RFT/MDT measurements in almost all wells in field D, and the density and resistivity data provided better pore pressure predictions than sonic velocity (though sonic data also provided reasonable predictions). However, Well D-14 is an exception, in which sonic velocity derived PP is scattered (-20% ~ +10%) around the hydrostatic gradient, and not

consistent with observed PP. However, density PPP in this particular well yielded a good fit to RFT/MDT measurements (Figure 8-7). The discrepancy of sonic log derived predictions in D-14 has already been previously described in this chapter, and is the result of anomalously fast sonic velocities that are thought to be spurious. However, aside from this well (D-14), the pore pressures predicted from sonic velocity are generally reasonably consistent with RFT/MDT measurements in field D.

In well Y-1, mud weight indicates moderate overpressure in the Gachsaran Formation while density and resistivity data suggest the formation to be normally pressured (Figure 8-9). There is no way to reliably assess whether the mud weight was pre-emptively kept high, based on the regional trend of nearby fields, or whether this formation is already overpressured. In deeper strata, a gas inflow and subsequent mud weight increase were observed in an interval of 2778-2818 m in the Sarvak Formation. This means that mud weight at that depth has been effectively equilibrated with the formation pressure, thus the driller decided to slightly increase the pressure in annulus. While no sonic or resistivity data was available at that depth interval, MDT results, which demonstrate hydrostatic pressures, indicate that the mud weight was significantly overbalanced when drilling through the formations above the Gadvan Formation. Despite a few data cloud clusters in the upper section of the Gadvan Formation, all sonic log predictions yielded a good match with MDT results in the Fahliyan Formation. It appears that the pressure transition zone in this well is within the Gadvan Formation, since MDT data shows a sudden pore pressure rise in the Zubeir Sand (Bottom section of the Gadvan Formation). Sonic velocity PPP follows the mud weight trend and successfully predicts the overpressure in that interval. However, resistivity-based prediction PPP seems to overestimate PP in the lower section of the Gadvan Formation, which is only mildly overpressured.

The A-6 well targeted hydrocarbon accumulations in the Sarvak, Gadvan (the Zubeir Member), and Fahliyan formations. Drilling of this well encountered no gas shows or anomalous total gas or connection gases, and the well was successfully controlled by mud pressure with no influxes. Mud weight has been increased from the Asmari Formation due to overpressure concerns, even though no sign of overpressure was observed. The

Sarvak Formation, 1000 meters below the Asmari Formation, is also normally pressured, and seems to support the indications that the Asmari Formation in normally pressured and was drilled overbalanced (Figure 8-10). Deeper in the well, mud weight remains constant, slightly above the hydrostatic gradient, until entering the Gadvan Formation. Pressure sampling in the Burgan Sand indicated mild overpressure, close to the mud weight. However, predicted pore pressure starts deviating from the hydrostatic gradient earlier in the Kazhdumi Formation, above the Burgan Sand. It is possible that the shale dominated Kazhdumi Formation, and the underlying Burgan Sand, could be overpressured, due to the Kazhdumi Formation's low permeability, while the adjacent permeable Sarvak Formation is normally pressured. However, there is no data to confirm or refute that possibility, and despite underbalanced drilling suggested by predicted pore pressure in the Burgan Sand, no pore pressure data is available to examine this. Even if the Kazhdumi Formation does contain overpressures, as the PP prediction suggests, these did not exceed the mud weight used in this formation, and thus no influx or notable gas peaks are likely to occur. Pore pressure predictions in the Gadvan and Fahliyan formations of this well are in agreement with mud weight and pressure test results. Bowers' PPP approaches the same values as Eaton's in these two formations, but underestimates the pore pressure in shallower zones.

Tight hole conditions have been encountered at 4040 m of well H-1, which were combatted by increasing mud weight, although this well had to be side-tracked twice due to stuck pipe events at 4360m depth. This could be indicative of underbalanced conditions in the Fahliyan Formation, but may also be related to stress-induced wellbore instability and provide no direct link to pore pressure gradient in this zone. Unfortunately, well H-1 did not contain any pressure test or log data in the Gachsaran Formation, and thus the accuracy of the PP prediction in this formation cannot be examined. However, based on regional data, it is anticipated that the Gachsaran Formation would contain overpressures. Sonic log data is available in deeper formations of well H-1, and both Eaton's sonic and resistivity derived PP suggest normal pore pressures, with only a slight predicted overpressure in the Kazhdumi to Dariyan formations (Figure 8-11). Bowers' PPP underestimates pore pressure in these zones. However, both of the Eaton and Bowers predictions provided good match to pore

pressure measurements in the underlying Gadvan and Fahliyan formations. Density log was only available in the Kazhdumi-Fahliyan interval of well H-1, but did not yield reliable predicted pressures when compared to pressure observations. Overall, the predicted PP in well H-1 indicate a gradual PP increase from hydrostatic pressures to mild and moderate overpressures in the Gadvan and Fahliyan formations.

The K-2 well contains an RFT measurement in the Sarvak Formation that confirms the hydrostatic gradient in this interval (Figure 8-12). However, mud weight is slightly above hydrostatic, and is believed to have been raised in anticipation of expected overpressures. Mud weight then remains constant until there is another slight weight increase in the Darian Formation, with this slightly elevated mud weight held constant until the mud weight is sharply increased in the Fahliyan Formation. There are no pressure measurements in the Gadvan Formation, but according to the regional trends, overpressure is expected. However, since there was no evidence of fluid influxes while drilling, the formation pressure must be considered to have been below the mud pressure. Recorded pore pressure in the Fahliyan Formation is greater than the mud pressure in the Gadvan Formation (as a proxy to pore pressure) and, hence, a hydrodynamic seal between these two formations must exist. In terms of PPP calculations, a few data points of sonic velocity and resistivity have provided accurate prediction of pore pressure in the Fahliyan Formation. Like well H-1, density PPP underestimates the pore pressure and is unreliable in this well.

In well J-4, the Gachsaran Formation is believed to be hosting significant overpressures, as the mud weight is almost as high as the lithostatic gradient (Figure 8-13). This well has been drilled to 4505 m depth, but was logged only over an interval of 2087-3213 m depth (Asmari to Sarvak formations). These formations are reported as normally pressured, which is confirmed with pressure measurements in the Sarvak Formation. Despite the Bowers' method underestimating pore pressure, Eaton method sonic velocity and density predictions suggest underbalanced drilling conditions in the Asmari and Pabdeh formations. The degree of underbalance was 2 MPa/km at its maximum and might have been ignored by the driller. There is no comprehensive drilling report to examine this, but since this field has the closest distance to the Zagros Deformation Front, these

formations could be under severe tectonic compressions and thus be highly overpressured. Eaton's pore pressure predictions in the Sarvak Formation, using the sonic velocity and density data, exhibit proximity good fit with mud weight and RFT/MDTs. Deeper in the well, mud weight was sharply increased in the Kazhdumi Formation and continued to be elevated in the Gadvan and Fahliyan formations. There is no log data from these formations in well J-4. However, a pressure test in the Fahliyan Formation confirmed a high magnitude of overpressure. Resistivity log was not available in well J-4 and resistivity-based PPP analysis hasn't been conducted in this well.

As a basin-scale overview, most of the pore pressure predictions in the studied wells of the Abadan Plain Basin are consistent with mud weight and direct pore pressure measurements. Bowers' pore pressure prediction provided accurate predictions in the Gadvan and Fahliyan formations, but underestimated pore pressure in the shallower sequences. The reason for this shallow underprediction is likely the poor definition of the loading curve due to limited availability of sonic log in the normally pressured deposits of this basin. Pore pressure predictions using resistivity data was observed to sometimes overestimate pore pressure at a range of depths. This is possibly due to the larger dynamic range of resistivity data, which is over several orders of magnitude (far larger than for sonic and density data), which means that resistivity-based predictions are more prone to large variations (even using an Eaton exponent of only 0.1), especially if there are any spurious measurements or issues such as saline drilling mud invasion into the formation (though this can often be overcome in practice with larger smoothing efforts or very careful data selection). Sonic and density-based shale PP predictions using the Eaton method provide the, overall, best fit to pore pressure observations, with density-based predictions offering a slightly better fit (due to less prediction variability, again due to the sonic velocity data having a lower dynamic range than density data). Nevertheless, there were still some sections in which density-based PP predictions underestimate observed pressures, such as in wells H-1 and K-2. According to the results of various pore pressure prediction methods, a useful approach for PPP in this kind of basins would include a combination of sonic, resistivity and density PPP calculations as complement to each other, and to provide a 'sense check' on all the log-based predictions. Furthermore, it is generally most important to always involve sonic-based PP predictions,

as these methods and parameters are more easily to other velocity data, such as VSPs and, most importantly, pre-drill seismic-based velocities.

8.6. Conclusion

In this chapter I presented an integrated approach to predicting pore pressure in carbonate deposits of the Abadan Plain Basin using standard shale-based PP prediction methods on shale interbeds. This included a validated shale discrimination scheme, data smoothing processes, derivation of NCTs and the most reliable input parameters for Bowers and Eaton method predictions. Furthermore, shale based PP prediction methods were tested using sonic velocity, density and resistivity data, both to test the validity of a range of petrophysical log types, but also to highlight how undertaking predictions with a range of log types and methods can be used together to improve overall PP predictions, sense check predictions and to assess uncertainty. It is particularly important to note that the shale-based PP prediction undertaken herein was quite successful within the Gadvan and Fahliyan formations, in which there is often an overpressure transition zone. In general, Eaton (1972) pore pressure predictions using sonic and density data provided the most reliable predictions, with density-based methods generally in better compliance with the measured pore pressure than sonic velocity and resistivity data. However, the shale-based pore pressure predictions also suffer from a number of issues, such as being occasionally significantly inaccurate (which suggests unreliability, and thus a risk for drilling safely), as well as there being the issue of potentially large data gaps due to a lack of shales (in addition to the lithological variability of the shales themselves). Thus, while the application of conventional shale-based predictions shows considerable promise and usefulness, I will also test and examine a new method, in the next chapter, that I have developed to specifically try and overcome the issues facing traditional PP prediction in carbonates.

CHAPTER 9- Compressibility Method for Pore Pressure Prediction

9.1. Introduction

Disequilibrium compaction is the primary origin of overpressure in many depositional environments, and is the most likely cause of overpressure in the Abadan Plain Basin (Haugland et al., 2013; Katahara, 2003, 2006; Luo et al., 1994; van Ruth et al., 2004; Yu and Hilterman, 2014; Zhang, 2013). Conventional methods for pore pressure prediction face several restrictions in carbonate environments, and require significant compromises and likely substantial modifications (Gruenwald et al., 2010; Huffman, 2013; Huffman et al., 2011; O'Connor et al., 2010; O'Connor et al., 2011; Wang et al., 2013). Pore structure in carbonate rocks also affects pressure predictions. For example, pores with low aspect ratio (e.g. fractures) lead to pore pressure overestimation, whilst vugs and moldic pores with high aspect ratios lead to underestimation (Wang et al., 2013). The pore system in carbonates is a complex combination of several pore types, which increases the risk of erroneous pore pressure prediction. Shale-based pore pressure prediction methods are a potentially effective tool for PPP in carbonates (as discussed in the previous chapter), but are restricted to (often thin) clay-rich interbedded layers that are assumed to represent the mechanical conditions of the surrounding rocks. This limits the application of such methods to only discrete intervals of a well. Shale deposits are rare in thick carbonate rocks and, while possessing great advantage of simple and easy to implement calculations, shale-based PPP methods fail to reliably predict pore pressure in many pure carbonate sediments. However, carbonate rocks can be characterised as poroelastic materials (Berryman, 2015; Hassanzadegan et al., 2016; Parra et al., 2004), though with more complex mechanical models than are typically applied to sands. This is the basis of two new methods proposed in this chapter that aim to predict pore pressure from carbonate rock compaction data, rather than purely from porosity (or a proxy for porosity, like p-wave velocity). These proposed techniques are only valid where disequilibrium compaction is the main mechanism responsible for overpressure generation, and thus the carbonate deposits of the Abadan Plain Basin are a suitable region to test these alternative methods. The first method is a porosity-based correlation for pore pressure, which is obtained from a comparative analysis of pore and bulk compressibility. The second method is a

mechanical model that predicts pore pressure during a mechanical compaction process. Empirical coefficients considered in these methods may differ for different geological settings, but the methods provide a potentially reliable tool to predict the onset and magnitude of overpressure.

9.2. Pore Pressure in Poroelastic Mediums

Disequilibrium compaction is a mechanical phenomenon that takes place over geological time. Mechanical state of a rock body in the earth can be defined by three principal stress regimes (Zoback et al., 1977). Stresses in a rock can be in any form of the following stress regimes (Zimmerman, 1991):

- "uniaxial: a state of stress with only one non-zero principal stress
- triaxial: a state of stress with all non-zero principal stresses but two of them are equal,
- polyaxial: the condition in which no principal stresses are zero nor necessarily equal."

There is also another classification of stresses comprised of 'uniaxial', 'biaxial' and 'triaxial' (also known as 'true triaxial') stresses which is more common in modern geomechanics. A 'triaxial' state of stress is the most common case in natural depositional environments. However, the laboratory tests are normally performed under controlled conditions in such a way that uniaxial or triaxial stress states persist. Whilst the first theory of one-dimensional consolidation was developed by Terzaghi (1923), a comprehensive theory of three dimensional consolidation under arbitrary states of stress was developed by Biot (Biot, 1941; Biot, 1955; Biot, 1973), and is commonly referred to as the theory of 'poroelasticity' (Detournay and Cheng, 1993). This theory includes the concepts of pore pressure and pore strain and, as a result, poroelastic materials behave differently than simple elastic materials (Nunziato and Cowin, 1979; Zimmerman, 1991). The vast majority of classic models for poroelastic materials were developed to study the soil deformation under certain load. However, there are similarities between rock and unconsolidated soil in terms of poroelasticity, and thus these theories are widely used in rock mechanics. According to Giles et al. (1998), it is possible to apply the poroelasticity theory to some kinds of sands, which behave like plastic under low stress, such as intergranular clays, sandstones without quartz; and mudstone clasts in particular. In a further

micro scale study, pore geometry was later considered an important factor in rock compressibility. For example, in a simple model in which pores are spherical (Dewey, 1947; Mackenzie, 1950), confining stress has the minimum effect on bulk compressibility and the compressibility increases as pores deviate from sphericity (Zimmerman, 1991). Formation compressibility, as a function of porosity, also plays a significant role in gas reservoirs and, according to Lowery (1984), can approach or exceed the gas compressibility in overpressured reservoirs.

A full field study of pressure regime in an oil and gas field requires comprehensive knowledge of the mechanical properties of the reservoir and cap rock, as well as paleo-temperature and paleo-pore pressure conditions. Such simulations are usually performed by basin modelling (BeicipFranlab, 2015; Paradigm, 2015; Platte River Associates, 2014; Schlumberger, 2015b). These packages evaluate seal capacity and fluid migration, and then create a hydrodynamic model of the basin. However, diagenetic evolutions of carbonate rocks complicate such models, and not all of the diagenetic processes are simulated. The problem arises in carbonate rocks where porosity evolves through several other processes (diagenesis), rather than normal mechanical compaction.

Most carbonate rocks in the Abadan Plain Basin were deposited under shallow marine environment. As Giles et al. (1998) discussed, the Plastic deformation associated with very shallow compaction is mostly mechanical rather than chemical. Mechanical deformation can be studied in terms of pore and solid phase (grain + matrix) changes in such a way that it can be divided into two main parameters: 'hard' and 'soft' portions of the poroelastic medium. Many rock mechanical studies such as Liu et al. (2009), Berryman (2005) and Mavko and Jizba (1991) examined the mechanical deformation of a rock in terms of changes in pore and solid phase, and are linked to effective stress via the Biot's poroelastic parameter, α. Biot's poroelastic parameter is the ratio of fluid volume gained (or lost) in a material element to the volume change of that element, when the pore pressure is allowed to return to its initial state (Detournay and Cheng, 1993). This constant is often assumed to be one (1) in many calculations, which implies the same amount of volumetric change as the amount of produced fluid (if the rock is not confined). Fatt (1958) has indicated that, according to Greetsma's (1957)

theoretical treatment of porous rock compressibility, α is pressure dependant and a function of bulk volume and solid material compressibility (Equation 9-1).

$$\propto = \frac{C_b - C_r}{C_b} \qquad \text{Equation 9-1}$$

Where C_r and C_b are the compressibility of rock matrix and bulk frame respectively. According to the concept of poroelasticity, a confined porous rock under a compressing load undergoes a process of deformation that includes compaction of the rock frame and pore fluid. During unconfined compaction, pore space reduces and applies loading force to the pore filling fluid. Depending on the sealing efficiency of the confining strata, some degrees of imbalance in the increasing load and fluid drainage from the pore space are generated which is then expressed as overpressure (disequilibrium compaction).

9.3. Porosity and Compressibility Correlations for Pore Pressure Prediction in Carbonates

9.3.1. Compressibility method for Pore Pressure Prediction (Atashbari and Tingay, 2012a)

A new method is introduced here that uses a series of sedimentary rock petrophysical attributes to obtain a correlation between pore pressure and porosity. The final correlation is a simple equation, which doesn't contain most of the parameters used during its derivation. That is because some of the rock's mechanical properties used in this analysis, such as pore volume compressibility, can be determined in terms of correlations with porosity. The primary concept of this method has been previously published by Atashbari and Tingay (2012a) for pore pressure prediction using compressibility data of a reservoir rock. This method includes compressibility data from core samples analysed in a laboratory. Such tests are often performed during special core analysis (SCAL) to evaluate petrophysical properties of a formation. The method is based on four basic definitions of compressibility by Zimmerman et al. (1986):

$$C_{bc} = \frac{-1}{V_b^i}\left[\frac{\partial V_b}{\partial P_c}\right]_{P_p} \qquad \text{Equation 9-2}$$

$$C_{bp} = \frac{1}{V_b^i}\left[\frac{\partial V_b}{\partial P_p}\right]_{P_c} \qquad \text{Equation 9-3}$$

$$C_{pc} = \frac{-1}{V_p^i}\left[\frac{\partial V_p}{\partial P_c}\right]_{P_p} \qquad \text{Equation 9-4}$$

$$C_{pp} = \frac{1}{V_p^i}\left[\frac{\partial V_p}{\partial P_p}\right]_{P_c} \qquad \text{Equation 9-5}$$

Where P_c is confining pressure, P_p is pore pressure, V_b is bulk volume of the rock, V_p is the pore volume, and the superscript i notation refers to the initial state of the media (before compression). For compressibility (C_{bc}, C_{bp}, C_{pc}, C_{pp}), the first subscript notation indicates the relevant volume change, and the second subscript notation indicates the pressure which is varied. The term to the right of the bracket indicates the pressure, which is kept constant. Equation 9-6 is obtained by dividing Equation 9-2 and Equation 9-3 by each other, assuming the same effect of pore and confining pressures on the bulk volume.

$$\partial_{pp} = \frac{C_{bc}\partial P_c}{C_{bp}} \qquad \text{Equation 9-6}$$

Herein, the negative sign in Equation 9-2 is removed, as it only relates to the direction of applied force in terms of volume change. It is assumed that both the confining and pore pressure result in the same magnitude of volume change if they are infinitesimal. Therefore, volume elements of both equations are cancelled, and compressibilities are undirected. This cancellation of parameters is not always correct, as pore pressure and confining pressure are measured separately in the laboratory tests (while confining pressure is varying, pore pressure is kept constant and *vice versa*). According to the magnitude of stress applied to a porous rock, and the way the rock responds to that stress, pore pressure and confining pressure would have different impacts on rock deformation (porosity loss). However, in reservoir conditions, there is a system of fluid flow in which the confining and pore pressures are iteratively dependent and act concurrently. Although, this hypothesis might be subject to criticism, the abovementioned assumption, in ideal conditions, satisfies the basic definitions of compressibility. Considering the infinitesimally small, and effectively same size, increments for all independent variables, differentiation becomes an equation:

$$d_{pp} = \frac{C_{bc} dP_c}{C_{bp}}$$ Equation 9-7

Where d_{pp} is the change in pore pressure and dP_c is the variable confining pressure. Values of C_{bc} come from SCAL tests, where the core sample is put in a core holder under an incremental confining pressure while the pore fluid is free to flow out of the system. The fourth variable, C_{bp}, remains unknown, but can be determined indirectly from the available parameters. Zimmerman et al. (1986) introduced a relationship between the bulk compressibility of rock against pore and confining pressures as follows:

$$C_{bp} = C_{bc} - C_r$$ Equation 9-8

Where C_{bp} and C_{bc} are the bulk compressibility of the rock against pore pressure and confining pressure respectively, and C_r is the compressibility of the rock matrix. Matrix compressibility is related to the porosity and pore compressibility by van Golf-Racht (1982):

$$C_r = \frac{\emptyset C_{pc}}{1-\emptyset}$$ Equation 9-9

Where Ø is porosity and the other terms are the same as previously described. Combining Equation 9-8 and Equation 9-9 into Equation 9-7 results in the following relationship for pore pressure prediction:

$$d_{pp} = \frac{(1-\emptyset) C_{bc} dP_c}{(1-\emptyset) C_{bc} - \emptyset C_{pc}}$$ Equation 9-10

The ultimate equation needs a calibration factor for each geological setting, which is achieved by the introduction of an empirical exponent γ. dP_c is interpreted as σ_{eff}, which is the difference between compacting stress and pore pressure (hydrostatic):

$$P_p = \left(\frac{(1-\emptyset) C_b \sigma_{eff}}{(1-\emptyset) C_b - \emptyset C_p} \right)^{\gamma}$$ Equation 9-11

This method was first used for PP prediction in one of the fields in the Abadan Plain Basin (Atashbari & Tingay, 2012; presented below), and has also since been successfully tested in the Gulf of Mexico in normally pressured formations with a γ exponent of 0.845 (in sequences in which pressures were underestimated using the Bowers and Eaton methods) (Morales Salazar, 2014). The majority of variables in Equation 9-11 are pore and rock compressibility values that are obtained from laboratory tests. Any technique to estimate those values from well log or seismic data will make the method a lot useful and applicable in wider range of wells. Despite the inherent complexity of carbonate pore systems, pore compressibility as a mechanical behaviour of a rock body could be correlated to porosity. The first attempt to relate these two parameters was performed by Hall (1953a), when he studied several carbonate and sandstone rocks and provided a combined graphical correlation for pore compressibility which was then converted to a numerical empirical relationship:

$$C_p = 0.2597\emptyset^{-0.45} \qquad \text{Equation 9-12}$$

Where C_p is pore volume compressibility in 1/GPa and Ø is the porosity in fraction. Van der Knaap (1959) provided another correlation for 23 limestone core samples from a single well. He related the fractional pore volume to the effective stress using the following equation:

$$\frac{V_{p_1}-V_p}{V_{p_1}} = \frac{7\times10^{-4}}{\emptyset}(\sigma - \bar{\sigma})^{0.42} \qquad \text{Equation 9-13}$$

Where V_p is pore volume, Ø is the porosity in fraction, and σ and $\bar{\sigma}$ are the compacting and hydrostatic pressures respectively in MPa. Those approaches were challenged by Newman (1973) following analysis of 256 samples from 40 reservoirs including 197 sandstone samples and 59 limestone samples. He concluded that considering a single correlation for several different rock types is unlikely to be valid due to the widely scattered data he analysed. Although considering different correlations for each rock type may provide better relationships, Newman (1973) found little or no relationship between pore compressibility and initial porosity in friable samples. He suggested a different relationship for every rock type and, for limestone, his correlation is approximated by correlation as the following equation:

$$C_p = 0.26 + \frac{0.09}{\emptyset}$$ **Equation 9-14**

Where C_p is pore volume compressibility in 1/GPa and Ø is the porosity in fraction. Horne (1997) also divided the relationships between pore volume compressibility and initial porosity into three main groups of limestones, sandstones, and unconsolidated sandstones (Figure 9-1). Like Newman (1973), Horne (1997) also believed that using the same correlation for all rock types was not appropriate. Horne's (1997) correlation for consolidated limestone is:

$$C = exp(4.026 - 23.07\emptyset + 44.28\emptyset^2) \times 10^{-6} \quad \text{, 1/psi}$$ **Equation 9-15**

The above equation in 1/GPa units becomes:

$$C = -7.55\left(-0.053 - e^{-22.21\emptyset}\right) \quad \text{, 1/GPa}$$ **Equation 9-16**

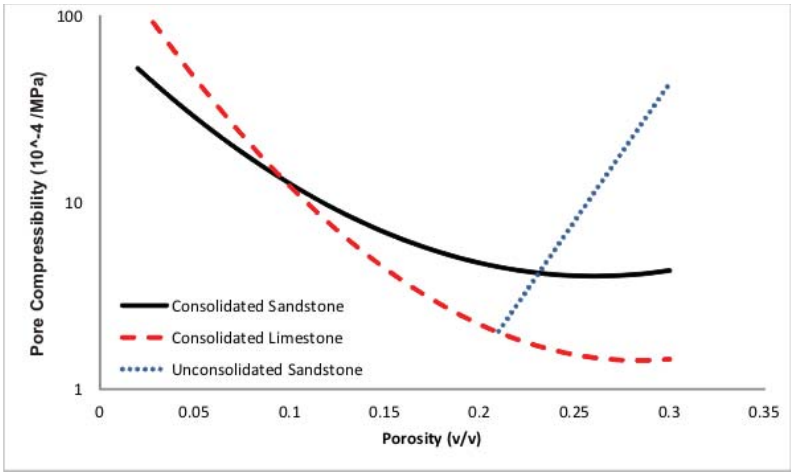

Figure 9-1 – The relationship between pore volume compressibility and porosity for sandstones, limestones and unconsolidated sandstones, modified after Horne (1997).

Jalalh (2006) continued this approach providing adapted correlations for limestone and sandstones separately as follows:

$$C_{p_{limestone}} = \left(\frac{1}{1.022^{-2}+1.681^{-2}\emptyset^{1.05}}\right) \times 10^{-6} \quad , 1/psi \qquad \text{Equation 9-17}$$

Where porosity is in percentage. Applying conversion to 1/GPa, the following correlation becomes:

$$C_{p_{limestone}} = \frac{1}{0.07+14.6\emptyset^{1.05}} \quad , 1/GPa \qquad \text{Equation 9-18}$$

The Jalalh (2006) correlation for sandstone is in the following form:

$$C_{p_{sandstone}} = \left(\frac{1}{-2.141^{-2}+4.064^{-2}\emptyset^{0.4652}}\right) \times 10^{-6} \quad , 1/psi \qquad \text{Equation 9-19}$$

$$C_{p_{sandstone}} = \frac{1}{-0.15+2.38\emptyset^{0.46}} \quad , 1/GPa \qquad \text{Equation 9-20}$$

The most recent laboratory test on carbonates of the Middle East was performed by Akhoundzadeh et al. (2011), who exclusively studied several samples of the Sarvak carbonate reservoir rock. Akhoundzadeh et al. (2011) provided a logarithmic correlation (Equation 9-21), which was used to determine the pore volume compressibility of the Sarvak Formation.

$$C_p = \left(\frac{1}{0.367+0.099\ln(\emptyset)}\right) \times 10^{-6} \quad , 1/psi \qquad \text{Equation 9-21}$$

This equation can be converted to metric units in the form of a power trend:

$$C_p = \frac{1}{-16.35+19\emptyset^{0.04}} \quad , 1/GPa \qquad \text{Equation 9-22}$$

Since the pore volume compressibilities are effective confining pressure dependant, there are different values of pore compressibility at different stresses for a single rock sample. Akhoundzadeh et al. (2011) proposed 11.3 MPa/km as the effective stress gradient, as a proxy

to the approximate effective confining stress acting under typical reservoir conditions. In his assumption, 1.0 psi/ft was considered as the lithostatic gradient and 0.5 psi/ft considered as the hydrostatic gradient. The available correlations are plotted along with Fahliyan Formation data in Figure 9-2. Jalalh's (2006) data is indicated as the best fitting correlation, and is used in further calculations herein. Concurrently, Akhoundzadeh et al.'s (2011) correlation has been used in wells A-6 and J-4, where the method was directly tested in the Sarvak formation.

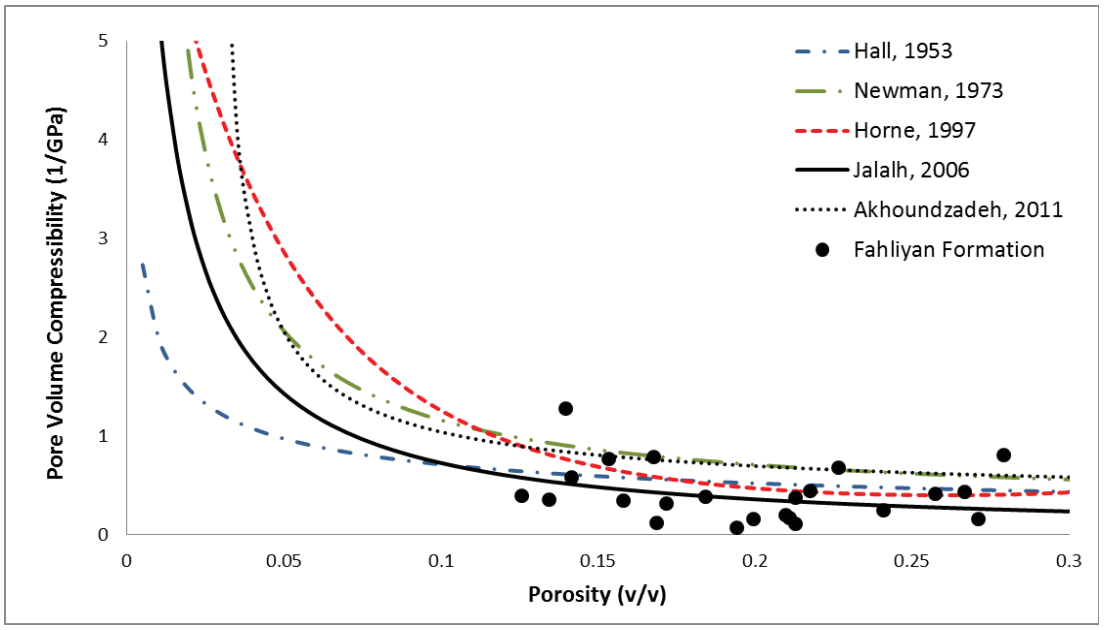

Figure 9-2 – The relationship between pore volume compressibility and porosity in the Fahliyan Formation alongside the correlations from published studies. The best matching correlations is Jalalh (2006).

The pore volume of core samples measured in the laboratory may differ from porosity measurement obtained from well logs. Therefore, an additional correlation is needed to convert core-measured porosity to log-measured porosity (Figure 9-3).

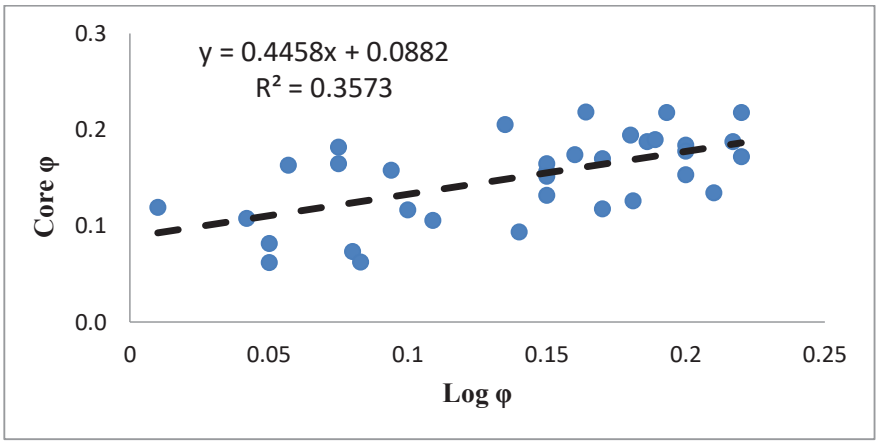

Figure 9-3 – Correlation between well log derived porosity and laboratory measured core porosity measurements in the Fahliyan Formation.

The correlated porosity is used in Equation 9-22 to estimate the pore volume compressibility. The correlated porosity and resulting pore volume compressibility measurements are then put into Equation 9-23 to predict pore pressure as a result of formation compaction.

9.3.2. Modified Compressibility method for Pore Pressure Prediction (Azadpour et al., 2015)

Through a series of personal discussions, Azadpour et al. (2015) provided a modified method of Equation 9-11, with the same approach, which uses Equation 9-4 and Equation 9-5 (instead of Equation 9-2 and Equation 9-3). This new relationship reduces the number of variables from 5 to 4 as following:

$$P_p = \left(\frac{(1-\emptyset)C_p\sigma_{eff}}{(1-\emptyset)C_p-\emptyset C_p}\right)^{\gamma'} \qquad \text{Equation 9-23}$$

Azadpour et al. (2015) successfully tested this method in an offshore carbonate gas reservoir in the Persian Gulf. C_p is repeated in the both numerator and denominator, and thus can be cancelled. Consequently, the above mentioned equation is simplified to an equation with only three variables:

$$P_p = \left(\frac{(1-\emptyset)\sigma_{eff}}{1-2\emptyset}\right)^{\gamma'}$$ Equation 9-24

In fact, this equation shows an exclusive correlation with porosity and seems to be a simplified approximation of Equation 9-11. In this approach, porosity is obtained from well logs. Total porosity was considered as the main variable in this process. Effective stress, which is the difference between total stress (overburden load) and pore pressure was obtained from Terzaghi (1925). σ_v is calculated by integrating the density of overlain formations according to the method presented in Chapter 6. Hydrostatic pore pressure is calculated using an average hydrostatic pressure gradient of 10.5 MPa/km. Given the porosity and effective stress values, pore pressure would be calculated from Equation 9-24, using am empirical exponent γ'. This pore pressure prediction method is a new method that uses well log data to provide a reliable approximation of pore pressure in a compacting porous rock under a load.

This new method of pore pressure prediction, using porosity and pore volume compressibility correlations, is tested in the Fahliyan Formation of the Abadan Plain Basin herein. Pore pressure has been predicted in eight wells using Equation 9-11 and Equation 9-24 with empirical exponents of 0.845 and 0.96 respectively. Figure 9-4 presents the predicted pore pressure as well as the mud weight, RFTs, hydrostatic pressure and lithostatic pressure in 8 wells. Two wells did not have well logs in the Fahliyan Formation and these are not shown in Figure 9-4. However, log measurements were available from the shallower Sarvak Formation, and these results are presented separately (Figure 9-5). The γ exponent of 0.845 in Equation 9-11 is the same as used by Morales Salazar (2014) in a study of the Gulf of Mexico. Alternatively, Azadpour et al. (2015) considered the γ exponent of Equation 9-23 to be 0.983 in a gas field in the Persian Gulf. However, these exponents overestimate pore pressure in the Abadan Plain Basin, and the best fitting value of 0.96 is used herein (using Equation 9-24).

Buoyancy forces, resulting from different densities of water and hydrocarbon, impose additional pressure on the top of the formation. As noted before, the Fahliyan Formation is not a hydrocarbon reservoir in all of the studied fields of the Abadan Plain Basin. Hence, the buoyancy force has been evaluated and additionally added to predicted pore pressure in wells containing a hydrocarbon column.

9.3.3. Results and Discussion of Pore Pressure Prediction using Porosity and Compressibility Correlations

Pore pressure predictions using porosity and pore volume compressibility correlations were conducted, and provided reasonably accurate estimates in most wells in the Abadan Plain Basin (Figure 9-4). However, there are a few cases of mismatch between predicted pore pressure and direct pressure measurements. For example, Predicted pore pressures are slightly higher than RFT measurements throughout the entire examined depth range in wells D-14 and D-15. The method used here estimates pore pressure as a result of porous rock compaction. Due to fluid withdrawal from the porous media, there would be a drop in pressure since early production started at the field. Chronologically, well D-14 was completed after D-15, and both were completed three years after well D-4. Equation 9-24 calculated the pore pressure as a result of compaction in which the influence of pressure disturbance on the reservoir may not have been seen. Hence, it is considered likely that the pore pressure in wells D-14 and D-15 are slightly overestimated by the prediction method because this method does not account for possible production-related depletion. Formation pressure is lower in wells D-14 and D-15 than the other wells of the field D (Figure 9-4). Furthermore, pore pressure is underestimated in well D-4 when the compressibility PP prediction method is used. As discussed earlier in Chapter 6, the density log in well D-4 provided a vertical stress that was lower in value than the rest of the wells in this basin, even the same field. The average vertical stress in well D-4 was 21.5 MPa/km while the other wells exhibited an average vertical stress of 24 MPa/km. Using the average regional overburden stress value, instead of the well's individual (and suspected to be spurious) overburden gradient, better predicts pore pressure in this well (dashed line in Figure 9-4).

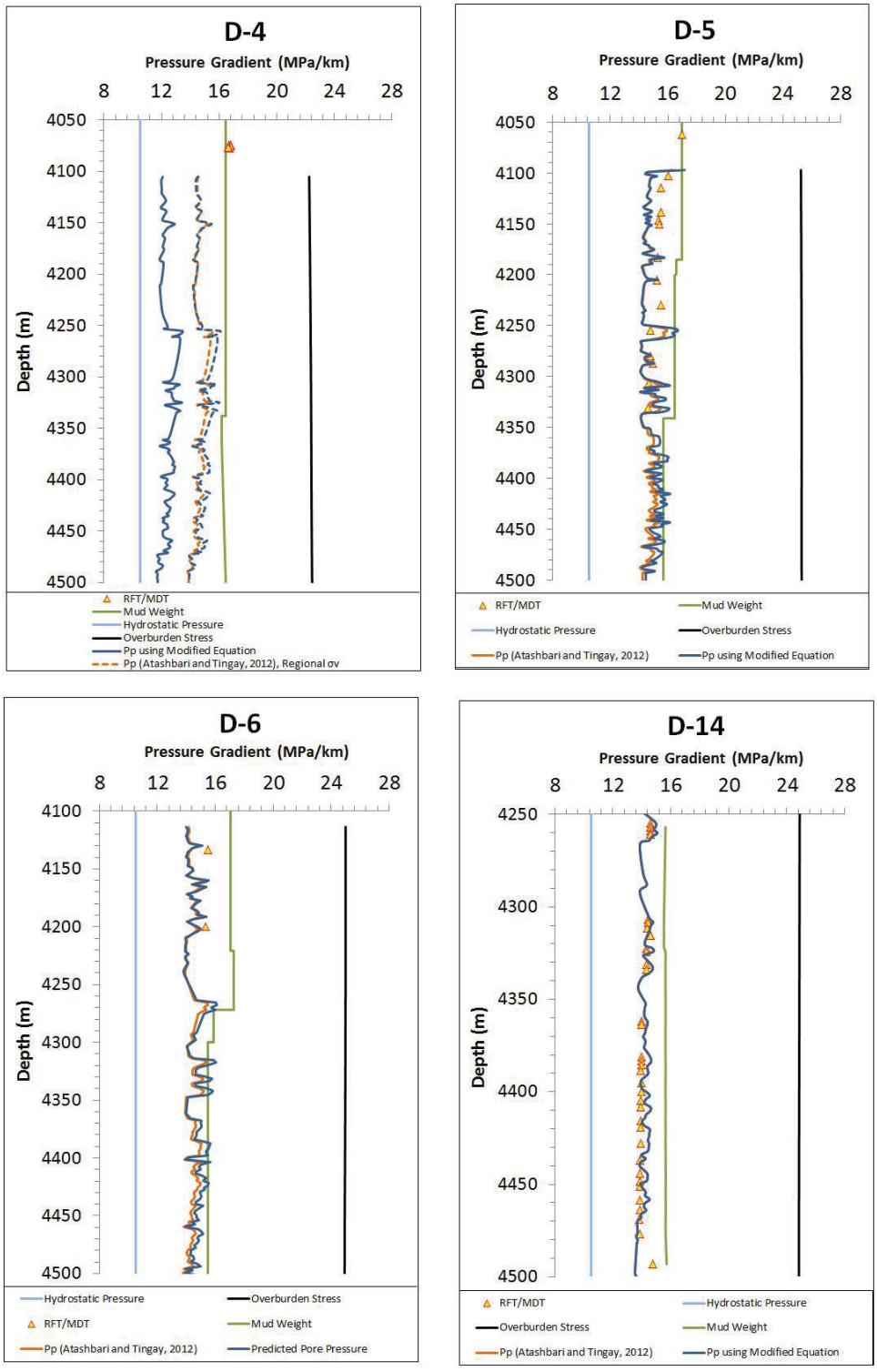

Figure 9-4 Pore pressure prediction using porosity and compressibility correlations in the Fahliyan Formation of the Abadan Plain Basin. Empirical exponent γ is set to 0.845 for Equation 9-11 analysis and 0.96 for Equation 9-24. The figure of well D-4 shows pore pressure prediction using both estimated overburden and regional overburden stress.

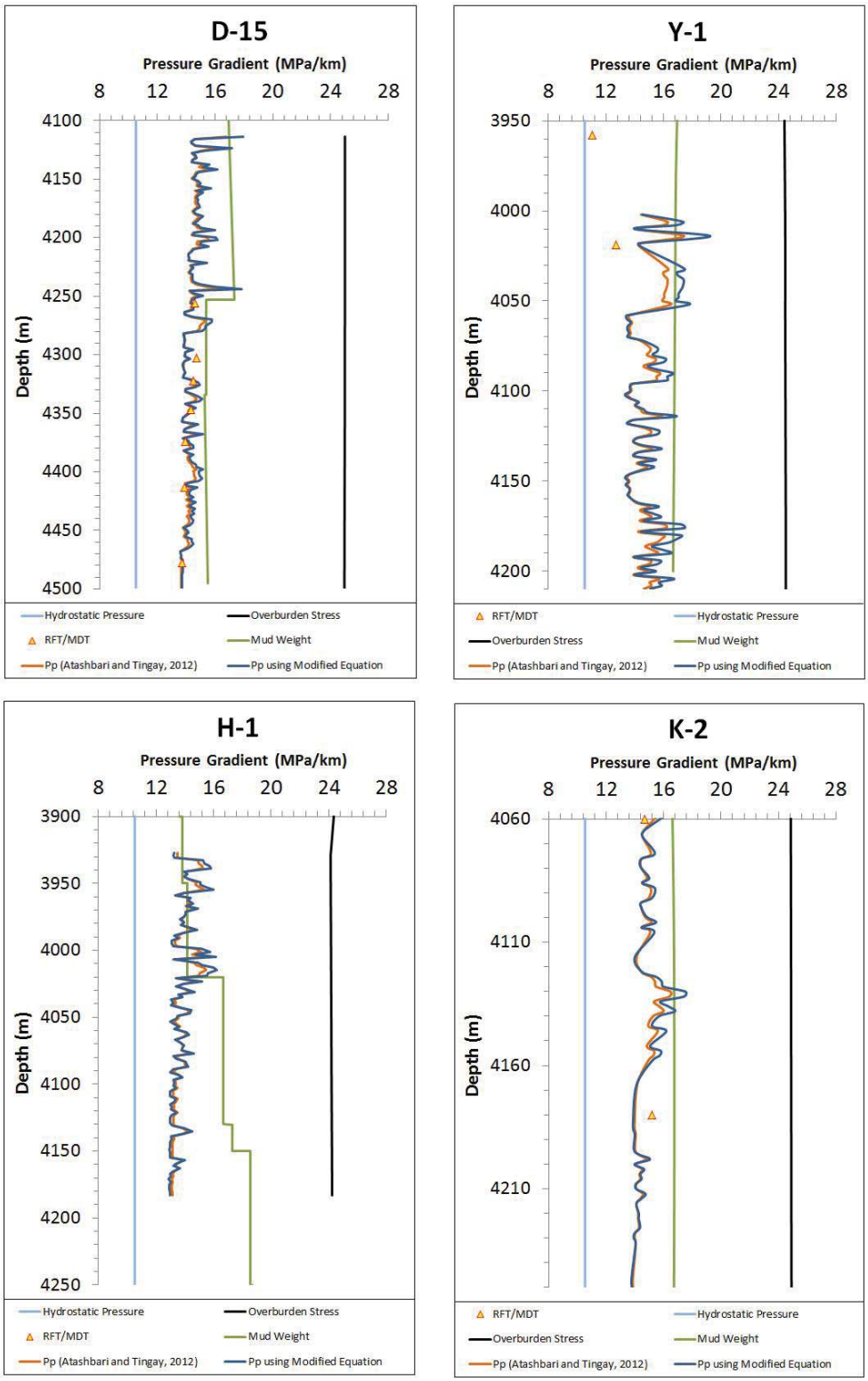

Figure 9-4 continued.

There are also some notable discrepancies between observed and predicted pore pressure in well Y-1, particularly where pore pressure is overestimated at 4019 m (Figure 9-4). However, this overestimate is largely due to a predicted sharp spike in PP, and is likely due to a lithology or porosity fluctuation, and not truly indicative of pore pressure (realistic pore pressure prediction for well planning would likely filter out this spike). Furthermore, it is hard to say whether, and by what degree, the predicted pressure is overestimated in this well, as there is an absence of deeper RFT/MDT data. In general, the predicted pressure in well Y-1 is reasonably consistent with mud weight. Pore pressure is also accurately predicted near the top of the Fahliyan Formation (at 4064 m) in well K-2 (Figure 9-4). However, there is a 1.3 MPa/km difference between the prediction and directly measured pore pressure at 4189 m.

Aside from the above discussed cases, the pore pressure predictions using this new method provide an overall satisfactory match with the field data. However, this method is limited to portions of the well with sufficient log information, which means that calibration is required for each formation separately. Pore pressure was properly predicted in the Fahliyan Formation using a γ of 0.96. Testing the method in the overpressured Gachsaran formation was not possible due to a lack of core sample and pressure measurements. This method was also applied to the normally pressured Sarvak Formation in wells A-6 and J-4 and, while it predicted pore pressure with close proximity in these wells (Figure 9-5).

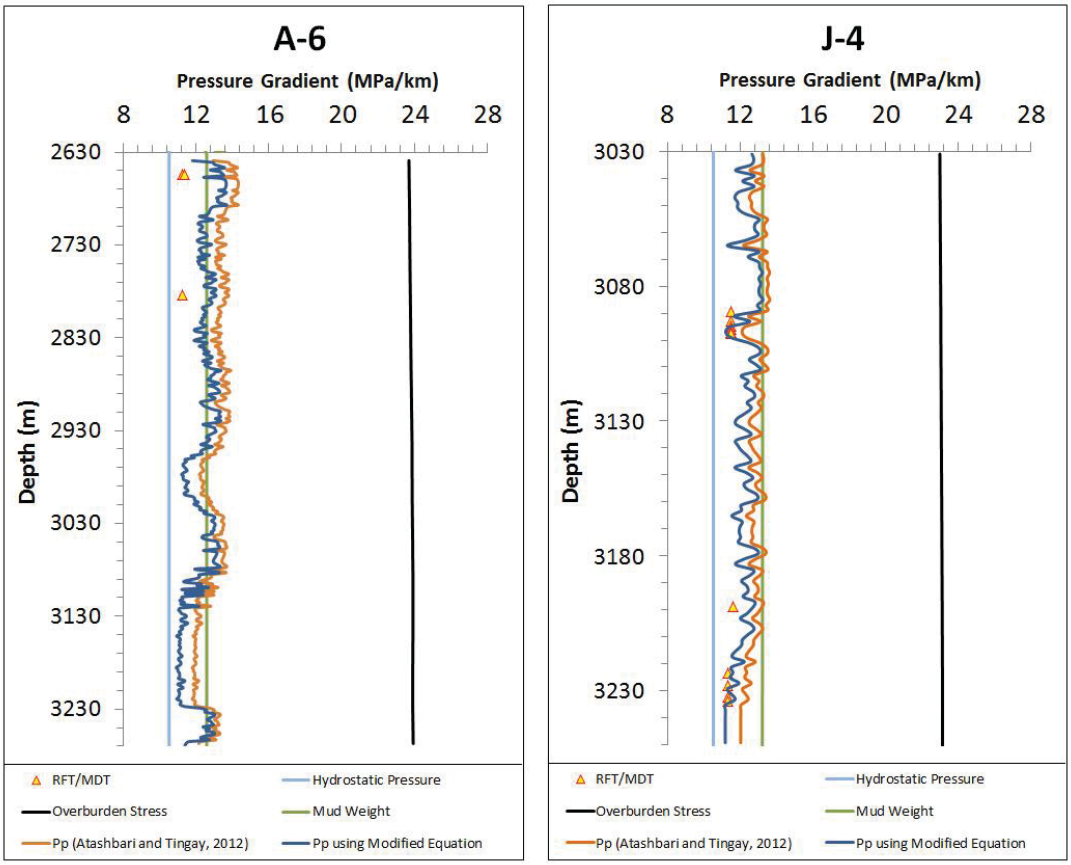

Figure 9-5 - Pore pressure prediction using porosity and compressibility correlations in the Sarvak Formation of wells A-6 and J-4. Empirical exponent γ is set to 0.845 for Equation 9-11 and 0.96 for Equation 9-24.

The log and core porosity correlation in well A-6 was performed using 186 data points, while well J-4 had no core analysis data (Figure 9-6). Although this correlation is not perfect ($R^2 = 0.05$), the pore pressure was calculated with acceptable range of approximation in wells A-6 and J-6. In the calculations of the pore compressibility of the Sarvak Formation, the porosity-pore volume compressibility correlation by Akhoundzadeh et al. (2011) has been employed and accurate predictions were obtained. This method slightly overestimates the pore pressure in well A-6 (1.2-1.8 MPa/km overestimation) while the predictions in well J-4 perfectly match the RFT/MDT. Using the same exponent in all wells of a similar geological setting provides reasonable results, which validates the accuracy of this technique and its appropriateness to be considered in further pore pressure analyses. I can herein conclude that this method is capable of predicting pore pressure in both of normally and abnormally

pressured formations. As with all pore pressure prediction methods, parameters of this technique need to be chosen with care.

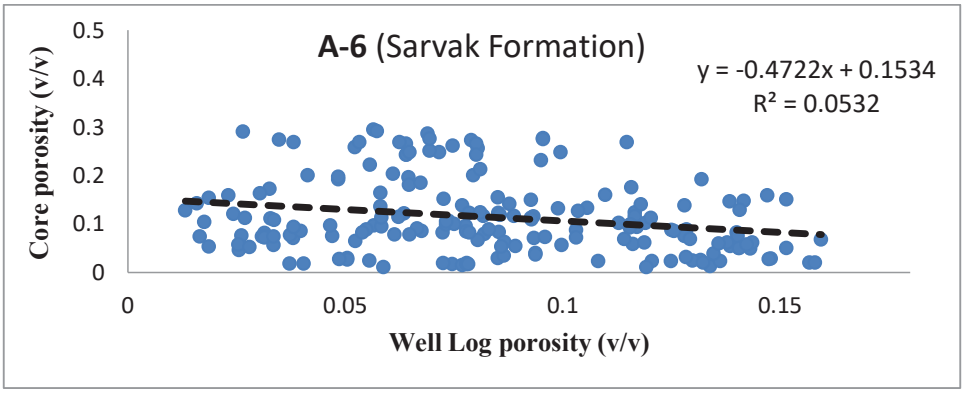

Figure 9-6 - Correlation between well log and laboratory porosity measurements in the Sarvak Formation of well A-6. This correlation is not perfect (R^2=0.05) and can result in false calculations. However, the pore pressure has been calculated using this correlation in the Sarvak Formation of wells A-6 and J-4. Slight overestimation in well A-6 can then be attributed to this poor correlation.

9.4. Pore Pressure Prediction Using Compaction Modelling

The regional and well-scale petrophysical analysis in Chapters 5 and 8 indicate that disequilibrium compaction is the dominant cause of overpressure in the Abadan Plain Basin. Overpressures generated by disequilibrium compaction can be mathematically modelled if the geological setting of the sediments is known. In this section, a generalised model of compaction is introduced to explain the hydrostratigraphic characteristics of the reservoir rock. The basic parameters that provide the geological conditions for overpressure from disequilibrium compaction are the compaction coefficient, sediment burial rate, geothermal gradient, and sealing conditions (Luo and Vasseur, 1992). Sealing conditions depend on permeability of both of the cap rock and reservoir if the reservoir formation is relatively thick, i.e. several hundreds of metres. According to Darcy's (1856) law, flow rate decreases with increasing thickness of the porous rock (length of the flow path); the thicker the formation, the lower the fluid can escape which results in greater overpressure. In shallow unconsolidated deposits, pore pressure normally stays in hydrostatic connection with the surface until the sediments reach a depth at which the seal starts to form. From this point, which is known as the fluid retention depth (FRD), the balance between pore fluid pressure and free surface water becomes lost. Swarbrick et al. (2002) provided a basis for estimating FRD during their study over several overpressures

in the Gulf of Mexico as well as North Africa, south-east Asia and the North Sea (Figure 9-7). Swarbrick (2012) projected pore pressure trends versus depth to the intersection with the hydrostatic pressure curve. That point has been defined as FRD.

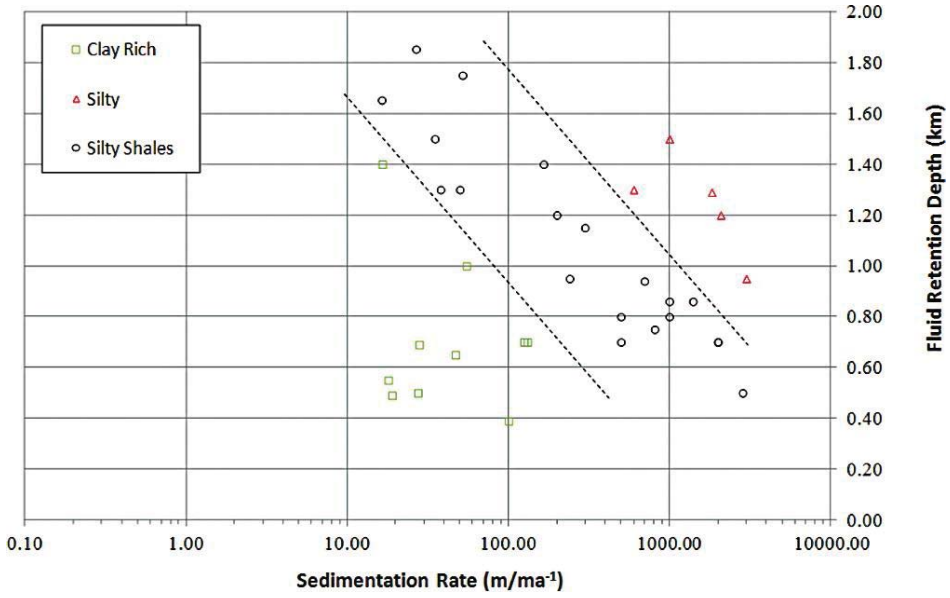

Figure 9-7 – The relationship between sedimentation rate and fluid retention (Swarbrick, 2012 updated from Swarbrick et al., 2002).The FRD is estimated from pore pressure trends, projected to the intersection with the hydrostatic pressure curve, and measured from the seabed. Others include North Africa, south-east Asia and the North Sea

Carbonate deposits of the Abadan Plain Basin exhibit some similarities with silty and silty shales in Figure 9-7 (discussed in Chapters 2 and 5) which gives FRD as a range, instead of a single depth. As discussed in Chapter 5, there has been a rapid sedimentation of 910-1366 m of the Aghajari Formation in 11 million years. The FRD of the southern fields, with an average 953 m thickness of the Aghajari Formation (a deposition rate of 86.6 m/Ma), is 1400-2200 m, while the FRD of the central and southern fields (a deposition rate of 114 m/Ma) becomes 1200-1800 m. It is believed that this rapid deposition is the primary origin of the disequilibrium compaction overpressure in the Gadvan and Fahliyan formations of the Abadan Plain Basin.

Given the FRD and rock and fluid properties, it is possible to estimate the maximum pore pressure resulted from undrained compaction of the Fahliyan Formation. According to

Terzaghi (1925), the grain configuration in a rock body is determined by the minimum potential energy. That means that in a porous elastic material, stresses are carried partly by pore fluid and partly by the rock frame and therefore, the stresses imposed on grains are at lowest. Compaction in such rocks is first applied to the pore space, which is far more compactible than matrix or grains. This is similar to the consolidation of soil or unconsolidated rocks. Biot (1941) provided a theoretical basis for three-dimensional consolidation for a soil sample under an unconfined load in the form of the heat conduction equation:

$$\frac{\partial^2 \sigma}{\partial_z{}^2} = \frac{1}{c}\frac{\partial \sigma}{\partial t} \qquad \text{Equation 9-25}$$

Where σ is the load on the sample, z is the sample thickness, c is a constant called the consolidation constant, and t is time. The consolidation constant noted above is defined as:

$$\frac{1}{c} = \alpha'^2 \frac{a}{k} + \frac{1}{Qk} \qquad \text{Equation 9-26}$$

Where k is the permeability; a is a coefficient called final compressibility; α' is a coefficient that measures the ratio of the liquid volume squeezed out to the volume change of the soil in an unconfined loading, and Q is a coefficient that measures the amount of liquid that can be forced into the sample under pressure while the volume of the sample is kept constant. Numerical definitions of the aforementioned constants are as follows:

$$\alpha' = \frac{2(1+\nu)}{3(1-2\nu)}\frac{G}{H} \qquad \text{Equation 9-27}$$

$$\frac{1}{Q} = \frac{1}{R} - \frac{\alpha'}{H} \qquad \text{Equation 9-28}$$

$$a = \frac{1-2\nu}{2G(1-\nu)} \qquad \text{Equation 9-29}$$

Where G is shear modulus, ν is Poisson's ratio, 1/H is a measure of the sample compressibility for a change in fluid pressure, and 1/R measures the change in liquid phase content for a given change in fluid pressure. The two elastic constants G and ν and the constant H and R are the four distinct constants which under the general assumptions of Biot (1941) define the physical proportions of an isotropic sample in equilibrium conditions. The remaining constants were

derived from these four constants. Since the hypothesis of soil consolidation is considered here, constants R and H are defined as the elastic properties of a sample of soil enclosed in a thin rubber bag (no stress applied to the soil). The amount of pore fluid drainage due to a negative pressure (-σ), through a thin tube passing through the walls of the bag is given by:

$$\boldsymbol{\theta = -\frac{\sigma}{R}} \qquad \textbf{Equation 9-30}$$

Where θ is the increment of liquid phase volume per unit volume of soil. The corresponding volume change (ε) of the soil is obtained from:

$$\boldsymbol{\epsilon = -\frac{\sigma}{H}} \qquad \textbf{Equation 9-31}$$

The basic assumptions of this model are:

- isotropy of the material;
- reversibility of stress-strain relations under final equilibrium conditions;
- linearity of stress-strain relations;
- small strains;
- existing air bubbles in the fluid (this assumption has been ignored in this study);
- incompressible pore fluid, and;
- fluid flows in the porous formation and the seal according to Darcy's (1856) law as follows,

$$\boldsymbol{\Delta P = \frac{qL\mu}{kA}} \qquad \textbf{Equation 9-32}$$

Where q is the rate of fluid flow, L is the length over which the pressure drop is taking place, μ is the fluid viscosity, k is the formation permeability and A is the cross sectional area to flow. Reversibility and linearity of stress-strain relations might be subject to criticism. However, it is noted that they constitute the basis of Terzaghi's (1925) theory (Biot, 1941). An analytical solution for Equation 9-25 with the following boundary conditions was provided by Biot (1941):

$\sigma=0$ for z=0 Equation 9-33

$\frac{\partial \sigma}{\partial z} = 0$ for z=h Equation 9-34

The first boundary condition expresses that the pressure of the liquid saturating the pores is zero because the permeability of the slab through which the load is applied is assumed to be large with respect to the soil. The second condition expresses that there is no fluid escape through the bottom of the sample container. Since disequilibrium compaction is a confined loading process, the first boundary condition isn't applicable and, therefore, an analytical solution doesn't seem attainable here. A new set of boundary conditions is required to be defined:

$\sigma= f(t,\rho)$ for z=0 Equation 9-35

$\frac{\partial \sigma}{\partial z} = 0$ for z=h Equation 9-36

The second condition is the same as Biot's (1941), while the first one accounts for a low permeability seal that allows fluid intrusion over the time (a function of time and density). Depth to the top of the cap rock and the reservoir formation are functions of time according to burial history. The overburden stress and rock properties such as reservoir compressibility and cap rock permeability are considered constant over time. Fluid flow in the permeable cap rock is also defined according to Darcy's (1856) law.

Equation 9-25, with new boundary conditions, is not analytically solvable. Instead, a partial differential equation (PDE) was used to find a numerical solution. PDEs are a set of equations that involve unknown functions and are defined in terms of independent variables and their partial derivatives (known as continuous variables). A computer program on the Matlab compiling platform has been generated that numerically solves Equation 9-25 for a given depth considering the burial and mechanical properties of the rock and the pore-filling fluid. The computer program used to solve Equation 9-25, provided in Appendix B., has been created using partial differential equations and a set of input parameters. The input parameters are the mechanical properties of reservoir rock, cap rock and pore fluid given in Table 9-1.

Table 9-1 – Input parameters in the Biot (1941) Consolidation model.

Reservoir Formation	Cap Rock	Pore Fluid
Poisson's ratio (ν)	Permeability (k_{cr})	Fluid viscosity (μ)
Young's modulus (E)	Thickness (h_{cr})	Fluid bulk modulus (K_f)
Bulk modulus (K)		Pore fluid gradient (psi/ft)
porosity (Φ)		
Area		
Compressibility (C)		
Permeability (k)		
Thickness (h)		
Depth to top of formation		
Fluid retention depth		

The computer program accepts the inputs in the following form (Figure 9-8) and compiles the data to give an estimated pore pressure as a result of sediment disequilibrium compaction. Some parameters are in imperial units, which are common in the oil and gas industry and have been used herein to make the method more user-friendly.

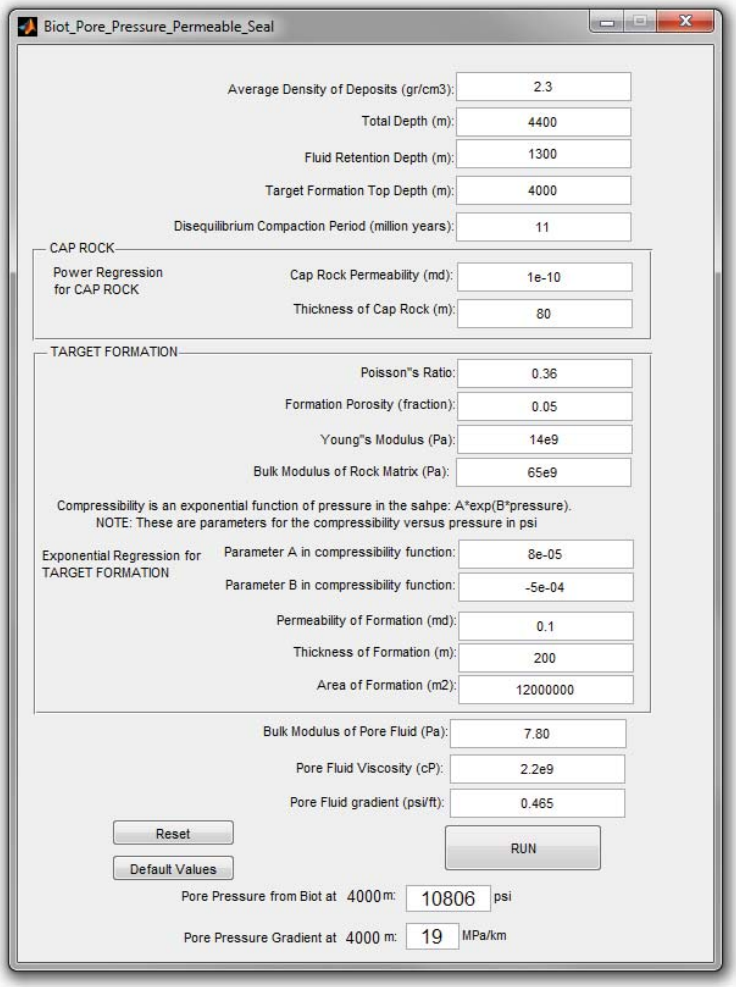

Figure 9-8 – computer program input layout for the Biot (1941) consolidation model. Estimated pore pressure of the Fahliyan Formation at 4000 m depth with a 160 m thick cap rock is 62 MPa (15.5 MPa/km).

The input dialog window also displays the calculated pore pressure and pressure gradient in psi/ft, which is then plotted as a depth-pressure cross plot in MPa/km (Figure 9-9). Typical data is used for field D to calculate pore pressure at the top of the Fahliyan Formation.

9.5. Results and Discussion of Pore Pressure Prediction Using Compaction Modelling

Pore pressure was predicted using the input values provided in Table 9-2. The Fahliyan Formation's values are those measured in laboratory or in-situ. The values of the Gadvan Formation are approximations from nearby fields. The results are also presented in Figure 9-9 as a time-dependant burial process. Predicted pore pressure has an approximately lithostatic-parallel gradient, which is a standard attribute of disequilibrium compaction overpressure resulting from purely vertical loading. Basically, a 400-metre deposit of the Fahliyan Formation capped by 80 metres of low permeability deposits of the Gadvan Formation over 11 Ma in a typical well is modelled as being expected to generate a pore pressure equal to 63-76 MPa for considering FRD at 2200 m and 1200 m respectively (Figure 9-9). These values indicate 21-34 MPa in excess of hydrostatic gradient.

Table 9-2 – Input values for the pore pressure calculation using Biot compaction model.

Parameter	Unit	Value
Average density of deposits from the surface to total depth	Gr/cm^3	2.3
Total depth	m	4400
Fluid retention depth	m	1255
FRD age	Ma	100
Parameters of Cap Rock		
Cap rock permeability	md	1.00E-10
Thickness of cap rock	m	80
Parameters of Target Formation		
Depth to top of target formation	m	4000
Bulk modulus	Pa	6.50E+10
Poisson's ratio	-	0.36
Young's modulus	Pa	1.40E+10
Coefficient A in rock compressibility	-	8.00E-05
Coefficient B in rock compressibility	-	-5.00E-04
Permeability	md	0.1
Thickness	m	400
Area of the formation	m^2	12000000
Parameters of Pore Fluid		
Bulk modulus	Pa	2.20E+09
Viscosity	cP	7.8
Pressure gradient	Psi/ft	0.465

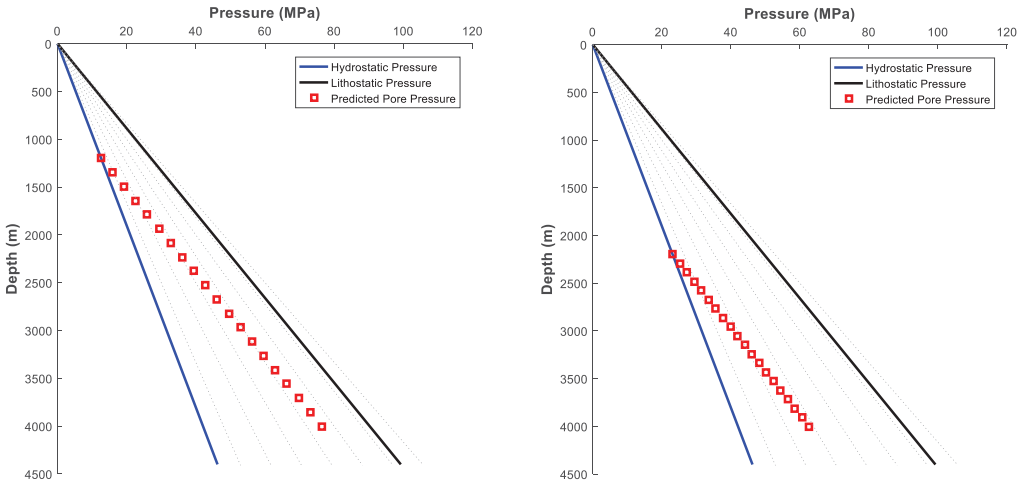

Figure 9-9 – Result of the Biot compaction model for the Fahliyan Formation considering permeable Gadvan shale as cap rock. The FRD is 1200 m in the right plot and 2200 m in the left one. Pore pressure has a lithostatic-parallel gradient from FRD to the top of the Fahliyan Formation.

The pore pressure trend is a sub-lithostatic pressure gradient, which is often observed where overpressure is generated by disequilibrium compaction (Darby and Funnell, 2001; Lee and Williams, 2000; Luo et al., 2003; Swarbrick et al., 2002). Since the compaction model is three-dimensional, mean stress instead of vertical stress can also be applied to predict pore pressure (Harrold et al., 1999). It must also be noted that lateral flow is not included in this model, but it is possible to consider lateral variations by performing a series of one dimensional simulations along a cross-section through the basin/field (Gordon and Flemings, 1998). This model, using typical data of the Fahliyan Formation and FRD at 2200 m, predicts a pore pressure as 16 MPa/km. Average pressure gradient within this formation is presented in Table 9-3, ranging between 12.7 and 15.4 MPa/km. Although the prediction can be more precise using more accurate inputs (which partly wasn't available to this research), there is a satisfactory agreement between the prediction and real pore pressure. This method is a more fundamental approach to pore pressure prediction, which requires precise input parameters. Normally, there is adequate information from a reservoir formation where core samples and pore fluid were tested in the laboratory. However, cap rocks (the Gadvan Formation in this in this study) are rarely considered for such studies and there is little data available. Thus, default parameters used in the calculations (as displayed as pre-defined values in the input dialog boxes) are rough estimates from nearby basins where the Gadvan Formation has been tested. Although the permeability of the cap rock is considered constant, there is a possibility to input

variable permeability (resulting from the compaction of the cap rock) into the model whenever such data is available. While this method was not completely tested on all wells (due to data unavailability), running this model on a typical overpressured well provided reasonable predictions. That has made this technique a reliable tool to verify the results of other methods under disequilibrium compaction process.

Table 9-3 – Average pore pressure measurements in the Fahliyan Formation

Well	Average measured pore pressure in the Fahliyan Formation (MPa/Km)
D-4	14.7
D-5	15.2
D-6	15.4
D-14	14.2
D-15	14.2
Y-1	12.7 (only one data point)
A-6	-
H-1	-
K-2	14.9
J-4	15.3

9.6. Conclusions

Although carbonate rocks are classified as non-stress sensitive, mechanical compaction could form the majority of the porosity loss in certain circumstances, such as deposition of the Fahliyan Formation capped by low permeability deposits of the Gadvan Formation. In such conditions, Pore pressure becomes sensitive to porosity variations. The porosity and pore volume compressibility correlations introduced in this chapter have provided reasonable results for pore pressure prediction. In the first method, pore volume compressibility was approximated from porosity log data, which was correlated with other well log data as well as laboratory core analysis. This compressibility data, along with porosity data, was then put into an equation derived herein to predict pore pressure via a new technique. Best matching empirical exponent γ seemed to be 0.845 using the Atashbari and Tingay (2012a) method and 0.96 for modified method (Equation 9-24) applied in the Fahliyan Formation in the Abadan Plain Basin. In the second method, a compaction model using Biot's (1941) theory of

consolidation was constructed in which a process of semi-confined compaction, starting from the fluid retention depth to the current depth of the reservoir formation, was modelled. The resultant modelled pore pressure follows a lithostatic-parallel gradient, which is as expected in disequilibrium compaction overpressure. The new methods proposed and tested in this chapter both aim to predict the approximate pore pressure due to the disequilibrium compaction in a formation of any lithology, and thus are not dependant only on use in shales. However, these methods need to be carefully calibrated with direct pressure measurements from offset wells for best results. Furthermore, their applicability for pore pressure prediction in overpressures generated by fluid expansion remains unconfirmed and thus, a good subject for further studies.

CHAPTER 10- Conclusions and Recommendation

This thesis was successful in achieving its stated aims of investigating the origin of overpressures throughout the Abadan Plain Basin and testing pore pressure prediction methods within the carbonate formations.

A dataset of well logs and drilling information from 10 wells in 6 fields of the Abadan Plain Basin was constructed and compiled in this research. This basin is prolific with hydrocarbon accumulations and, drilling and well completion operations are often at the risk of blowouts due to abnormally high pore pressures. This study provides a basin-wide pressure model to understand the pressure distribution regime and investigate its implications for well drilling and field developments. In the Abadan Plain Basin, overpressures can reach almost lithostatic magnitudes (22.0 MPa/km), and are occasionally occur in the Gachsaran Formation (mostly in the fields at the northern end of the basin) and entirely in the Gadvan and Fahliyan formations. A south-west to north-east oriented increase in formation burial depth of both the Gachsaran and Gadvan formations was observed, which is due to the post-collisional crust shortening and thickening and development of formations within a foreland setting. Both the formations get deeper towards the north-east of the basin towards the Zagros fold belt. The Gachsaran Formation becomes thicker and overpressured along this direction while it is normally pressured in the southern fields. However, despite having a similar burial depth trend with the Gachsaran Formation, thickness of the Gadvan Shale as a sealing layer has a different trend and seems inconsecutive to the Zagros folding. Pore pressure doesn't vary significantly across the Gadvan and Fahliyan formations and both of them are entirely overpressured in this basin.

Several mechanisms are capable of generating overpressures in carbonates, whereas only disequilibrium compaction (DC) has been identified as the primary origin of overpressure. Moderate to high overpressures in the Gachsaran Formation are mainly a result of undrained loading which pressurized the entrapped pore fluid in the isolated pore space, as well as partly gypsum to Anhydrite transformation. Whilst there is a high contingency of kerogen maturation,

and clay diagenesis in the Gadvan Formation, the magnitudes of these mechanisms aren't comparable to DC, which is a result of undrained compaction of very low permeable deposits. Examination of the sealing potential of the upper Gachsaran Formation and lower Gadvan formation indicates that these units represent good top seals that are able to maintain and seal overpressure, and thus supports the evidence of these sections being pore pressure transition zones. Analysis of sonic velocity-VES plots (Bowers type plots) was used to first characterise the range of normally pressured 'loading curve' properties, and was then compared with the properties of overpressured sequences. Overpressured sequences plot predominately within the loading curve zone, suggesting disequilibrium compaction as the likely primary cause of overpressure in the region. Analysis of sonic-density and resistivity-density cross plots yielded further support for disequilibrium compaction as being the dominant overpressure generation mechanisms in the basin, and provided no strong evidence for significant pressure transfer, and occasionally minor evidence to suggest the existence of fluid expansion overpressure generation mechanisms at the basin-scale. Northern fields in this basin are believed to be solely overpressured by DC, whilst southern fields are predominately overpressured by DC but may have a small contribution from fluid expansion, likely as a result of hydrocarbon-water buoyancy force.

Conventional pore pressure prediction methods can't give reliable estimations if used in carbonate sediments. It's because carbonate deposits of the Sarvak and Fahliyan formations of the Abadan Plain Basin are associated with extensive fracturing, which further creates brecciation patterns in the rocks. Pressure solution and stylolites filled with calcite and dolomite cements are also frequently evident in these formations. Although in-situ stresses significantly affect some of those processes, the overall porosity evolution isn't entirely controlled by stress. Therefore, porosity in this kind of deposits is 'stress-insensitive'. Instead of conventional pore pressure prediction methods, a new dataset, comprising of sonic, resistivity and density logs of carefully discriminated shale interbeds, which are assumed to be in hydrodynamic equilibrium with, and represent the surround formations, was incorporated with Eaton (1972) and Bowers (1995) methods to predict pore pressure in the Abadan Plain Basin. In General, Eaton's (1972) pore pressure predictions using sonic and density data provided the most reliable predictions, with density-based methods generally in better compliance with the measured pore pressure than sonic

velocity and resistivity data. These three set of logs provided most accurate predictions when utilised together.

Alternatively, the fact that overpressures are generated by disequilibrium compaction in this basin enabled successfully employing two new methods based on the compressibility attributes of carbonate rocks to predict pore pressure. In the first method, pore volume compressibility was approximated from porosity log data, which was correlated with other well log data as well as laboratory core analysis. This compressibility data, along with porosity data, was then put into an equation derived herein to predict pore pressure via a new technique. Best matching empirical exponent γ seemed to be 0.845 using the Atashbari and Tingay (2012a) method and 0.96 for modified method (Equation 9-24) applied in the Fahliyan Formation in the Abadan Plain Basin. In the second method, a compaction model using Biot's (1941) theory of consolidation was constructed in which a process of semi-confined compaction, starting from the fluid retention depth to the current depth of the reservoir formation, was modelled. These methods aim to predict the approximate pore pressure due to the disequilibrium compaction in a formation of any lithology, and thus are not dependant only on use in shales.

There are several areas related to the topic of this thesis that can be subject for further studies. First area is investigating the origin of overpressure in deeper formation of the Abadan Plain Basin. Typical fluid expansion type overpressuring mechanisms, such as kerogen-to-gas maturation or clay diagenesis (and associated mechanisms, such as load transfer) may potentially act at deeper, and yet unexplored, sections of this basin, which require extra analysis. Secondly, the shale-based pore pressure predictions suffer from a number of issues, such as being occasionally significantly inaccurate (which suggests unreliability, and thus a risk for drilling safely), as well as there being the issue of potentially large data gaps due to a lack of shales (in addition to the lithological variability of the shales themselves). Defining and performing appropriate shale discrimination is another are of interest for more research. Finally, the applicability of compressibility method for pore pressure prediction in overpressures generated by fluid expansion remains unconfirmed and thus, a good subject for further studies.

Appendix A-
Integrated Data of Studied Wells

This appendix contains formation tops, age and lithology, as well as GR, sonic, resistivity, and density logs of the studied wells. Pressure-depth plot is also included in the figures.

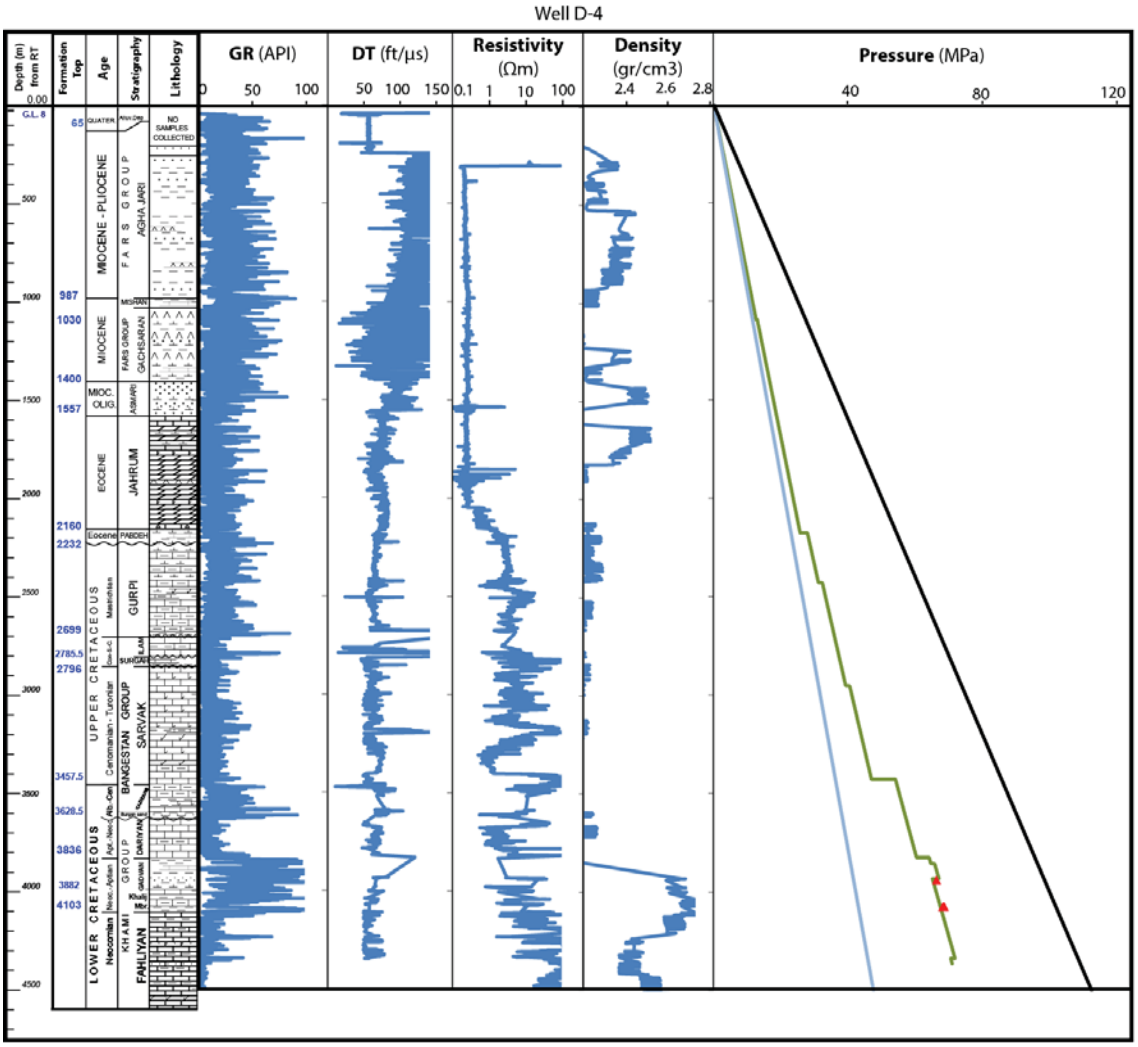

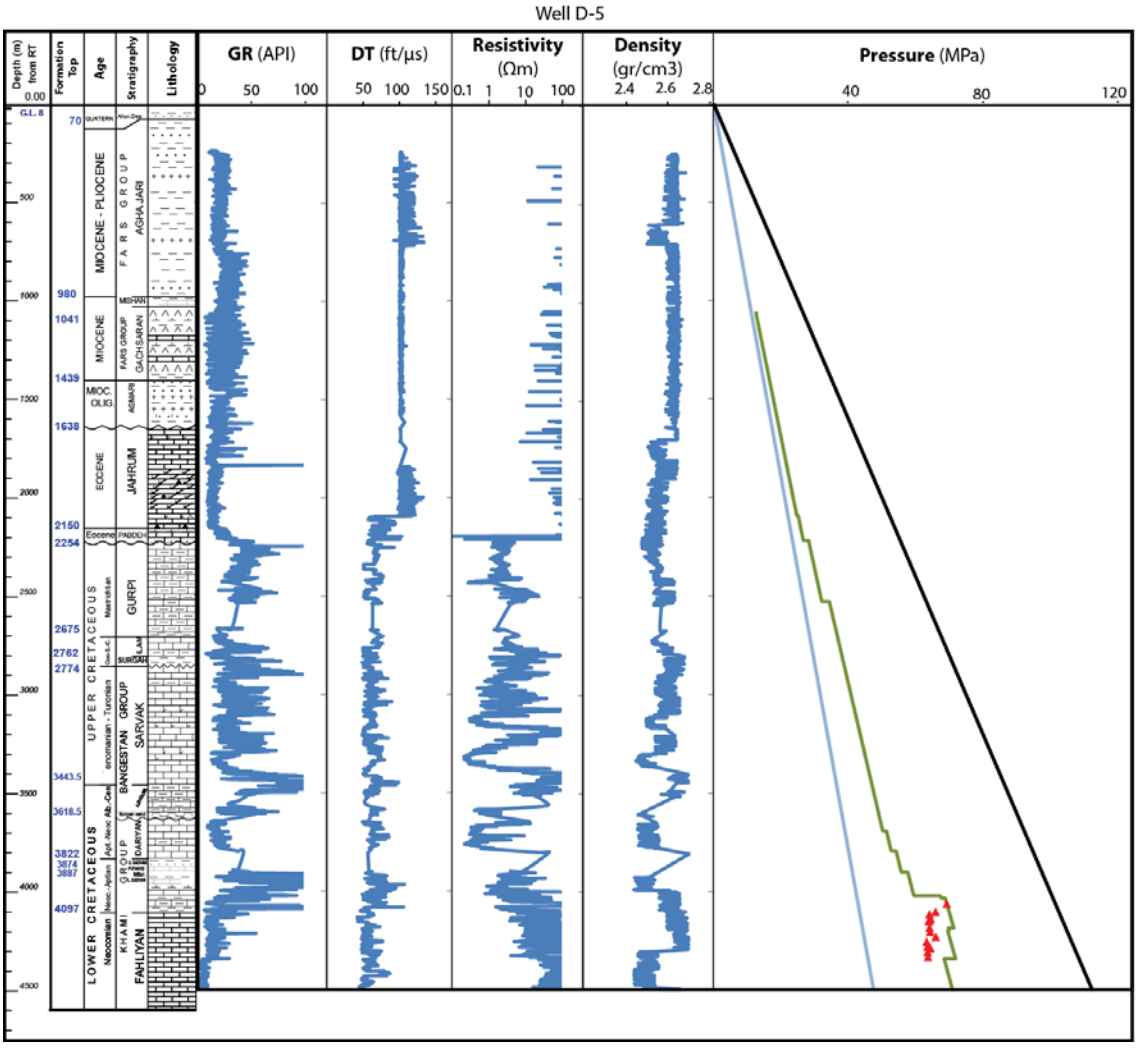
Well D-5
Depth (m) from RT
Formation Top
Age
Stratigraphy
Lithology
GR (API)
DT (ft/µs)
Resistivity (Ωm)
Density (gr/cm3)
Pressure (MPa)
G.L. 8
70
980
1041
1439
1638
2150
2254
2675
2762
2774
3443.5
3618.5
3822
3874
3887
4097
MIOCENE - PLIOCENE
MIOCENE
MIOC. OLIG.
ECCENE
Eocene
UPPER CRETACEOUS
LOWER CRETACEOUS
FARS GROUP
AGHAJARI
MISHAN
GACHSARAN
ASMARI
JAHRUM
PABDEH
GURPI
SURGAH
BANGESTAN GROUP
SARVAK
DARIYAN
KHAMI
FAHLIYAN

Well D-6

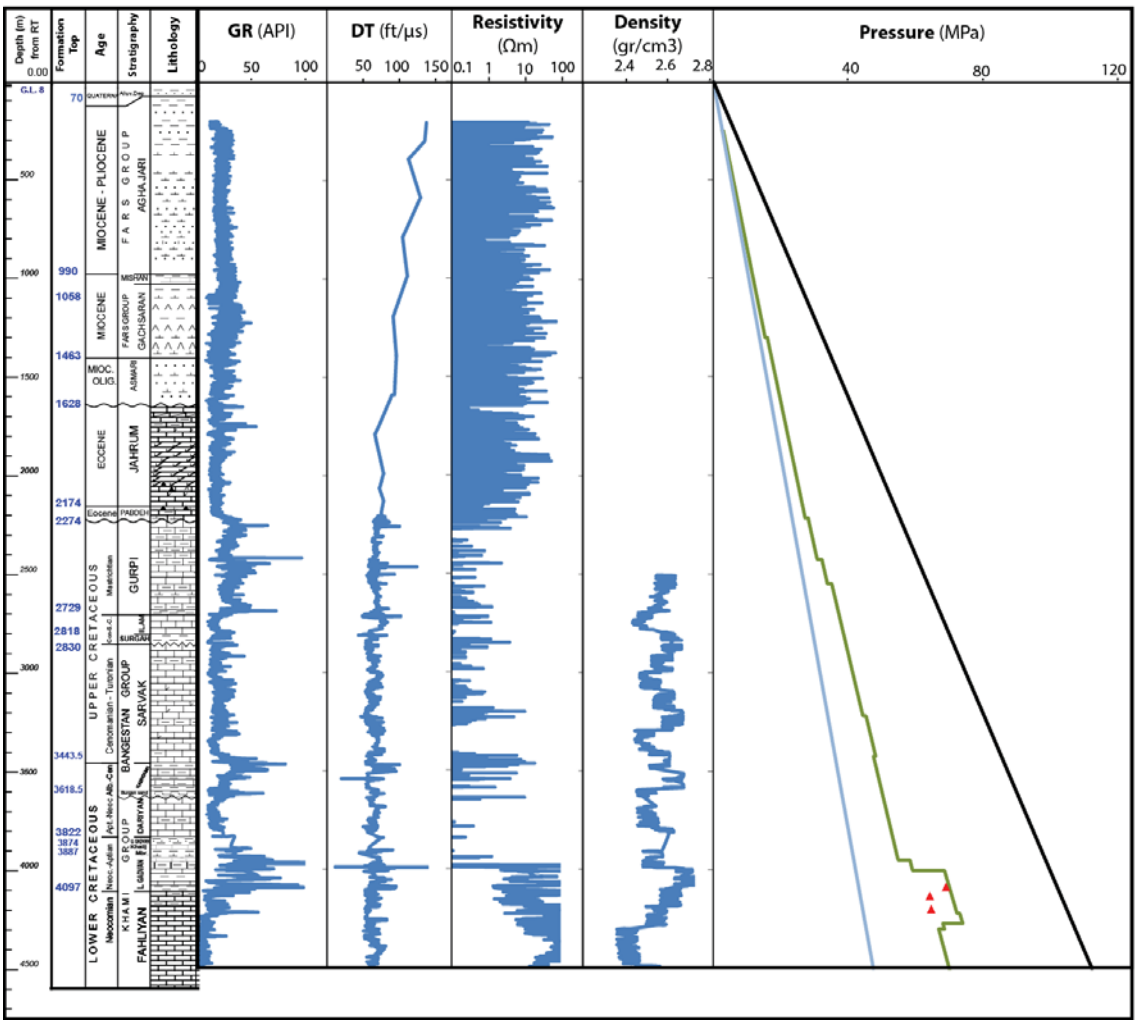
Depth (m) from RT
Formation Top
Age
Stratigraphy
Lithology
GR (API)
DT (ft/µs)
Resistivity (Ωm)
Density (gr/cm3)
Pressure (MPa)
G.L. 8
70
990
1058
1463
1628
2174
2274
2729
2818
2830
3443.5
3618.5
3822
3874
3887
4097
MIOCENE - PLIOCENE
MIOCENE
MIOC. OLIG.
ECENE
Eocene
Maastrichtian
Cenomanian - Turonian
Alb.-Cen.
Jurassic
Neocomian
FARS GROUP
AGHAJARI
MISHAN
GACHSARAN
ASMARI
JAHRUM
PABDEH
GURPI
SURMAH
BANGESTAN GROUP
SARVAK
KHAMI GROUP
GADVAN
FAHLIYAN

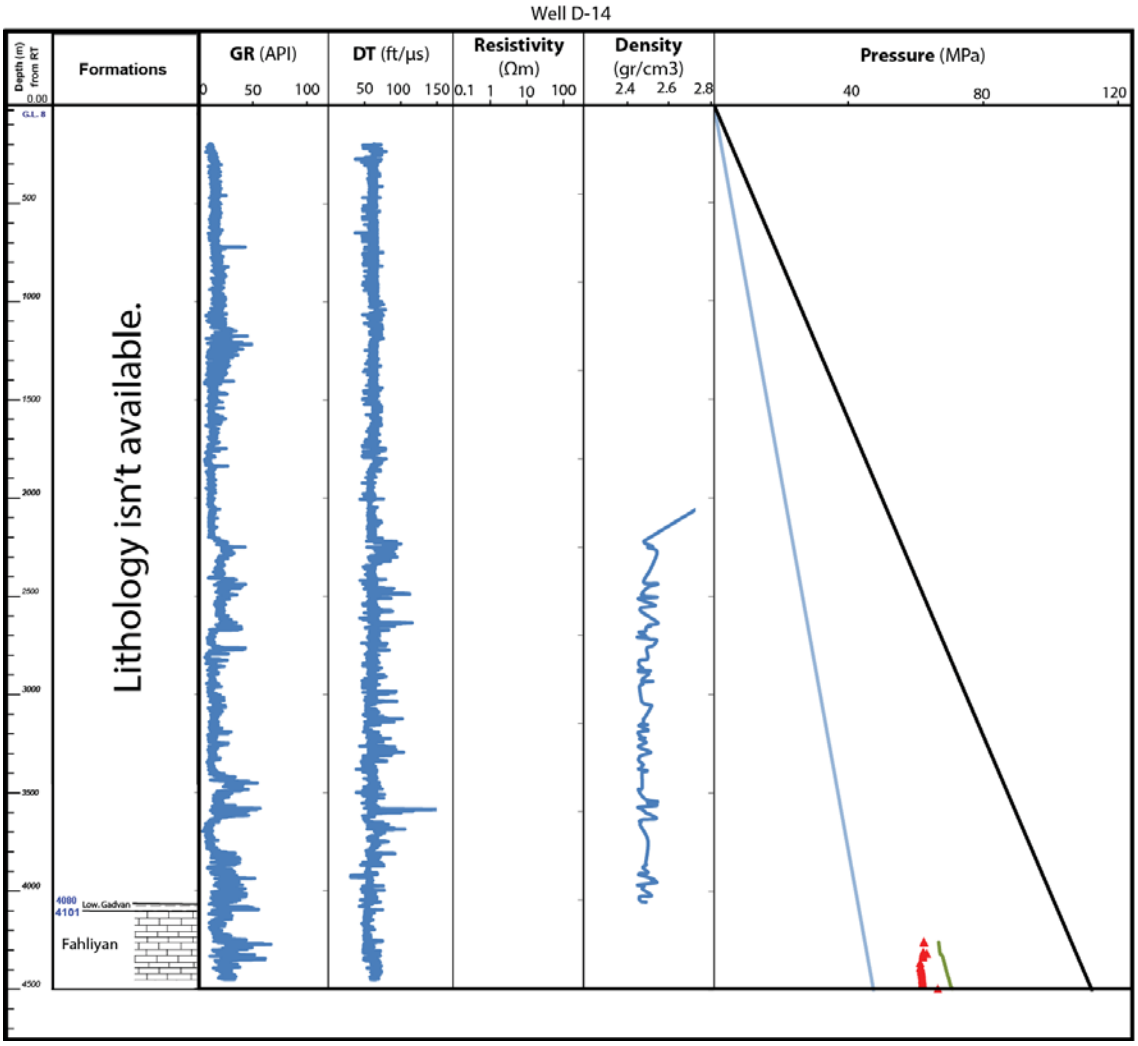
Well D-14
Depth (m) from RT
Formations
GR (API)
0 50 100
DT (ft/µs)
50 100 150
Resistivity (Ωm)
0.1 1 10 100
Density (gr/cm3)
2.4 2.6 2.8
Pressure (MPa)
40 80 120
0.00
G.L. 8
500
1000
1500
2000
2500
3000
3500
4000
4500
Lithology isn't available.
4080
4101
Low. Gadvan
Fahliyan

Well D-15

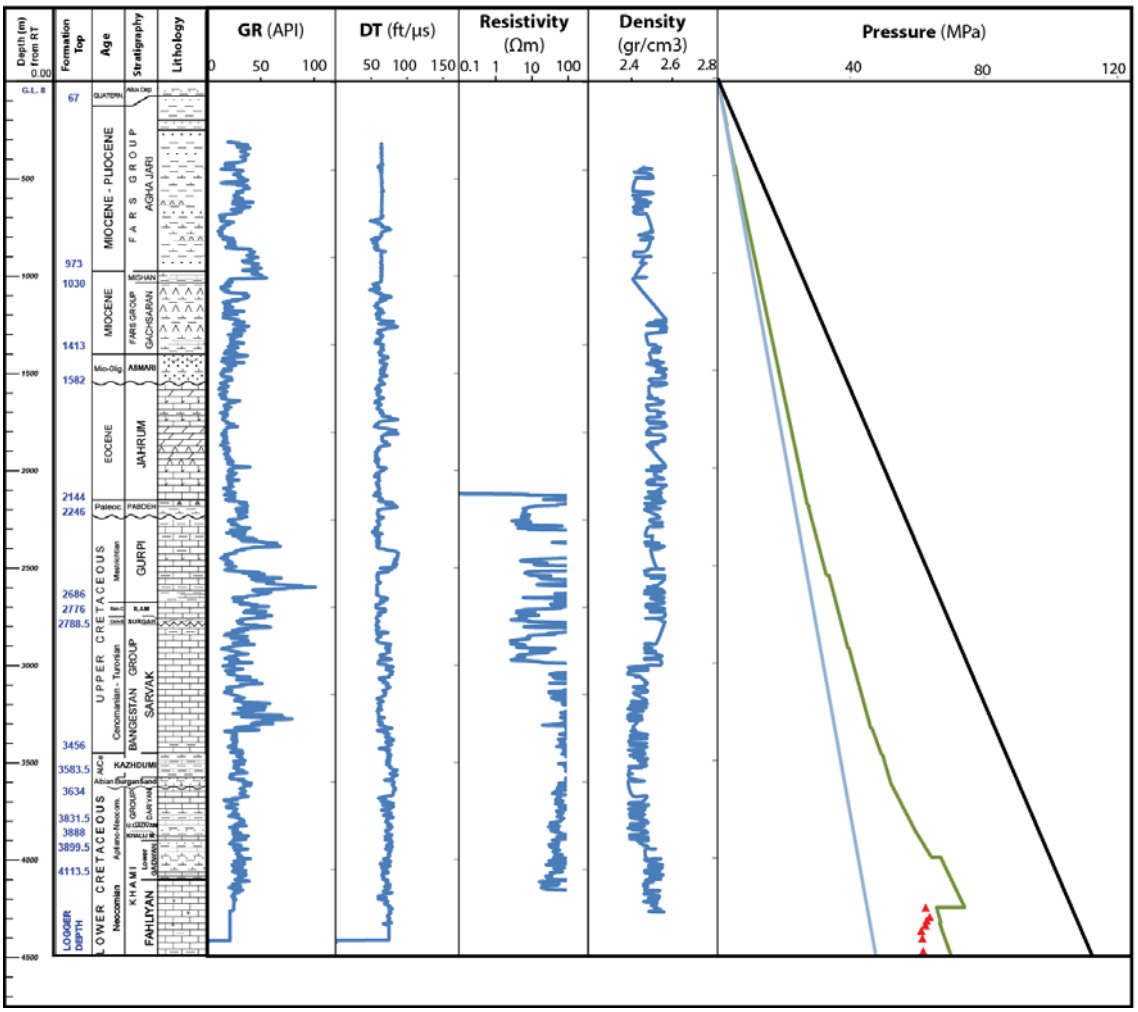
Depth (m) from RT
Formation Top
Age
Stratigraphy
Lithology
GR (API)
DT (ft/µs)
Resistivity (Ωm)
Density (gr/cm3)
Pressure (MPa)
MIOCENE - PLIOCENE
FARS GROUP
AGHA JARI
MIOCENE
MISHAN
GACHSARAN
ASMARI
EOCENE
JAHRUM
PABDEH
UPPER CRETACEOUS
GURPI
BANGESTAN GROUP
SARVAK
KAZHDUMI
LOWER CRETACEOUS
KHAMI
FAHLIYAN
LOGGER DEPTH

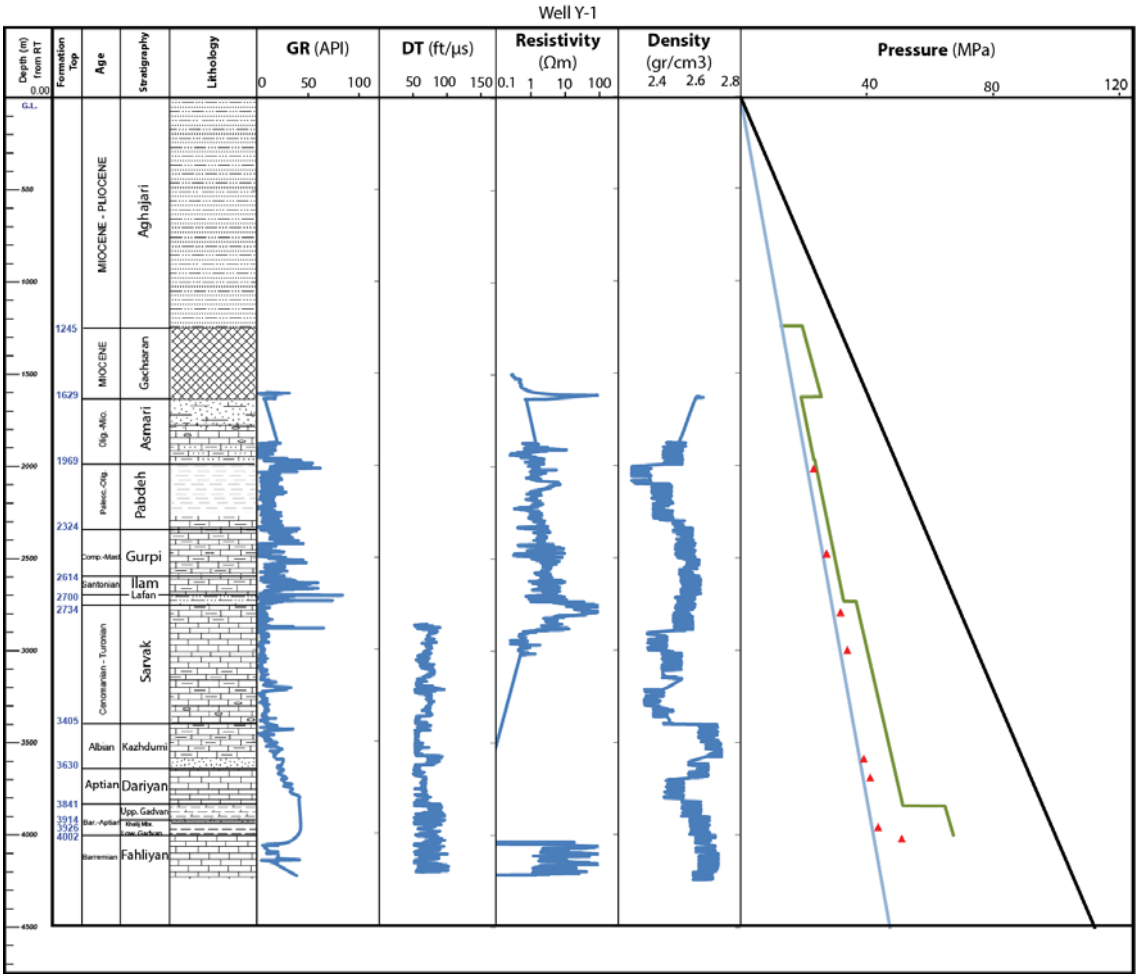
Well Y-1
Depth (m) from RT
Formation Top
Age
Stratigraphy
Lithology
GR (API)
0 50 100
DT (ft/µs)
50 100 150
Resistivity (Ωm)
0.1 1 10 100
Density (gr/cm3)
2.4 2.6 2.8
Pressure (MPa)
40 80 120
0.00
G.L.
1245
1629
1969
2324
2614
2700
2734
3405
3630
3841
3914
3925
4002
MIOCENE - PLIOCENE
MIOCENE
Olig.-Mio.
Paleoc.-Olig.
Comp.-Maas.
Santonian
Cenomanian - Turonian
Albian
Aptian
Barr.-Aptian
Barremian
Aghajari
Gachsaran
Asmari
Pabdeh
Gurpi
Ilam
Lafan
Sarvak
Kazhdumi
Dariyan
Upp. Gadvan
Khaij Mbr.
Low. Gadvan
Fahliyan
500
1000
1500
2000
2500
3000
3500
4000
4500

Well A-6

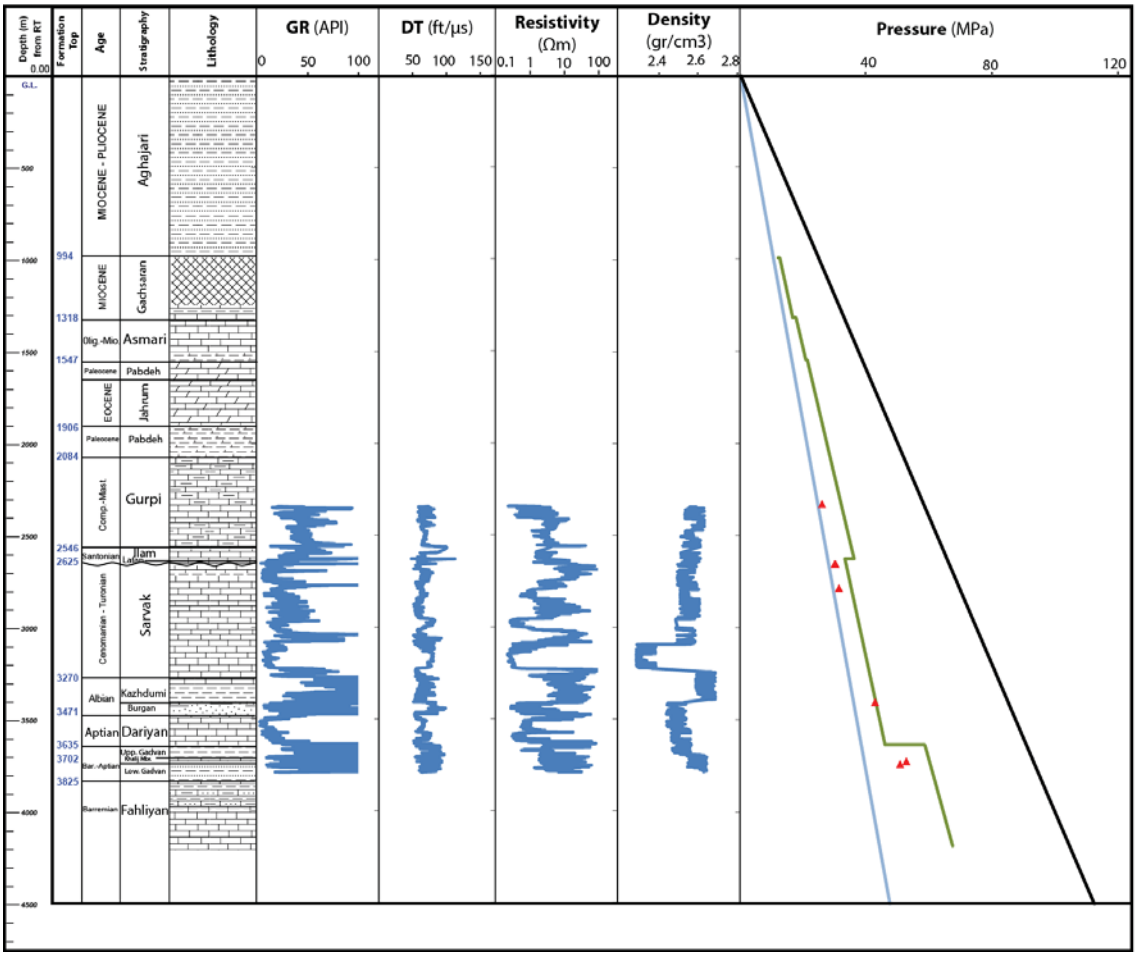
Depth (m) from RT
Formation Top
Age
Stratigraphy
Lithology
GR (API)
0 50 100
DT (ft/µs)
50 100 150
Resistivity (Ωm)
0.1 1 10 100
Density (gr/cm3)
2.4 2.6 2.8
Pressure (MPa)
40 80 120
G.L.
0.00
994
1318
1547
1906
2084
2546
2625
3270
3471
3635
3702
3825
MIOCENE - PLIOCENE
Aghajari
MIOCENE
Gachsaran
Olig.-Mio.
Asmari
Paleocene
Pabdeh
EOCENE
Jahrum
Paleocene
Pabdeh
Comp.-Maast.
Gurpi
Santonian
Ilam
Cenomanian - Turonian
Sarvak
Albian
Kazhdumi
Burgan
Aptian
Dariyan
Upp. Gadvan
Khaki Mbr.
Mar.-Aptian
Low. Gadvan
Barremian
Fahliyan

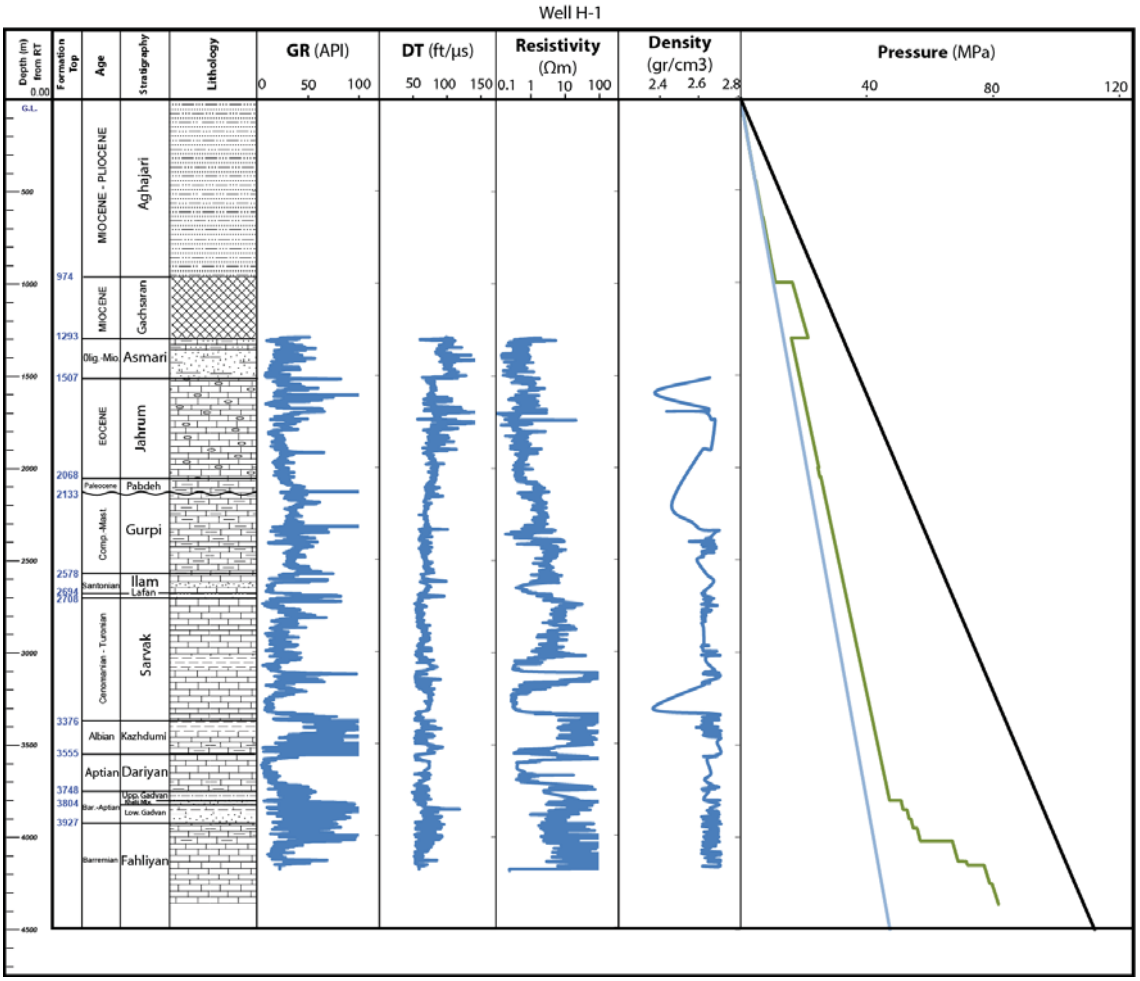
Well H-1
Depth (m) from RT
Formation Top
Age
Stratigraphy
Lithology
GR (API)
0 50 100
DT (ft/µs)
50 100 150
Resistivity (Ωm)
0.1 1 10 100
Density (gr/cm3)
2.4 2.6 2.8
Pressure (MPa)
40 80 120
G.L.
0.00
974
1293
1507
2068
2133
2578
2694
2708
3376
3555
3748
3804
3927
MIOCENE - PLIOCENE
Aghajari
MIOCENE
Gachsaran
Olig.-Mio.
Asmari
EOCENE
Jahrum
Paleocene
Pabdeh
Comp.-Mast.
Gurpi
Santonian
Ilam
Lafan
Cenomanian - Turonian
Sarvak
Albian
Kazhdumi
Aptian
Dariyan
Upp. Gadvan
Bar.-Aptian
Kbeli Mb.
Low. Gadvan
Barremian
Fahliyan

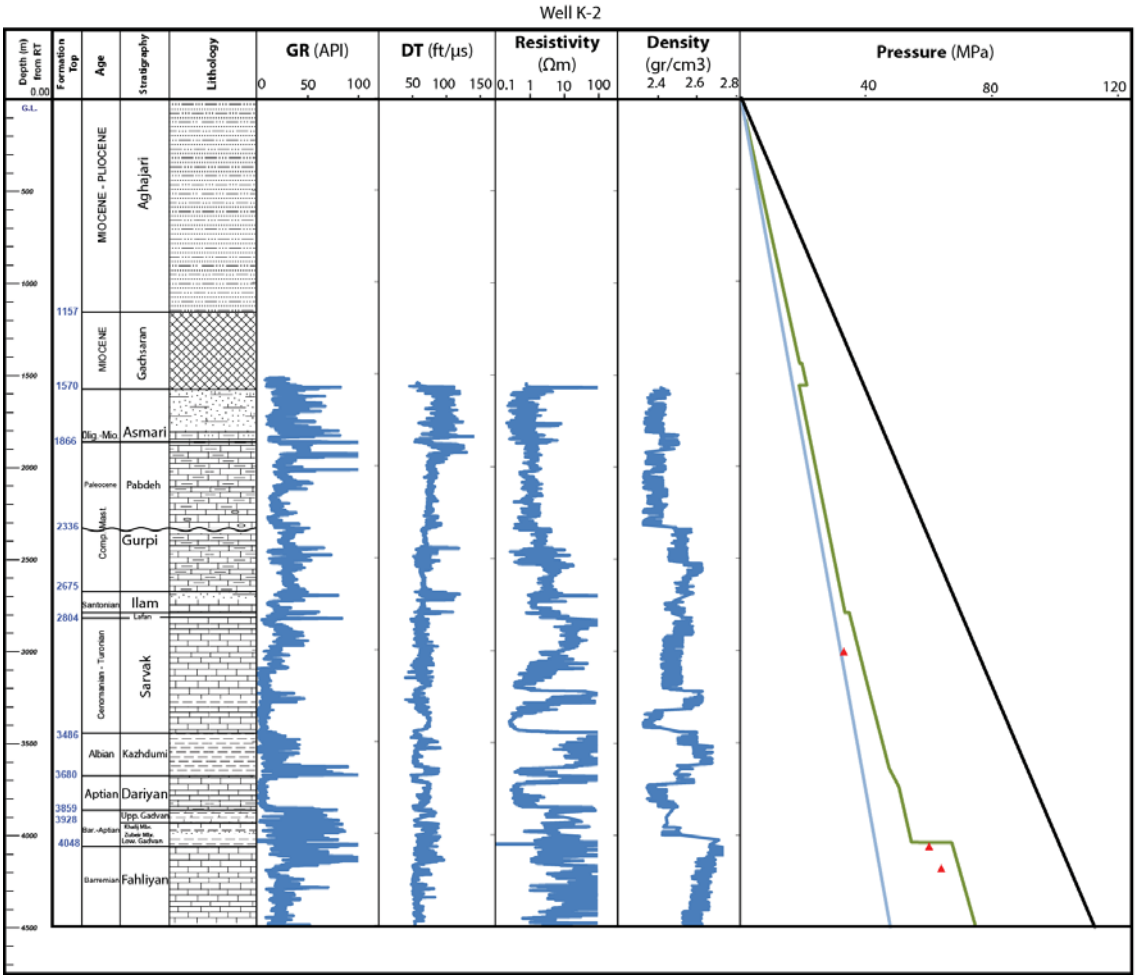
Well K-2
Depth (m) from RT
Formation Top
Age
Stratigraphy
Lithology
GR (API)
0 50 100
DT (ft/µs)
50 100 150
Resistivity (Ωm)
0.1 1 10 100
Density (gr/cm3)
2.4 2.6 2.8
Pressure (MPa)
40 80 120
0.00
G.L.
1157
1570
1866
2336
2675
2804
3486
3680
3859
3928
4048
MIOCENE - PLIOCENE
MIOCENE
Oligo -Mio
Paleocene
Comp. Mast.
Santonian
Cenomanian - Turonian
Albian
Aptian
Bar.-Aptian
Barremian
Aghajari
Gachsaran
Asmari
Pabdeh
Gurpi
Ilam
Lafan
Sarvak
Kazhdumi
Dariyan
Upp. Gadvan
Khaki Mbr.
Zubair Mbr.
Low. Gadvan
Fahliyan

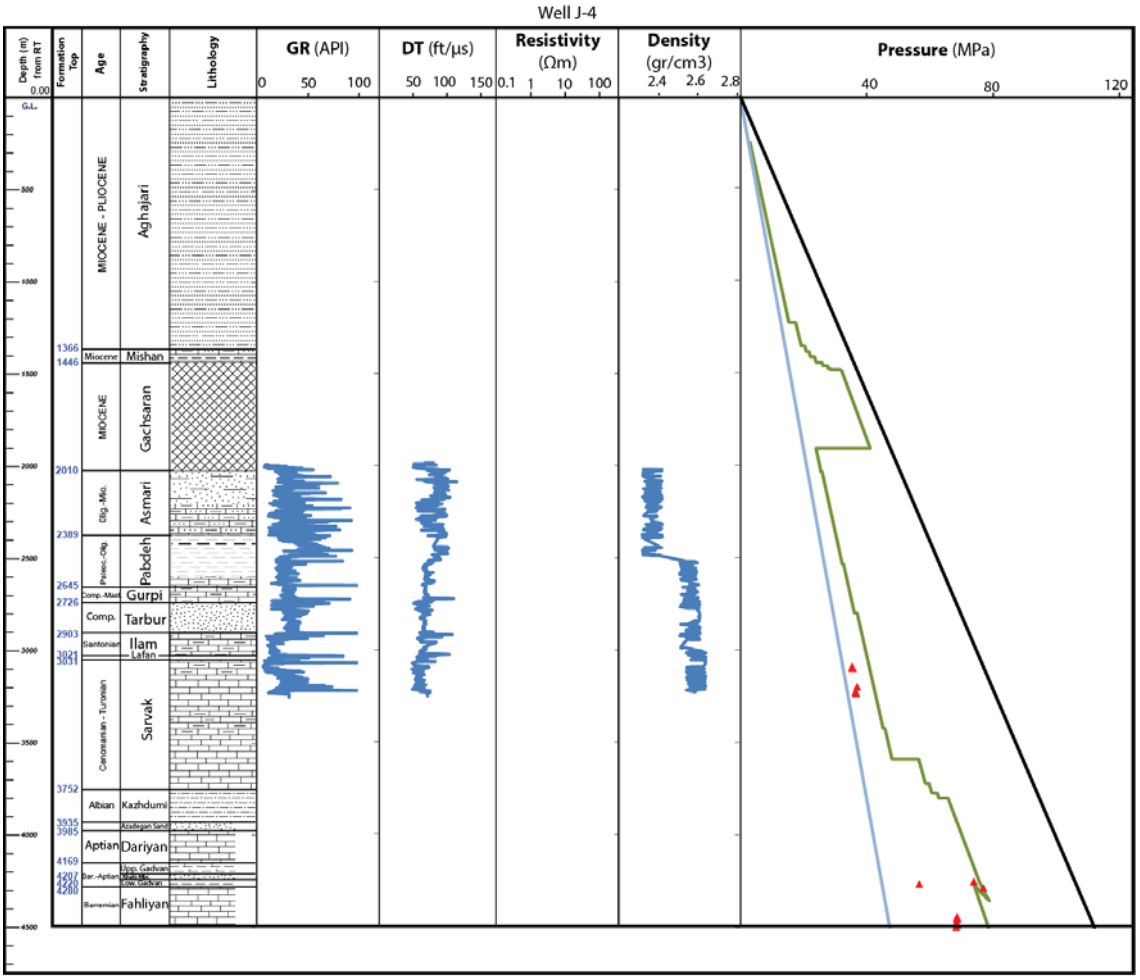
Well J-4
Depth (m) from RT
Formation Top
Age
Stratigraphy
Lithology
GR (API)
0 50 100
DT (ft/µs)
50 100 150
Resistivity (Ωm)
0.1 1 10 100
Density (gr/cm3)
2.4 2.6 2.8
Pressure (MPa)
40 80 120
0.00
G.L.
500
1000
1500
2000
2500
3000
3500
4000
4500
1366
1446
2010
2389
2645
2726
2903
3021
3031
3752
3935
3985
4169
4207
4220
4280
MIOCENE - PLIOCENE
Aghajari
Miocene
Mishan
MIOCENE
Gachsaran
Oligo.-Mio.
Asmari
Paleoc.-Olig.
Pabdeh
Comp.-Maas.
Gurpi
Comp.
Tarbur
Santonian
Ilam
Lafan
Cenomanian - Turonian
Sarvak
Albian
Kazhdumi
Kazhdumi Sand
Aptian
Dariyan
Upp. Gadvan
Bar.-Aptian
Mid. Gadvan
Low. Gadvan
Barremian
Fahliyan

Appendix B-

MatLab code for Biot Compaction Model

```
function varargout = Biot_Pore_Pressure_Permeable_Seal(varargin)
% BIOT_PORE_PRESSURE_PERMEABLE_SEAL MATLAB code for
Biot_Pore_Pressure_Permeable_Seal.fig
%      BIOT_PORE_PRESSURE_PERMEABLE_SEAL, by itself, creates a new
BIOT_PORE_PRESSURE_PERMEABLE_SEAL or raises the existing
%      singleton*.
%
%      H = BIOT_PORE_PRESSURE_PERMEABLE_SEAL returns the handle to a new
BIOT_PORE_PRESSURE_PERMEABLE_SEAL or the handle to
%      the existing singleton*.
%
%
BIOT_PORE_PRESSURE_PERMEABLE_SEAL('CALLBACK',hObject,eventData,handles,...)
calls the local
%      function named CALLBACK in BIOT_PORE_PRESSURE_PERMEABLE_SEAL.M with
the given input arguments.
%
%      BIOT_PORE_PRESSURE_PERMEABLE_SEAL('Property','Value',...) creates a
new BIOT_PORE_PRESSURE_PERMEABLE_SEAL or raises the
%      existing singleton*.  Starting from the left, property value pairs
are
%      applied to the GUI before
Biot_Pore_Pressure_Permeable_Seal_OpeningFcn gets called.  An
%      unrecognized property name or invalid value makes property
application
%      stop.  All inputs are passed to
Biot_Pore_Pressure_Permeable_Seal_OpeningFcn via varargin.
%
%      *See GUI Options on GUIDE's Tools menu.  Choose "GUI allows only one
%      instance to run (singleton)".
%
% See also: GUIDE, GUIDATA, GUIHANDLES

% Edit the above text to modify the response to help
Biot_Pore_Pressure_Permeable_Seal

% Last Modified by GUIDE v2.5 05-Aug-2016 20:07:15

% Begin initialization code - DO NOT EDIT
gui_Singleton = 1;
gui_State = struct('gui_Name',       mfilename, ...
                   'gui_Singleton',  gui_Singleton, ...
                   'gui_OpeningFcn',
@Biot_Pore_Pressure_Permeable_Seal_OpeningFcn, ...
                   'gui_OutputFcn',
@Biot_Pore_Pressure_Permeable_Seal_OutputFcn, ...
                   'gui_LayoutFcn',  [] , ...
                   'gui_Callback',   []);
if nargin && ischar(varargin{1})
    gui_State.gui_Callback = str2func(varargin{1});
end

if nargout
    [varargout{1:nargout}] = gui_mainfcn(gui_State, varargin{:});
else
    gui_mainfcn(gui_State, varargin{:});
```

```
end
% End initialization code - DO NOT EDIT


% --- Executes just before Biot_Pore_Pressure_Permeable_Seal is made
visible.
function Biot_Pore_Pressure_Permeable_Seal_OpeningFcn(hObject, eventdata,
handles, varargin)
% This function has no output args, see OutputFcn.
% hObject    handle to figure
% eventdata  reserved - to be defined in a future version of MATLAB
% handles    structure with handles and user data (see GUIDATA)
% varargin   command line arguments to Biot_Pore_Pressure_Permeable_Seal
(see VARARGIN)

% Choose default command line output for Biot_Pore_Pressure_Permeable_Seal
handles.output = hObject;

% Update handles structure
guidata(hObject, handles);

% UIWAIT makes Biot_Pore_Pressure_Permeable_Seal wait for user response
(see UIRESUME)
% uiwait(handles.figure1);


% --- Outputs from this function are returned to the command line.
function varargout = Biot_Pore_Pressure_Permeable_Seal_OutputFcn(hObject,
eventdata, handles)
% varargout  cell array for returning output args (see VARARGOUT);
% hObject    handle to figure
% eventdata  reserved - to be defined in a future version of MATLAB
% handles    structure with handles and user data (see GUIDATA)

% Get default command line output from handles structure
varargout{1} = handles.output;



function Nu_Callback(hObject, eventdata, handles)
% hObject    handle to Nu (see GCBO)
% eventdata  reserved - to be defined in a future version of MATLAB
% handles    structure with handles and user data (see GUIDATA)

% Hints: get(hObject,'String') returns contents of Nu as text
%        str2double(get(hObject,'String')) returns contents of Nu as a
double


% --- Executes during object creation, after setting all properties.
function Nu_CreateFcn(hObject, eventdata, handles)
% hObject    handle to Nu (see GCBO)
% eventdata  reserved - to be defined in a future version of MATLAB
% handles    empty - handles not created until after all CreateFcns called

% Hint: edit controls usually have a white background on Windows.
%       See ISPC and COMPUTER.
```

```
if ispc && isequal(get(hObject,'BackgroundColor'),
get(0,'defaultUicontrolBackgroundColor'))
    set(hObject,'BackgroundColor','white');
end



function Phi_Callback(hObject, eventdata, handles)
% hObject    handle to Phi (see GCBO)
% eventdata  reserved - to be defined in a future version of MATLAB
% handles    structure with handles and user data (see GUIDATA)

% Hints: get(hObject,'String') returns contents of Phi as text
%        str2double(get(hObject,'String')) returns contents of Phi as a
double


% --- Executes during object creation, after setting all properties.
function Phi_CreateFcn(hObject, eventdata, handles)
% hObject    handle to Phi (see GCBO)
% eventdata  reserved - to be defined in a future version of MATLAB
% handles    empty - handles not created until after all CreateFcns called

% Hint: edit controls usually have a white background on Windows.
%       See ISPC and COMPUTER.
if ispc && isequal(get(hObject,'BackgroundColor'),
get(0,'defaultUicontrolBackgroundColor'))
    set(hObject,'BackgroundColor','white');
end



function E_Callback(hObject, eventdata, handles)
% hObject    handle to E (see GCBO)
% eventdata  reserved - to be defined in a future version of MATLAB
% handles    structure with handles and user data (see GUIDATA)

% Hints: get(hObject,'String') returns contents of E as text
%        str2double(get(hObject,'String')) returns contents of E as a
double


% --- Executes during object creation, after setting all properties.
function E_CreateFcn(hObject, eventdata, handles)
% hObject    handle to E (see GCBO)
% eventdata  reserved - to be defined in a future version of MATLAB
% handles    empty - handles not created until after all CreateFcns called

% Hint: edit controls usually have a white background on Windows.
%       See ISPC and COMPUTER.
if ispc && isequal(get(hObject,'BackgroundColor'),
get(0,'defaultUicontrolBackgroundColor'))
    set(hObject,'BackgroundColor','white');
end



function Rhob_Callback(hObject, eventdata, handles)
```

```
% hObject    handle to Rhob (see GCBO)
% eventdata  reserved - to be defined in a future version of MATLAB
% handles    structure with handles and user data (see GUIDATA)

% Hints: get(hObject,'String') returns contents of Rhob as text
%        str2double(get(hObject,'String')) returns contents of Rhob as a
double


% --- Executes during object creation, after setting all properties.
function Rhob_CreateFcn(hObject, eventdata, handles)
% hObject    handle to Rhob (see GCBO)
% eventdata  reserved - to be defined in a future version of MATLAB
% handles    empty - handles not created until after all CreateFcns called

% Hint: edit controls usually have a white background on Windows.
%       See ISPC and COMPUTER.
if ispc && isequal(get(hObject,'BackgroundColor'),
get(0,'defaultUicontrolBackgroundColor'))
    set(hObject,'BackgroundColor','white');
end



function Kf_Callback(hObject, eventdata, handles)
% hObject    handle to Kf (see GCBO)
% eventdata  reserved - to be defined in a future version of MATLAB
% handles    structure with handles and user data (see GUIDATA)

% Hints: get(hObject,'String') returns contents of Kf as text
%        str2double(get(hObject,'String')) returns contents of Kf as a
double


% --- Executes during object creation, after setting all properties.
function Kf_CreateFcn(hObject, eventdata, handles)
% hObject    handle to Kf (see GCBO)
% eventdata  reserved - to be defined in a future version of MATLAB
% handles    empty - handles not created until after all CreateFcns called

% Hint: edit controls usually have a white background on Windows.
%       See ISPC and COMPUTER.
if ispc && isequal(get(hObject,'BackgroundColor'),
get(0,'defaultUicontrolBackgroundColor'))
    set(hObject,'BackgroundColor','white');
end



function TD_Callback(hObject, eventdata, handles)
% hObject    handle to TD (see GCBO)
% eventdata  reserved - to be defined in a future version of MATLAB
% handles    structure with handles and user data (see GUIDATA)

% Hints: get(hObject,'String') returns contents of TD as text
%        str2double(get(hObject,'String')) returns contents of TD as a
double
```

```
% --- Executes during object creation, after setting all properties.
function TD_CreateFcn(hObject, eventdata, handles)
% hObject    handle to TD (see GCBO)
% eventdata  reserved - to be defined in a future version of MATLAB
% handles    empty - handles not created until after all CreateFcns called

% Hint: edit controls usually have a white background on Windows.
%       See ISPC and COMPUTER.
if ispc && isequal(get(hObject,'BackgroundColor'),
get(0,'defaultUicontrolBackgroundColor'))
    set(hObject,'BackgroundColor','white');
end



function FRD_Callback(hObject, eventdata, handles)
% hObject    handle to FRD (see GCBO)
% eventdata  reserved - to be defined in a future version of MATLAB
% handles    structure with handles and user data (see GUIDATA)

% Hints: get(hObject,'String') returns contents of FRD as text
%        str2double(get(hObject,'String')) returns contents of FRD as a
double


% --- Executes during object creation, after setting all properties.
function FRD_CreateFcn(hObject, eventdata, handles)
% hObject    handle to FRD (see GCBO)
% eventdata  reserved - to be defined in a future version of MATLAB
% handles    empty - handles not created until after all CreateFcns called

% Hint: edit controls usually have a white background on Windows.
%       See ISPC and COMPUTER.
if ispc && isequal(get(hObject,'BackgroundColor'),
get(0,'defaultUicontrolBackgroundColor'))
    set(hObject,'BackgroundColor','white');
end



function Ftop_Callback(hObject, eventdata, handles)
% hObject    handle to Ftop (see GCBO)
% eventdata  reserved - to be defined in a future version of MATLAB
% handles    structure with handles and user data (see GUIDATA)

% Hints: get(hObject,'String') returns contents of Ftop as text
%        str2double(get(hObject,'String')) returns contents of Ftop as a
double



% --- Executes during object creation, after setting all properties.
function Ftop_CreateFcn(hObject, eventdata, handles)
% hObject    handle to Ftop (see GCBO)
% eventdata  reserved - to be defined in a future version of MATLAB
% handles    empty - handles not created until after all CreateFcns called
```

```
% Hint: edit controls usually have a white background on Windows.
%       See ISPC and COMPUTER.
if ispc && isequal(get(hObject,'BackgroundColor'),
get(0,'defaultUicontrolBackgroundColor'))
    set(hObject,'BackgroundColor','white');

end



function tt_Callback(hObject, eventdata, handles)
% hObject    handle to tt (see GCBO)
% eventdata  reserved - to be defined in a future version of MATLAB
% handles    structure with handles and user data (see GUIDATA)

% Hints: get(hObject,'String') returns contents of tt as text
%        str2double(get(hObject,'String')) returns contents of tt as a
double


% --- Executes during object creation, after setting all properties.
function tt_CreateFcn(hObject, eventdata, handles)
% hObject    handle to tt (see GCBO)
% eventdata  reserved - to be defined in a future version of MATLAB
% handles    empty - handles not created until after all CreateFcns called

% Hint: edit controls usually have a white background on Windows.
%       See ISPC and COMPUTER.
if ispc && isequal(get(hObject,'BackgroundColor'),
get(0,'defaultUicontrolBackgroundColor'))
    set(hObject,'BackgroundColor','white');
end



function Acon_Callback(hObject, eventdata, handles)
% hObject    handle to Acon (see GCBO)
% eventdata  reserved - to be defined in a future version of MATLAB
% handles    structure with handles and user data (see GUIDATA)

% Hints: get(hObject,'String') returns contents of Acon as text
%        str2double(get(hObject,'String')) returns contents of Acon as a
double


% --- Executes during object creation, after setting all properties.
function Acon_CreateFcn(hObject, eventdata, handles)
% hObject    handle to Acon (see GCBO)
% eventdata  reserved - to be defined in a future version of MATLAB
% handles    empty - handles not created until after all CreateFcns called

% Hint: edit controls usually have a white background on Windows.
%       See ISPC and COMPUTER.
if ispc && isequal(get(hObject,'BackgroundColor'),
get(0,'defaultUicontrolBackgroundColor'))
    set(hObject,'BackgroundColor','white');
end
```

```
function Bcon_Callback(hObject, eventdata, handles)
% hObject    handle to Bcon (see GCBO)
% eventdata  reserved - to be defined in a future version of MATLAB
% handles    structure with handles and user data (see GUIDATA)

% Hints: get(hObject,'String') returns contents of Bcon as text
%        str2double(get(hObject,'String')) returns contents of Bcon as a
double


% --- Executes during object creation, after setting all properties.
function Bcon_CreateFcn(hObject, eventdata, handles)
% hObject    handle to Bcon (see GCBO)
% eventdata  reserved - to be defined in a future version of MATLAB
% handles    empty - handles not created until after all CreateFcns called

% Hint: edit controls usually have a white background on Windows.
%       See ISPC and COMPUTER.
if ispc && isequal(get(hObject,'BackgroundColor'),
get(0,'defaultUicontrolBackgroundColor'))
    set(hObject,'BackgroundColor','white');
end



function k_Callback(hObject, eventdata, handles)
% hObject    handle to k (see GCBO)
% eventdata  reserved - to be defined in a future version of MATLAB
% handles    structure with handles and user data (see GUIDATA)

% Hints: get(hObject,'String') returns contents of k as text
%        str2double(get(hObject,'String')) returns contents of k as a
double


% --- Executes during object creation, after setting all properties.
function k_CreateFcn(hObject, eventdata, handles)
% hObject    handle to k (see GCBO)
% eventdata  reserved - to be defined in a future version of MATLAB
% handles    empty - handles not created until after all CreateFcns called

% Hint: edit controls usually have a white background on Windows.
%       See ISPC and COMPUTER.
if ispc && isequal(get(hObject,'BackgroundColor'),
get(0,'defaultUicontrolBackgroundColor'))
    set(hObject,'BackgroundColor','white');
end


% --- Executes on button press in RUN.
function RUN_Callback(hObject, eventdata, handles)
% hObject    handle to RUN (see GCBO)
% eventdata  reserved - to be defined in a future version of MATLAB
% handles    structure with handles and user data (see GUIDATA)
%clf( figure(1));
%clf( figure(2));
```

```
clf( figure(3));


Nu=str2num(get(handles.Nu,'String'));
E=str2num(get(handles.E,'String'));
Phi=str2num(get(handles.Phi,'String'));
Rhob=str2num(get(handles.Rhob,'String'));
Krock=str2num(get(handles.Krock,'String'));
Kf=str2num(get(handles.Kf,'String'));
TD=str2num(get(handles.TD,'String'));
FRD=str2num(get(handles.FRD,'String'));
Ftop=str2num(get(handles.Ftop,'String'));
tt=str2num(get(handles.tt,'String'));
Acon=str2num(get(handles.Acon,'String'));
Bcon=str2num(get(handles.Bcon,'String'));
k_CR=str2num(get(handles.k_CR,'String'));
k=str2num(get(handles.k,'String'));
h=str2num(get(handles.h,'String'));
Area=str2num(get(handles.Area,'String'));
h_CR=str2num(get(handles.h_CR,'String'));
Mu=str2num(get(handles.Mu,'String'));
Pf_gradient=str2num(get(handles.Pf_gradient,'String'));


Crock=1/Krock;
Cf=1/Kf;
kc=k*0.858e-6;  %cm/sec
kc=kc*0.01;  %m/sec

k_CR=k_CR*9.869233e-16; % m2

Mu=Mu*0.001 ;        %Pa.s

res_vol=h*Area;
pore_vol=h*Area*Phi;

G=E/(2*(1+Nu));%Pa
P0=(Ftop-FRD)*Rhob*1000*9.81*145.04e-6; %psi
P0=P0*6894.757; %Pa

%z=h;%m
t=tt*365*24*60*60*1000000;%sec

c=Acon*exp(Bcon*P0*0.0001450377);%Psi-1
c=c/6897;   %Pa-1
H=(1/c)/Phi;%???????
R=-P0/c; % P0 is considered as negative pressure and compressibility is
considered as "increment of liquid phase volume per unit volume of soil"

%%%%
K=E/(3*(1-(2*Nu)));

%=============== from here, Biot theory will be modeled ================

alpha=2*(1+Nu)*G/(3*H*(1-2*Nu));
%alpha=1
a=(1-2*Nu)/(2*G*(1-Nu));
Q=1/(1/R-(alpha/H));
Cc=1/((alpha*alpha*a/kc)+(1/(Q*kc)));
```

```
nt=1000;
dt=t/nt;%sec?
nz=100;% --> dz=3m

tvec=zeros(100,1);
pvec=zeros(100,1);
dvec=zeros(100,1);
dz=h/nz;
z=linspace(0,h,nz+1);

d=linspace(0,TD,nz+1);
%while d<=4000
Ph=d*3.28*Pf_gradient; % psi
Ph=Ph*6894.757; %Pa
Plit=d*Rhob*1000*9.81*145.04e-6;
Plit=Plit*6894.757; %Pa


DeltaP=zeros(nz+1);


figure (3);
hold on
set (gca,'Ydir','reverse')

Phplot=plot(Ph/1000000,d,'-b');    %MPa
set(Phplot,'linewidth',2);
Plithplot=plot(Plit/1000000,d,'-k');     %MPa
set(Plithplot,'linewidth',2);

temp_Depth_for_plot=linspace(FRD,Ftop,20);
for iii=1:length(temp_Depth_for_plot)
Ftop=temp_Depth_for_plot(iii);

for ik=1:nt
    tMY=ik*dt/3600/24/365/1000000;
    Depth=tMY*(Ftop-FRD)/tt;%(m) ... meters per ... million years
    P0=(Rhob*1000*9.8*Depth)-DeltaP(end);%(Pa)

    Depth_for_CR=tMY*(Ftop-h_CR)/tt;%(m) ... meters per ... million years
    P0_for_CR=(Rhob*1000*9.8*Depth_for_CR); %(Pa)
    P0_for_CR=P0_for_CR*0.000145037743897;   %psi
    %c=18e-6*0.00014504;        % if want to consider constant
compressibiliy

    Sigma_n_1=P0*ones(nz+1,1);
    A=zeros(nz+1,nz+1);
    b=zeros(nz+1,1);
    A(1,1)=1;
    A(1,2)=-1;
    %b(1,1)=P0;
    XX=dz^2/(Cc*dt);
    for I=2:nz
        A(I,I-1)=1;
        A(I,I+1)=1;
        A(I,I)=-(2+XX);
        b(I,1)=-XX*Sigma_n_1(I);
    end
    A(nz+1,nz+1)=1;
```

```
    A(nz+1,nz)=-1;
    Sigma_n=A\b;
    if rem(ik,0.1*nt)==0
%         plot(Sigma_n,-z);
        tvec(ik/0.1/nt)=tMY;    %million year
        pvec(ik/0.1/nt)=Sigma_n(1);
        dvec(ik/0.1/nt)=tMY*(Ftop-FRD)/tt;
    end
    Sigma_n_1=Sigma_n+Ph((round((FRD/TD)*length(Ph))));


    Qrate=k_CR*Area*(Sigma_n_1'+P0-
Ph((round(((FRD+z)/TD)*length(Ph))))/(Mu*h_CR); % m3 per second
    DeltaP=Qrate*t/(Cf*pore_vol); %Pa per second    note that the flow rate
has been multiplied by dt t achieve the volume of the fluid exits the
formation

end

PPPBiot_plot=plot((Sigma_n_1(end))/1000000,(Ftop),'rs','linewidth',2);
%MPa
% set(PPPBiot_plot,'linewidth',2);
label = [num2str((Sigma_n_1(end))*0.000145037743897/(Ftop*3.28),2) '
psi/ft'];
text(Ftop, (Sigma_n_1(end))*0.000145037743897, label , 'horizontal','left',
'vertical','top');
set(gca,'XAxisLocation','top')

end

hleg2=legend ('Hydrostatic Pressure','Lithostatic Pressure','Predicted Pore
Pressure');
set(hleg2,'Location','NorthEast');
xlabel('Pressure (MPa)','FontSize',12,'FontWeight','bold');
ylabel('Depth (m)','FontSize',12,'FontWeight','bold');

virtual_depth(1)= 0;
for i=1:1:9

virtual_depth(i)=i*490;     %m
virtual_depth(1)= 0;
virtual_pressure_12(i)=virtual_depth(i)*12/1000;     %MPa/km
virtual_pressure_14(i)=virtual_depth(i)*14/1000;     %MPa/km
virtual_pressure_16(i)=virtual_depth(i)*16/1000;     %MPa/km
virtual_pressure_18(i)=virtual_depth(i)*18/1000;     %MPa/km
virtual_pressure_20(i)=virtual_depth(i)*20/1000;     %MPa/km
virtual_pressure_22(i)=virtual_depth(i)*22/1000;     %MPa/km
virtual_pressure_24(i)=virtual_depth(i)*24/1000;     %MPa/km
end

plot(virtual_pressure_12,virtual_depth,':','Color', [.5 .5 .5]);
plot(virtual_pressure_14,virtual_depth,':','Color', [.5 .5 .5]);
plot(virtual_pressure_16,virtual_depth,':','Color', [.5 .5 .5]);
plot(virtual_pressure_18,virtual_depth,':','Color', [.5 .5 .5]);
plot(virtual_pressure_20,virtual_depth,':','Color', [.5 .5 .5]);
plot(virtual_pressure_22,virtual_depth,':','Color', [.5 .5 .5]);
plot(virtual_pressure_24,virtual_depth,':','Color', [.5 .5 .5]);

grid off
```

```
 depth=num2str(Ftop);
 set(handles.depth,'string',depth);

Biot_PP=num2str(round(Sigma_n_1(end)*0.0001450377));
set(handles.result1,'String',Biot_PP);

set(handles.result2,'string',num2str((Sigma_n_1(end))*1000/(Ftop*1000000),2
));

guidata(hObject,handles);


% --- Executes during object creation, after setting all properties.
function result1_CreateFcn(hObject, eventdata, handles)
% hObject    handle to result1 (see GCBO)
% eventdata  reserved - to be defined in a future version of MATLAB
% handles    empty - handles not created until after all CreateFcns called



function result1_Callback(hObject, eventdata, handles)
% hObject    handle to result1 (see GCBO)
% eventdata  reserved - to be defined in a future version of MATLAB
% handles    structure with handles and user data (see GUIDATA)

% Hints: get(hObject,'String') returns contents of result1 as text
%        str2double(get(hObject,'String')) returns contents of result1 as a
double


% --- Executes on button press in Reset.
function Reset_Callback(hObject, eventdata, handles)
% hObject    handle to Reset (see GCBO)
% eventdata  reserved - to be defined in a future version of MATLAB
% handles    structure with handles and user data (see GUIDATA)

set(handles.Nu,'string','');
set(handles.Phi,'string','');
set(handles.E,'string','');
set(handles.Rhob,'string','');
set(handles.Krock,'string','');
set(handles.Kf,'string','');
set(handles.TD,'string','');
set(handles.FRD,'string','');
set(handles.Ftop,'string','');
set(handles.tt,'string','');
set(handles.Acon,'string','');
set(handles.Bcon,'string','');
set(handles.k_CR,'string','');
set(handles.k,'string','');
set(handles.h,'string','');
set(handles.Area,'string','');
set(handles.h_CR,'string','');
set(handles.Mu,'string','');
set(handles.Pf_gradient,'string','');
set(handles.result1,'string','');
set(handles.result2,'string','');
```

```
function result2_Callback(hObject, eventdata, handles)
% hObject    handle to result2 (see GCBO)
% eventdata  reserved - to be defined in a future version of MATLAB
% handles    structure with handles and user data (see GUIDATA)

% Hints: get(hObject,'String') returns contents of result2 as text
%        str2double(get(hObject,'String')) returns contents of result2 as a
double


% --- Executes during object creation, after setting all properties.
function result2_CreateFcn(hObject, eventdata, handles)
% hObject    handle to result2 (see GCBO)
% eventdata  reserved - to be defined in a future version of MATLAB
% handles    empty - handles not created until after all CreateFcns called

% Hint: edit controls usually have a white background on Windows.
%       See ISPC and COMPUTER.
if ispc && isequal(get(hObject,'BackgroundColor'),
get(0,'defaultUicontrolBackgroundColor'))
    set(hObject,'BackgroundColor','white');
end


% --- Executes on button press in DefaultValues.
function DefaultValues_Callback(hObject, eventdata, handles)
% hObject    handle to DefaultValues (see GCBO)
% eventdata  reserved - to be defined in a future version of MATLAB
% handles    structure with handles and user data (see GUIDATA)

set(handles.Nu,'string',0.36);
set(handles.Phi,'string','0.05');
set(handles.E,'string','14e9');
set(handles.Rhob,'string','2.3');
set(handles.Krock,'string','65e9');
set(handles.Kf,'string','2.2e9');
set(handles.TD,'string','4400');
set(handles.FRD,'string','1300');
set(handles.Ftop,'string','4000');
set(handles.tt,'string','11');
set(handles.Acon,'string','8e-05');
set(handles.Bcon,'string','-5e-04');
set(handles.k_CR,'string','1e-10');
set(handles.k,'string','0.1');
set(handles.h,'string','200');
set(handles.Area,'string','12000000');
set(handles.h_CR,'string','80');
set(handles.Mu,'string','7.80');
set(handles.Pf_gradient,'string','0.465');
set(handles.result1,'string','');
set(handles.result2,'string','');



% --- Executes on button press in togglebutton1.
function togglebutton1_Callback(hObject, eventdata, handles)
% hObject    handle to togglebutton1 (see GCBO)
```

```
% eventdata  reserved - to be defined in a future version of MATLAB
% handles    structure with handles and user data (see GUIDATA)

% Hint: get(hObject,'Value') returns toggle state of togglebutton1



function k_CR_Callback(hObject, eventdata, handles)
% hObject    handle to k_CR (see GCBO)
% eventdata  reserved - to be defined in a future version of MATLAB
% handles    structure with handles and user data (see GUIDATA)

% Hints: get(hObject,'String') returns contents of k_CR as text
%        str2double(get(hObject,'String')) returns contents of k_CR as a
double


% --- Executes during object creation, after setting all properties.
function k_CR_CreateFcn(hObject, eventdata, handles)
% hObject    handle to k_CR (see GCBO)
% eventdata  reserved - to be defined in a future version of MATLAB
% handles    empty - handles not created until after all CreateFcns called

% Hint: edit controls usually have a white background on Windows.
%       See ISPC and COMPUTER.
if ispc && isequal(get(hObject,'BackgroundColor'),
get(0,'defaultUicontrolBackgroundColor'))
    set(hObject,'BackgroundColor','white');
end



function h_Callback(hObject, eventdata, handles)
% hObject    handle to h (see GCBO)
% eventdata  reserved - to be defined in a future version of MATLAB
% handles    structure with handles and user data (see GUIDATA)

% Hints: get(hObject,'String') returns contents of h as text
%        str2double(get(hObject,'String')) returns contents of h as a
double


% --- Executes during object creation, after setting all properties.
function h_CreateFcn(hObject, eventdata, handles)
% hObject    handle to h (see GCBO)
% eventdata  reserved - to be defined in a future version of MATLAB
% handles    empty - handles not created until after all CreateFcns called

% Hint: edit controls usually have a white background on Windows.
%       See ISPC and COMPUTER.
if ispc && isequal(get(hObject,'BackgroundColor'),
get(0,'defaultUicontrolBackgroundColor'))
    set(hObject,'BackgroundColor','white');
end



function Area_Callback(hObject, eventdata, handles)
```

```
% hObject    handle to Area (see GCBO)
% eventdata  reserved - to be defined in a future version of MATLAB
% handles    structure with handles and user data (see GUIDATA)

% Hints: get(hObject,'String') returns contents of Area as text
%        str2double(get(hObject,'String')) returns contents of Area as a
double


% --- Executes during object creation, after setting all properties.
function Area_CreateFcn(hObject, eventdata, handles)
% hObject    handle to Area (see GCBO)
% eventdata  reserved - to be defined in a future version of MATLAB
% handles    empty - handles not created until after all CreateFcns called

% Hint: edit controls usually have a white background on Windows.
%       See ISPC and COMPUTER.
if ispc && isequal(get(hObject,'BackgroundColor'),
get(0,'defaultUicontrolBackgroundColor'))
    set(hObject,'BackgroundColor','white');
end



function h_CR_Callback(hObject, eventdata, handles)
% hObject    handle to h_CR (see GCBO)
% eventdata  reserved - to be defined in a future version of MATLAB
% handles    structure with handles and user data (see GUIDATA)

% Hints: get(hObject,'String') returns contents of h_CR as text
%        str2double(get(hObject,'String')) returns contents of h_CR as a
double


% --- Executes during object creation, after setting all properties.
function h_CR_CreateFcn(hObject, eventdata, handles)
% hObject    handle to h_CR (see GCBO)
% eventdata  reserved - to be defined in a future version of MATLAB
% handles    empty - handles not created until after all CreateFcns called

% Hint: edit controls usually have a white background on Windows.
%       See ISPC and COMPUTER.
if ispc && isequal(get(hObject,'BackgroundColor'),
get(0,'defaultUicontrolBackgroundColor'))
    set(hObject,'BackgroundColor','white');
end



function Mu_Callback(hObject, eventdata, handles)
% hObject    handle to Mu (see GCBO)
% eventdata  reserved - to be defined in a future version of MATLAB
% handles    structure with handles and user data (see GUIDATA)

% Hints: get(hObject,'String') returns contents of Mu as text
%        str2double(get(hObject,'String')) returns contents of Mu as a
double
```

```
% --- Executes during object creation, after setting all properties.
function Mu_CreateFcn(hObject, eventdata, handles)
% hObject    handle to Mu (see GCBO)
% eventdata  reserved - to be defined in a future version of MATLAB
% handles    empty - handles not created until after all CreateFcns called

% Hint: edit controls usually have a white background on Windows.
%       See ISPC and COMPUTER.
if ispc && isequal(get(hObject,'BackgroundColor'),
get(0,'defaultUicontrolBackgroundColor'))
    set(hObject,'BackgroundColor','white');
end



function Pf_gradient_Callback(hObject, eventdata, handles)
% hObject    handle to Pf_gradient (see GCBO)
% eventdata  reserved - to be defined in a future version of MATLAB
% handles    structure with handles and user data (see GUIDATA)

% Hints: get(hObject,'String') returns contents of Pf_gradient as text
%        str2double(get(hObject,'String')) returns contents of Pf_gradient
as a double


% --- Executes during object creation, after setting all properties.
function Pf_gradient_CreateFcn(hObject, eventdata, handles)
% hObject    handle to Pf_gradient (see GCBO)
% eventdata  reserved - to be defined in a future version of MATLAB
% handles    empty - handles not created until after all CreateFcns called

% Hint: edit controls usually have a white background on Windows.
%       See ISPC and COMPUTER.
if ispc && isequal(get(hObject,'BackgroundColor'),
get(0,'defaultUicontrolBackgroundColor'))
    set(hObject,'BackgroundColor','white');
end



function Krock_Callback(hObject, eventdata, handles)
% hObject    handle to Krock (see GCBO)
% eventdata  reserved - to be defined in a future version of MATLAB
% handles    structure with handles and user data (see GUIDATA)

% Hints: get(hObject,'String') returns contents of Krock as text
%        str2double(get(hObject,'String')) returns contents of Krock as a
double


% --- Executes during object creation, after setting all properties.
function Krock_CreateFcn(hObject, eventdata, handles)
% hObject    handle to Krock (see GCBO)
% eventdata  reserved - to be defined in a future version of MATLAB
% handles    empty - handles not created until after all CreateFcns called

% Hint: edit controls usually have a white background on Windows.
```

```
%       See ISPC and COMPUTER.
if ispc && isequal(get(hObject,'BackgroundColor'),
get(0,'defaultUicontrolBackgroundColor'))
    set(hObject,'BackgroundColor','white');
end



function Acon_CR_Callback(hObject, eventdata, handles)
% hObject    handle to Acon_CR (see GCBO)
% eventdata  reserved - to be defined in a future version of MATLAB
% handles    structure with handles and user data (see GUIDATA)

% Hints: get(hObject,'String') returns contents of Acon_CR as text
%        str2double(get(hObject,'String')) returns contents of Acon_CR as a
double


% --- Executes during object creation, after setting all properties.
function Acon_CR_CreateFcn(hObject, eventdata, handles)
% hObject    handle to Acon_CR (see GCBO)
% eventdata  reserved - to be defined in a future version of MATLAB
% handles    empty - handles not created until after all CreateFcns called

% Hint: edit controls usually have a white background on Windows.
%       See ISPC and COMPUTER.
if ispc && isequal(get(hObject,'BackgroundColor'),
get(0,'defaultUicontrolBackgroundColor'))
    set(hObject,'BackgroundColor','white');
end



function Bcon_CR_Callback(hObject, eventdata, handles)
% hObject    handle to k_CR (see GCBO)
% eventdata  reserved - to be defined in a future version of MATLAB
% handles    structure with handles and user data (see GUIDATA)

% Hints: get(hObject,'String') returns contents of k_CR as text
%        str2double(get(hObject,'String')) returns contents of k_CR as a
double


% --- Executes during object creation, after setting all properties.
function Bcon_CR_CreateFcn(hObject, eventdata, handles)
% hObject    handle to k_CR (see GCBO)
% eventdata  reserved - to be defined in a future version of MATLAB
% handles    empty - handles not created until after all CreateFcns called

% Hint: edit controls usually have a white background on Windows.
%       See ISPC and COMPUTER.
if ispc && isequal(get(hObject,'BackgroundColor'),
get(0,'defaultUicontrolBackgroundColor'))
    set(hObject,'BackgroundColor','white');
end
```

References

Abdollahie Fard, I., S. A. Alavi, and M. Mokhtari, 2006a, Structural framework of the Abadan Plain (Southwest of Iran) and noth of Persian Gulf based on geophysical data (translated from Persian title): Journal of Science, University of Tehran, v. 32, p. 107-120.

Abdollahie Fard, I., A. Braathen, M. Mokhtari, and S. A. Alavi, 2006b, Interaction of the Zagros Fold–Thrust Belt and the Arabian-type, deep-seated folds in the Abadan Plain and the Dezful Embayment,SW Iran: Petroleum Geoscience, v. 12, p. 347-362.

Agard, P., J. Omrani, L. Jolivet, H. Whitechurch, B. Vrielynck, W. Spakman, P. Monie, B. Meyer, and R. Wortel, 2011, Zagros orogeny: a subduction-dominated process: Geological Magazine, v. 148, p. 692-725.

Aharonov, E., and R. Katsman, 2009, Interaction between pressure solution and clays in stylolite development: Insights from modeling: American Journal of Science, v. 309, p. 607-632.

Ahmed, A., R. Hussain, L. Anis, B. H. Tan, and A. Mohaideen, 2011, Real Time Pore Pressure Prediction Using LWD And Borehole Seismic Data Assists In Mitigating Risk On An Appraisal Well Offshore Malaysia, SPE/IADC Drilling Conference and Exhibition, Amsterdam, The Netherlands, SPE/IADC Drilling Conference and Exhibition.

Akhoundzadeh, H., J. Moghadasi, and B. Habibnia, 2011, Correlation of Pore Volume Compressibility with Porosity in One of the Iranian Southern Carbonate Reservoirs: 3rd National Iranian Conference of Petroleum Engineering.

Al Naqib, K. M., 1967, Geology of the Arabian Peninsula; southwestern Iraq: US Geological Survey Professional Paper, v. 560 G.

Ala, M. A., R. R. F. Kinghorn, and M. Rahman, 1980, Organic Geochemistry and Source Rock Characteristics of The Zagros Petroleum Province, Southwest Iran: Journal of Petroleum Geology, v. 3, p. 61-89.

Alavi, M., 1994, Tectonics of the Zagros Orogenic Belt of Iran - New Data and Interpretations: Tectonophysics, v. 229, p. 211-238.

Alavi, M., 2004, Regional Stratigraphy Of The Zagros Fold-Thrust Belt Of Iran And Its Proforeland Evolution: American Journal of Science, v. 304, p. 1-20.

Alavi, M., 2007, Structures of the Zagros fold-thrust belt in Iran: American Journal of Science, v. 307, p. 1064-1095.

Ali, S. A., W. J. Clark, W. R. Moore, and J. R. Dribus, 2010, Diagenesis and reservoir quality: Oilfield Review, v. 22, p. 14-27.

Allahkarampour Dill, M., A. Seyrafian, and H. Vaziri-Moghaddam, 2010, The Asmari Formation, north of the Gachsaran (Dill anticline), southwest Iran: facies analysis, depositional environments and sequence stratigraphy: Carbonates and Evaporites, v. 25, p. 145-160.

Allen, M., J. Jackson, and R. Walker, 2004, Late Cenozoic reorganization of the Arabia-Eurasia collision and the comparison of short-term and long-term deformation rates: Tectonics, v. 23, p. TC2008.

Amthor, J. E., E. W. Mountjoy, and H. G. Machel, 1994, Regional-Scale Porosity and Permeability Variations in Upper Devonian Leduc Buildups - Implications for Reservoir Development and Prediction in Carbonates: AAPG Bulletin-American Association of Petroleum Geologists, v. 78, p. 1541-1559.

Anderson, R. A., D. S. Ingram, and A. M. Zanier, 1973, Determining Fracture Pressure-Gradients from Well Logs: Journal of Petroleum Technology, v. 25, p. 1259-1268.

Aquitaine, E., A. Reeckmann, and G. Friedman, 1982, Exploration for carbonate petroleum reservoirs, New York, John Wiley & Sons, Inc.

ARAMCO, 1968, Oil and the Middle East: Dhahran, Saudi Arabia, Arabian American Oil Company.

Archie, G. E., 1952, Classification of Carbonate Reservoir Rocks and Petrophysical Considerations: AAPG Bulletin-American Association of Petroleum Geologists, v. 36, p. 278-298.

Arvandan Oil and Gas Co., 2014, Darquain Oil Field.

Ashton, F. E., and J. E. Klovan, 1971, A Late Devonian reef tract on northeastern Banks Island, NWT: Bulletin of Canadian Petroleum Geology, v. 19, p. 730-781.

Asquith, G. B., and C. R. Gibson, 1982, Basic well log analysis for geologists, American Association of Petroleum Geologists.

Atashbari, V., and M. R. Tingay, 2012a, Pore Pressure Prediction in a Carbonate Reservoir, SPE Oil and Gas India Conference and Exhibition, Mumbai, India Society of Petroleum Engineers.

Atashbari, V., and M. R. Tingay, 2012b, Pore Pressure Prediction in Carbonate Reservoirs, SPE Latin America and Caribbean Petroleum Engineering Conference, Mexico City, Mexico, Society of Petroleum Engineers.

Athy, L. F., 1930a, Compaction and oil migration: AAPG Bulletin, v. 14, p. 25-35.

Athy, L. F., 1930b, Density, porosity, and compaction of sedimentary rocks: AAPG Bulletin, v. 14, p. 1-24.

Azadpour, M., and N. Shad Manaman, 2015, Determination of Pore Pressure from Sonic Log: a Case Study on One of Iran Carbonate Reservoir Rocks: Iranian Journal of Oil & Gas Science and Technology, v. 4, p. 37-50.

Azadpour, M., N. Shad Manaman, A. Kadkhodaie-Ilkhchi, and M.-R. Sedghipour, 2015, Pore pressure prediction and modeling using well-logging data in one of the gas fields in south of Iran: Journal of Petroleum Science and Engineering, v. 128, p. 15-23.

Badri, M. A., C. Sayers, R. A. Hussein, and A. Graziano, 2001, Pore Pressure Prediction Data Using Seismic Velocities and Log Data in the Offshore Nile Delta, Egypt, SPE Middle East Oil Show, Bahrain, Copyright 2001, Society of Petroleum Engineers Inc.

Bagrintseva, K. I., 1977, Carbonate Oil and Gas Reservoir rocks: Moscow, Nedra Publishing House, 231 p.

Bahadori, A., E. J. M. Carranza, and B. Soleimani, 2011, Geochemical analysis of evaporite sedimentation in the Gachsaran Formation, Zeloi oil field, southwest Iran: Journal of Geochemical Exploration, v. 111, p. 97-112.

Bahroudi, A., 2003, The Effect of Mechanical Characteristics of Basal Decollement and Basement Structures on Deformation of the Zagros Basin, Uppsala University Library.

Bahroudi, A., and H. A. Koyi, 2004, Tectono-sedimentary framework of the Gachsaran Formation in the Zagros foreland basin: Marine and Petroleum Geology, v. 21, p. 1295-1310.

Baker Hughes INTEQ, 1993, Formation Pressure Evaluation.

Baker, P. A., M. Kastner, J. D. Byerlee, and D. A. Lockner, 1980, Pressure solution and hydrothermal recrystallization of carbonate sediments — An experimental study: Marine Geology, v. 38, p. 185-203.

Baltensperger, P., W. Zanussi, S. Bordoloi, and S. Nath, 2012, Overpressured Carbonate Reservoirs, Offshore Sarawak; Methods of Pore Pressure Prediction: Petroleum Geoscience Conference & Exhibition.

Barker, C., 1990, Calculated Volume and Pressure Changes During the Thermal Cracking of Oil to Gas in Reservoirs (1): AAPG Bulletin, v. 74, p. 1254-1261.

Bathurst, R. G., 1972, Carbonate sediments and their diagenesis, v. 12, Elsevier.

BeicipFranlab, 2015, Petroleum System Assessmen (TemisFlow).

Bell, J. S., 1996, Petro Geoscience 1. IN SITU STRESSES IN SEDIMENTARY ROCKS (PART 1): MEASUREMENT TECHNIQUES: 1996.

Berberian, M., 1995, Master "blind" thrust faults hidden under the Zagros folds: active basement tectonics and surface morphotectonics: Tectonophysics, v. 241, p. 193–195, 197, 199–224.

Berberian, M., and G. C. P. King, 1981, Towards a Paleogeography and Tectonic Evolution of Iran: Canadian Journal of Earth Sciences, v. 18, p. 210-265.

Berryman, J. G., 2005, Estimates and rigorous bounds on pore-fluid enhanced shear modulus in poroelastic media with hard and soft anisotropy: International Journal of Damage Mechanics.

Berryman, J. G., 2015, Poroelasticity of carbonates with fractured grains and fluid-saturated pores: International Journal for Numerical and Analytical Methods in Geomechanics, v. 39, p. 1527-1546.

Bethke, C. M., 1985, A Numerical-Model of Compaction-Driven Groundwater-Flow and Heat-Transfer and Its Application to the Paleohydrology of Intracratonic Sedimentary Basins: Journal of Geophysical Research-Solid Earth and Planets, v. 90, p. 6817-6828.

Beydoun, Z. R., M. W. Hughes Clarke, and R. Stoneley, 1992, Petroleum in the Zagros Basin: A Late Tertiary Foreland Basin Overprinted onto the Outer Edge of a Vast Hydrocarbon-Rich Paleozoic-Mesozoic Passive-Margin Shelf, AAPG Memoir 55 Foreland Basins and Fold Belts, p. 309-339.

Bhagwan, S., O. D. Singh, R. Awadhesh, and B. N. Talukdar, 1998, Occurrence Of Overpressures And Its Implications For Hydrocarbon Exploration In North East India, SPE India Oil and Gas Conference and Exhibition, New Delhi, India, Society of Petroleum Engineers.

Bhattacharyya, A., and G. M. Friedman, 1979, Experimental compaction of ooids and lime mud and its implication for lithification during burial: Journal of Sedimentary Research, v. 49, p. 1279-1286.

Biot, M. A., 1941, General theory of three-dimensional consolidation: Journal of applied physics, v. 12, p. 155-164.

Biot, M. A., 1955, Theory of Elasticity and Consolidation for a Porous Anisotropic Solid: Journal of Applied Physics, v. 26, p. 182-185.

Biot, M. A., 1973, Nonlinear and semilinear rheology of porous solids: Journal of Geophysical Research, v. 78, p. 4924-4937.

Bishop, C. M., 2006, Pattern recognition and machine learning, springer.

Blanc, E. J. P., M. B. Allen, S. Inger, and H. Hassani, 2003, Structural styles in the Zagros Simple Folded Zone, Iran: Journal of the Geological Society, v. 160, p. 401-412.

Blount, D. N., and C. H. Moore, 1969, Depositional and Non-Depositional Carbonate Breccias, Chiantla Quadrangle, Guatemala: Geological Society of America Bulletin, v. 80, p. 429-442.

Boles, J. R., and S. G. Franks, 1979, Clay Diagenesis in Wilcox Sandstones of Southwest Texas - Implications of Smectite Diagenesis on Sandstone Cementation: Journal of Sedimentary Petrology, v. 49, p. 55-70.

Borge, H., 2002, Modelling generation and dissipation of overpressure in sedimentary basins: an example from the Halten Terrace, offshore Norway: Marine and Petroleum Geology, v. 19, p. 377-388.

Bowers, G. L., 1994, Pore pressure estimation from velocity data: accounting from overpressure mechanisms besides undercompaction: Proceedings of the IADC/SPE drilling conference, Dallas, 1994,(IADC/SPE), 1994, pp 515–530: International Journal of Rock Mechanics and Mining Sciences & Geomechanics Abstracts, p. 276.

Bowers, G. L., 1995, Pore Pressure Estimation From Velocity Data: Accounting for Overpressure Mechanisms Besides Undercompaction: SPE Drilling & Completion, v. 10, p. 89-95.

Bowers, G. L., 2001, Determining an Appropriate Pore-Pressure Estimation Strategy, 2001 Offshore Technology Conference, Houston, Texas.

Bowers, G. L., 2002, Detecting high overpressure: The Leading Edge, v. 21, p. 174-177.

Bowers, G. L., and T. J. Katsube, 2001, The Role of Shale Pore Structure on the Sensitivity of Wire-Line Logs to Overpressure, *in* A. Huffman, and G. Bowers, eds., AAPG Memoir 76: Pressure Regimes in Sedimentary Basins and Their Prediction, American Association of Petroleum Geologists.

Bradley, J. S., 1975, Abnormal formation pressure: AAPG Bulletin, v. 59, p. 957-973.

Bradley, J. S., and D. E. Powley, 1994, Pressure compartments in sedimentary basins: a review.

Bramkamp, R. A., and R. W. Powers, 1955, Two Persian Gulf Lagoons: Journal of Sedimentary Research, v. 25, p. 139-A-140.

British Petroleum, 2014, Statistical Review of World Energy 2014.

Brocher, T. M., 2005, Empirical Relations between Elastic Wavespeeds and Density in the Earth's Crust: Bulletin of the Seismological Society of America, v. 95, p. 2081-2092.

Broni-Bediako, E., and R. Amorin, 2010, Effects of Drilling Fluid Exposure to Oil and Gas Workers Presented with Major Areas of Exposure and Exposure Indicators: Research Journal of Applied Sciences, Engineering and Technology, p. 710-719.

Brown, A., 1997, Porosity Variation in Carbonates as a Function of Depth: Mississippian Madison Group, Williston Basin: AAPG Special Volumes, v. 69.

Bruce, B., and G. Bowers, 2002, Pore Pressure Terminology: The Leading Eadge.

Budd, D. A., 2001, Permeability Loss with Depth in the Cenozoic Carbonate Platform of West-Central Florida: AAPG Bulletin, v. 85, p. 1253-1272.

Budd, D. A., 2002, The Relative Roles of Compaction and Early Cementation in the Destruction of Permeability in Carbonate Grainstones: A Case Study from the Paleogene of West-Central Florida, U.S.A: Journal of Sedimentary Research, v. 72, p. 116-128.

Burley, S., J. t. Mullis, and A. Matter, 1989, Timing diagenesis in the Tartan Reservoir (UK North Sea): constraints from combined cathodoluminescence microscopy and fluid inclusion studies: Marine and Petroleum Geology, v. 6, p. 98-120.

Burrus, J., 1998, Overpressure models for clastic rocks, their relation to hydrocarbon expulsion: a critical reevaluation: Memoirs-American Association of Petroleum Geologists, p. 35-64.

Burrus, J., K. Osadetz, S. Wolf, B. Doligez, K. Visser, and D. Dearborn, 1996, A two-dimensional regional basin model of Williston Basin hydrocarbon systems: AAPG bulletin, v. 80, p. 265-290.

Burst, J. F., 1969, Diagenesis of Gulf Coast clayey sediments and its possible relation to petroleum migration: AAPG Bulletin, v. 53, p. 73-93.

Buryakovskiy, L. A., R. D. Djevanshir, and G. V. Chilingarian, 1991, Mathematical simulation of sediment compaction: Journal of Petroleum Science and Engineering, v. 5, p. 151-161.

Buryakovsky, L. A., R. D. Djevanshir, G. V. Chilingar, H. H. Rieke Iii, and J. O. Robertson Jr, 2002, Chapter 4 Smectite-illite transformations during diagenesis and catagenesis as related to overpressures, *in* V. A. S. G.V. Chilingar, and J. O. Robertson, eds., Origin and Prediction of Abnormal Formation Pressures, v. Volume 50, Elsevier, p. 97-122.

Caenn, R., and G. V. Chillingar, 1996, Drilling fluids: State of the art: Journal of Petroleum Science and Engineering, v. 14, p. 221-230.

Caillet, G., 1993, The caprock of the Snorre Field, Norway: a possible leakage by hydraulic fracturing: Marine and Petroleum Geology, v. 10, p. 42-50.

Calladine, C. R., 1986, Gaussian curvature and shell structures, The mathematics of surfaces: Oxford, Clarendon Press.

Cannon, G. E., and R. C. Craze, 1938, Excessive Pressures and Pressure Variations with Depth of Petroleum Reservoirs in the Gulf Coast Region of Texas and Louisiana.

Cannon, G. E., and R. S. Sullins, 1946, Problems Encountered In Drilling Abnormal Pressure Formations, American Petroleum Institute.

Carstens, H., and H. Dypvik, 1981, Abnormal formation pressure and shale porosity: AAPG Bulletin, v. 65, p. 344-350.

Chanson, H., 1999, The hydraulics of open channel flow : an introduction: London, Arnold.

Chatterjee, A., S. Mondal, P. Basu, and B. K. Patel, 2012, Pore Pressure Prediction Using Seismic Velocities for Deepwater High Temperature- High Pressure Well in Offshore Krishna Godavari Basin, India, SPE Oil and Gas India Conference and Exhibition, Mumbai, India, Society of Petroleum Engineers.

Cheng, C. H., and M. N. Toksöz, 1979, Inversion of seismic velocities for the pore aspect ratio spectrum of a rock: Journal of Geophysical Research: Solid Earth, v. 84, p. 7533-7543.

Chierici, G. L., G. Ciucci, M., G. Sclocchi, and L. Terzi, 1978, Water Drive From Interbedded Shale Compaction In Sup.erPressured Gas Reservoirs —A Model Study: JOURNALOFPETROLWM TECHNOLOGY, p. 937-946.

Chilingar, G. V., H. J. Bissell, and K. H. Wolf, 1979, DIAGENESIS OF CARBONATE SEDIMENTS AND EPIGENESIS: Diagenesis in sediments and sedimentary rocks, v. 25, p. 247.

Chilingar, G. V., J. O. Robertson Jr, and H. H. Rieke Iii, 2002, Chapter 2 Origin of abnormal formation pressures, *in* V. A. S. G.V. Chilingar, and J. O. Robertson, eds., Origin and Prediction of Abnormal Formation Pressures, v. Volume 50, Elsevier, p. 21-67.

Choquette, P. W., and L. C. Pray, 1970, Geologic nomenclature and classification of porosity in sedimentary carbonates: AAPG bulletin, v. 54, p. 207-250.

Christensen, N. I., and W. D. Mooney, 1995, Seismic velocity structure and composition of the continental crust: A global view: Journal of Geophysical Research: Solid Earth, v. 100, p. 9761-9788.

Connolly, C. A., L. M. Walter, H. Baadsgaard, and F. J. Longstaffe, 1990, Origin and evolution of formation waters, Alberta Basin, Western Canada sedimentary Basin. I. Chemistry: Applied Geochemistry, v. 5, p. 375-395.

Conybeare, D. M., and H. F. Shaw, 2000, Fracturing, overpressure release and carbonate cementation in the Everest Complex, North Sea: Clay Minerals, v. 35, p. 135-149.

Coogan, A. H., 1970, Measurements of compaction in oolitic grainstone: Journal of Sedimentary Research, v. 40.

Couzens-Schultz, B. A., and K. Azbel, 2014, Predicting pore pressure in active fold–thrust systems: An empirical model for the deepwater Sabah foldbelt: Journal of Structural Geology, v. 69, p. 465-480.

Cox, B., L. A. Romo, B. D. Champion, K. D. Card, S. P. Barton, and Z. Maung, 2007, Extreme Drilling Environment Forces Evolution of Rotary Steerable Systems and Rotary Steerable Bit Technology: SPE/IADC Drilling Conference.

Cox, S. F., 1995, Faulting processes at high fluid pressures: an example of fault valve behavior from the Wattle Gully Fault, Victoria, Australia: Journal of Geophysical Research: Solid Earth, v. 100, p. 12841-12859.

Craig, D., 1988, Caves and Other Features of Permian Karst in San Andres Dolomite, Yates Field Reservoir, West Texas, *in* N. James, and P. Choquette, eds., Paleokarst, Springer New York, p. 342-363.

Croizé, D., K. Bjørlykke, J. Jahren, and F. Renard, 2010, Experimental mechanical and chemical compaction of carbonate sand: Journal of Geophysical Research: Solid Earth, v. 115, p. B11204.

Cui, H., 2012, Carbonate Diagenesis (stories behind the microscopic images), University of Maryland.

Daniel, R. B., 2001, Pressure prediction for a Central Graben wildcat well, UK North Sea: Marine and Petroleum Geology, v. 18, p. 235-250.

Darby, D., and R. H. Funnell, 2001, Overpressure associated with a convergent plate margin: East Coast Basin, New Zealand: Petroleum Geoscience, v. 7, p. 291-299.

Darcy, H., 1856, The Public Fountains of the City of Dijon, Paris.

Dehghani, G. A., and J. Makris, 1983, The gravity field and crustal structure of Iran, Geodynamics project (geotraverse) in Iran, Geological Survey of Iran, p. 51-68.

Delhomme, J. P., 2007, The quest for permeability evaluation in wireline logging Aquifer systems management; Darcy's legacy in a world of impending water shortage: London, UK, Taylor & Francis Group.

DELLWIG, L. F., 1955, ORIGIN OF THE SALINA SALT OF MICHIGAN: Journal of Sedimentary Petrology, v. 25, p. 83-110.

DeMets, C., R. G. Gordon, and D. F. Argus, 2010, Geologically current plate motions: Geophysical Journal International, v. 181, p. 1-80.

DeMets, C., R. G. Gordon, D. F. Argus, and S. Stein, 1990, Current Plate Motions: Geophysical Journal International, v. 101, p. 425-478.

Derby, J. R., 1984, Exploration for Carbonate Reservoirs or.

Detournay, E., and A. H.-D. Cheng, 1993, Fundamentals of Poroelasticity, *in* C. Fairhurst, ed., Emmanuel Detournay and Alexander H.-D. Cheng, v. II, Analysis and Design Method Pergamon Press, p. 113-171.

Devereux, S., 1998, Practical Well Planning and Drilling Manual, PennWell.

Devine, P. E., 2014, Toward Understanding Overpressure in a Basin with Burial and Uplift: Preliminary Results of a Study Measuring Undercompaction with DT Logs, Society of Petroleum Engineers.

Dewey, J. F., M. L. Helman, S. D. Knott, E. Turco, and D. H. W. Hutton, 1989, Kinematics of the western Mediterranean: Geological society, London, Special Publications, v. 45, p. 265-283.

Dewey, J. M., 1947, The Elastic Constants of Materials Loaded with Non-Rigid Fillers: Journal of Applied Physics, v. 18, p. 578-581.

Dickinson, G., 1951, Geological Aspects of Abnormal Reservoir Pressures in the Gulf Coast Region of Louisiana, U.S.A, World Petroleum Congress.

Dickinson, G., 1953, Geological Aspects of Abnormal Reservoir Pressure in Gulf Coast Luisiana: AAPG Bulletin, v. 37, p. 410-432.

Dobrynin, V., and V. Serebryakov, 1978, Methods for Prediction of Abnormally-High Formation Pressure: Nedra, Moscow, v. 231.

Dravis, J. J., and I. D. Muir, 1993, Deep-Burial Brecciation in the Devonian Upper Elk Point Group, Rainbow Basin, Alberta, Western Canada, Paleokarst Related Hydrocarbon Reservoirs, v. 18, SEPM Society for Sedimentary Geology, p. 119-166.

Dunham, R. J., 1962, Classification of carbonate rocks according to depositional textures.

Durney, D. W., 1972, Solution-transfer, an important geological deformation mechanism: Nature, v. 235, p. 315-317.

Dutta, N. C., 2002, Deepwater geohazard prediction using prestack inversion of large offset P-wave data and rock model: The Leading Edge, v. 21, p. 193-198.

Dvorkin, J., and M. Prasad, 2001, Velocity To Porosity Transform In Marine Sediments.

Eaton, B. A., 1972, The Effect of Overburden Stress on Geopressure Prediction from Well Logs: SPE Journal of Petroleum Technology.

Eaton, B. A., 1975, The Equation for Geopressured Prediction from Well Logs, 50thAnnualFall Meetingof the Societyof Petroleum Engineers of AIME, Dallas, Texas.

England, W., A. Mackenzie, D. Mann, and T. Quigley, 1987, The movement and entrapment of petroleum fluids in the subsurface: Journal of the Geological Society, v. 144, p. 327-347.

Enos, P., and L. H. Sawatsky, 1981, Pore Networks in Holocene Carbonate Sediments: Journal of Sedimentary Petrology, v. 51, p. 961-985.

Falcon, N. L., 1961, Major Earth-Flexuring in the Zagros Mountains of South-West Iran: Quarterly Journal of the Geological Society, v. 117, p. 367-376.

Falcon, N. L., 1974, Southern Iran: Zagros Mountains: Geological Society, London, Special Publications, v. 4, p. 199-211.

Fall, A., P. Eichhubl, S. P. Cumella, R. J. Bodnar, S. E. Laubach, and S. P. Becker, 2012, Testing the basin-centered gas accumulation model using fluid inclusion observations: Southern Piceance Basin, Colorado: AAPG bulletin, v. 96, p. 2297-2318.

Fatt, I., 1953, The Effect of Overburden Pressure on Relative Permeability.

Fatt, I., 1958, Compressibility of Sandstones at Low to Moderate Pressures: AAPG Bulletin, v. 42.

Fertl, W. H., 1976, Abnormal formation pressures : implications to exploration, drilling, and production of oil and gas resources / Walter H. Fertl, with a contribution by George V. Chilingarian and Herman H. Rieke, III: Amsterdam, New York, Elsevier Scientific Pub. Co.

Fertl, W. H., 1980, Evaluation Of Fractured Reservoir Rocks Using Geophysical Well Logs, SPE Unconventional Gas Recovery Symposium, Pittsburgh, Pennsylvania, Society of Petroleum Engineers.

Fertl, W. H., R. E. Chapman, and R. F. Hotz, 1994, Studies in abnormal pressures / edited by Walter H. Fertl, Richard E. Chapman, and Rod F. Hotz: Amsterdam, New York, Elsevier.

Fertl, W. H., and G. V. Chilingarian, 1977, Importance of Abnormal Formation Pressures (includes associated paper 6560): Journal of Petroleum Technology, v. 29, p. 347-354.

Fertl, W. H., and G. V. Chilingarian, 1987, Abnormal Formation Pressures and Their Detection by Pulsed Neutron Capture Logs: Journal of Petroleum Science and Engineering, v. 1, p. 23-38.

Fertl, W. H., and P. A. Wichmann, 1977, How to determine static BHT from well log data: Journal Name: World Oil; (United States); Journal Volume: 184:1, p. Medium: X; Size: Pages: 105-106.

Feyzullayev, A., and I. Lerche, 2009, Occurrence and nature of overpressure in the sedimentary section of the South Caspian Basin, Azerbaijan: Energy, Exploration & Exploitation, v. 27, p. 345-366.

Field D Owner, 2003, Well D-4 Geological Analysis.

Field D Owner, 2004, Well D-6 Stratigraphic & Sedimentological Characterisation of the Cored Intervals.

Field D Owner, 2005, Well D-14 Integrated Formation Evaluation.

Fillippone, W. R., 1982, Estimation of Formation Parameters And the Prediction of Overpressures From Seismic Data.

Finkbeiner, T., M. Zoback, P. Flemings, and B. Stump, 2001, Stress, Pore Pressure, and Dynamically Constrained Hydrocarbon Columns in the South Eugene Island 330 Field, Northern Gulf of Mexico: AAPG Bulletin, v. 85, p. 1007-1031.

Fischer, M. P., and M. S. Wilkerson, 2000, Predicting the orientation of joints from fold shape: Results of pseudo–three-dimensional modeling and curvature analysis: Geology, v. 28, p. 15-18.

Folk, R. L., 1959, Practical petrographic classification of limestones: AAPG Bulletin, v. 43, p. 1-38.

Folk, R. L., 1974, The natural history of crystalline calcium carbonate: effect of magnesium content and salinity: Journal of Sedimentary Research, v. 44.

Gaarenstroom, L., R. Tromp, and A. BRANDENBURG, 1993, Overpressures in the Central North Sea: implications for trap integrity and drilling safety: Geological Society, London, Petroleum Geology Conference series, p. 1305-1313.

Gardner, G. H. F., G. L.W., and G. A.R., 1974, Formation velocity and density - the diagnostic basics for stratigraphic traps: Geophysics v. 39, p. 770–780.

Garrison, R. E., 1981, Diagenesis of oceanic carbonate sediments: a review of the DSDP perspective.

Geertsma, J., 1957, A remark on the analogy between thermoelasticity and the elasticity of saturated porous media: Journal of the Mechanics and Physics of Solids, v. 6, p. 13-16.

Ghazi, M., G. Quaranta, J. Duplay, R. Hadjamor, M. Khodja, H. A. Amar, and Z. Kessaissia, 2011, Life-Cycle Impact Assessment of oil drilling mud system in Algerian arid area: Resources, Conservation and Recycling, v. 55, p. 1222-1231.

Ghorbani, M., 2002, A preamble to the economic geology of Iran (Translated from Persian).

Giles, M. R., 1987, Mass-Transfer and Problems of Secondary Porosity Creation in Deeply Buried Hydrocarbon Reservoirs: Marine and Petroleum Geology, v. 4, p. 188-204.

Giles, M. R., 1997, Diagenesis : a quantitative perspective : implications for basin modelling and rock property prediction, Dordrecht ;, Kluwer Academic Publishers.

Giles, M. R., S. L. Indrelid, and D. M. D. James, 1998, Compaction - The Great Unknown in Basin Modelling: Geological society, London, Special Publications, v. 141.

Gill, W. D., and M. A. Ala, 1972, Sedimentology of Gachsaran Formation (Lower Fars Series), Southwest Iran: AAPG Bulletin, v. 56, p. 1965-1974.

Godfrey, N., B. Beaudoin, S. Klemperer, and M. W. Group, 1997, Ophiolitic basement to the Great Valley forearc basin, California, from seismic and gravity data: Implications for crustal growth at the North American continental margin: Geological Society of America Bulletin, v. 109, p. 1536-1562.

Goldhammer, R. K., 1997, Compaction and decompaction algorithms for sedimentary carbonates: Journal of Sedimentary Research, v. 67, p. 26-35.

Goodwyne, O. K., 2012, Pressure prediction and underbalanced drilling in the deepwater niger delta, Durham University, United Kingdom.

Gordon, D. S., and P. B. Flemings, 1998, Generation of overpressure and compaction-driven fluid flow in a Plio-Pleistocene growth-faulted basin, Eugene Island 330, offshore Louisiana: Basin Research, v. 10, p. 177-196.

Goulty, N. R., 1998, Relationships Between Porosity and Effective Stress in Shales: First Break (European Association of Geoscientists and Engineers), v. 16.

Grauls, D., and J. Baleix, 1994, Role of overpressures and in situ stresses in fault-controlled hydrocarbon migration: a case study: Marine and Petroleum Geology, v. 11, p. 734-742.

Grauls, D., and C. Cassignol, 1993, Identification of a zone of fluid pressure-induced fractures from log and seismic data-a case history: First Break, v. 11.

Green, D. H., and H. F. Wang, 1986, Fluid Pressure Response to Undrained Compression in Saturated Sedimentary-Rock: Geophysics, v. 51, p. 948-956.

Gressier, J.-B., R. Mourgues, L. Bodet, J.-Y. Matthieu, O. Galland, and P. Cobbold, 2010, Control of pore fluid pressure on depth of emplacement of magmatic sills: An experimental approach: Tectonophysics, v. 489, p. 1-13.

Gretener, P. E., 1981, Pore Pressure: Fundamentals, General Ramification and Implications for Structural Geology: Education course note series AAPG Dept. of Education

Gruenwald, R. M., J. Buitrago, J. Dessay, A. Huffman, C. Moreno, J. M. G. Munoz, C. Diaz, and K. S. Tawengi, 2010, Pore Pressure Prediction Based on High Resolution Velocity Inversion in Carbonate Rocks, Offshore Sirte Basin - Libya: AAPG Annual Convention & Exhibition.

Gutierrez, M. A., N. R. Braunsdor, and B. A. Couzens, 2006, Calibration and ranking of pore-pressure prediction models: The Leading Edge, v. 25, p. 1516-1523.

Haghi Pour, A., and A. Aghanabati, 1988, Geological Map of Iran (1:2500000): Geological Survey of Iran.

Hall, H. N., 1953a, Compressibility of Reservoir Rocks: Journal of Petroleum Technology, v. 5, p. 17-19.

Hall, H. N., 1953b, Compressibility of Reservoir Rocks.

Hamilton, E. L., 1978, Sound velocity–density relations in sea-floor sediments and rocks: The Journal of the Acoustical Society of America, v. 63, p. 366-377.

Hanshaw, B. B., and J. D. Bredehoeft, 1968, On the Maintenance of Anomalous Fluid Pressures: II. Source Layer at Depth: Geological Society of America Bulletin, v. 79, p. 1107.

Hardie, L. A., 1965, Phase equilibria involving minerals of the system $CaSO_4$ - Na_2SO_4 - H_2O, The Johns Hopkins University, Baltimore, Md.

Hardie, L. A., 1967, The Gypsum-Anhydrite Equilibrium at One Atmosphere Pressure: The American Mineralogist, v. 52, p. 171-200.

Harris, W. H., and R. Matthews, 1968, Subaerial diagenesis of carbonate sediments: efficiency of the solution-reprecipitation process: Science, v. 160, p. 77-79.

Harrold, T. W. D., R. E. Swarbrick, and N. R. Goulty, 1999, Pore Pressure Estimation from Mudrock Porosities in Tertiary Basins, Southeast Asia: AAPG Bulletin, v. 83, p. 1057-1067.

Hart, B. S., P. B. Flemings, and A. Deshpande, 1995, Porosity and Pressure - Role of Compaction Disequilibrium in the Development of Geopressures in a Gulf-Coast Pleistocene Basin: Geology, v. 23, p. 45-48.

Hasegawa, H. S., J. Adams, and K. Yamazaki, 1985, Upper crustal stresses and vertical stress migration in eastern Canada: Journal of Geophysical Research: Solid Earth, v. 90, p. 3637-3648.

Hassanzadegan, A., R. Guérizec, T. Reinsch, G. Blöcher, G. Zimmermann, and H. Milsch, 2016, Static and Dynamic Moduli of Malm Carbonate: A Poroelastic Correlation: Pure and Applied Geophysics, p. 1-15.

Haugland, M., J. Zhang, R. Sarker, A. Axon, K. Azbel, R. Wilhelm, B. Couzens-Schultz, B. Tichelaar, J. Wieseneck, K. Hansen, and I. Zhang, 2013, Pore Pressure Prediction in Unconventional Resources, 6th International Petroleum Technology Conference, Beijing, China, 2013, International Petroleum Technology Conference.

Hedberg, H. D., 1926, The effect of gravitational compaction on the structure of sedimentary rocks: AAPG Bulletin, v. 10, p. 1035-1072.

Hedberg, H. D., 1936, Gravitational compaction of clays and shales: American Journal of Science, v. Series 5 Vol. 31, p. 241-287.

Hedberg, H. D., 1974, Relation of methane generation to undercompacted shales, shale diapirs, and mud volcanoes: AAPG Bulletin, v. 58, p. 661-673.

Hedberg, H. D., 1978, Methane Generation and Petroleum Migration.

Hedberg, H. D., 1980, Methane generation and petroleum migration.

Henning, A., N. Yassir, A. A. Addis, and A. Warrington, 2002, Pore-Pressure Estimation in an Active Thrust Region and Its Impact on Exploration and Drilling, *in* A. R. Huffman, and G. L. Bowers, eds., Pressure Regimes in Sedimentary Basins and Their Prediction, v. AAPG Memoir 76, p. 89-105.

Hermanrud, C., L. Wensaas, G. M. G. Teige, H. M. Nordgard Bolas, S. Hansen, and E. Vik, 1998, Shale Porosities from Well Logs on Haltenbanken (Offshore Mid-Norway) Show No Influence of Overpressuring, *in* B. E. Law, G. F. Ulmishek, and V. I. Slavin, eds., AAPG Memoir 70: Abnormal Pressures in Hydrocarbon Environments, The American Association of Petroleum Geologists, p. 65 - 85.

Hessami, K., H. A. Koyi, C. J. Talbot, H. Tabasi, and E. Shabanian, 2001, Progressive unconformities within an evolving foreland fold-thrust belt, Zagros Mountains: Journal of the Geological Society, v. 158, p. 969-981.

Heydari, E., 2000, Porosity Loss, Fluid Flow, and Mass Transfer in Limestone Reservoirs: Application to the Upper Jurassic Smackover Formation, Mississippi: AAPG Bulletin, v. 84, p. 100-118.

Hoesni, M. J., 2004, Origins of overpressure in the Malay Basin and its influence on petroleum systems Durham University.

Holbrook, P. W., D. A. Maggiori, and R. Hensley, 1995, Real-Time Pore Pressure and Fracture Gradient Evaluation in All Sedimentary Lithologies: SPE Formation Evaluation.

Hooyman, P. J., C. M. Sayers, A. Malinverno, N. Smirnov, G. Fiume, A. Prince, J. C. d. L. Mojarro, M. T. Romero, and O. M. Gonzalez, 2003, Calibrated Predrill Pore Pressure Prediction from 3D Seismic for the Cocuite Field, Veracruz Basin, Offshore Technology Conference, Houston, Texas.

Horne, R. N., 1997, Modern well test analysis [electronic resource] : a computer-aided approach: Palo Alto, CA, Palo Alto, CA : Petroway.

Hospers, J., 1971, The Geology of the Niger Delta Area, H.M. Stationery Office.

Hottmann, C. E., and R. K. Johnson, 1965, Estimation of Formation Pressures from Log-Derived Shale Properties: Journal of Petroleum Technology, v. 17, p. 717-722.

Howard, W. V., 1928, A Classification of Limestone Reservoirs: AAPG Bulletin, v. 12, p. 1153-1161.

Howard, W. V., and M. W. David, 1936, Development of porosity in limestones: AAPG Bulletin, v. 20, p. 1389-1412.

HOWER, J., E. V. ESLINGER, M. E. HOWER, and E. A. PERRY, 1976, Mechanism of burial metamorphism of argillaceous sediment: 1. Mineralogical and chemical evidence: Geological Society of America Bulletin, v. 87, p. 725-737.

Hubbert, M. K., and W. W. Rubey, 1961, Role Of Fluid Pressure In Mechanics Of Overthrust Faulting, The Geological Society of America, Inc.

Huffman, A., 2013, Geophysical Pore Pressure Prediction in Complex Geologic Environments, Offshore Libya, 2013 Offshore Technology Conference, Houston, TX, USA.

Huffman, A. R., J. S. Meyer, R. M. Gruenwald, J. Buitrago, J. Suarez, C. Diaz, J. M. Munoz, and J. Dessay, 2011, Recent Advances in Pore Pressure Prediction In Complex Geologic Environments, SPE Middle East Oil and Gas Show and Conference, Manama, Bahrain, Society of Petroleum Engineers.

Hurai, V., M. Huraiová, M. Slobodník, and R. Thomas, 2015, Geofluids: Developments in Microthermometry, Spectroscopy, Thermodynamics, and Stable Isotopes, Elsevier.

Hyams, D., 2009, CurveExpert.

Imbt, W. C., and S. P. Ellison, 1946, Porosity In Limestone And Dolomite Petroleum Reservoir, Drilling and Production Practice, New York, American Petroleum Institute.

Ingraffea, A. R., 1987, 3 - THEORY OF CRACK INITIATION AND PROPAGATION IN ROCK, *in* B. K. Atkinson, ed., Fracture Mechanics of Rock: London, Academic Press, p. 71-110.

International Seismological Centre, 2014, Event Catalogue, Thatcham, United Kingdom, Internatl. Seis. Cent.

Ireland, T., J. Joseph, N. Colley, S. Richardson, P. Reignier, T. Zimmerman, A. Hastings, and I. Traboulay, 1992, The MDT Tool: A Wireline Testing Breakthrough: Oilfield Review, p. 58-65.

Issler, D. R., 1992, A New Approach to Shale Compaction and Stratigraphic Restoration, Beaufort-Mackenzie Basin and Mackenzie Corridor, Northern Canada: AAPG Bulletin-American Association of Petroleum Geologists, v. 76, p. 1170-1189.

Jalalh, A. A., 2006, Compressibility of porous rocks: Part II. New relationships: Acta Geophysica, v. 54, p. 399-412.

James, G. A., and J. G. Wynd, 1965, Stratigraphic nomenclature of Iranian Oil Consortium Agreement Area: AAPG Bulletin, v. 49, p. 2182-2245.

James, N. P., and P. W. Choquette, 1983, Diagenesis 6. Limestones — The Sea Floor Diagenetic Environment: 1983.

Jenkins, S., R. Swarbrick, A. Mallon, and S. O'Connor, 2012, Pressure in Miocene carbonate exploration targets: INDONESIAN PETROLEUM ASSOCIATION Thirty-Sixth Annual Convention & Exhibition,.

Johnson, P. R., and I. C. F. Stewart, 1995, Magnetically Inferred Basement Structure in Central Saudi-Arabia: Tectonophysics, v. 245, p. 37-52.

Jones, P. H., 1969, Hydrodynamics of Geopressure in the Northern Gulf of Mexico Basin: Journal of Petroleum Technology.

Jowett, E. C., L. M. Cathles, and B. W. Davis, 1993, Predicting Depths of Gypsum Dehydration in Evaporitic Sedimentary Basins: AAPG Bulletin-American Association of Petroleum Geologists, v. 77, p. 402-413.

Kadyrov, T., and A. Tutuncu, 2012, Sonic Log-derived Pore Pressure Prediction in a West Kazakhstan Dolomite Field: 74th EAGE Conference and Exhibition incorporating EUROPEC 2012.

Katahara, K., 2003, Analysis of Overpressure on the Gulf of Mexico Shelf, Offshore Technology Conference, Houston, Texas.

Katahara, K., 2006, Overpressure And Shale Properties: Stress Unloading Or Smectite-illite Transformation?, Society of Exploration Geophysicists.

Katahara, K., 2007, Overpressure and shale properties: Stress unloading or smectite-illite transformation?, 2006 SEG Meeting, p. expanded abstract PPP 1.2.

Katahara, K., 2008, What is shale to a petrophysicist?: The Leading Edge, v. 27, p. 738-741.

Katahara, K., and J. Corrigan, 2001, AAPG Memoir 76, Chapter 7: Effect of Gas on Poroelastic Response to Burial or Erosion.

Kendall, C. G. S. C., and W. Schlager, 1981, Carbonates and relative changes in sea level: Marine Geology, v. 44, p. 181-212.

Kerans, C., 1990, Depositional systems and karst geology of the Ellenburger Group (Lower Ordovician), subsurface West Texas.

Kerans, C., 1993, Description and interpretation of karst-related breccia fabrics, Ellenburger Group, West Texas.

King Hubbert, M., and W. W. Rubey, 1959, Role of Fluid Pressure in Mechanics of Overthrust Faulting: Geological Society of America Bulletin, v. 70, p. 115.

King, R. C., M. Neubauer, R. R. Hillis, and S. D. Reynolds, 2010, Variation of vertical stress in the Carnarvon Basin, NW Shelf, Australia: Tectonophysics, v. 482, p. 73-81.

Kinsman, D. J. J., 1965, Dolomitization and evaporite development, including anhydrite in lagoonal sediments, Persian Gulf: The Geological Society of America, p. 108-109.

Koepnick, R. B., 1984, Distribution and vertical permeability of stylolites within a lower Cretaceous carbonate reservoir, Abu Dhabi, United Arab Emirates: Stylolites and Associated Phenomena: Relevance to Hydrocarbon Reservoirs, Abu Dhabi National Reservoir Foundation Special Publication, p. 261-278.

Koepnick, R. B., 1987, Distribution and Permeability of Stylolite-Bearing Horizons Within a Lower Cretaceous Carbonate Reservoir in the Middle East: SPE Formation Evaluation, v. 2, p. 137 - 142.

Krushin, J., 2013, A True Shale Compaction Model With Pore Pressure Prediction, 2013 Offshore Technology Conference, Houston, TX, USA.

Kulander, B., S. Dean, and B. Ward Jr, 1990, Natural Fractures in Core: Chapter 2.

Lacombe, O., K. Amrouch, F. Mouthereau, and L. Dissez, 2007, Calcite twinning constraints on late Neogene stress patterns and deformation mechanisms in the active Zagros collision belt: Geology, v. 35, p. 263-266.

Lahann, R., 2000, Impact of diagenesis on compaction modeling and compaction equilibrium, Drilling and exploiting overpressured reservoirs: A research workshop for the millennium; April 4-6, 2000: London, UK.

Lahann, R. W., D. K. McCarty, and J. C. C. Hsieh, 2001, Influence of Clay Diagenesis on Shale Velocities and Fluid-Pressure, Offshore Technology Conference, Houston, Texas.

Lahann, R. W., and R. E. Swarbrick, 2011, Overpressure generation by load transfer following shale framework weakening due to smectite diagenesis: Geofluids, v. 11, p. 362-375.

Land, L. S., 1967, Diagenesis of skeletal carbonates: Journal of Sedimentary Research, v. 37.

Lash, G. G., and T. Engelder, 2005, An analysis of horizontal microcracking during catagenesis: Example from the Catskill delta complex: AAPG bulletin, v. 89, p. 1433-1449.

Law, B. E., J. R. Hatch, G. C. Kukal, and C. W. Keighin, 1983, Geologic implications of coal dewatering: AAPG Bulletin, v. 67, p. 2255-2260.

Lee, M.-K., and D. D. Williams, 2000, Paleohydrology of the Delaware Basin, Western Texas: Overpressure Development, Hydrocarbon Migration, and Ore Genesis: AAPG Bulletin, v. 84, p. 961-974.

Lee, Y., and D. Deming, 2002, Overpressures in the Anadarko Basin, Southwestern Oklahoma: Static or Dynamic?: AAPG Bulletin, v. 86, p. 145-160.

Leftwich Jr, J. T., and T. Engelder, 1994, The characteristics of geopressure profiles in the Gulf of Mexico Basin.

Leturmy, P., and C. Robin, 2010, Tectonic and stratigraphic evolution of Zagros and Makran during the Mesozoic-Cenozoic: introduction: Geological Society, London, Special Publications, v. 330, p. 1-4.

Li Menggang, Z. H., Niu Chengcheng, 2015, Casing Program Optimization and Application in Complex Formation of the YD Oilfield Drilling Petroleum Techniques.

Li, Z. H., T. V. Gerya, and J. P. Burg, 2010, Influence of tectonic overpressure on P–T paths of HP–UHP rocks in continental collision zones: thermomechanical modelling: Journal of Metamorphic Geology, v. 28, p. 227-247.

Lindberg, P., R. Riise, and W. H. Fertl, 1980, OCCURRENCE AND DISTRIBUTION OF OVERPRESSURES IN THE NORTHERN NORTH SEA AREA, SPE Annual Technical Conference and Exhibition, Dallas, Texas, 1980 Copyright 1980, American Institute of Mining, Metallurgical, and Petroleum Engineers, Inc.

Lisle, R. J., 1995, Detection of zones of abnormal strains in structures using Gaussian curvature analysis: American Association of Petroleum Geologists Bulletin, v. 78, p. 1811–1819.

Liu, H.-H., J. Rutqvist, and J. Berryman, 2009, On therelationshipbetweenstressandelasticstrainforporous and fracturedrock: International Journalof RockMechanics&MiningSciences, v. 46.

Longman, M. W., 1985, Fracture porosity in reef talus of a Miocene pinnacle-reef reservoir, Nido B Field, the Philippines, Carbonate Petroleum Reservoirs, Springer, p. 547-560.

Loucks, R. G., and P. Mescher, 2001, Paleocave facies classification and associated pore types, American Association of Petroleum Geologists, Southwest Section, Annual Meeting, Dallas, Texas,.

Loucks, R. G., P. K. Mescher, and G. A. McMechan, 2004, Three-dimensional architecture of a coalesced, collapsed-paleocave system in the Lower Ordovician Ellenburger Group, central Texas: AAPG Bulletin, v. 88, p. 545-564.

Lowery, J. D., 1984, Geologic Occurrence of Geopressured Reservoirs, Society of Petroleum Engineers.

Lucia, F. J., 1983, Petrophysical parameters estimated from visual descriptions of carbonate rocks: a field classification of carbonate pore space: Journal of Petroleum Technology, v. 35, p. 629-637.

Lucia, F. J., 1995, Lower Paleozoic cavern development, collapse, and dolomitization, Franklin Mountains, El Paso, Texas.

Lucia, F. J., 1999, Carbonate Reservoir Characterization, Springer.

Lucia, F. J., 2007, Carbonate reservoir characterization: an integrated approach, Springer Science & Business Media.

Lucia, F. J., and R. C. Murray, 1967, Origin and Distribution of Porosity in Crinoidal Rock, 7th World Petroleum Congress, Mexico City, Mexico, World Petroleum Congress.

Lucia, J. F., J. W. Jennings Jr., M. Rahnis, and F. O. Meyer, 2001, Permeability and rock fabric from wireline logs, Arab-D reservoir, Ghawar field, Saudi Arabia: GeoArabia, v. 6, p. 619-646.

Ludwig, W. J., J. E. Nafe, and C. L. Drake, 1970, Seismic refraction, in The Sea: A.E. Maxwell, v. 4, p. 53-84.

Lun, Z., C. Yefei, N. Zhengfu, W. Xuelin, L. Lifang, and C. Xi, 2013, Stress sensitive experiments for abnormal overpressure carbonate reservoirs: A case from the Kenkiyak fractured-porous oil field in the littoral Caspian Basin: PETROL. EXPLOR. DEVELOP, v. 40, p. 208–215.

Luo, M., M. R. Baker, and D. V. Lemone, 1994, Distribution and Generation of the Overpressure System, Eastern Delaware Basin, Western Texas and Southern New-Mexico: Aapg Bulletin-American Association of Petroleum Geologists, v. 78, p. 1386-1405.

Luo, X., W. Dong, J. Yang, and W. Yang, 2003, Overpressuring mechanisms in the Yinggehai basin, south China sea: AAPG bulletin, v. 87, p. 629-645.

Luo, X., Z. Wang, L. Zhang, W. Yang, and L. Liu, 2007, Overpressure generation and evolution in a compressional tectonic setting, the southern margin of Junggar Basin, northwestern China: AAPG Bulletin, v. 91, p. 1123-1139.

Luo, X. R., and G. Vasseur, 1992, Contributions of Compaction and Aquathermal Pressuring to Geopressure and the Influence of Environmental-Conditions: Aapg Bulletin-American Association of Petroleum Geologists, v. 76, p. 1550-1559.

Macdonald, G. J. F., 1953, Anhydrite-Gypsum Equilibrium Relations: American Journal of Science, v. 251, p. 884-898.

Mackenzie, J. K., 1950, The Elastic Constants of a Solid Containing Spherical Holes: Proceedings of the Physical Society of London Section B, v. 63, p. 2-11.

Magara, K., 1975, Reevaluation of montmorillonite dehydration as cause of abnormal pressure and hydrocarbon migration: AAPG Bulletin, v. 59, p. 292-302.

Magara, K., 1980, COMPARISON OF POROSITY-DEPTH RELATIONSHIPS OF SHALE AND SANDSTONE*: Journal of Petroleum Geology, v. 3, p. 175-185.

Magner, E., 1963, Porosity and Bulk Density of Sedimentary Rocks: U.S. Atomic Energy Commission: WASHINGTON.

Mann, D. M., and A. S. Mackenzie, 1990, Prediction of pore fluid pressures in sedimentary basins: Marine and Petroleum Geology, v. 7, p. 55-65.

Marine, I. W., and S. J. Fritz, 1981, Osmotic Model to Explain Anomalous Hydraulic Heads: Water Resources Research, v. 17, p. 73-82.

Matheron, G., 1973, The Intrinsic Random Functions and Their Applications: Advances in Applied Probability, v. 5, p. 439-468.

Mavko, G., and D. Jizba, 1991, Estimating Grain-Scale Fluid Effects on Velocity Dispersion in Rocks: Geophysics, v. 56, p. 1940-1949.

Mazzullo, S., 2004, Overview of porosity evolution in carbonate reservoirs: Kansas Geological Society Bulletin, v. 79, p. 20-28.

McClusky, S., S. Balassanian, A. Barka, C. Demir, S. Ergintav, I. Georgiev, O. Gurkan, M. Hamburger, K. Hurst, H. Kahle, K. Kastens, G. Kekelidze, R. King, V. Kotzev, O. Lenk, S. Mahmoud, A. Mishin, M. Nadariya, A. Ouzounis, D. Paradissis, Y. Peter, M. Prilepin, R. Reilinger, I. Sanli, H. Seeger, A. Tealeb, M. N. Toksöz, and G. Veis, 2000, Global Positioning System constraints on plate kinematics and dynamics in the eastern Mediterranean and Caucasus: Journal of Geophysical Research: Solid Earth, v. 105, p. 5695-5719.

McQuarrie, N., 2004, Crustal scale geometry of the Zagros fold–thrust belt, Iran: Journal of Structural Geology, v. 26, p. 519-535.

McQuillan, H., 1985, Fracture-controlled production from the Oligo-Miocene Asmari Formation in Gachsaran and Bibi Hakimeh fields, southwest Iran, Carbonate Petroleum Reservoirs, Springer, p. 511-523.

Meissner, F. F., 1984, Petroleum Geology of the Bakken Formation Williston Basin, North Dakota and Montana.

Melim, L. A., F. S. Anselmetti, and G. P. Eberli, 2001, The Importance of Pore Type on Permeability of Neogene Carbonates, Great Bahama Bank, Subsurface Geology of a Prograding Carbonate Platform Margin, Great Bahama Bank, v. 70, SEPM Society for Sedimentary Geology, p. 217-238.

Meunier, A., B. Velde, and B. Velde, 2004, Illite: origins, evolution, and metamorphism.

Miller, J. A., 1985, Depositional and reservoir facies of the Mississippian Leadville Formation, northwest Lisbon field, Utah, Carbonate Petroleum Reservoirs, Springer, p. 161-173.

Miller, T. W., C. H. Luk, and D. L. Olgaard, 2002, The interrelationships between overpressure mechanisms and in-situ stress, *in* A. R. Huffman, and G. L. Bowers, eds., Pressure regimes in sedimentary basins and their prediction: AAPG Memoir 76, p. 13-20.

Milliman, J. D., 1974, Marine carbonates, Springer.

Ministry of Environment Office British Columbia, 2010, Flowing Artesian Wells: Water Stewardship Information Series.

Moallemi, S. A., and M. Kermanshah, 2012, Significances of integrated study of Abadan Plain depositional basin (translated from Persian title): Exploration and Production, v. 94, p. 20-22.

Mohammadlou, M. H., and M. B. Mørk, 2012, Integrated Permeability Analysis in Tight and Brecciated Carbonate Reservoir.

Mokhtari, M., A. M. Farahbod, C. Lindholm, M. Alahyarkhani, and H. Bungum, 2004, An Approach to a Comprehensive Moho Depth Map and Crust and Upper Mantle Velocity Model for Iran: Iranian Int. J. Sci., v. 5, p. 223-244.

Molinaro, M., J. C. Guezou, P. Leturmy, S. A. Eshraghi, and D. F. de Lamotte, 2004, The origin of changes in structural style across the Bandar Abbas syntaxis, SE Zagros (Iran): Marine and Petroleum Geology, v. 21, p. 735-752.

Momper, J. A., 1980, Generation of Abnormal Pressures Through Organic Matter Transformations: ABSTRACT: AAPG Bulletin, v. 64, p. 753-753.

Moore, C. H., 1988, Upper Jurassic Smackover Platform Dolomitization Northwestern Gulf of Mexico a Tale of Two Waters.

Moore, C. H., 1989, Carbonate diagenesis and porosity, Elsevier.

Moore, C. H., 2001, Carbonate Reservoirs: Porosity, Evolution & Diagenesis in a Sequence Stratigraphic Framework: Porosity Evolution and Diagenesis in A Sequence Stratigraphic Framework, v. 55, Elsevier.

Moore, C. H., and W. J. Wade, 2013a, Chapter 5 - Carbonate Diagenesis: Introduction and Tools, *in* H. M. Clyde, and J. W. William, eds., Carbonate Reservoirs Porosity and Diagenesis in a Sequence Stratigraphic Framework, v. Volume 67, Elsevier, p. 67-89.

Moore, C. H., and W. J. Wade, 2013b, Chapter 10 - Burial Diagenetic Environment, *in* H. M. Clyde, and J. W. William, eds., Carbonate Reservoirs Porosity and Diagenesis in a Sequence Stratigraphic Framework, v. Volume 67, Elsevier, p. 239-284.

Moore, C. H., and W. J. Wade, 2013c, Chapter 11 - Natural Fracturing in Carbonate Reservoirs, *in* H. M. Clyde, and J. W. William, eds., Carbonate Reservoirs Porosity and Diagenesis in a Sequence Stratigraphic Framework, v. Volume 67, Elsevier, p. 285-300.

Morales Salazar, J. P., 2014, Geomecánica aplicada a la perforación de pozos en formaciones de lutitas y carbonatos utilizando datos sónicos y sísmicos, UNIVERSIDAD NACIONAL AUTÓNOMA DE MÉXICO, Mexico.

Morley, C., 1992, Hydrocarbon generation-a possible cause of elevated pore pressures in the Osen-Roa thrust sheet, Norway: Journal of structural geology, v. 14, p. 743-747.

Morris, P., 1977, Basement structure as suggested by aeromagnetic surveys in southwest Iran: Second Geological Symposium of Iran, p. 193-224.

Morris, R. C., and P. A. Dickey, 1957, Modern evaporite deposition in Peru: AAPG Bulletin, v. 41, p. 2467-2474.

Morton-Thompson, D., and A. M. Woods, 1992, Development Geology Reference Manual, American Association of Petroleum Geologists, 556 p.

Motiei, H., 1993, Petroleum Geology of Zagros (in Persian): Geology of Iran: Tehran, Iran, Geological Survey of Iran.

Motiei, H., 1995, Geology of Iran (in Persian): Tehran, Iran, Geological Survey of Iran.

Mouchet, J.-P., and A. Mitchell, 1989, Abnormal Pressures While Drilling: Origins, Prediction, Detection, Evaluation, v. 2, Editions Technip.

Mouthereau, F., O. Lacombe, J. Tensi, N. Bellahsen, S. Kargar, and K. Amrouch, 2007, Mechanical Constraints on the Development of the Zagros Folded Belt (Fars), *in* O. Lacombe, F. Roure, J. Lavé, and J. Vergés, eds., Thrust Belts and Foreland Basins: Frontiers in Earth Sciences, Springer Berlin Heidelberg, p. 247-266.

Mouthereau, F., O. Lacombe, and J. Vergés, 2012, Building the Zagros collisional orogen: Timing, strain distribution and the dynamics of Arabia/Eurasia plate convergence: Tectonophysics, v. 532–535, p. 27-60.

Murray, A. N., 1930, Limestone oil reservoirs of the northeastern United States and of Ontario, Canada: Economic Geology, v. 25, p. 452-469.

Murray, R. C., 1960, Origin of Porosity in Carbonate Rocks: SEPM Journal of Sedimentary Research, v. Vol. 30, p. 59-84.

Murris, R. J., 1980, Middle-East - Stratigraphic Evolution and Oil Habitat: AAPG Bulletin-American Association of Petroleum Geologists, v. 64, p. 597-618.

Nairn, A., and A. S. Alsharhan, 1997, Sedimentary Basins and Petroleum Geology of the Middle East: Burlington, Elsevier Science.

Narr, W., D. W. Schechter, and L. B. Thompson, 2006, Naturally fractured reservoir characterization, Richardson, TX: Society of Petroleum Engineers.

Nashaat, M., 1998, Abnormally High Formation Pressure and Seal Impacts on Hydrocarbon Accumulations in the Nile Delta and North Sinai Basins, Egypt, *in* B. E. Law, G. F. Ulmishek, and V. I. Slavin, eds., AAPG Memoir 70: Abnormal Pressures in Hydrocarbon Environments, The American Association of Petroleum Geologists, p. 161 - 180.

Neff, J. M., S. McKelvie, and J. R.C. Ayers, 2000, Environmental Impacts of Synthetic Based Drilling Fluids, New Orleans.

Nelson, R., 2001, Geologic analysis of naturally fractured reservoirs, Gulf Professional Publishing.

Neugebauer, J., 1973, The diagenetic problem of chalk - the role of pressure solution and pore fluid: Neues Jawbuch Geologie Palaeontologie Abhondlunge, v. 143, p. 223-245.

Neuzil, C. E., 1995, Abnormal Pressures as Hydrodynamic Phenomena: American Journal of Science, v. 295, p. 742-786.

Neuzil, C. E., 2000, Osmotic generation of 'anomalous' fluid pressures in geological environments: Nature, v. 403, p. 182-184.

Newman, G. H., 1973, Pore-Volume Compressibility of Consolidated, Friable, and Unconsolidated Reservoir Rocks Under Hydrostatic Loading: Journal of Petroleum Technology, v. 25, p. 129-134.

Niemann, J. C., 2002, Developing a more rigorous methodology for the determination of pressure from resistivity measurements: SEG/EAGE Summer Research Workshop - Geopressure: Conceptual Advances, applications, and Future Challenges.

Nilforoushan, F., F. Masson, P. Vernant, C. Vigny, J. Martinod, M. Abbassi, H. Nankali, D. Hatzfeld, R. Bayer, F. Tavakoli, A. Ashtiani, E. Doerflinger, M. Daignières, P. Collard, and J. Chéry, 2003, GPS network monitors the Arabia-Eurasia collision deformation in Iran: Journal of Geodesy, v. 77, p. 411-422.

Nordgren, R. P., 1972, Propagation of a Vertical Hydraulic Fracture: Society of Petroleum Engineers Journal, v. 12, p. 306-&.

Nunziato, J. W., and S. C. Cowin, 1979, A nonlinear theory of elastic materials with voids: Archive for Rational Mechanics and Analysis, v. 72, p. 175-201.

Nurmi, R., M. Charara, M. Waterhouse, and R. Park, 1990, Heterogeneities in carbonate reservoirs: detection and analysis using borehole electrical imagery: Geological Society, London, Special Publications, v. 48, p. 95-111.

O'connor, S., R. Swarbrick, S. Jenkins, S. Green, and P. Clegg, 2010, Modeling Pore Pressure Profiles in Carbonates, Geoscience Conference $ Exhibition, Manama, Bahrain.

O'Connor, S., R. Swarbrick, S. Jenkins, S. Green, and P. Clegg, 2010, Modeling Pore Pressure Profiles in Carbonates, AAPG GEO 2010 Middle East Geoscience Conference & Exhibition, Manama, Bahrain.

O'Connor, S., R. Swarbrick, and R. Lahann, 2011, Geologically-driven pore fluid pressure models and their implications for petroleum exploration. Introduction to thematic set: Geofluids, v. 11, p. 343-348.

Osborne, M. J., and R. E. Swarbrick, 1997a, How Overpressure and Diagenesis Interact in Sedimentary Basins – Consequences for Porosity Preservation in HPHT Reservoir Sandstones: International Conference on Petroleum Systems of SE Asia and Australasia.

Osborne, M. J., and R. E. Swarbrick, 1997b, Mechanisms for generating overpressure in sedimentary basins; a reevaluation: AAPG Bulletin, v. 81, p. 1023-1041.

Owen, E. R., 2008, One Hundred Years of Middle Eastern Oil, Middle East Brief, Massachusetts, Brandeis University, Crown Center for Middle East Studies.

Oxford English Dictionary, 2015, "osmosis, n.", Oxford University Press.

Paradigm, 2015, SKUA-GOCAD.

Parra, J., C. Hackert, and S. Pride, 2004, A Double–Porosity Poroelastic Model to Relate P–Wave Attenuation to Fluid Flow in Vuggy Carbonate Rock, *in* S. Ove, ed., Elsevier Geo-Engineering Book Series, v. Volume 2, Elsevier, p. 483-488.

Patrick, J. F., 2002, Consolidation and Settlement Analysis, The Civil Engineering Handbook, Second Edition: New Directions in Civil Engineering, CRC Press.

Pavlova, N. N., 1975, Deformation and Reservoir Properties of Rocks: Moscow, Nedra Publishing House, 240 p.

Pennebaker, E. S., 1968, An Engineering Interpretation of Seismic Data, Society of Petroleum Engineers.

Perry Jr, E. A., and J. Hower, 1972, Late-stage dehydration in deeply buried pelitic sediments: AAPG Bulletin, v. 56, p. 2013-2021.

Philip, H., A. Cisternas, A. Gvishiani, and A. Gorshkov, 1989, The Caucasus - an Actual Example of the Initial-Stages of Continental Collision: Tectonophysics, v. 161, p. 1-21.

Pinna, G., J. M. Carcione, and F. Poletto, 2011, Kerogen to oil conversion in source rocks. Pore-pressure build-up and effects on seismic velocities: Journal of Applied Geophysics, v. 74, p. 229-235.

Platte River Associates, I., 2014, BasinMod.

Porter, E., and W. James, 1986, Influence of pressure, salinity, temperature and grain size on silica diagenesis in quartzose sandstones: Chemical geology, v. 57, p. 359-369.

Posnjak, E., 1940, Deposition of calcium sulfate from sea water.: American Journal of Science, v. 238, p. 559-568.

Poston, S. W., and R. R. Berg, 1997, Overpressured Gas Reservoirs, Society of Petroleum Engineers.

Pray, L. C., and P. W. Choquette, 1966, Genesis of carbonate reservoir Facies: ABSTRACT: AAPG Bulletin, v. 50, p. 632-632.

Proshlyakov, B. K., 1974, Secondary Changes of Oil and Gas Reservoir Rocks: Moscow, Nedra Publishing House, 232 p.

Rajabi, M., S. Sherkati, B. Bohloli, and M. Tingay, 2010, Subsurface fracture analysis and determination of in-situ stress direction using FMI logs: An example from the Santonian carbonates (Ilam Formation) in the Abadan Plain, Iran: Tectonophysics, v. 492, p. 192-200.

Ramdhan, A. M., 2010, Overpressure and compaction in the lower kutai basin, indonesia, Durham University, United Kingdom.

Ramdhan, A. M., and N. R. Goulty, 2010, Overpressure-generating mechanisms in the Peciko Field, Lower Kutai Basin, Indonesia: Petroleum Geoscience, v. 16, p. 367-376.

Ramdhan, A. M., and N. R. Goulty, 2011, Overpressure and mudrock compaction in the Lower Kutai Basin, Indonesia: A radical reappraisal: AAPG bulletin, v. 95, p. 1725-1744.

Ramsay, J. G., 1967, Folding and fracturing of rocks: New York, McGraw-Hill.

Ransom, R. C., 1986, A Method For Calculation Pore Pressures From Well Logs: The Log Analyst, v. XXVII.

Raymer, L. L., E. R. Hunt, and J. S. Gardner, 1980, An Improved Sonic Transit Time-To-Porosity Transform, 21st Annual Logging Symposium, Lafayette, Louisiana Society of Petrophysicists and Well-Log Analysts.

Read, J. F., 1982, Carbonate platforms of passive (extensional) continental margins: Types, characteristics and evolution: Tectonophysics, v. 81, p. 195-212.

Research Institute of Petroleum Industry, 2005a, Reservoir Geology of the Azadegan Field.

Research Institute of Petroleum Industry, 2005b, Reservoir Geology of the Field A, Tehran, Iran, p. 41.

Robertson, A. H. F., 2000, Mesozoic-Tertiary Tectonic-Sedimentary Evolution of a South Tethyan Oceanic Basin and its Margins in Southern Turkey: Geological society, London, Special Publications, v. 173, p. 97-138.

Rocha, L. A. S., J. L. Falcão, C. J. C. Gonçalves, C. Toledo, K. Lobato, S. Leal, and H. Lobato, Fracture Pressure Gradient in Deepwater, Society of Petroleum Engineers.

Rockenbach, B., 2006, Interpolation.

Roehl, P. O., and R. Weinbrandt, 1985, Geology and Production Characteristics of Fractured Reservoirs in the Miocene Monterey Formation, West Cat Canyon Oilfield, Santa Maria Valley, California, Carbonate Petroleum Reservoirs, Springer, p. 525-545.

Royden, L., and C. E. Keen, 1980, Rifting process and thermal evolution of the continental margin of Eastern Canada determined from subsidence curves: Earth and Planetary Science Letters, v. 51, p. 343-361.

Rudolph, M. L., M. Manga, M. Tingay, and R. J. Davies, 2015, Influence of seismicity on the Lusi mud eruption: Geophysical Research Letters, v. 42, p. 7436-7443.

Runnegar, B., 1985, Shell microstructures of Cambrian molluscs replicated by phosphate: Alcheringa: An Australasian Journal of Palaeontology, v. 9, p. 245-257.

Rusmussen, C. E., and K. I. Williams, 2006, Gaussian Processes for Machine Learning the MIT Press.

Rutter, E. H., and D. Elliott, 1976, The Kinetics of Rock Deformation by Pressure Solution [and Discussion], v. 283, 203-219 p.

Saadatinejad, M. R., and K. Sarkarinejad, 2011, Application of the spectral decomposition technique for characterizing reservoir extensional system in the Abadan Plain, southwestern Iran: Mar Pet Geol, v. 28, p. 1205-1217.

Sahagian, D. L., and A. A. Proussevitch, 1992, Bubbles in volcanic systems: Nature, v. 359, p. 485-485.

Sahay, B., 1999, Pressure Regimes in Oil and Gas Exploration, Sunil Sachdev.

Saller, A. H., and N. Henderson, 1998, Distribution of porosity and permeability in platform dolomites: Insight from the Permian of west Texas: AAPG bulletin, v. 82, p. 1528-1550.

Salz, L. B., 1977, RELATIONSHIP BETWEEN FRACTURE PROPAGATION PRESSURE AND PORE PRESSURE, SPE Annual Fall Technical Conference and Exhibition, Denver, Colorado, 1977 Copyright 1977, American Institute of Mining, Metallurgical, and Petroleum Engineers, Inc.

Sam Boggs, J., and J. Boggs, Sam . 2009, Carbonaceous sedimentary rocks

Petrology of Sedimentary Rocks, Cambridge University Press.

Sarkarinejad, K., and A. Azizi, 2008, Slip partitioning and inclined dextral transpression along the Zagros Thrust System, Iran: Journal of Structural Geology, v. 30, p. 116-136.

Sassen, R., and C. H. Moore, 1988, Framework of hydrocarbon generation and destruction in eastern Smackover trend: AAPG Bulletin, v. 72, p. 649-663.

Sattarzadeh, Y., J. W. Cosgrove, and C. Vita-Finzi, 1999, The interplay of faulting and folding during the evolution of the Zagros deformation belt: Geological society, London, Special Publications, v. 169, p. 187-196.

Sayers, C. M., P. J. Hooyman, N. Smirnov, G. Fiume, A. Prince, J. C. d. L. Mojarro, M. T. Romero, and O. M. Gonzalez, 2002, Pore Pressure Prediction for the Cocuite Field, Veracruz Basin, SPE Annual Technical Conference and Exhibition, San Antonio, Texas, Copyright 2002, Society of Petroleum Engineers Inc.

Sayers, C. M., G. M. Johnson, and G. Denyer, 2000, Predrill Pore Pressure Prediction Using Seismic Data, IADC/SPE Drilling Conference, New Orleans, Louisiana, Copyright 2000, IADC/SPE Drilling Conference.

Sayers, C. M., and M. J. Woodward, 2001, Predrill Pore Pressure Prediction Using 4C Seismic Data.

Schlumberger, 2006, Fundamentals of Formation Testing: 225 Schlumberger Drive: Sugar Land, Texas.

Schlumberger, 2009, Log interpretation charts.

Schlumberger, 2015a, Connection Gas.

Schlumberger, 2015b, PetroMod Petroleum Systems Modeling Software.

Schlumberger, 2015c, Trip Gas.

SCHMIDT, V., and D. A. MCDONALD, 1979, The Role of Secondary Porosity in the Course of Sandstone Diagenesis, Aspects of Diagenesis, v. 26, SEPM (Society for Sedimentary Geology), p. 175-207.

Schmoker, J. W., 1984, Empirical relation between carbonate porosity and thermal maturity: An approach to regional porosity prediction: AAPG Bulletin, v. 68, p. 1697-1703.

Schmoker, J. W., and R. B. Halley, 1982, Carbonate porosity versus depth; a predictable relation for South Florida: AAPG Bulletin, v. 66, p. 2561-2570.

Scholle, P. A., 1977, Chalk diagenesis and its relation to petroleum exploration: oil from chalks, a modern miracle?: AAPG Bulletin, v. 61, p. 982-1009.

Scholle, P. A., and R. B. Halley, 1989, Burial diagenesis: Out of sight, out of mind!: SHORT COURSES IN GEOLOGY, v. 4.

Sclater, J. G., and P. A. F. Christie, 1980, Continental Stretching - an Explanation of the Post-Mid-Cretaceous Subsidence of the Central North-Sea Basin: Journal of Geophysical Research, v. 85, p. 3711-3739.

Sepehr, M., and J. W. Cosgrove, 2004, Structural framework of the Zagros Fold–Thrust Belt, Iran: Marine and Petroleum Geology, v. 21, p. 829-843.

Serebryakov, V. A., G. V. Chilingar, and S. A. Katz, 1995, Methods of Estimating and Predicting Abnormal Formation Pressures: Journal of Petroleum Science and Engineering, v. 13, p. 113-123.

Shaker, S., 2007, Calibration of Geopressure Predictions using the Normal Compaction Trend: Perception and Pitfall: CSEG RECORDER, p. 29-35.

Shanley, K. W., R. M. Cluff, and J. W. Robinson, 2004, Factors controlling prolific gas production from low-permeability sandstone reservoirs: Implications for resource assessment, prospect development, and risk analysis: AAPG bulletin, v. 88, p. 1083-1121.

Sharief, F. A., 1982, Lithofacies Distribution of the Permian-Triassic Rocks in the Middle East: Journal of Petroleum Geology, v. 4, p. 299-310.

Sheldon, H. A., J. Wheeler, R. H. Worden, and M. J. Cheadle, 2003a, An Analysis of the Roles of Stress, Temperature, and pH in Chemical Compaction of Sandstones: Journal of Sedimentary Research, v. 73, p. 64-71.

Sheldon, H. A., J. Wheeler, R. H. Worden, and M. J. Cheadle, 2003b, An Analysis of the Roles of Stress, Temperature, and pH in Chemical Compaction of Sandstones: Journal of Sedimentary Research, v. 73.

Sherman, C., C. Fletcher, and K. Rubin, 1999, Marine and meteoric diagenesis of Pleistocene carbonates from a nearshore submarine terrace, Oahu, Hawaii: Journal of Sedimentary Research, v. 69.

Shinn, E. A., R. B. Halley, J. H. Hudson, and B. H. Lidz, 1977, Limestone compaction: An enigma: Geology, v. 5.

Shinn, E. A., and D. M. Robbin, 1983, Mechanical and Chemical Compaction in Fine-Grained Shallow-Water Limestones: Journal of Sedimentary Petrology, v. 53, p. 595-618.

Sibley, D. F., and H. Blatt, 1976, Intergranular pressure solution and cementation of the Tuscarora orthoquartzite: Journal of Sedimentary Research, v. 46, p. 881-896.

Sibson, R. H., 1990, Conditions for Fault-Valve Behavior: Deformation Mechanisms, Rheology and Tectonics, v. 54, p. 15-28.

Sibson, R. H., 2003, Brittle-failure controls on maximum sustainable overpressure in different tectonic regimes: AAPG bulletin, v. 87, p. 901-908.

Skempton, A. W., 1969, The consolidation of clays by gravitational compaction: Quarterly Journal of the Geological Society, v. 125, p. 373-411.

Slotnick, M., 1936, On seismic computations, with applications, I: Geophysics, v. 1, p. 9-22.

Smith, J., 1971, The dynamics of shale compaction and evolution of pore-fluid pressures: Journal of the International Association for Mathematical Geology, v. 3, p. 239-263.

Smolen, J. J., and L. R. Litsey, 1979, Formation Evaluation Using Wireline Formation Tester Pressure Data: Journal of Petroleum Technology, v. 31, p. 25-32.

Soleimani, B., and A. Bahadori, 2014, The Miocene Gachsaran Formation evaporite cap rock, Zeloi oilfield, SW Iran: Carbonates and Evaporites, p. 1-20.

Spencer, C. W., 1987, Hydrocarbon generation as a mechanism for overpressuring in Rocky Mountain region: AAPG bulletin, v. 71, p. 368-388.

Stoecklin, J., 1968, Structural history and tectonics of Iran: a review: AAPG Bulletin, v. 52, p. 1229-1258.

Stoessell, R. K., and C. H. Moore, 1983, water-rock interactions: The American Associaiion of Petroleum Geologists Bulletin, v. 67, p. 896-906.

Stoneley, R., 1990, The Middle East Basin: a summary overview: Geological Society, London, Special Publications, v. 50, p. 293-298.

Stueber, A. M., and L. M. Walter, 1991, Origin and chemical evolution of formation waters from Silurian-Devonian strata in the Illinois basin, USA: Geochimica et Cosmochimica Acta, v. 55, p. 309-325.

Swarbrick, R., 2012, Review of pore-pressure prediction challenges in high-temperature areas: The Leading Edge, v. 31, p. 1288-1294.

Swarbrick, R. E., 1995, Distribution and Generation of the Overpressure System, Eastern Delaware Basin, Western Texas and Southern New Mexico: DISCUSSION AND REPLY: AAPG Bulletin, v. 79, p. 1817-1821.

Swarbrick, R. E., 2001, Challenges of porosity based pore pressure prediction: 63rd EAGE Conference & Exhibition.

Swarbrick, R. E., and M. J. Osborne, 1996, The nature and diversity of pressure transition zones: Petroleum Geoscience, v. 2, p. 111-116.

Swarbrick, R. E., and M. J. Osborne, 1998, Memoir 70, Chapter 2: Mechanisms that Generate Abnormal Pressures: an Overview.

Swarbrick, R. E., M. J. Osborne, and G. S. Yardley, 2002, Comparison of Overpressure Magnitude Resulting from the Main Generating Mechanisms, *in* A. Huffman, and G. Bowers, eds., Pressure Regimes in Sedimentary Basins and Their Prediction, v. AAPG Memoir 76, American Association of Petroleum Geologists.

Szabo, F., and A. Kheradpir, 1978, Permian and Triassic Stratigraphy, Zagros Basin, South-West Iran: Journal of Petroleum Geology, v. 1, p. 57-82.

Takin, M., 1972, Iranian Geology and Continental Drift in the Middle East: Nature, v. 235, p. 147-150.

Tang, H., J. Luo, K. Qiu, Y. Chen, and C. P. Tan, 2011, Worldwide Pore Pressure Prediction: Case Studies and Methods, SPE Asia Pacific Oil and Gas Conference and Exhibition, Jakarta, Indonesia, Society of Petroleum Engineers.

Teige, G. M. G., C. Hermanrud, L. Wensaas, and H. M. N. Bolas, 1999, The lack of relationship between overpressure and porosity in North Sea and Haltenbanken shales: Marine and Petroleum Geology, v. 16, p. 321-335.

Terzaghi, K., 1925, Principles of soil mechanics, IV—Settlement and consolidation of clay: Engineering News-Record, v. 95, p. 874-878.

Terzaghi, K., and R. B. Peck, 1967, Soil Mechanics in Engineering Practice, John Wiley and Sons, Inc.

Terzaghi, K. v., 1923, Die berechnung der durchlassigkeitsziffer des tones aus dem verlauf der hydrodynamischen spannungserscheinungen: Sitzungsberichte der Akademie der Wissenschaften in Wien, Mathematisch-Naturwissenschaftliche Klasse, Abteilung IIa, v. 132, p. 125-138.

Testa, G., and S. Lugli, 2000, Gypsum–anhydrite transformations in Messinian evaporites of central Tuscany (Italy): Sedimentary Geology, v. 130, p. 249-268.

Tingay, M., 2014, Initial pore pressures under the Lusi mud volcano, Indonesia: Interpretation, v. 3, p. SE33-SE49.

Tingay, M. R. P., 2003, In Situ Stress and Overpressures of Brunei Darussalam, The University of Adelaide.

Tingay, M. R. P., R. R. Hillis, C. K. Morley, R. E. Swarbrick, and E. C. Okpere, 2003, Variation in vertical stress in the Baram Basin, Brunei: tectonic and geomechanical implications: Marine and Petroleum Geology, v. 20, p. 1201-1212.

Tingay, M. R. P., R. R. Hillis, R. E. Swarbrick, C. K. Morley, and A. R. Damit, 2007, 'Vertically transferred' overpressures in Brunei: Evidence for a new mechanism for the formation of high-magnitude overpressure: Geology, v. 35, p. 1023.

Tingay, M. R. P., R. R. Hillis, R. E. Swarbrick, C. K. Morley, and A. R. Damit, 2009, Origin of overpressure and pore-pressure prediction in the Baram province, Brunei: AAPG Bulletin, v. 93, p. 51-74.

Tingay, M. R. P., C. K. Morley, A. Laird, O. Limpornpipat, K. Krisadasima, S. Pabchanda, and H. R. Macintyre, 2013, Evidence for overpressure generation by kerogen-to-gas maturation in the northern Malay Basin: AAPG Bulletin, v. 97, p. 639-672.

Toksöz, M. N., C. H. Cheng, and A. Timur, 1976, Velocities of seismic waves in porous rocks: Geophysics, v. 41, p. 621-645.

Traugott, M., 1997, Pore/fracture pressure determinations in deep water: World oil, v. 218, p. 68-70.

Turcotte, D., 1974, Are transform faults thermal contraction cracks?: Journal of Geophysical Research, v. 79, p. 2573-2577.

U.S. Army Corps of Engineers, 2001, Drilling Fluids, *in* R. L. DAVIS, ed., Engineering and Design - Geotechnical Investigations Washington, DC, DEPARTMENT OF THE ARMY.

Ungerer, P., E. Behar, and D. Discamps, 1981, Tentative calculation of the overall volume expansion of organic matter during hydrocarbon genesis from geochemistry data. Implications for primary migration: Advances in organic geochemistry, v. 10, p. 129-135.

Van der Knaap, W., 1959, Nonlinear behavior of elastic porous media: Trans. AIME, v. 216, p. 179-187.

van Golf-Racht, T. D., 1982, Fundamentals of fractured reservoir engineering, Elsevier.

Van Ruth, P., R. Hillis, R. Swarbrick, and P. Tingate, 2000, Mud weights, transient pressure tests, and the distribution of overpressure in the North West Shelf, Australia: Petroleum Exploration Society of Australia Journal, v. 28, p. 59-66.

van Ruth, P., R. Hillis, and P. Tingate, 2004, The origin of overpressure in the Carnarvon Basin, Western Australia: implications for pore pressure prediction: Petroleum Geoscience, v. 10, p. 247-257.

Vasil, P. R., and R. M. Mitcham Jr., 1979, Global Cycles of Relative Changes of Sea Level from Seismic Stratigraphy: Resources, Comparative Structure, and Eustatic Changes in Sea Level, Geological and Geophysical Investigations of Continental Margins, v. 29, Geologic History and Areal Geology, p. 469-472.

Velde, B., and G. Vasseur, 1992, Estimation of the Diagenetic Smectite to Illite Transformation in Time-Temperature Space: American Mineralogist, v. 77, p. 967-976.

Vernant, P., F. Nilforoushan, D. Hatzfeld, M. R. Abbassi, C. Vigny, F. Masson, H. Nankali, J. Martinod, A. Ashtiani, R. Bayer, F. Tavakoli, and J. Chéry, 2004, Present-day crustal deformation and plate kinematics in the Middle East constrained by GPS measurements in Iran and northern Oman: Geophysical Journal International, v. 157, p. 381-398.

Walderhaug, O., 1994, Precipitation rates for quartz cement in sandstones determined by fluid-inclusion microthermometry and temperature-history modeling: Journal of Sedimentary Research, v. 64.

Waldschmidt, W. A., P. E. Fitzgerald, and C. Lunsford, 1956, Classification of porosity and fractures in reservoir rocks: AAPG Bulletin, v. 40, p. 953-974.

Wang, R., Z. Wang, X. Shan, H. Qiu, and T. Li, 2013, Factors influencing pore-pressure prediction in complex carbonates based on effective medium theory: Petroleum Science, v. 10, p. 494-499.

Waples, D. W., 2001, Mechanisms for generating overpressure in sedimentary basins: A reevaluation: Discussion: AAPG Bulletin, v. 85, p. 2118.

Waples, D. W., and G. D. Couples, 1998a, Some thoughts on porosity reduction - rock mechanics, overpressure and fluid flow: Geological society, London, Special Publications, v. 141.

Waples, D. W., and G. D. Couples, 1998b, Some thoughts on porosity reduction — rock mechanics, overpressure and fluid flow: Geological society, London, Special Publications, v. 141, p. 73-81.

Weakley, R. R., 1990, Determination Of Formation Pore Pressures In Carbonate Environments From Sonic Logs, Annual Technical Meeting, Calgary, Alberta, Petroleum Society of Canada.

Weller, J. M., 1959, Compaction of sediments: AAPG Bulletin, v. 43, p. 273-310.

West, G., J. Hall, and S. Seaton, 2006, Drilling Engineering, *in* R. F. Mitchel, ed., Petroleum Engineering Handbook: Richardson, TX, Society of Petroleum Engineerins.

Western Atlas International Inc, 1992, Introduction to Wireline Log Analysis.

Wilson, J. L., 1975, Carbonate facies in geologic history, Springer.

Wyllie, M. R. J., A. R. Gregory, and L. W. Gardner, 1956, Elastic wave velocities in heterogeneous and porous media: Geophysics, v. 21, p. 41-70.

Xinong, X. I. E., W. Zhenfeng, L. I. Sitian, Z. Minqiang, and Y. Jihai, 2003, Characteristics of Overpressure Systems and Their Significance in Hydrocarbon Accumulation in the Yinggehai and Qiongdongnan Basins, China: Acta Geologica Sinica - English Edition, v. 77, p. 258-266.

Xu, S., G. Chen, Y. Zhu, J. Zhang, M. Payne, M. Deffenbaugh, L. Song, and J. H. Dunsmuir, 2007, Carbonate Rock Physics: Analytical Models and Validations Using Computational Approaches and Lab/Log Measurements, International Petroleum Technology Conference.

Yardley, G. S., and R. E. Swarbrick, 2000, Lateral transfer: a source of additional overpressure?: Marine and Petroleum Geology, v. 17.

Yassir, N., and M. A. Addis, 2002, Relationships between Pore Pressure and Stress in Different Tectonic Settings, *in* A. H. a. G. Bowers, ed., AAPG Memoir 76: Pressure Regimes in Sedimentary Basins and Their Prediction, The American Association of Petroleum Geologists, p. 79 - 88.

Yassir, N. A., and J. S. Bell, 1994, Relationships between Pore Pressure, Stresses, and Present-Day Geodynamics in the Scotian-Shelf, Offshore Eastern Canada: AAPG Bulletin-American Association of Petroleum Geologists, v. 78, p. 1863-1880.

Yilmaz, Y., 1993, New Evidence and Model on the Evolution of the Southeast Anatolian Orogen: Geological Society of America Bulletin, v. 105, p. 251-271.

Young, A., and P. F. Low, 1965, Osmosis in argillaceous rocks: Geological notes: AAPG Bulletin, v. 49, p. 1004-1007.

Yu, H., and F. J. Hilterman, 2014, The effect of pressure on rock properties in the Gulf of Mexico: Comparison between compaction disequilibrium and unloading: Interpretation, v. 2, p. SB1-SB15.

Zabihi Naeini, E., and H. Siahkoohi, 2006, Overpressure detection frequency attributes: 8th SEGJ International Symposium, p. 1-4.

Zahm, C. K., L. C. Zahm, and J. A. Bellian, 2010, Integrated fracture prediction using sequence stratigraphy within a carbonate fault damage zone, Texas, USA: Journal of Structural Geology, v. 32, p. 1363-1374.

Zeinalzadeh, A., R. Moussavi-Harami, A. Mahboubi, and V. A. Sajjadian, 2015, Basin and petroleum system modeling of the Cretaceous and Jurassic source rocks of the gas and oil reservoirs in Darquain field, south west Iran: Journal of Natural Gas Science and Engineering, v. 26, p. 419-426.

Zencher, F., M. Bonafede, and R. Stefansson, 2006, Near-lithostatic pore pressure at seismogenic depths: a thermoporoelastic model: Geophysical Journal International, v. 166, p. 1318-1334.

Zhang, J. C., 2011, Pore pressure prediction from well logs: Methods, modifications, and new approaches: Earth-Science Reviews, v. 108, p. 50-63.

Zhang, J. C., 2013, Effective stress, porosity, velocity and abnormal pore pressure prediction accounting for compaction disequilibrium and unloading: Marine and Petroleum Geology, v. 45, p. 2-11.

Zhao, Z., 2013, Mechanisms of Generating Overpressure and Its Influences on Super-Low Permeability Reservoirs of Upper Es4 Member, Chexi Depression, 6th International Petroleum Technology Conference, Beijing, China, 2013, International Petroleum Technology Conference.

Zimmerman, R. W., 1991, Compressibility of Sandstones: Development in Petroleum Science, v. 29: Amsterdam, The Netherlands, Elsevier Science Publishers B.V.

Zimmerman, R. W., W. H. Somerton, and M. S. King, 1986, Compressibility of porous rocks: Journal of Geophysical Research: Solid Earth, v. 91, p. 12765-12777.

Zoback, M., J. Healy, and J. Roller, 1977, Preliminary stress measurements in central California using the hydraulic fracturing technique: pure and applied geophysics, v. 115, p. 135-152.

Zoback, M. D., 2007, Reservoir Geomechanics: New York, cambridge university press.